DIRECT OPTICAL MEASUREMENTS OF THE LAURENTIAN GREAT LAKES PART II: AN OPTICAL ATLAS

by

R.P. Bukata, J.H. Jerome and J.E. Bruton

Aquatic Physics and Systems Division

National Water Research Institute

Canada Centre for Inland Waters

May 1985

NWRI Contribution #85-25

EXECUTIVE SUMMARY

Historically, optical properties of natural water masses and their influence on the social/technical impact of such waters have been inferred utilizing a wide variety of scientific, non-scientific, and quasi-scientific methods and techniques. Direct visual impressions of aquatic colour and clarity have long been reported as the need and/or opportunity has presented itself. Secchi discs have for many decades been included as part of limnological and oceanographic research vessel payloads. The development and continual modification of submersible electronic instrumentation has added another dimension to the overall capability of evaluating the aquatic environment through direct measurements of the optical characteristics of natural waters. The launching of environmental satellites, coupled with the development and application of airborne remote sensing devices, has added yet another dimension.

The Environmental Optics Section at the National Water Research Institute has concerned itself with the study of inland lakes utilizing their optical properties as revealed from both *in situ* data collected beneath the air-water interface and remotely-sensed data collected above the air-water interface. This report focuses on the former, in particular on the *in situ* data collected by the Environmental Optics Section since 1973 in four of the Laurentian Great Lakes (no direct measurements were performed in Lake Michigan), and presents such data in the form of an optical atlas.

These direct optical measurements were performed as part of the CCIW Surveillance Program utilizing transmissometer systems (Martek XMS and Multiband Transmission Temperature Profiler MTTP) and irradiance meter systems (Techtum QSM Quanta Spectrometer). The principal highlights of these measurements are presented in graphical, pictorial, and/or tabular form in such a manner as to allow, where possible, maximum ease in intercomparing the properties of Lake Erie, Ontario, Superior, and Huron/Georgian Bay.

The optical properties and parameters included within this atlas are surface transmission contours, summer photic depths, transmission transects, relationships between beam attenuation coefficient and Secchi disc depth, relationships between irradiance attenuation coefficient and beam attenuation coefficient, relationships between irradiance attenuation coefficient and Secchi disc depth, spectral band (blue, green, and red) values of irradiance attenuation coefficients, spectral dependence of irradiance attenuation coefficients, and horizontal optical layering.

In addition to the above intercomparable Great Lakes optical properties, discussions are presented on the determination of subsurface sighting range, photosynthetic available radiation, "optical cross sections", and water quality parameters from direct measurements of optical parameters.

This optical atlas is the second part of a two-part report concerning the *in situ* optical measurements performed by the Environmental Optics Section at NWRI. Its companion volume "Direct Optical Measurements of the Laurentian Great Lakes Part I: Theoretical Concepts and Measurement Techniques" presents an expanded discussion of the nature of the optical interactions occurring among impinging electromagnetic radiations and the aquatic components defining a natural water mass. Consequently, Part I of this report may provide a valuable background to the material presented in this atlas.

RÉSUMÉ ADMINISTRATIF

Au cours des années, on a déduit à partir de diverses méthodes et techniques scientifiques, intuitives et pseudo-scientifiques les propriétés optiques des étendues d'eaux naturelles, leur influence sur la société et leurs répercussions techniques. Pendant longtemps, l'évaluation de la couleur de l'eau et de sa transparence a reposé sur les constatations visuelles directes, selon que les besoins apparaissaient ou que les occasions se présentaient. Depuis plusieurs dizaines d'années maintenant, les disques de Secchi font partie du matériel que l'on retrouve à bord de tout navire de recherche limnologique ou océanographique. La mise au point et la constante amélioration d'instruments électroniques sous-marins ont ajouté une nouvelle dimension à la capacité globale d'évaluer le milieu aquatique en mesurant directement les caractéristiques optiques des eaux naturelles. Le lancement de satellites environnementaux, en plus de l'élaboration et l'utilisation pratique de télécapteurs aéroportés, a permis d'accéder à une dimension de plus.

La Section de la spectro-optique de l'environnement à l'Institut national de recherche sur les eaux s'est vouée à l'étude des lacs de l'intérieur, en ayant recours aux propriétés optiques qui ont été précisées au moyen de données recueillies sur place en-dessous de l'interface air/eau et par télécapteurs au-dessus de l'interface. Le rapport met l'accent surtout sur les données recueillies sur place

par la Section de la spectro-optique de l'environnement depuis 1973 dans quatre des Grand Lacs laurentiens (aucune mesure n'a été effectuée dans le lac Michigan) et fournit ces données sous la forme d'un atlas optique.

Ces mesures optiques directes ont été prises à l'aide de transmissomètres (le Martek XMS et le bathyphotothermogramme) et d'appareils de mesure de l'éclairement énergétique (spectromètre de quanta Techtum), dans le cadre du Programme de surveillance du CCEI. Les principaux résultats de ces mesures apparaissent sous forme de graphiques et de tableaux qui facilitent autant que possible la comparaison des propriétés entre les eaux des lacs Erié, Ontario, Supérieur, et Huron (Baie Georgienne).

Les propriétés et les paramètres optiques figurant dans cet atlas sont les suivants: la transmission en surface, la profondeur limite de la visibilité en été, les transects de la mesure de la transmission optique, les relations entre le coefficient d'extinction du faisceau et la profondeur limite de la visibilité du disque de Secchi, les relations entre le coefficient d'extinction de l'éclairement énergétique et le coefficient d'extinction du faisceau, les relations entre le coefficient d'extinction de l'éclairement énergétique et la profondeur limite de la visibilité du disque de Secchi, les valeurs du spectre de bandes (bleu, vert et rouge) des coefficients d'extinction de l'éclairement énergétique, la dépendance spectrale des coefficients d'extinction de l'éclairement énergétique et la superposition spectrale de la lumière selon la profondeur.

En plus de comparer les propriétés optiques des eaux provenant des Grand Lacs, l'atlas présente des discussions sur la détermination de la visibilité sous-marine, du rayonnement disponible pour la photosynthèse, de "coupes transversales" optiques et de paramètres de la qualité de l'eau à partir de mesures directes de paramètres optiques.

Cet "atlas optique" constitue le deuxième volet d'un rapport en deux parties qui rassemble les données sur les mesures optiques prises in situ par la Section de la spectro-optique de l'environnement due INRE. Le premier volume, Direct Optical Measurements of the Laurentian Great Lakes Part I: Theoretical Concepts and Measurement Techniques, présente des analyses détaillées sur la nature des interactions optiques qui agissent sur le rayonnement électromagnétique incident et les composants aquatiques qui définissent les étendues d'eau naturelles. La première partie du rapport constitue donc une information de base valable pour la lecture de cet "atlas".

ABSTRACT

The Environmental Optics Section at the National Water Research Institute has been actively engaged in various aspects of in situ and remote optical sensing of inland lakes since 1972. During that time considerable optical data have been directly acquired for four of the Laurentian Great Lakes (Lake Michigan has been excluded). This report presents, in atlas form, a review of such directly acquired optical data along with short narratives, where appropriate, which illustrate similarities and/or differences among the Great Lakes.

The optical properties and parameters considered herein include surface transmission, summer photic depth, transmission transects, beam attenuation coefficient, irradiance attenuation coefficient, Secchi disc depth, optical layering, sighting range, photosynthetic available radiation, scattering, absorption and water quality determinations. These properties and parameters are presented in pictorial, graphical, and/or tabular form in this atlas.

RÉSUMÉ

Depuis 1972, la Section de la spectro-optique de l'environnement à l'Institut national de recherche sur les eaux a conduit des travaux sur divers aspects des données recueillies sur place et au moyen de télécapteurs optiques dans les lacs de l'intérieur. Au cours de cette période, on a obtenu une foule de données optiques sur quatre des Grands Lacs laurentiens (on a exclu le lac Michigan). Le rapport présente sous forme d'atlas un aperçu de ces données en plus de courtes descriptions, lorsqu'elles s'imposent, pour illustrer les similitudes et les différences des Grands Lacs.

Les propriétés et les paramètres optique à l'étude sont les suivants: transmission en surface, profondeur limite de la visibilité en été, transects de la mesure de la transmission optique, coefficient d'extinction du faisceau, coefficient d'extinction de l'éclairement énergétique, profondeur limite de la visibilité au disque de Secchi, superposition spectrale de la lumière selon la profondeur, angle de champ, énergie radiante utilisable par les organismes photosynthétiques, dispersion, absorption et autres indicateurs de la qualité de l'eau. Ces propriétés et paramètres apparaissent sous forme d'images, de graphiques et de tableaux dans l'atlas.

TABLE OF CONTENTS

FIGURE CAPTIONS

Figure 1 Near-surface transmission contours of Lake Superior, May 12-26, 1973.

Figure 2 Near-surface transmission contours of Lake Superior, June 15-29, 1973.

Figure 3 Near-surface transmission contours of Lake Superior, July 26-August 9, 1973.

Figure 4 Near-surface transmission contours of Lake Superior, September 5-18, 1973.

Figure 5 Near-surface transmission contours of Lake Superior, October 9-29, 1973.

Figure 6 Near-surface transmission contours of Lake Superior, November 13-30, 1973.

Figure 7 Near-surface transmission contours of Lake Huron, April 24-May 2, 1974.

Figure 8 Near-surface transmission contours of Lake Huron, May 14-18, 1974.

Figure 9 Near-surface transmission contours of Lake Huron, June 22-29, 1974.

Figure 10 Near-surface transmission contours of Lake Huron, July 22-28, 1974.

Figure 11 Near-surface transmission contours of Lake Huron, August 26-September 1, 1974.

Figure 120 Spectral dependence of scattering cross sections of pure water, total suspended mineral and chlorophyll *a*.

Figure 121 Subsurface irradiance reflectance spectra for various suspended mineral concentrations in a water mass for which the dissolved organic concentration is kept fixed at 2.0 g carbon m^{-3} and the chlorophyll *a* concentration at 0.05 mg m^{-3}.

Figure 122 Subsurface irradiance reflectance spectra for various chlorophyll *a* and suspended mineral concentrations in a water mass for which the dissolved organic carbon concentration is kept fixed at 2.0 g carbon m^{-3}.

Figure 123 Subsurface irradiance reflectance spectra for various dissolved organic carbon concentrations in a water mass for which the suspended mineral concentration is kept fixed at 0.05 g m^{-3} and the chlorophyll *a* concentration at 1.0 mg m^{-3}.

Figure 124 Subsurface predictive water quality methodology based on the subsurface irradiance reflectances at 550 nm and 670 nm. Each point on the duo-isoplethic curves is defined by the coordinates (Chl *a*, suspended mineral).

Figure 125 Comparison between measured and calculated concentrations of chlorophyll *a* using *in situ* measurements of subsurface irradiance reflectances at 520 nm and 670 nm and the duo-isoplethic methodology of Figure 124.

Figure 126 Comparison between measured and calculated concentrations of suspended mineral using *in situ* measurements of subsurface irradiance reflectances at 520 nm and 670 nm and the duo-isoplethic methodology of Figure 124.

Figure 127 Predicted relationship between subsurface irradiance reflectance at 650 nm (red) and suspended mineral concentration for a water mass in which the dissolved organic carbon concentration is permitted to vary between zero and 5 g carbon m^{-3} and the chlorophyll *a* concentration is permitted to vary between 0.05 and 20.0 mg m^{-3}.

Figure 128 Relationship between the measured total suspended mineral concentration and the measured subsurface irradiance reflectance at 670 nm.

Figure 129 Relationship between total suspended mineral concentration and the beam attenuation coefficient.

INTRODUCTION

Direct measurements of the optical properties of the water masses found in four of the Laurentian Great Lakes (no measurements were taken in Lake Michigan) have been routinely performed in conjunction with the Canada Centre for Inland Waters Surveillance Program, by the Environmental Optics Section at the National Water Research Institute since 1973. These measurements were performed by the use of transmissometer systems (Martek XMS and Multiband Transmission Temperature Profiler MTTP) and irradiance meter systems (Techtum QSM Quanta Spectrometer). The use of these instruments and the nature of the data analyses associated with them have been extensively discussed elsewhere (see, for example, Bukata et al, 1979; Jerome et al, 1983; Jerome et al, 1984; as well as Part I of this report).

This report presents, in atlas form, the principal highlights of these measurements. The data will be presented in graphical, pictorial, and/or tabular form, in such a manner that, where possible, intercomparison among the four Great Lakes will be readily apparent. Included within this atlas will be surface transmission contours, summer photic depths, transmission transects, relationships between beam attenuation coefficient and Secchi disc depth, relationships between irradiance attenuation coefficient and beam attenuation coefficient, relationships between irradiance attenuation coefficient and Secchi disc depth, spectral band (blue,

green and red) values of irradiance attenuation coefficients, spectral dependence of irradiance attentuation coefficients, and horizontal optical layering.

In addition, discussions are presented concerning the determination of subsurface sighting range, photosynthetic available radiation, "optical cross sections", and water quality parameters from direct measurements of optical parameters.

SURFACE TRANSMISSION CONTOURS

Figures 1-32 illustrate contours of transmission values at a depth of 1 metre as directly measured in the Great Lakes at various intervals from 1973 to 1979. All measurements were performed with MARTEK XMS transmissometers of 1 m or 0.25 m path lengths and a Wratten 45 optical filter. Specific breakdown of these figures are given in Table 1. The data for Lakes Superior, Huron, Erie and Georgian Bay are presented on a per-cruise basis. The data from Lake Ontario are presented on a seasonal basis. Such a presentation was possible for Lake Ontario since considerably more attention was given to this lake during the surveillance activities of the past decade. Consequently, the data collected during the months of March, April and May (17 cruises during the years 1974-79) were averaged to represent a spring condition. Similarly, the data collected during the months June, July and August (22 cruises during 1974-79) were averaged to represent a summer condition; the data collected during September, October and November (20 cruises during 1974-79) were averaged to represent an autumn condition; the data collected during December and March (5 cruises during 1974-79) were averaged to represent a winter condition. The surface transmission contours for Lake Ontario waters are, therefore, a more realistic representation of the inherent properties of the lake than are the corresponding contours for the other Great Lake water regimes which are based solely on single cruise

values. Such single cruise values are, understandably, much more vulnerable to aberrant meteorological conditions occurring prior to or during the measurement interval.

The salient features of the surface transmission contours of Figures 1-32 include:

a) In general Lake Superior displays a high degree of clarity (transmission values >~60% for 1 m path length). The lowest lake-wide values of transmission occur in September, while the highest lake-wide values occur during May and June. Areas of generally low transmission throughout the year include the tip of the western basin (near Duluth), the north shore area (Thunder, Black and Nipigon Bays), and the south shore (west of the Keweenaw Peninsula).

b) While not as optically transparent as Lake Superior, Lake Huron also displays a high degree of clarity (transmission values >~50% for 1 m path length). The lowest lake-wide values of transmission occur in May, while the highest lake-wide values occur during July and August. Areas of generally low transmission throughout the year include Saginaw Bay (transmission <5% for 1 m path length), the inflow into the North Channel from the St. Mary's River, and coastal portions of the southern tip of Lake Huron.

c) Transmission values observed in Georgian Bay are comparable to those transmission values observed at mid-lake stations in Lake

Huron (55-70% for 1 m path length). Areas of generally low transmission include the north shore (near the mouth of the French River and the entrance to the North Channel) and the Nottawasaga Bay areas.

d) In general Lake Erie displays a low degree of optical clarity combined with a high degree of spatial variability. Throughout the year, measured transmission values range from as low as 1% for a 0.25 m path length (corresponding to ~1×10^{-6}% for a 1 m path length) to as high as 90% for a 0.25 m path length (corresponding to ~66% for a 1 m path length). While a seasonal variation is in evidence (lowest transmission in April and November; highest transmission in June), the most noteable feature is the transmission gradient along the lake from west-to-east. The shallowest western basin of Lake Erie is characterized by the least clarity, while the intermediate depth central basin is often characterized by a clarity intermediate to those characterizing the shallow western and deep eastern basins.

e) Lake Ontario generally displays an optical transmission intermediate to the optical transmissions displayed by Lake Erie and the Upper Lakes. Lake Ontario transmission values usually lie in the range 50-85% for 0.25 m path length (~6-52% for 1 m path length). The lowest lake-wide transmission values occur during the summer, the highest during the spring and winter.

Areas of generally lowest transmission values throughout the year include Hamilton Harbour, Niagara River plume region, Toronto area, Black Bay, and, in general, the nearshore zone. These regions are particularly evident in the yearly-average contours of Figure 32.

f) Throughout most of the year (summer possibly excluded), a distinct "onion skin" pattern is evident in the surface transmission contours of Lake Ontario, the clarity increasing with distance from shore. Of particular interest in Figure 32 is the maximum transmission contour (the 74% contour line) which is in almost direct alignment with the 180 m depth contour.

g) Such "onion skin" patterns are not readily recognizable features of the transmission contours of the other lakes, although more extensive surveillance techniques might extract such a pattern for the Upper Lakes.

h) The largest seasonal variations in optical clarity are observed in the lower Great Lakes while the minimal seasonal variations in optical clarity are observed in the upper Great Lakes.

TABLE 1

Figure	Lake	Path Length	Date
1	Superior	1 m	May 12-26, 1973
2	Superior	1 m	June 15-29, 1973
3	Superior	1 m	July 26-Aug 9, 1973
4	Superior	1 m	Sept. 5-18, 1973
5	Superior	1 m	Oct. 9-29, 1973
6	Superior	1 m	Nov. 13-30, 1973
7	Huron	1 m	Apr. 24-May 2, 1974
8	Huron	1 m	May 14-18, 1974
9	Huron	1 m	June 22-29, 1974
10	Huron	1 m	July 22-28, 1974
11	Huron	1 m	Aug. 26-Sept. 1, 1974
12	Huron	1 m	Sept. 30-Oct. 6, 1974
13	Huron	1 m	Dec. 4-10, 1974
14	Georgian Bay	1 m	Apr. 28-May 1, 1974
15	Georgian Bay	1 m	May 18-22, 1974
16	Georgian Bay	1 m	June 17-22, 1974
17	Georgian Bay	1 m	July 28-Aug. 2, 1974
18	Georgian Bay	1 m	Sept. 1-6, 1974
19	Georgian Bay	1 m	Oct. 6-11, 1974
20	Georgian Bay	1 m	Dec. 5-7, 1974
21	Erie	0.25 m	Apr. 3-10, 1975
22	Erie	0.25 m	May 12-25, 1975
23	Erie	0.25 m	June 24-29, 1975
24	Erie	0.25 m	Aug. 5-11, 1975
25	Erie	0.25 m	Oct. 6-11, 1975
26	Erie	0.25 m	Oct. 27-31, 1975
27	Erie	0.25 m	Nov. 25-30, 1975
28	Ontario	0.25 m	Mar,Apr.,May 1974-79
29	Ontario	0.25 m	June,July,Aug. 1974-79
30	Ontario	0.25 m	Sept.,Oct.,Nov.,1974-79
31	Ontario	0.25 m	Dec., Mar. 1974-79
32	Ontario	0.25 m	Mar.-Dec. 1974-79

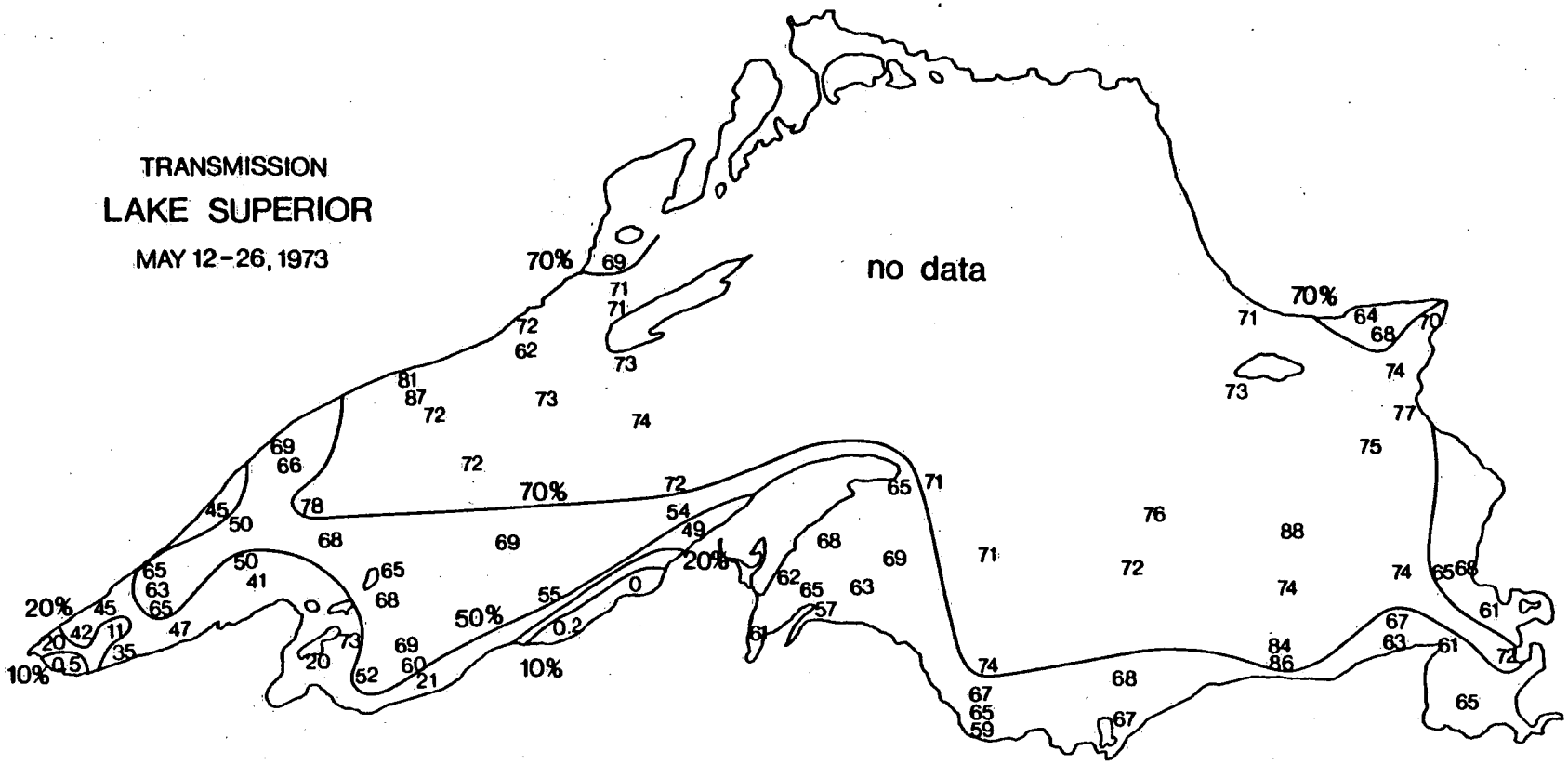
TRANSMISSION
LAKE SUPERIOR
MAY 12-26, 1973
no data
70%
70%
70%
50%
20%
20%
10%
10%
69
71
71
72
62
73
81
87
72
73
74
69
66
72
78
72
54
49
45
50
68
69
65
71
76
88
50
41
65
63
65
45
47
68
55
0
0.2
62
65
63
68
69
71
72
74
74
65
68
61
67
63
61
72
20
42
11
35
0.5
20
73
69
60
21
52
61
57
84
86
74
68
67
65
59
67
65
18

FIG. 1

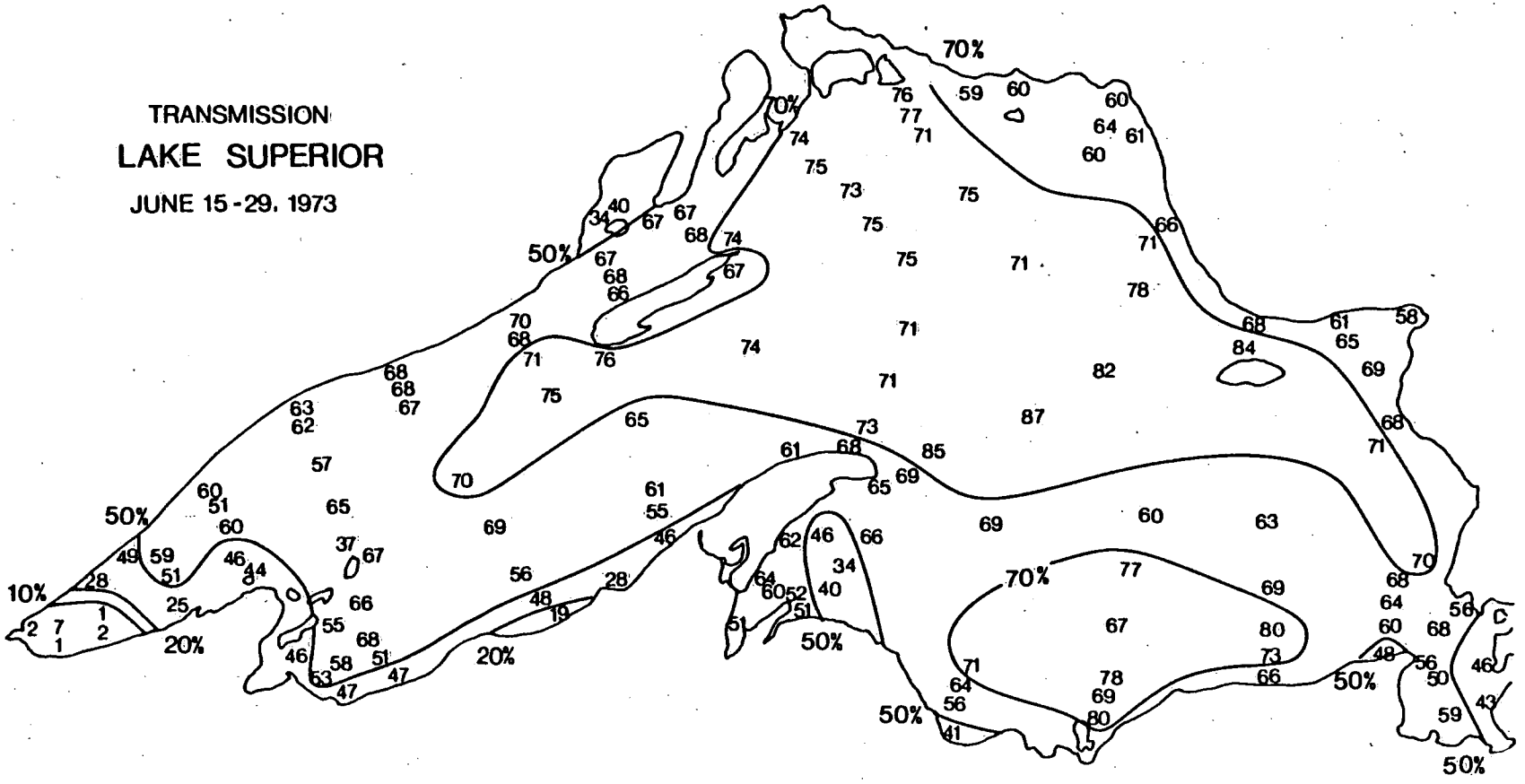

FIG. 2

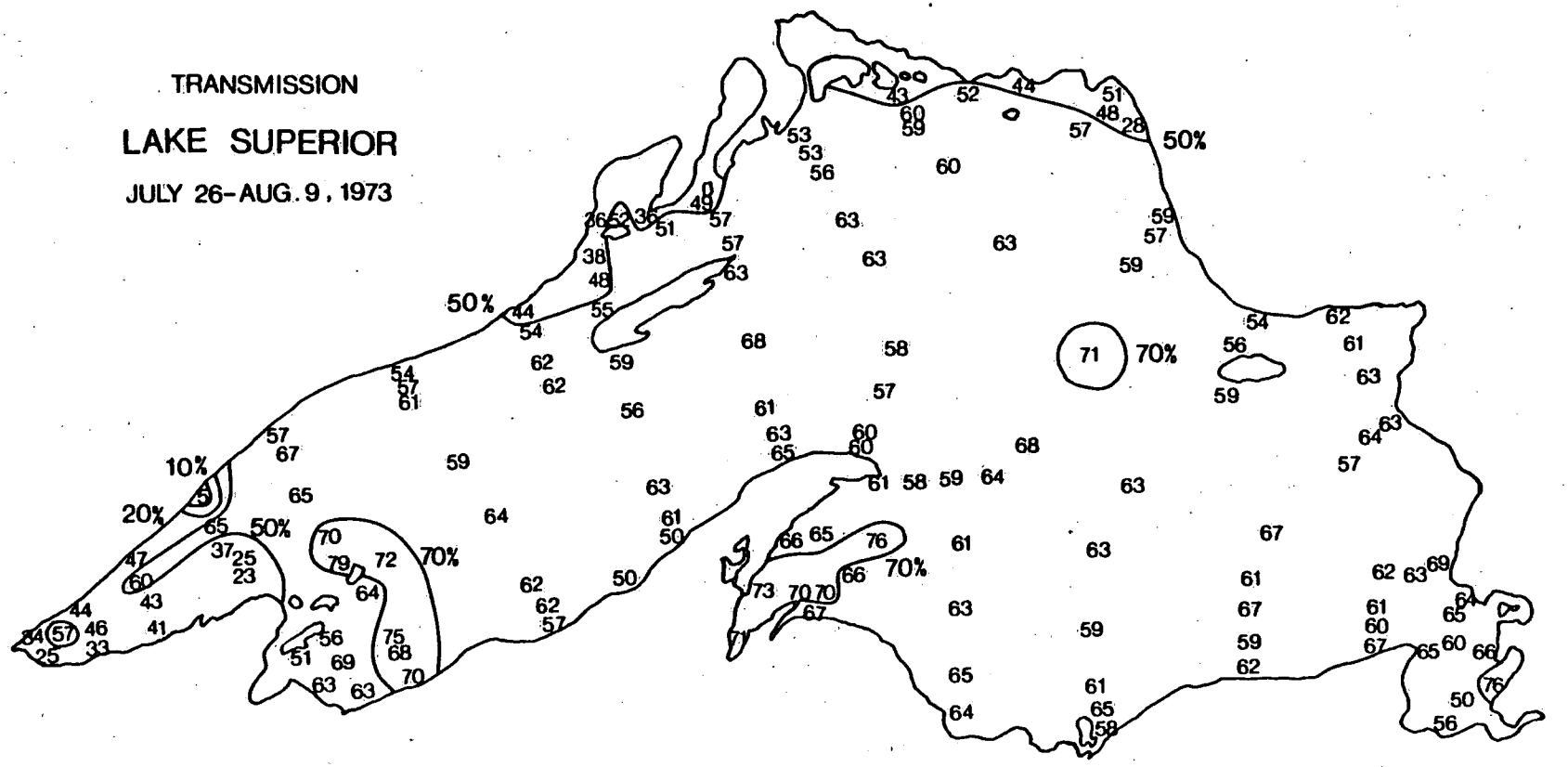

FIG. 3

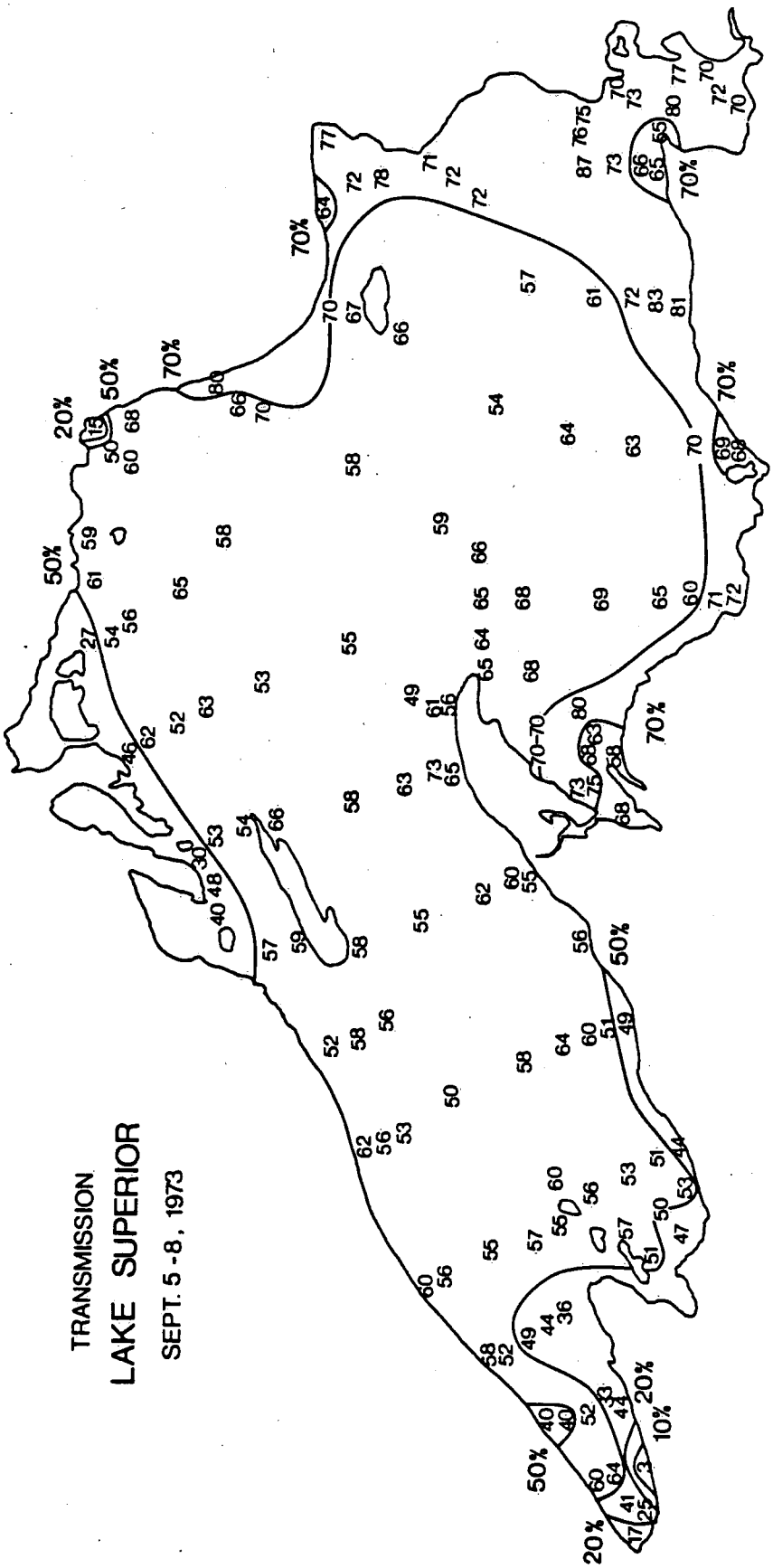

FIG. 4

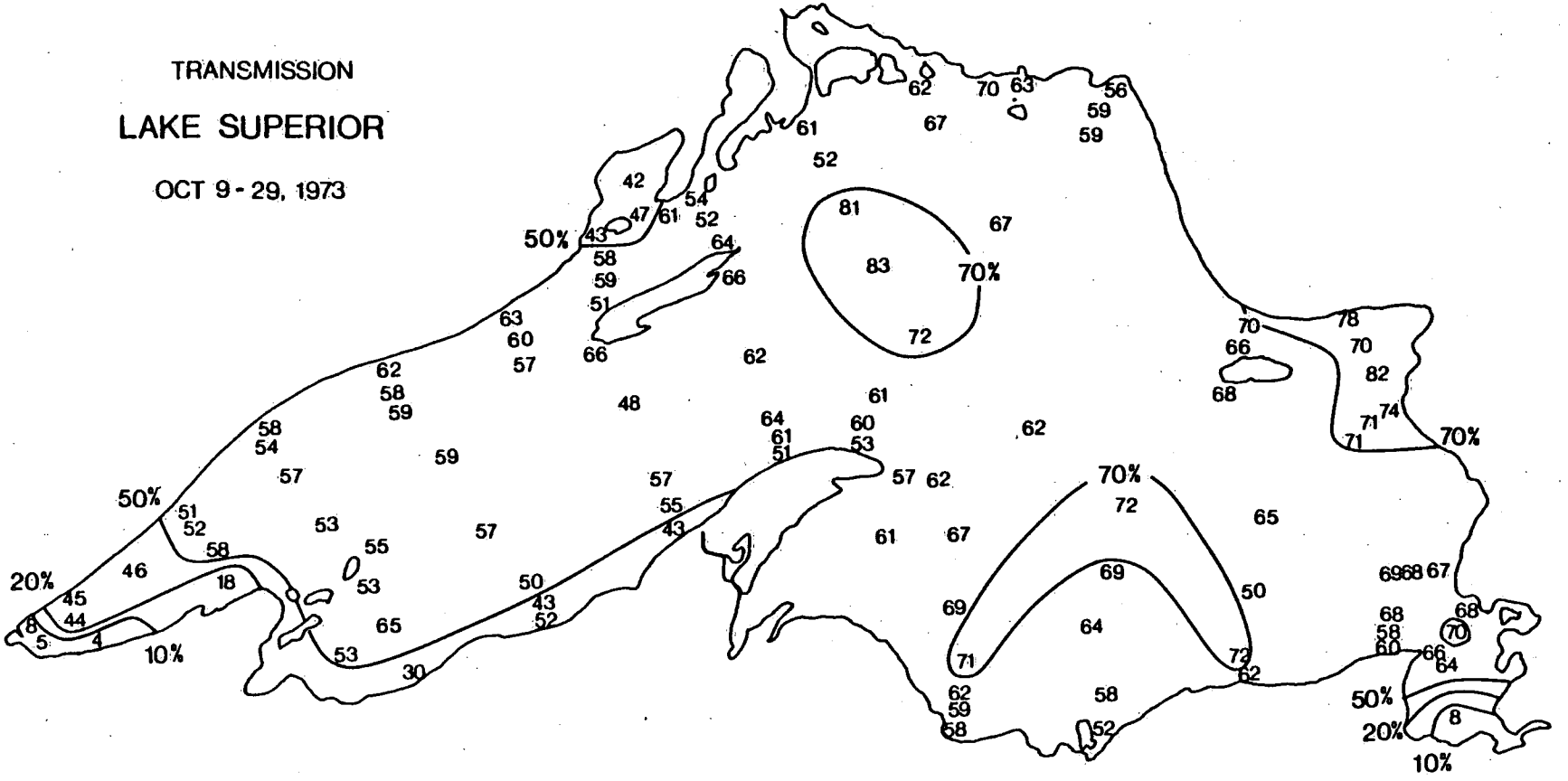

FIG. 5

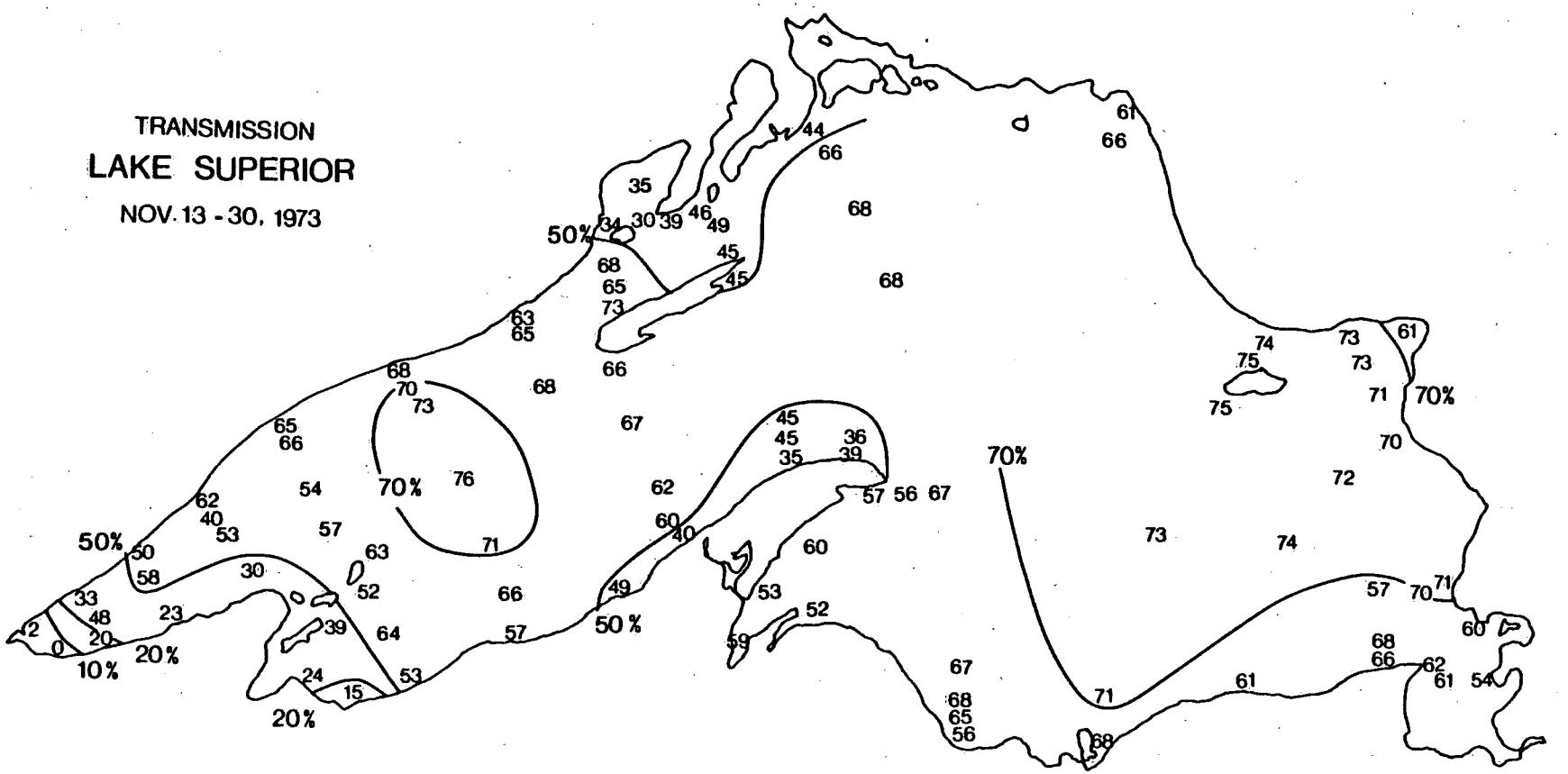

FIG. 6

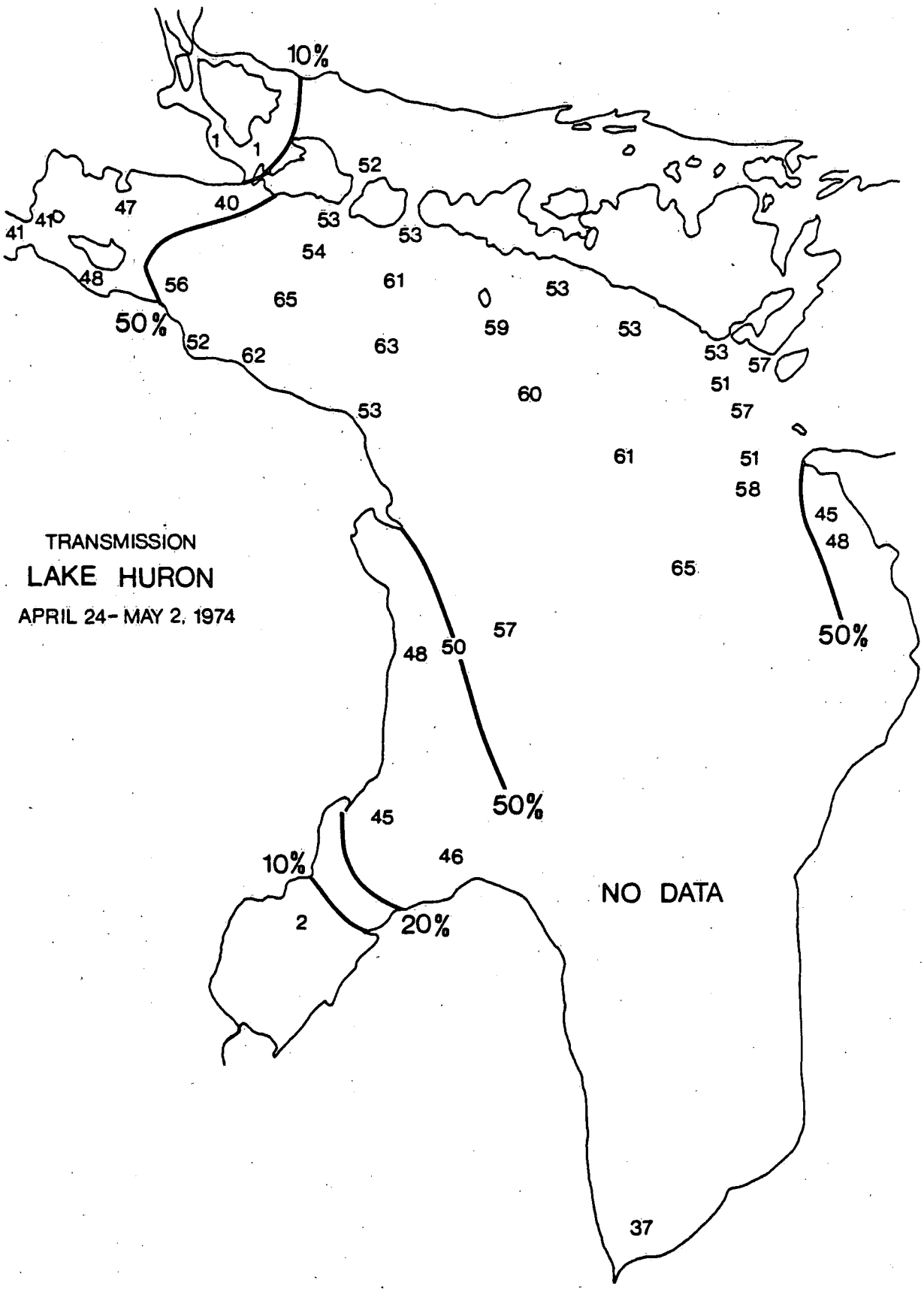
TRANSMISSION
LAKE HURON
APRIL 24- MAY 2, 1974
10%
50%
50%
50%
10%
20%
NO DATA
1
1
52
47
40
41
41
53
53
54
48
56
61
65
53
59
53
53
57
63
62
52
51
60
57
53
61
51
58
45
48
65
57
48
50
45
46
2
37

FIG. 7

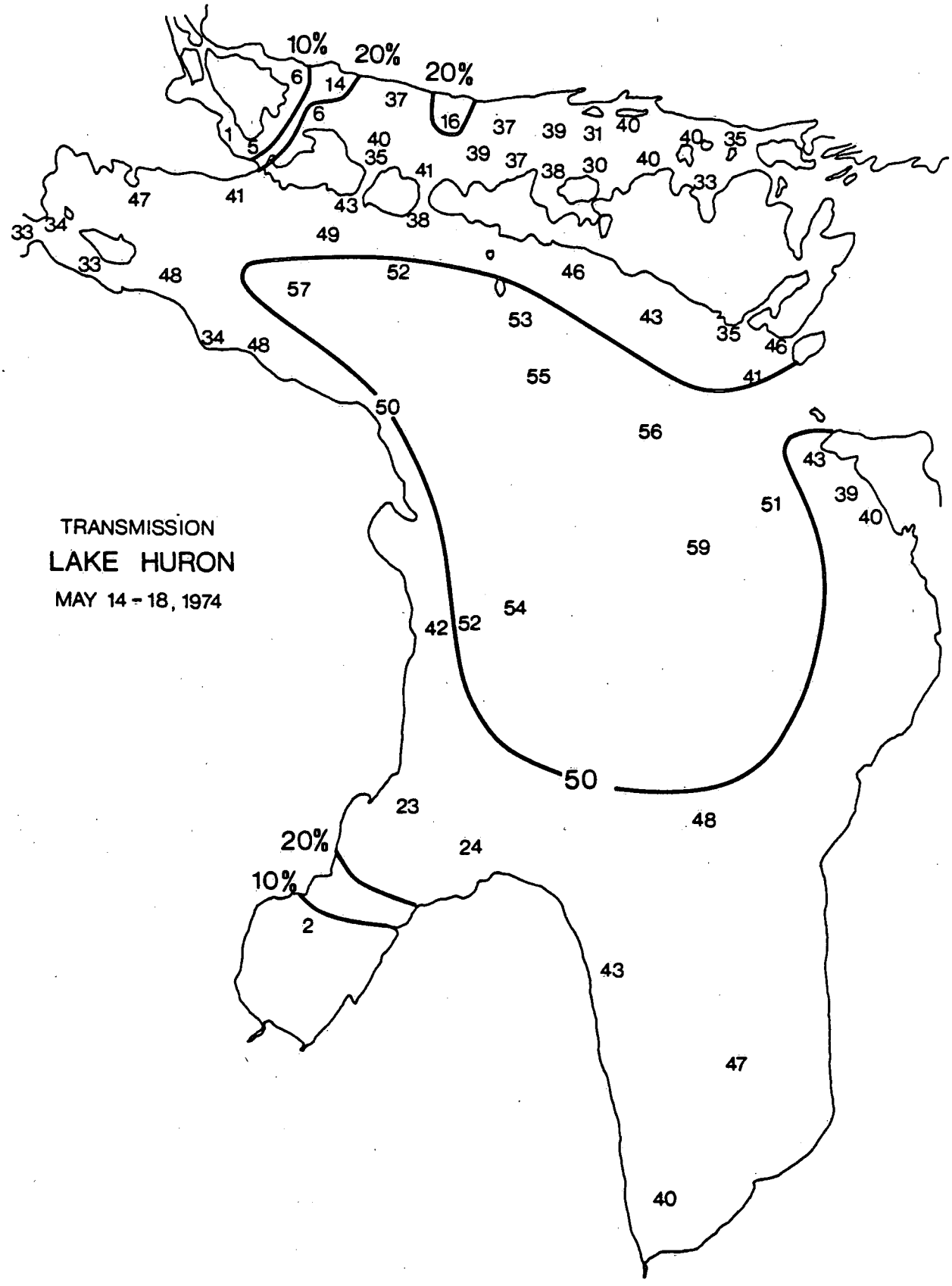
TRANSMISSION
LAKE HURON
MAY 14 - 18, 1974
10%
20%
20%
6
14
37
6
16
1
5
37
39
31
40
40
35
40
35
41
39
37
38
30
40
33
47
41
43
38
33
34
49
33
48
52
46
57
53
43
35
46
34
48
55
41
50
56
43
39
40
51
59
54
42
52
50
23
48
20%
24
10%
2
43
47
40

FIG. 8

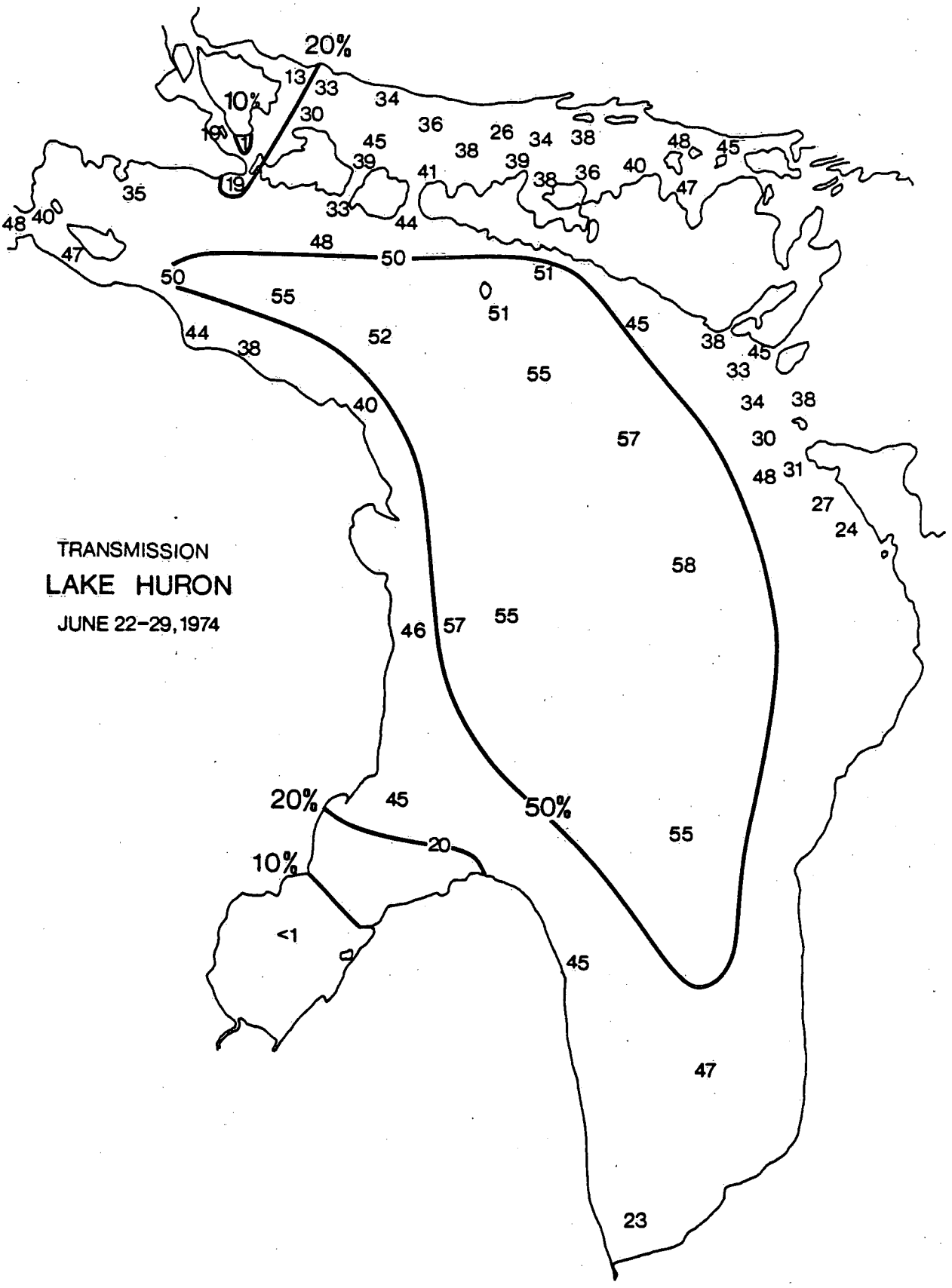

FIG. 9

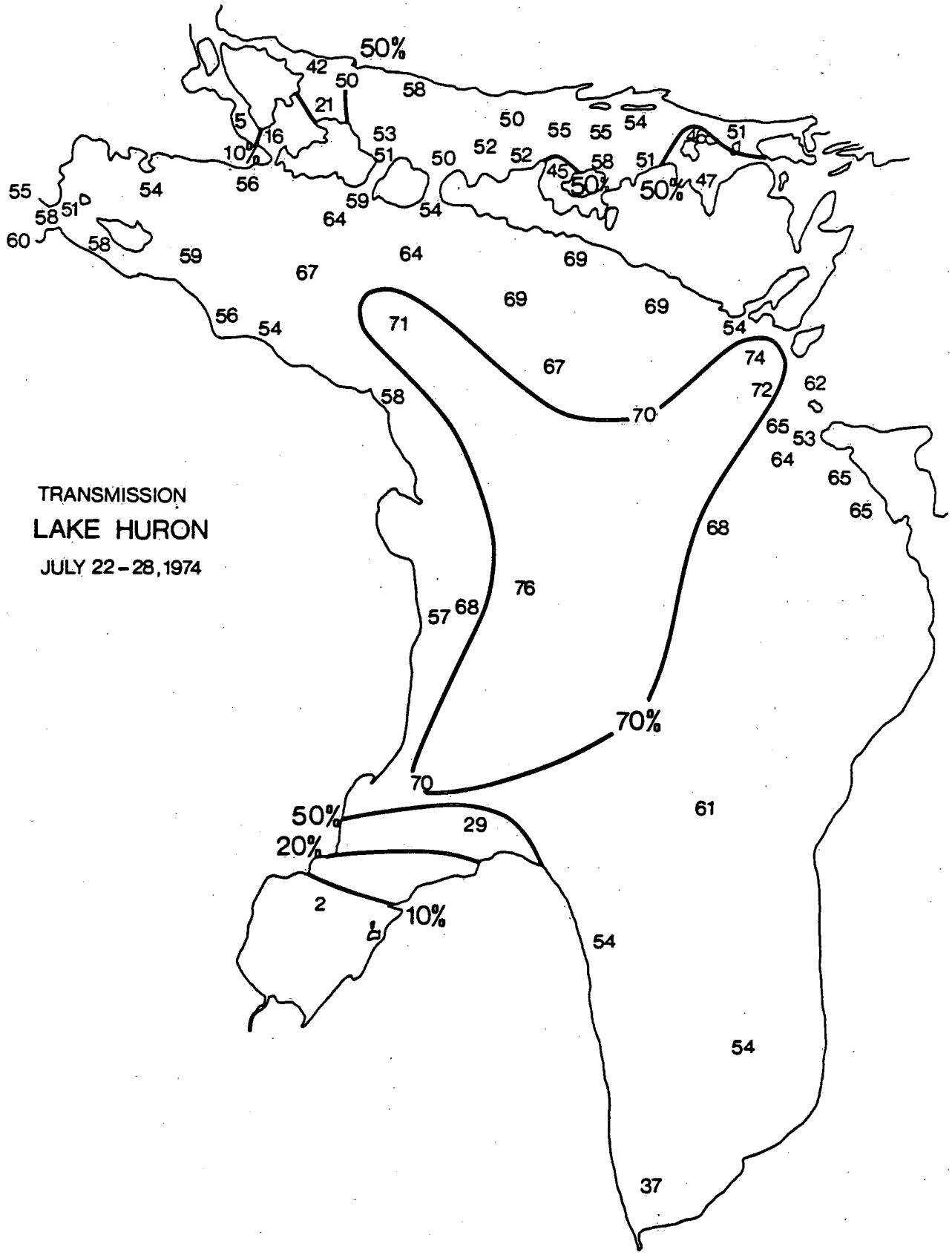
TRANSMISSION
LAKE HURON
JULY 22-28, 1974
50%
42
50
58
21
5
16
10%
53
51
50
52
52
55
55
54
46
51
45
58
51
50%
50%
47
55
54
56
59
64
54
58
51
60
58
59
67
64
69
56
54
71
69
69
54
67
74
72
62
58
70
65
53
64
65
65
68
76
57
68
70%
70
50%
29
61
20%
2
10%
54
54
37

FIG. 10

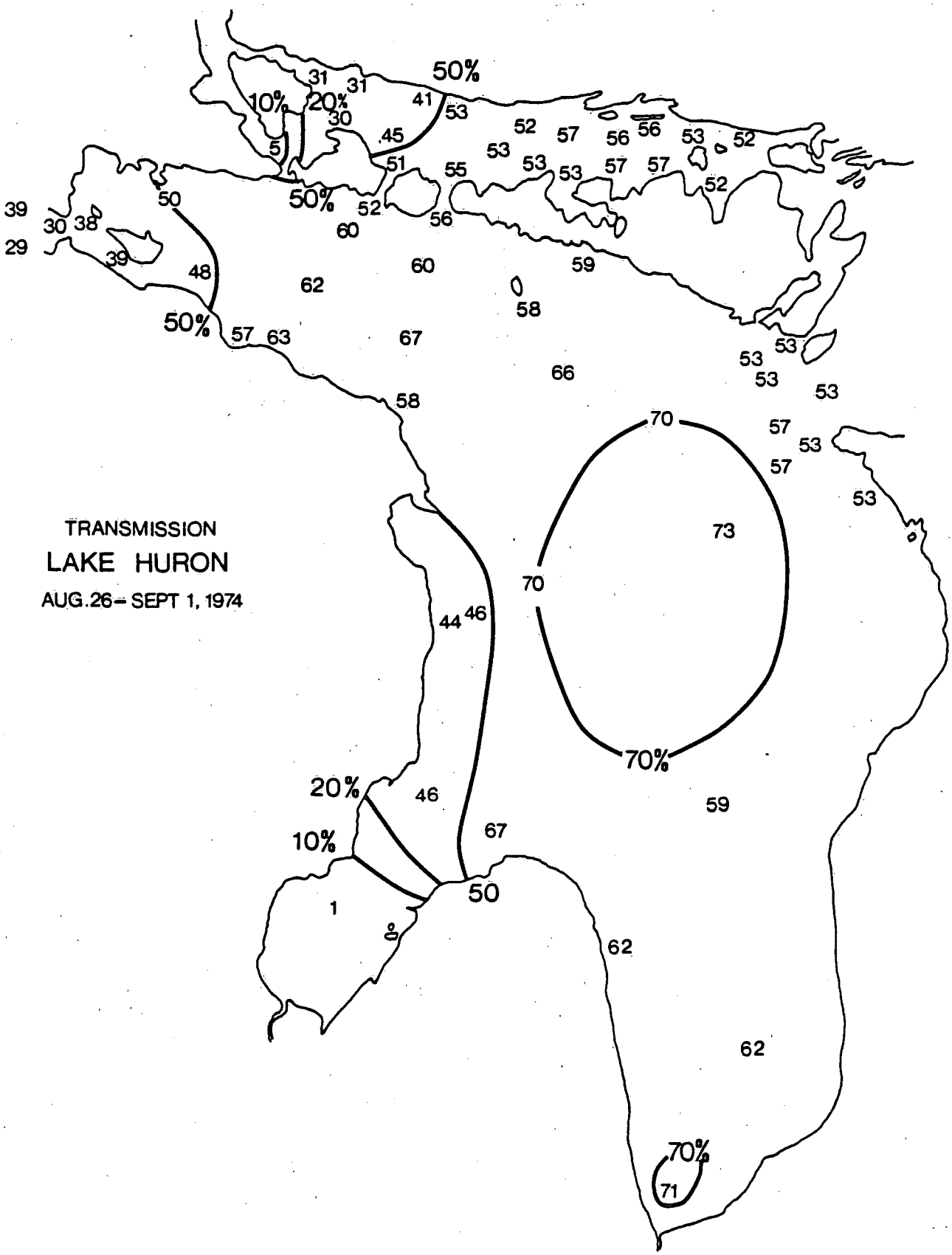
TRANSMISSION
LAKE HURON
AUG.26– SEPT 1, 1974
50%
10%
20%
70%
31
31
41
53
30
45
5
51
52
57
56
56
53
52
53
53
53
57
57
52
55
39
30
38
29
39
50
50%
52
56
60
48
62
60
59
58
50%
57
63
67
53
53
66
53
53
58
70
57
53
57
53
73
70
44
46
70%
20%
46
59
10%
67
50
1
62
62
70%
71

FIG. 11

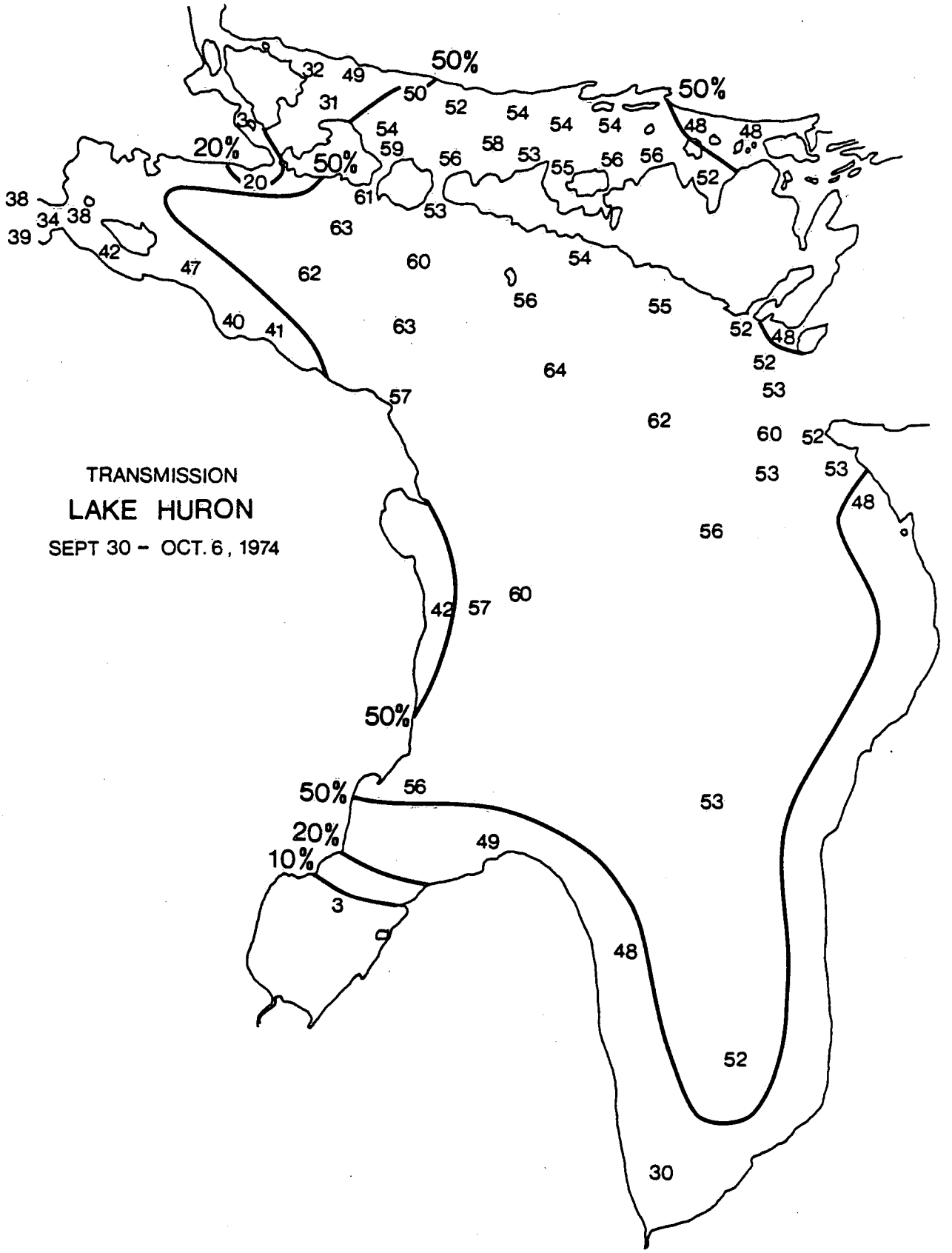
TRANSMISSION
LAKE HURON
SEPT 30 - OCT. 6, 1974
50%
50%
20%
50%
50%
50%
20%
10%
32
49
31
50
52
54
54
54
48
48
54
59
58
56
53
55
56
56
52
20
61
53
38
34
38
39
42
63
47
62
60
54
56
55
40
41
63
52
48
64
52
53
57
62
60
52
53
53
48
56
42
57
60
56
53
49
3
48
52
30

FIG. 12

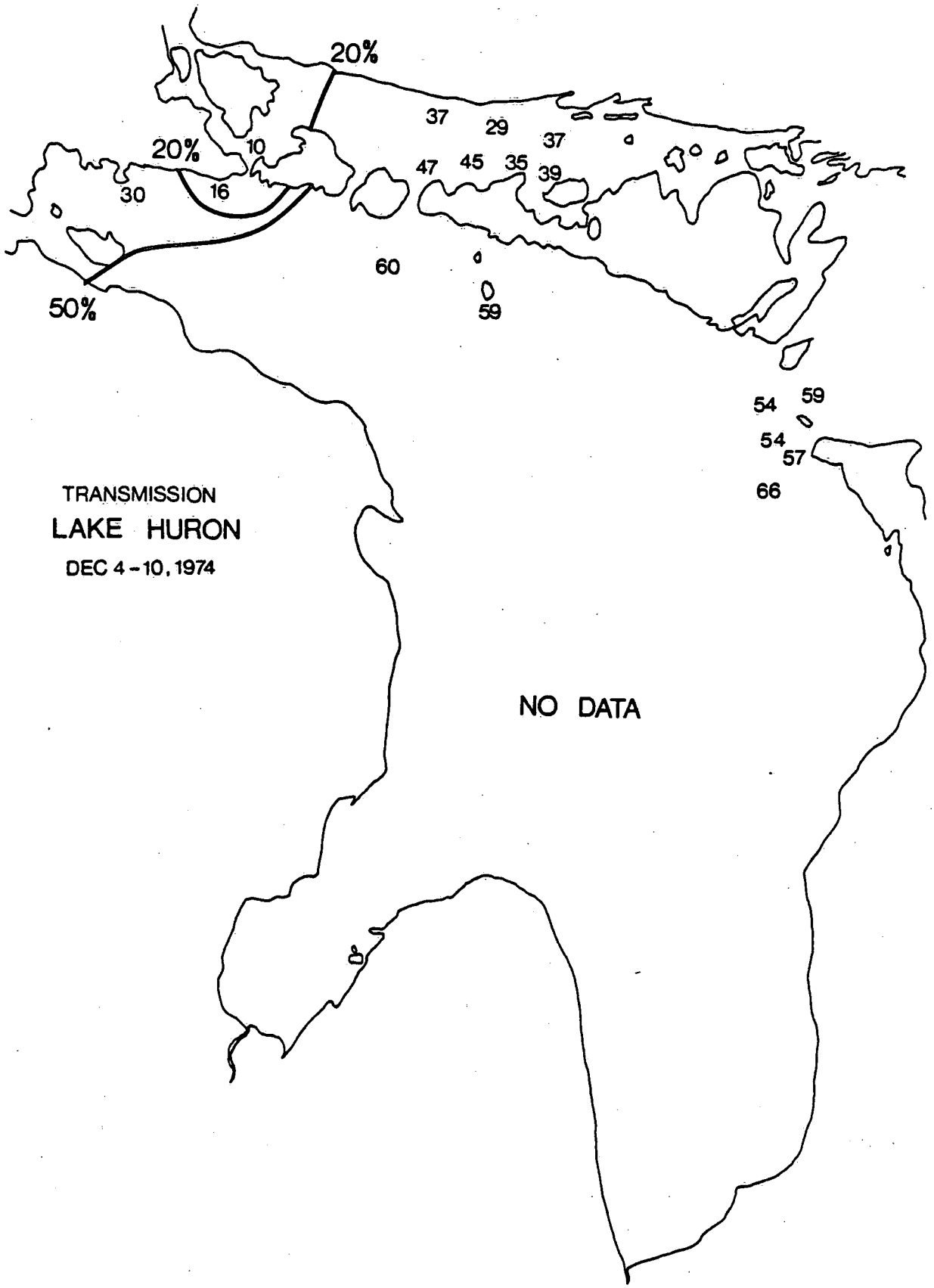
20%
37
29
37
20%
10
47
45
35
39
30
16
60
50%
59
54
59
54
57
66
TRANSMISSION
LAKE HURON
DEC 4 - 10, 1974
NO DATA

FIG. 13

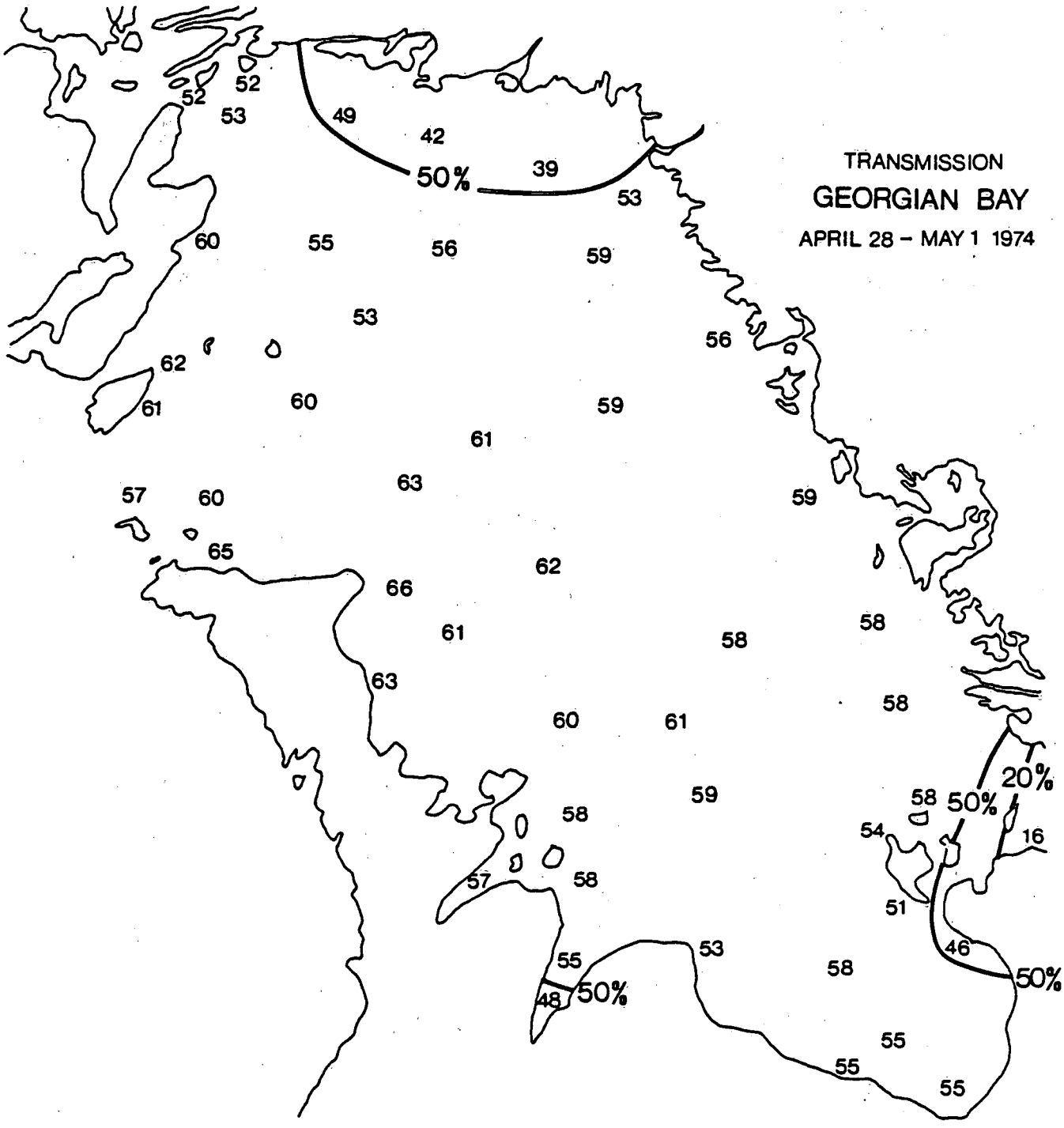
TRANSMISSION
GEORGIAN BAY
APRIL 28 – MAY 1 1974
52
52
53
49
42
50%
39
53
60
55
56
59
53
56
62
61
60
59
61
63
57
60
59
65
62
66
61
58
58
63
58
60
61
59
58
20%
58
50%
54
16
57
58
51
46
55
53
58
50%
48
55
55
55

FIG. 14

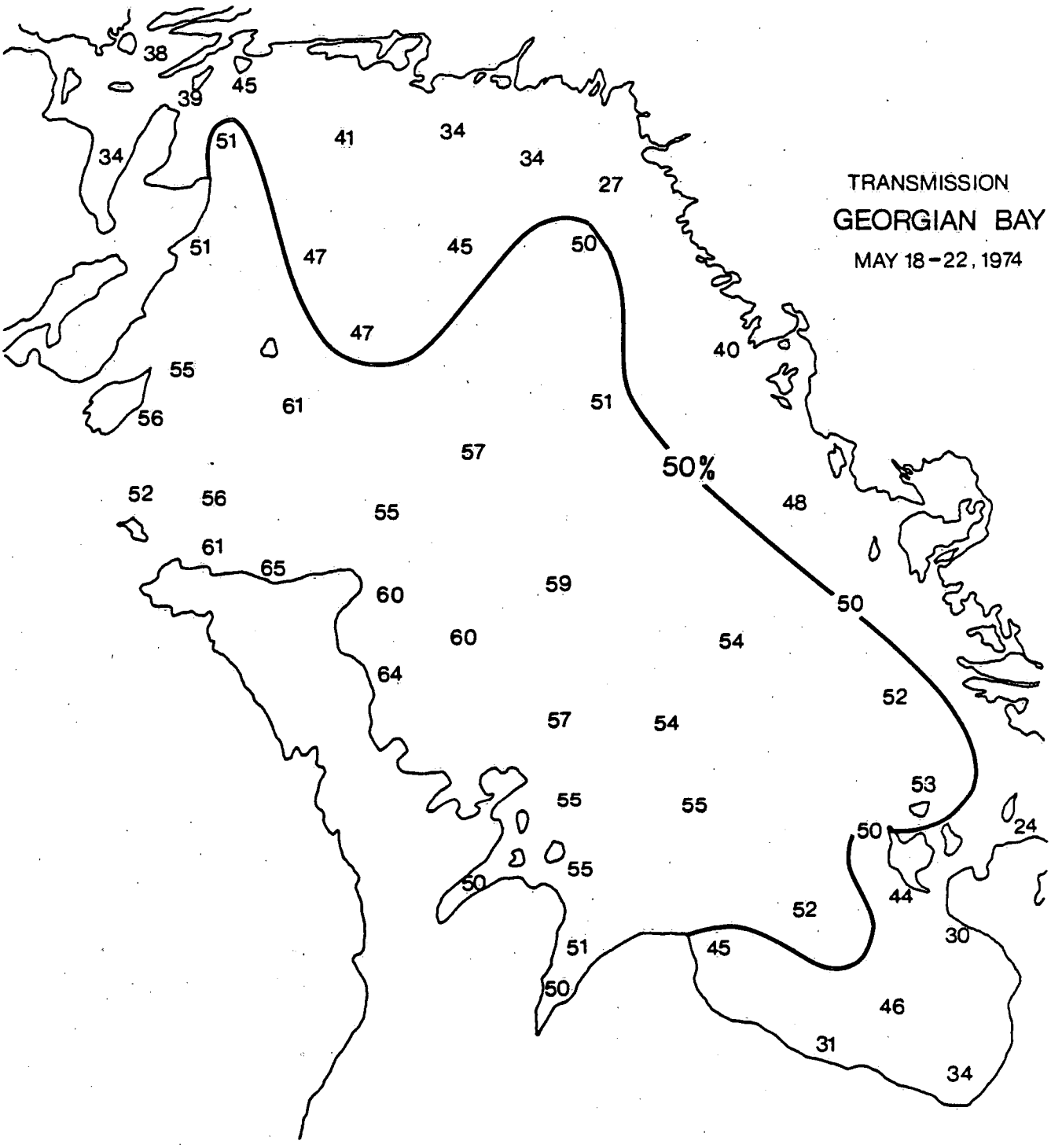
TRANSMISSION
GEORGIAN BAY
MAY 18-22, 1974
50%
38
39
45
34
51
41
34
34
27
51
47
45
50
47
40
55
56
61
51
57
52
56
55
48
61
65
60
59
50
60
54
64
52
57
54
53
55
55
50
24
55
50
44
52
30
51
45
50
46
31
34

FIG. 15

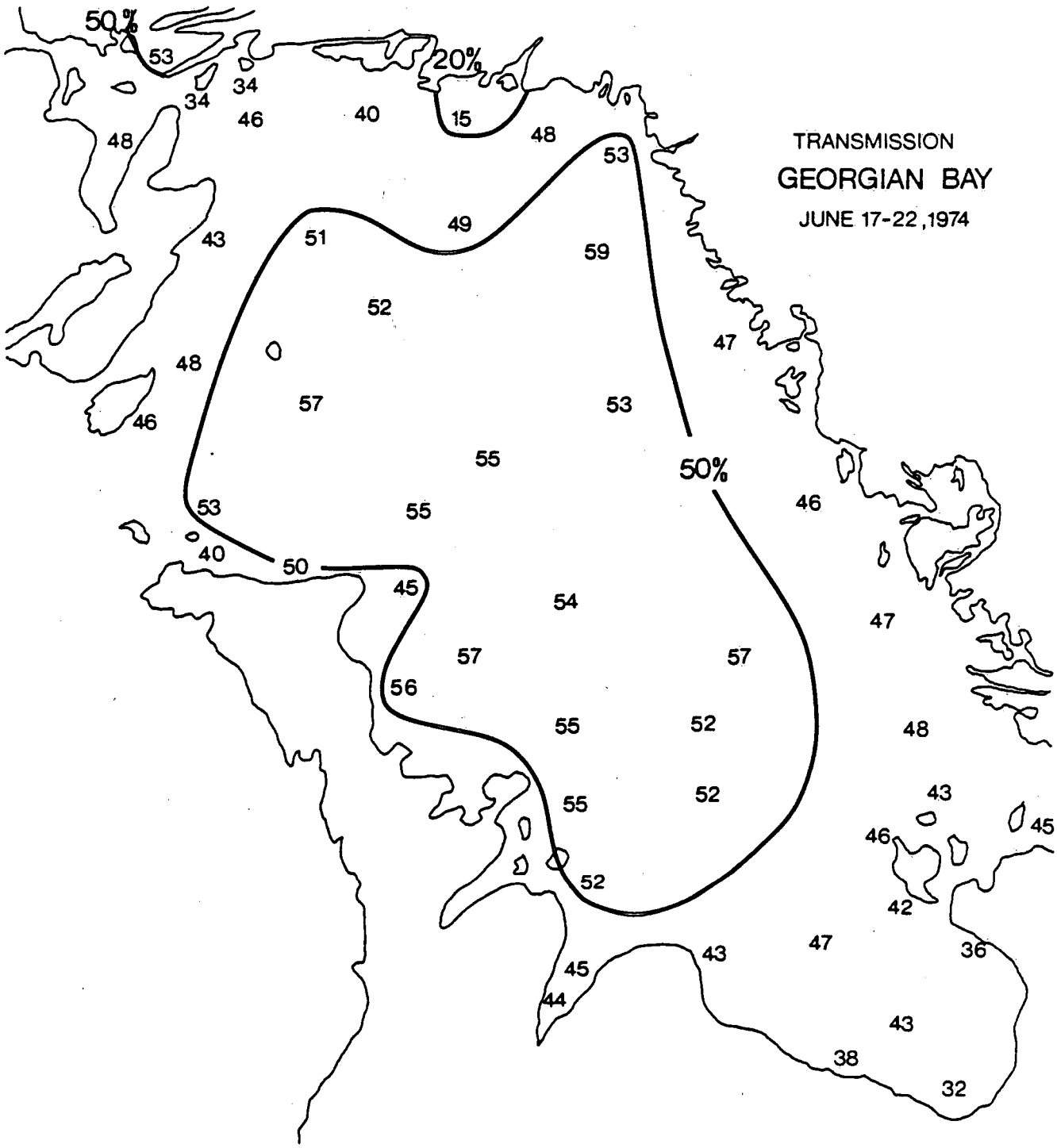
TRANSMISSION
GEORGIAN BAY
JUNE 17-22, 1974
50%
20%
50%
53
34
34
46
40
15
48
48
53
49
43
51
59
52
48
47
57
53
46
55
50%
53
55
46
40
50
45
54
47
57
57
56
55
52
48
55
52
43
46
45
52
42
47
36
45
43
44
43
38
32

FIG. 16

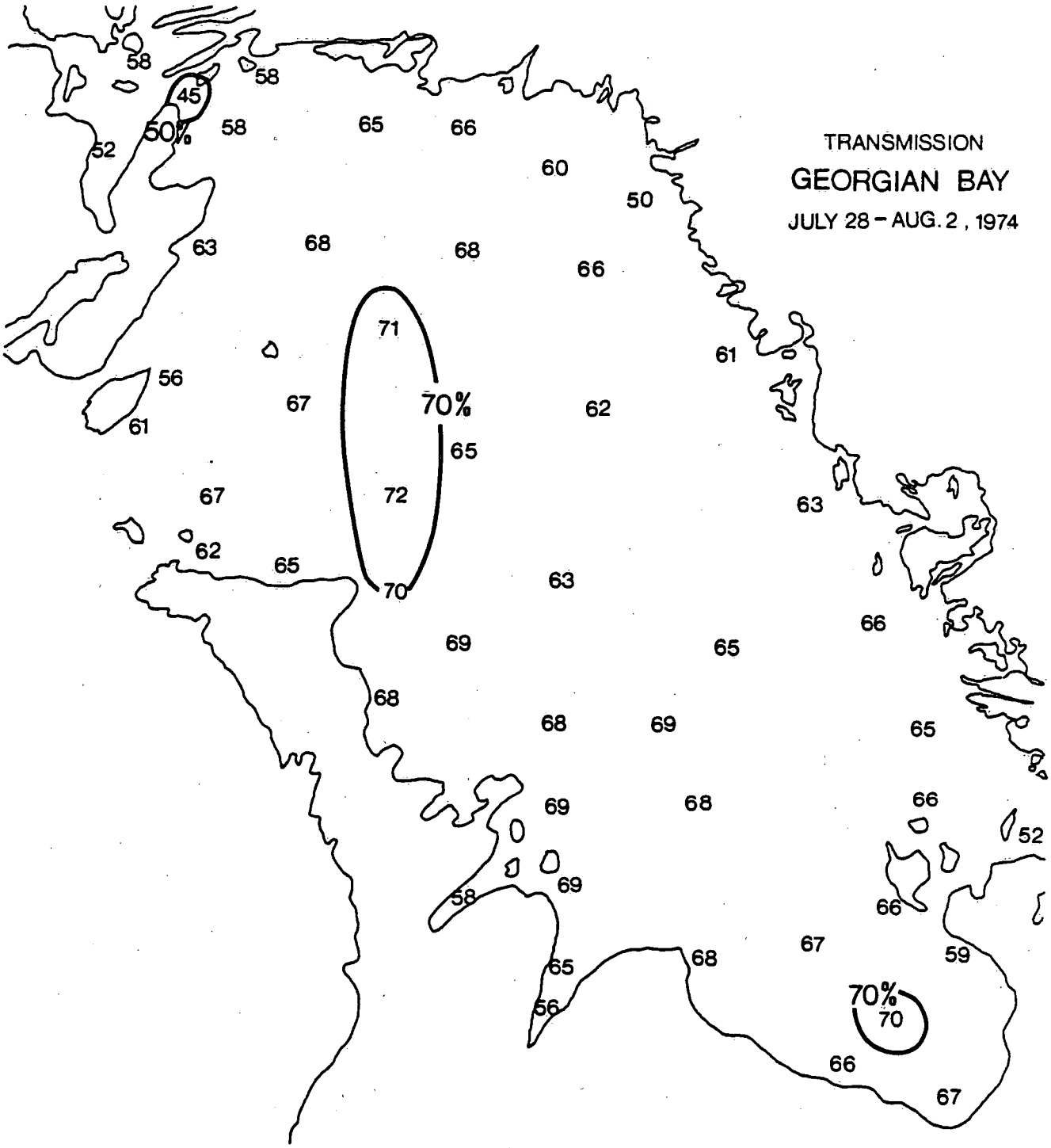
TRANSMISSION
GEORGIAN BAY
JULY 28 - AUG. 2, 1974
58
58
45
50%
58
65
66
52
60
50
63
68
68
66
71
61
56
67
70%
62
61
65
67
72
63
62
65
70
63
66
69
65
68
68
69
65
69
68
66
52
58
69
66
67
59
65
68
56
70%
70
66
67

FIG. 17

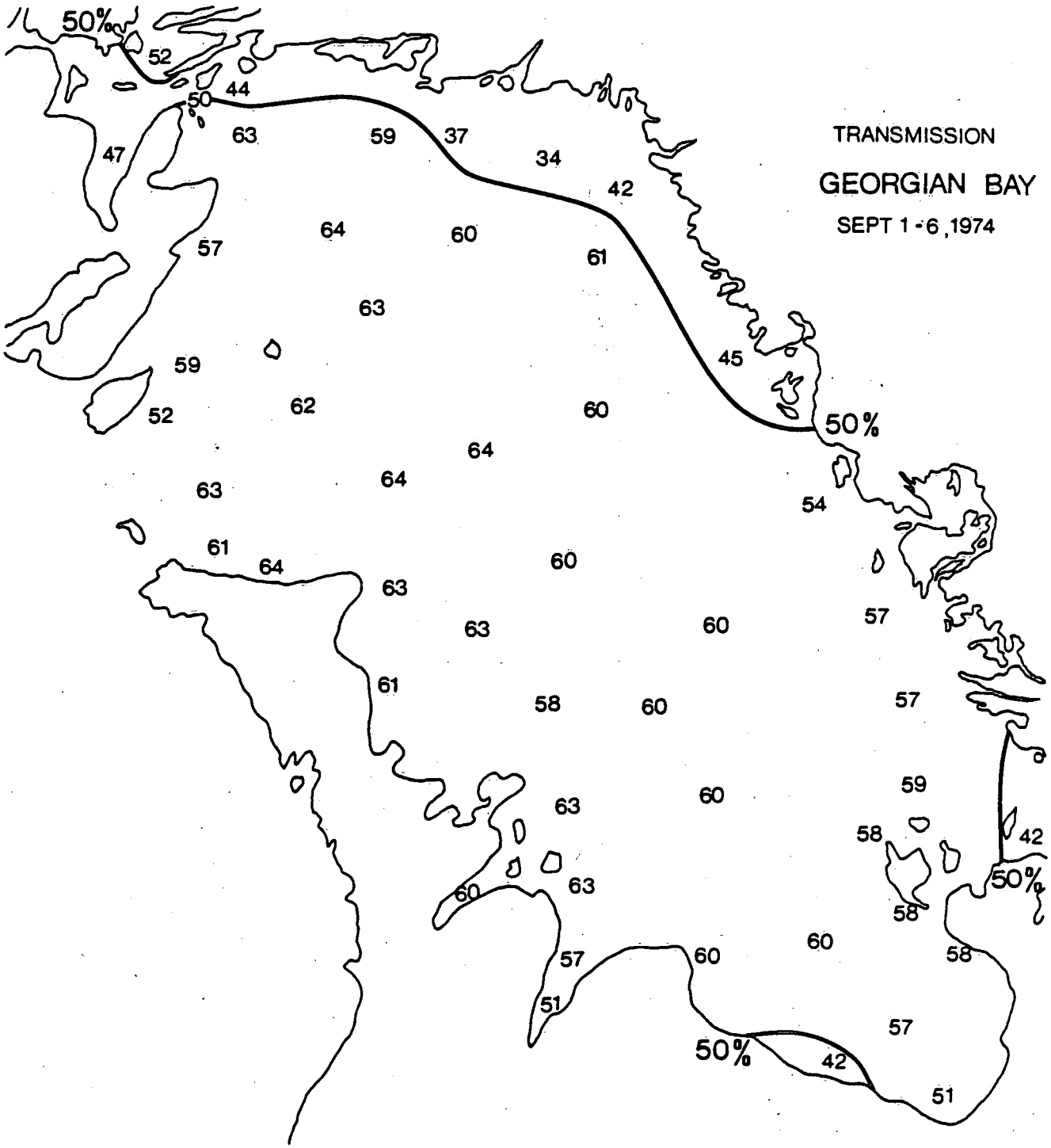
TRANSMISSION
GEORGIAN BAY
SEPT 1-6, 1974
50%
52
44
50
63
59
37
34
42
47
57
64
60
61
63
59
45
52
62
60
50%
64
63
64
54
61
64
60
63
57
63
60
61
58
60
57
59
63
60
58
42
63
60
50%
58
57
60
60
58
51
57
50%
42
51

FIG. 18

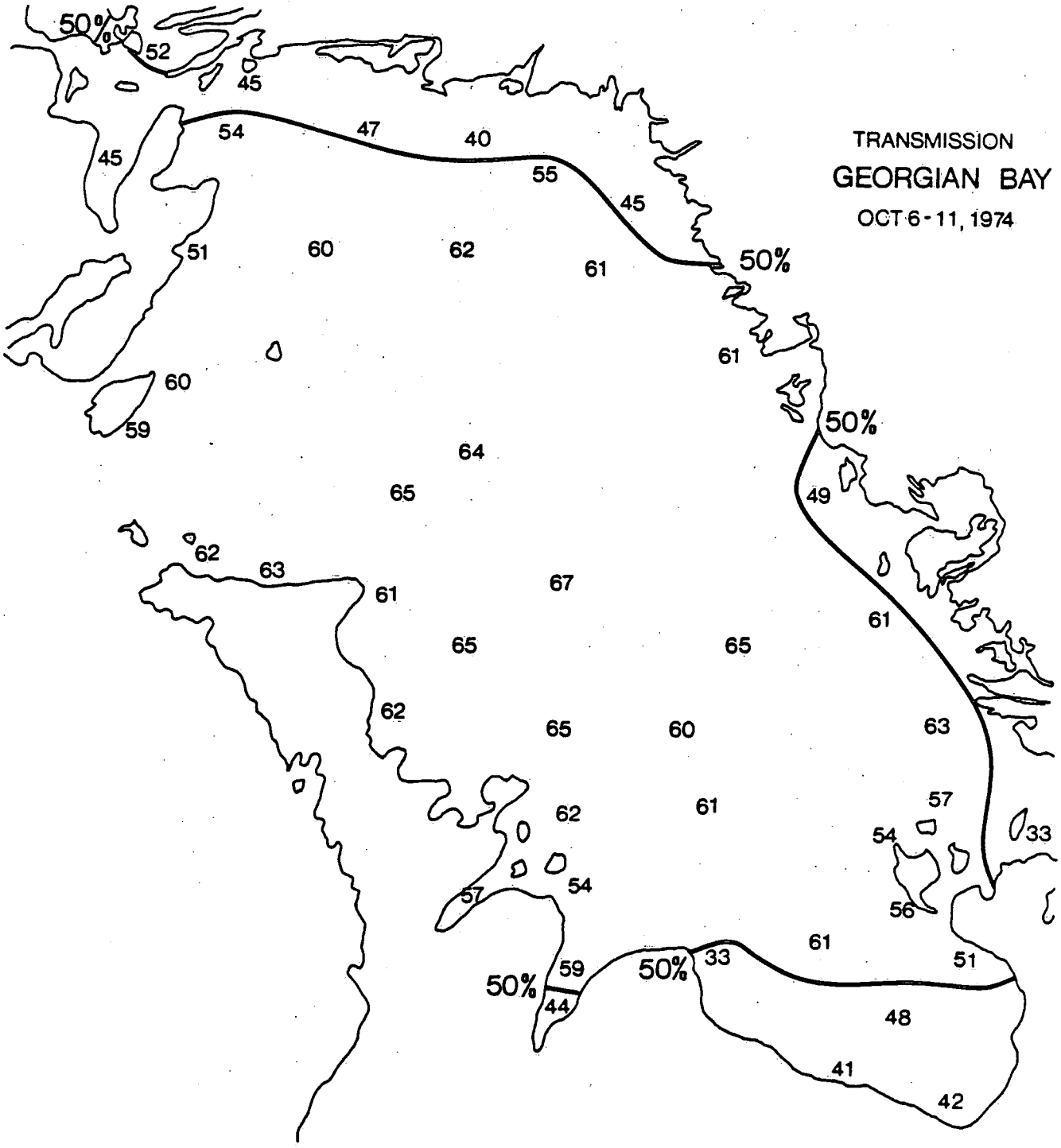
TRANSMISSION
GEORGIAN BAY
OCT 6 - 11, 1974
50%
52
45
54
47
40
55
45
45
51
60
62
61
50%
61
60
59
50%
64
65
49
62
63
61
67
61
65
65
62
65
60
63
62
61
57
54
33
57
54
56
61
50%
59
50%
33
51
44
48
41
42

FIG. 19

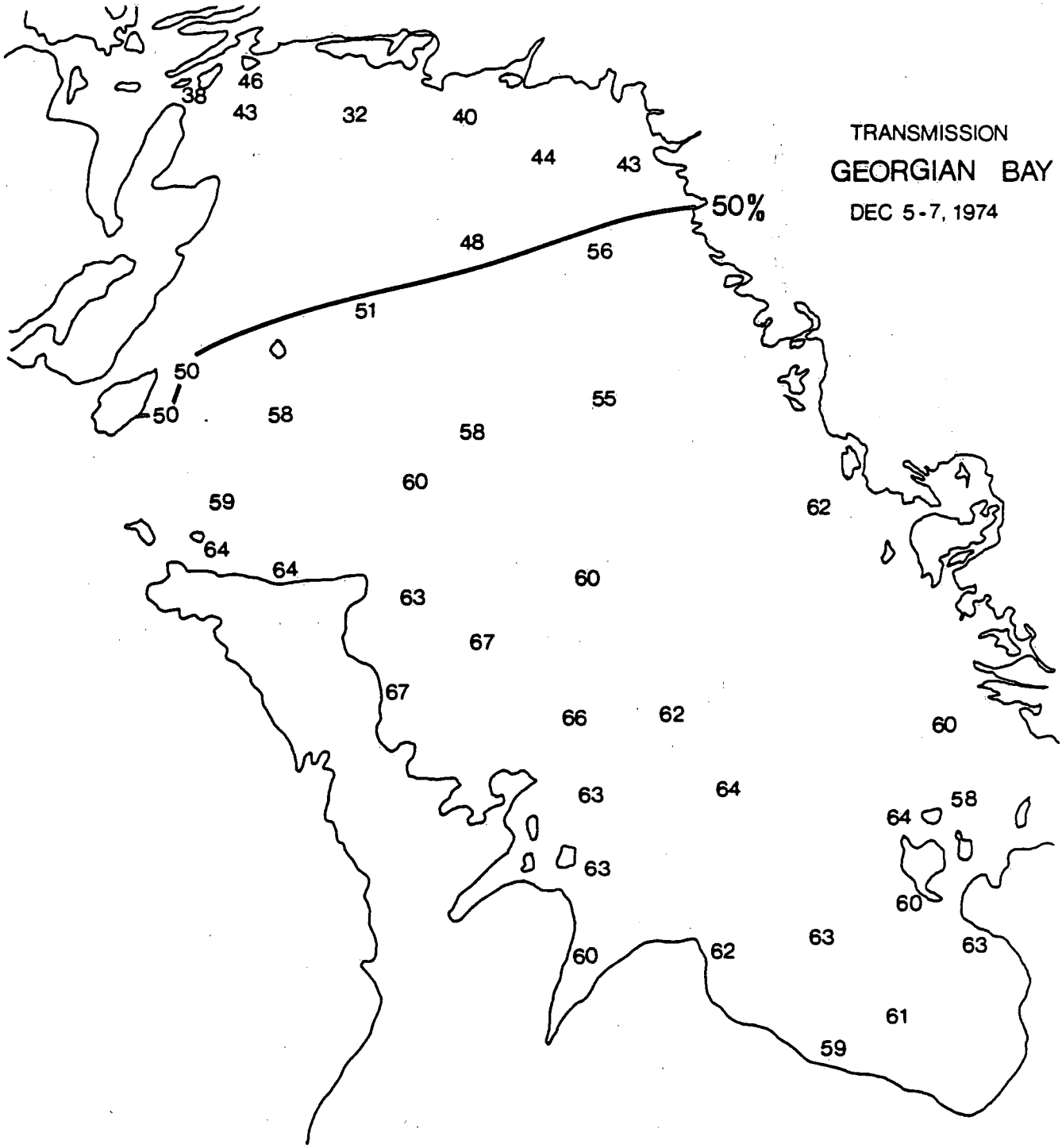
TRANSMISSION
GEORGIAN BAY
DEC 5-7, 1974
50%
38
46
43
32
40
44
43
48
56
51
50
50
58
55
58
60
59
62
64
64
60
63
67
67
66
62
60
63
64
64
58
63
60
63
60
62
63
61
59

FIG. 20

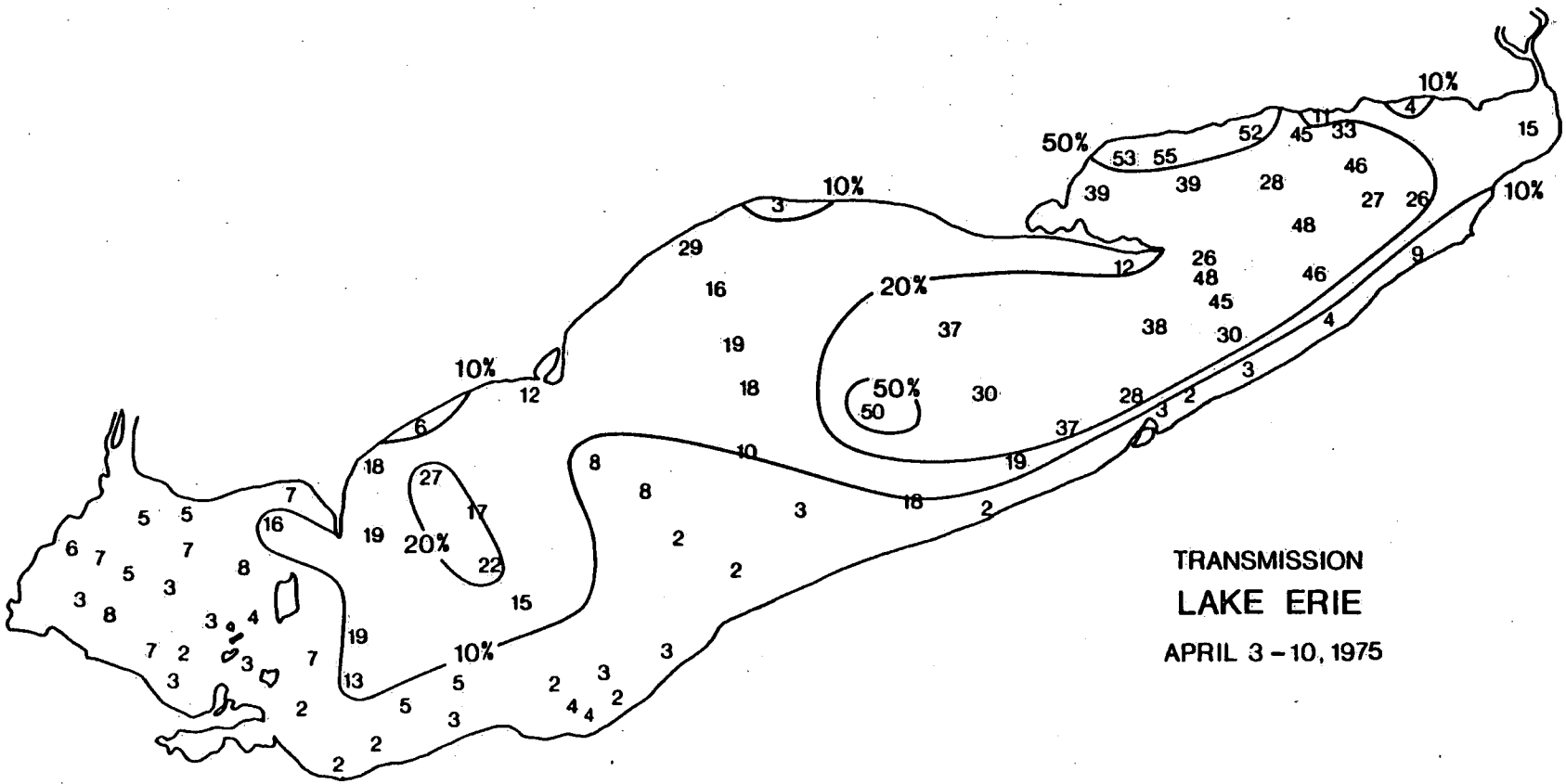

FIG. 21

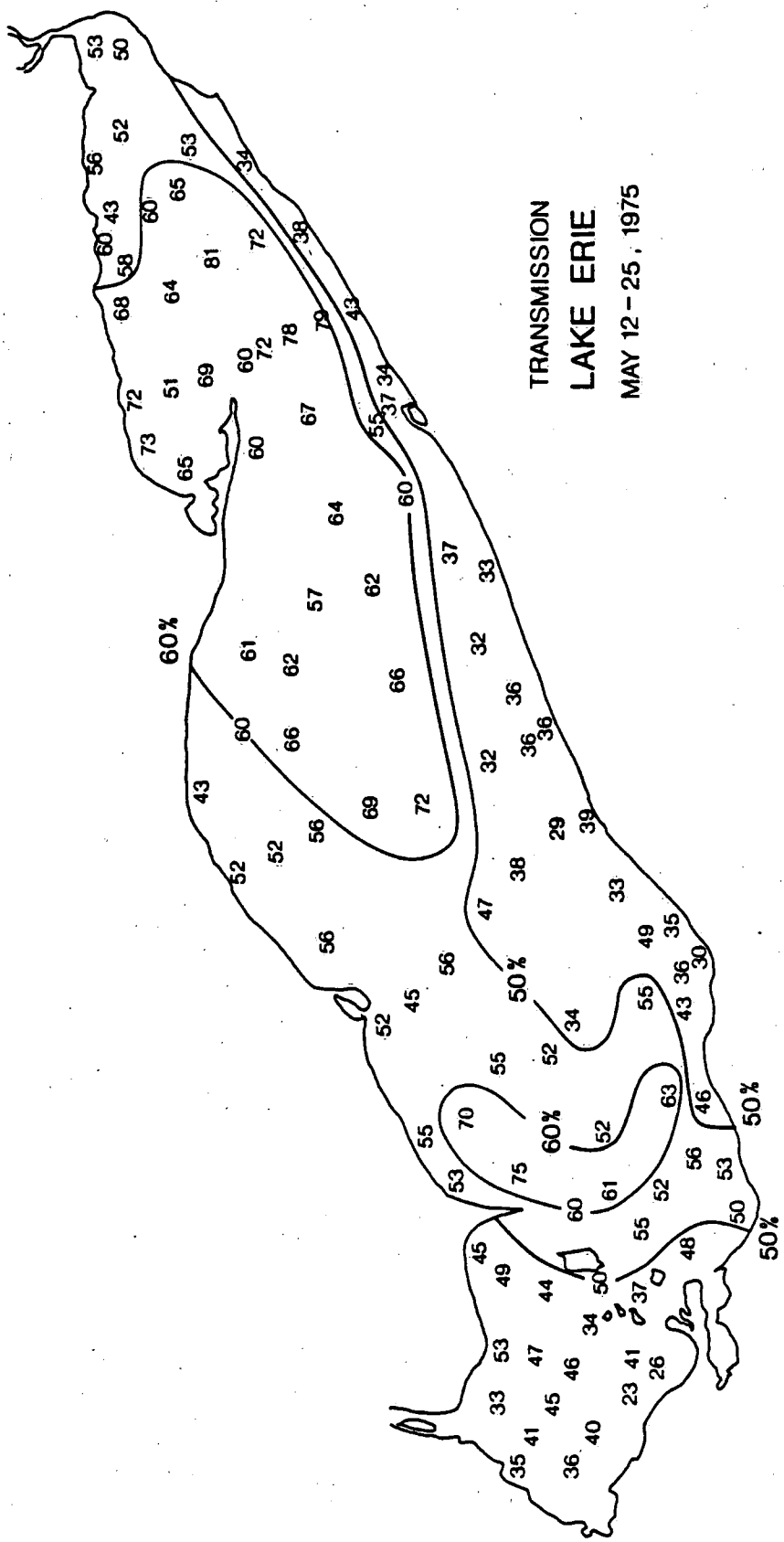

FIG. 22

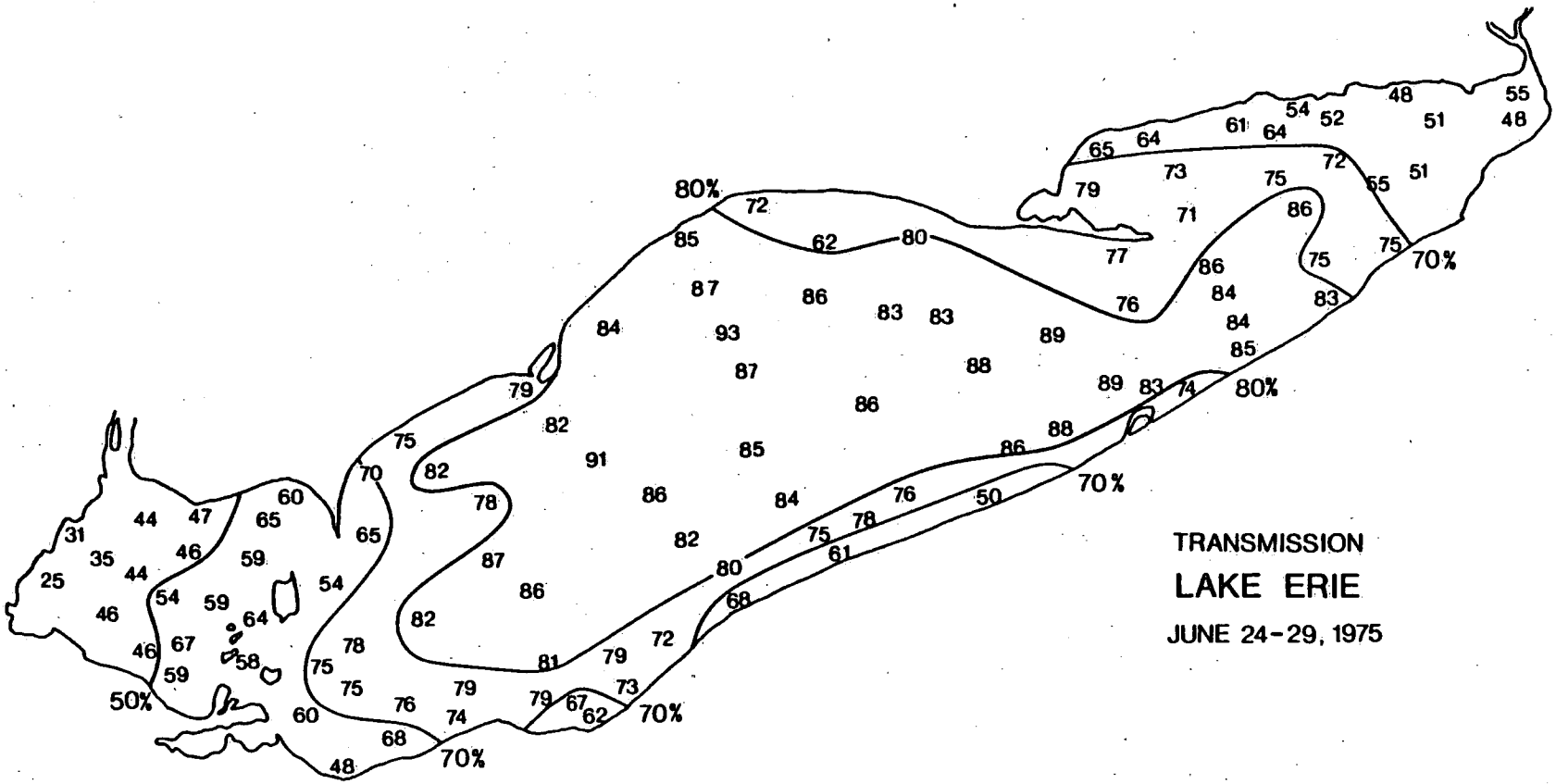

FIG. 23

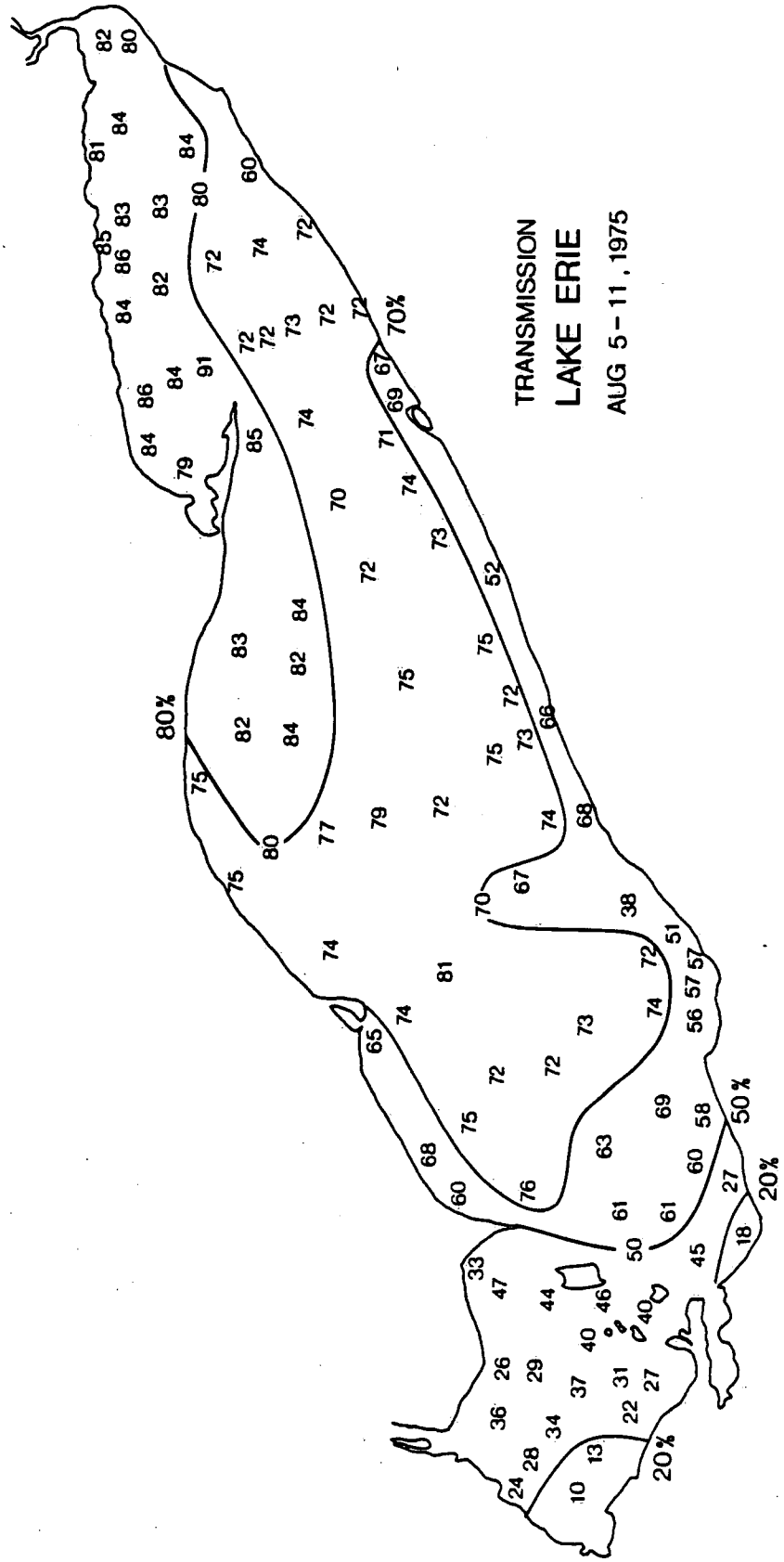

FIG. 24

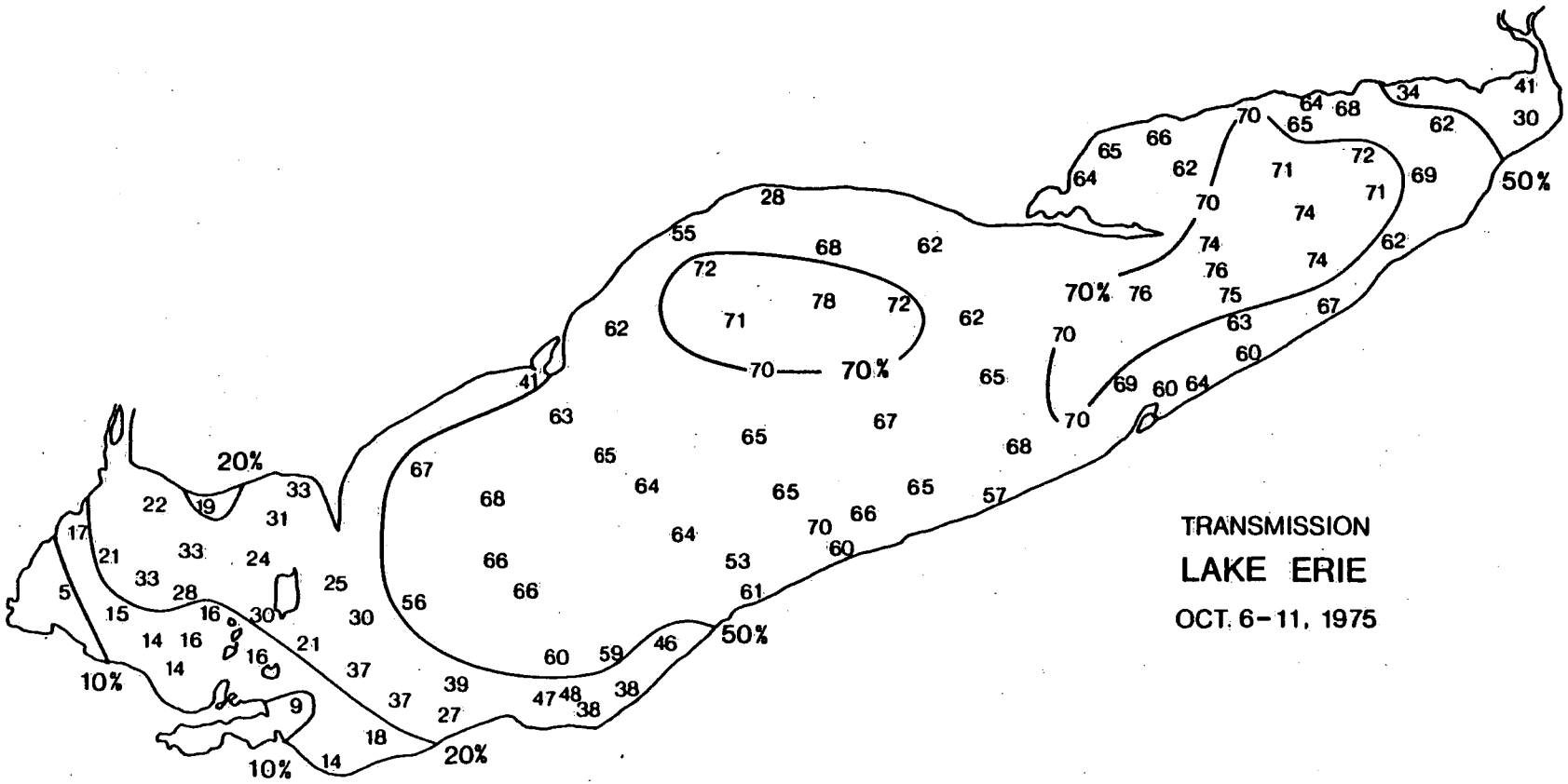

FIG. 25

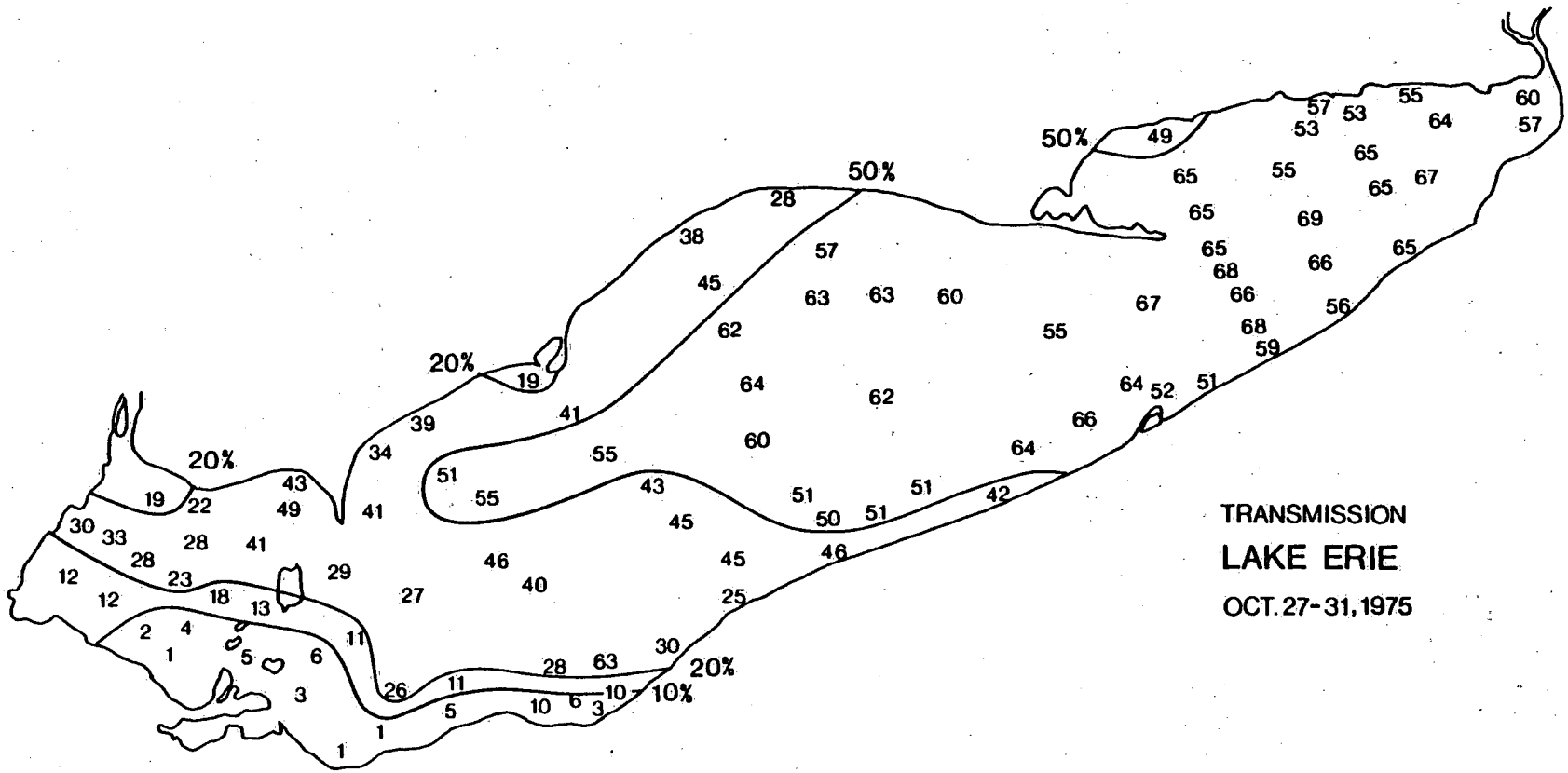

FIG. 26

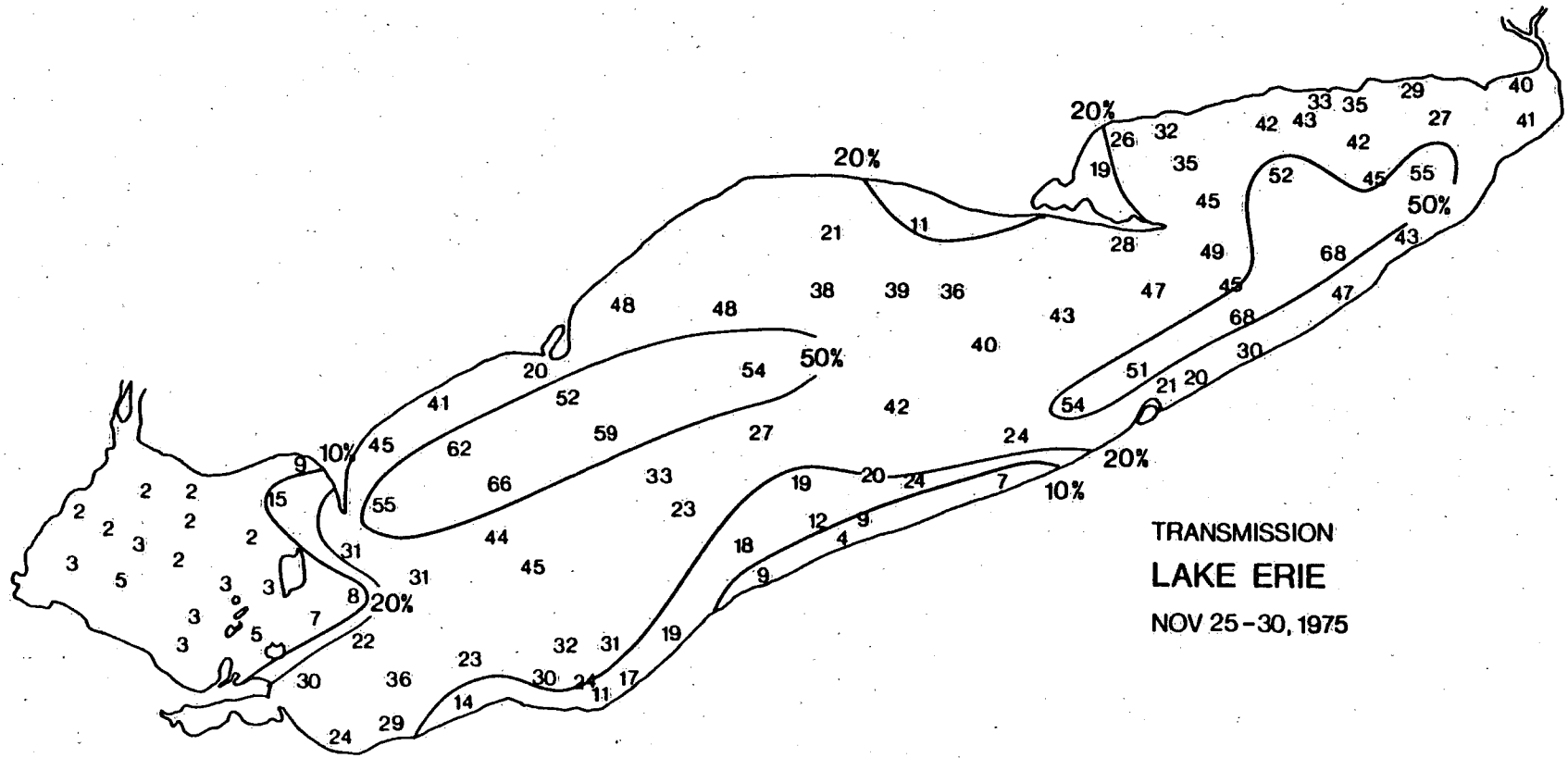

FIG. 27

1 of 1

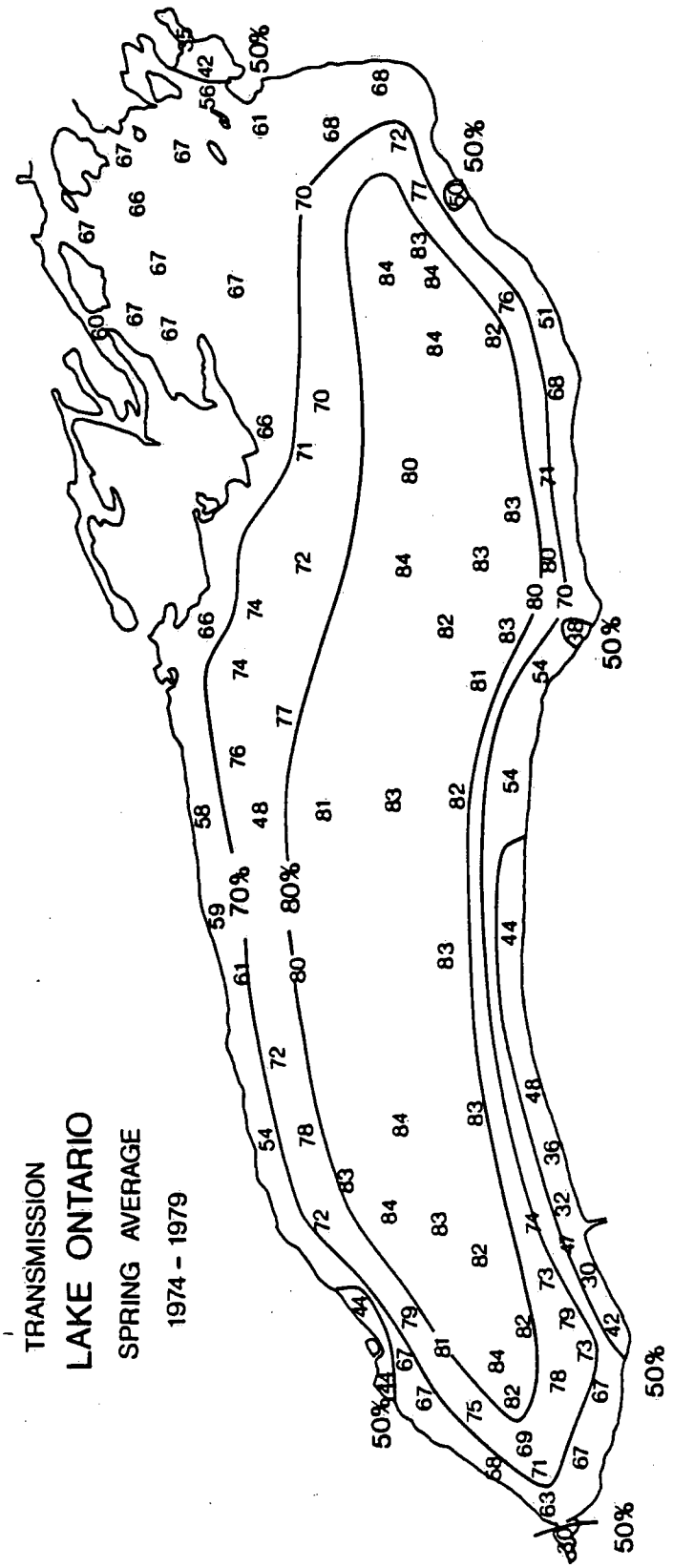
TRANSMISSION
LAKE ONTARIO
SPRING AVERAGE
1974 - 1979
50%
70%
80%

FIG. 28

TRANSMISSION

LAKE ONTARIO

SUMMER AVERAGE

1974 - 1979

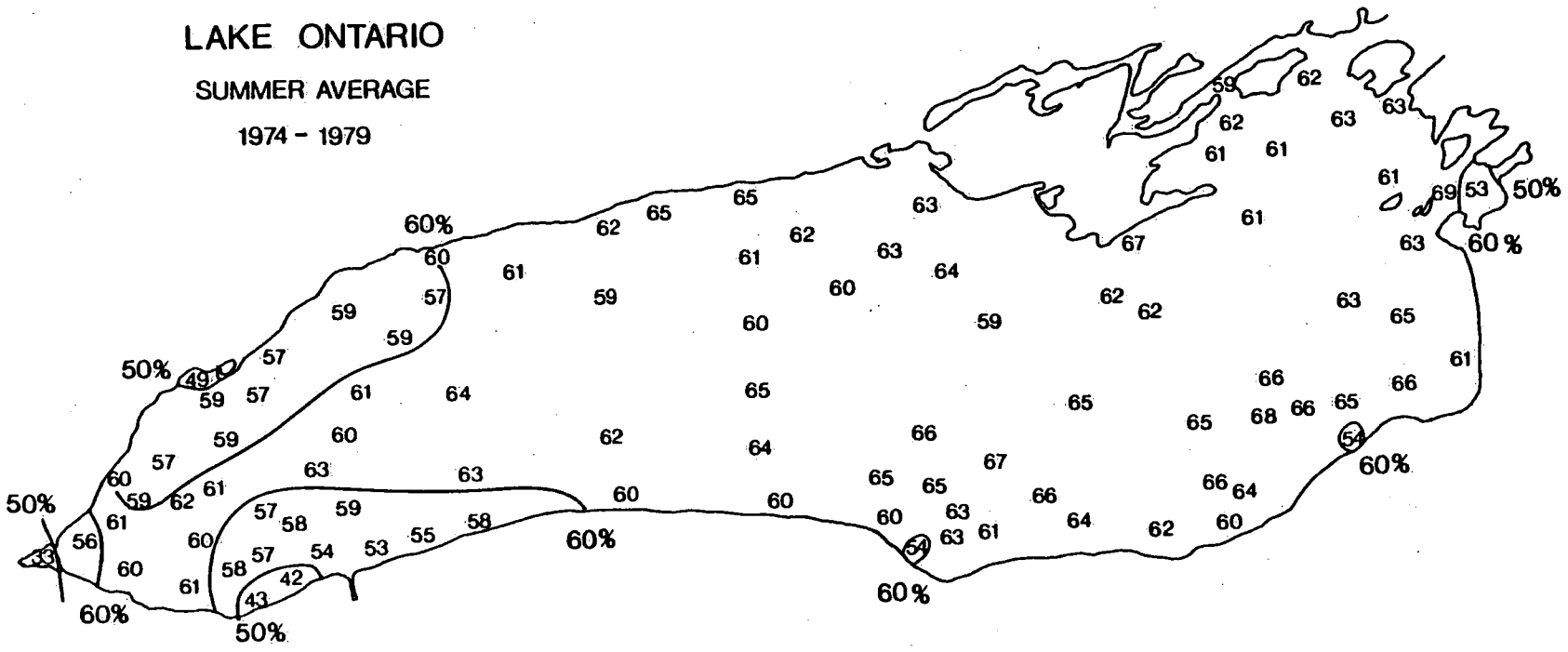

FIG. 29

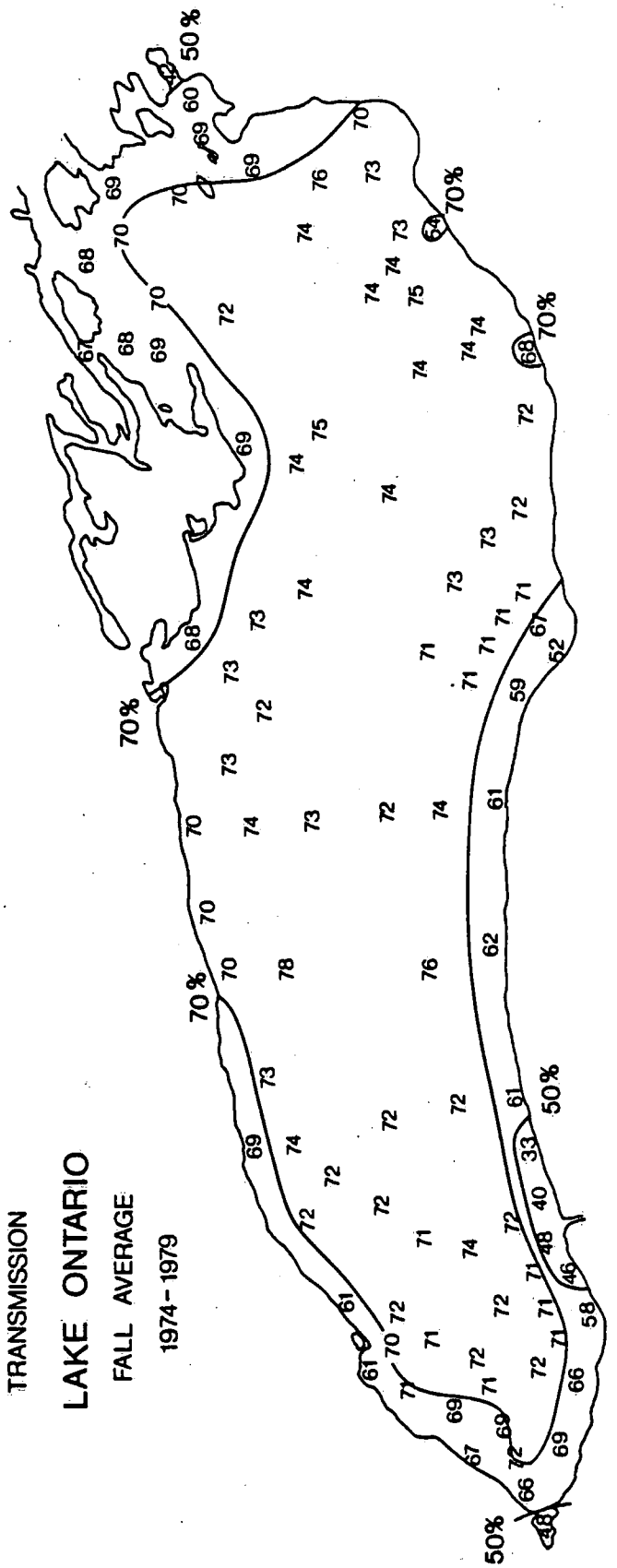
TRANSMISSION
LAKE ONTARIO
FALL AVERAGE
1974 - 1979
50%
70%
70%
70%
50%
50%

FIG. 30

TRANSMISSION

LAKE ONTARIO

WINTER AVERAGE
1974-1979

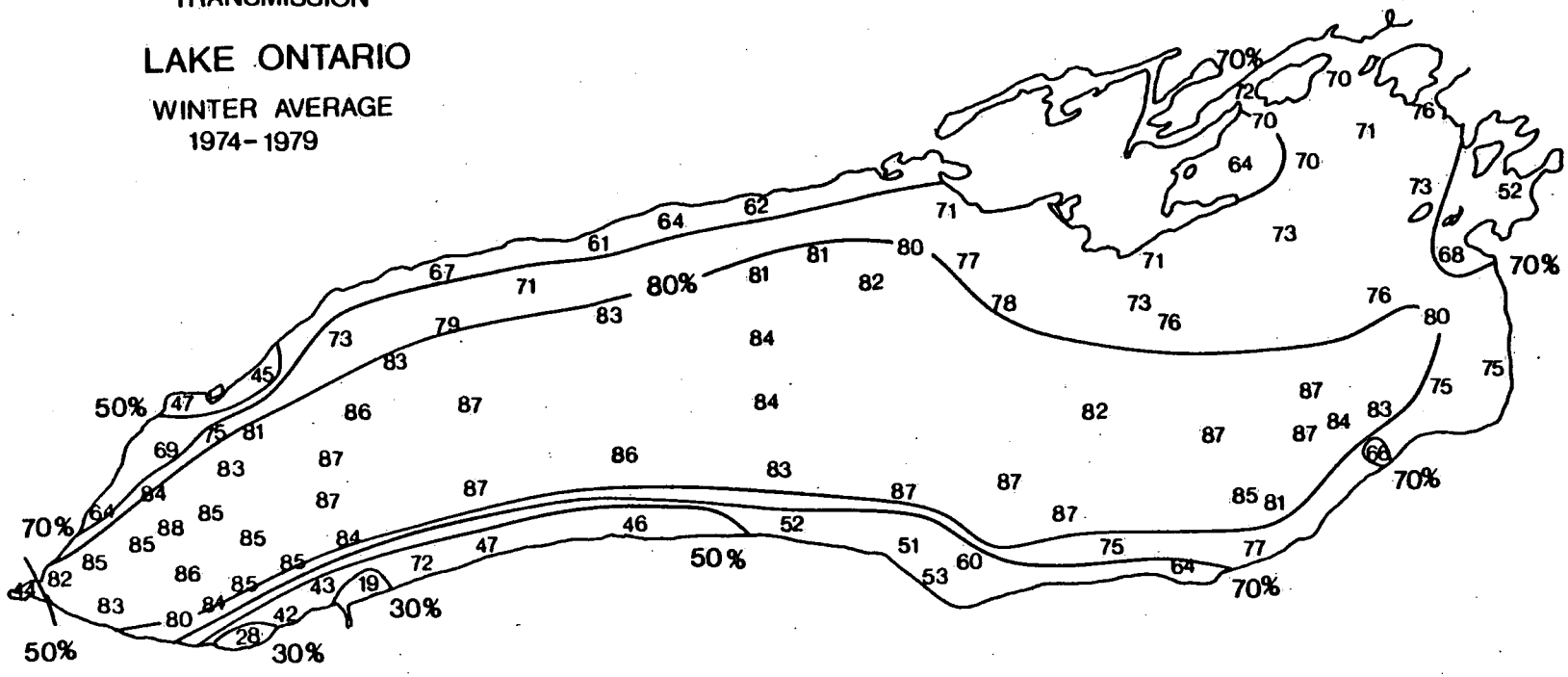

FIG. 31

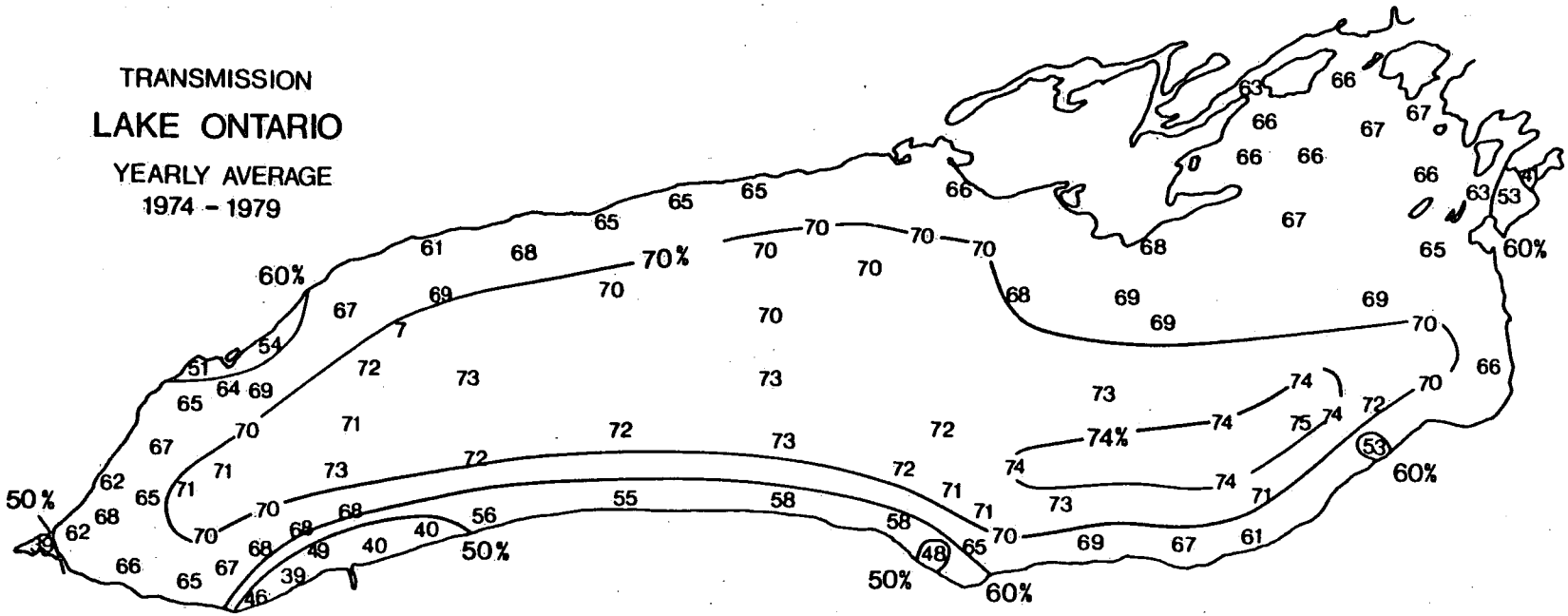
TRANSMISSION
LAKE ONTARIO
YEARLY AVERAGE
1974 - 1979
60%
70%
50%
50%
50%
60%
60%
74%

FIG. 32

PHOTIC DEPTH

Figures 33-41 illustrate contours of the calculated photic depths (defined as the depth of the 1% subsurface irradiance level). The optical surface transmission data were combined for periods shown in Table 2 to provide a "summer" value of photic depth for Lakes Superior, Huron and Erie and Georgian Bay. The wealth of Lake Ontario data once again enabled a more statistically rigorous seasonal analysis for that lake. Since the optical surface transmission data were utilized in the determination of photic depth, there is an understandable similarity between the surface transmission contours and the photic depth contours for each body of water.

Salient features of the photic depth contours of Figures 33-41 include:

a) For the summer period, the Upper Lakes (including Georgian Bay) are characterized by consistently large values of photic depths (>20 metres with values >30 metres not uncommon).

b) For the summer period, the Lower Lakes are characterized by consistently smaller values of photic depths (<20 metres with values <15 metres not uncommon).

c) In general, the areas of low transmission in each lake (as listed in the previous section) are reflected as areas of small photic depths, while the areas of high transmission in each lake (as listed in the previous section) are reflected as areas of large photic depths.

d) The "onion skin" pattern in the photic depth contours of Lake Ontario which is so distinctly prominent in spring and winter (and the yearly average shown in Figure 41) is very indistinct in the fall and totally absent in the summer during which time the entirety of Lake Ontario is characterized by photic depths of ~11-14 metres (see Figure 38).

TABLE 2

Figure	Lake	Date
33	Superior	June-Oct., 1973
34	Huron	May-Oct., 1974
35	Georgian Bay	May-Oct., 1974
36	Erie	May-Oct., 1975
37	Ontario	Mar-May, 1974-79
38	Ontario	June-Aug, 1974-79
39	Ontario	Sept.-Nov., 1974-79
40	Ontario	Dec., Mar., 1974-79
41	Ontario	Mar.- Dec., 1974-79

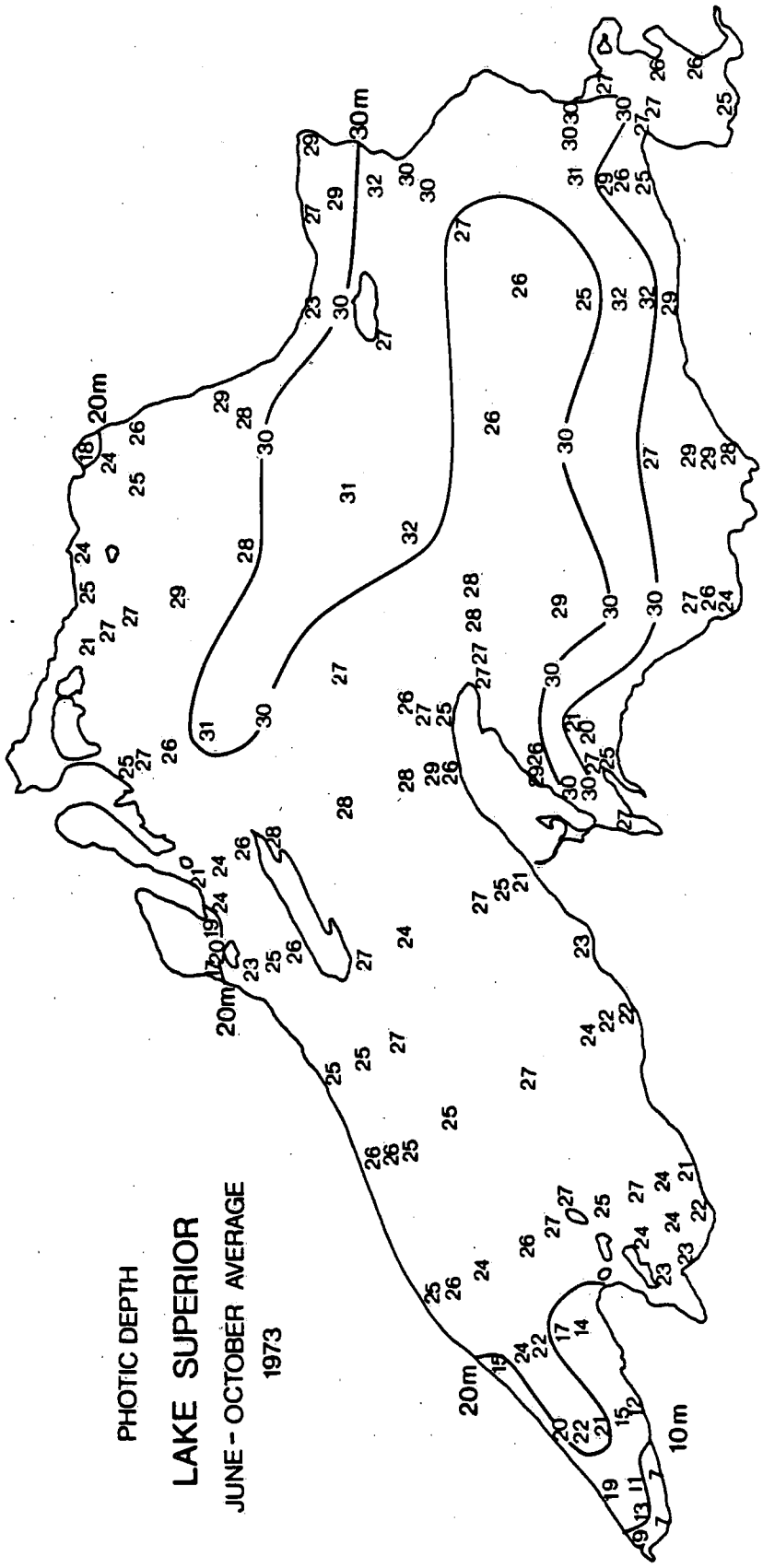
PHOTIC DEPTH
LAKE SUPERIOR
JUNE - OCTOBER AVERAGE
1973
20m
30m
20m
20m
10m

FIG. 33

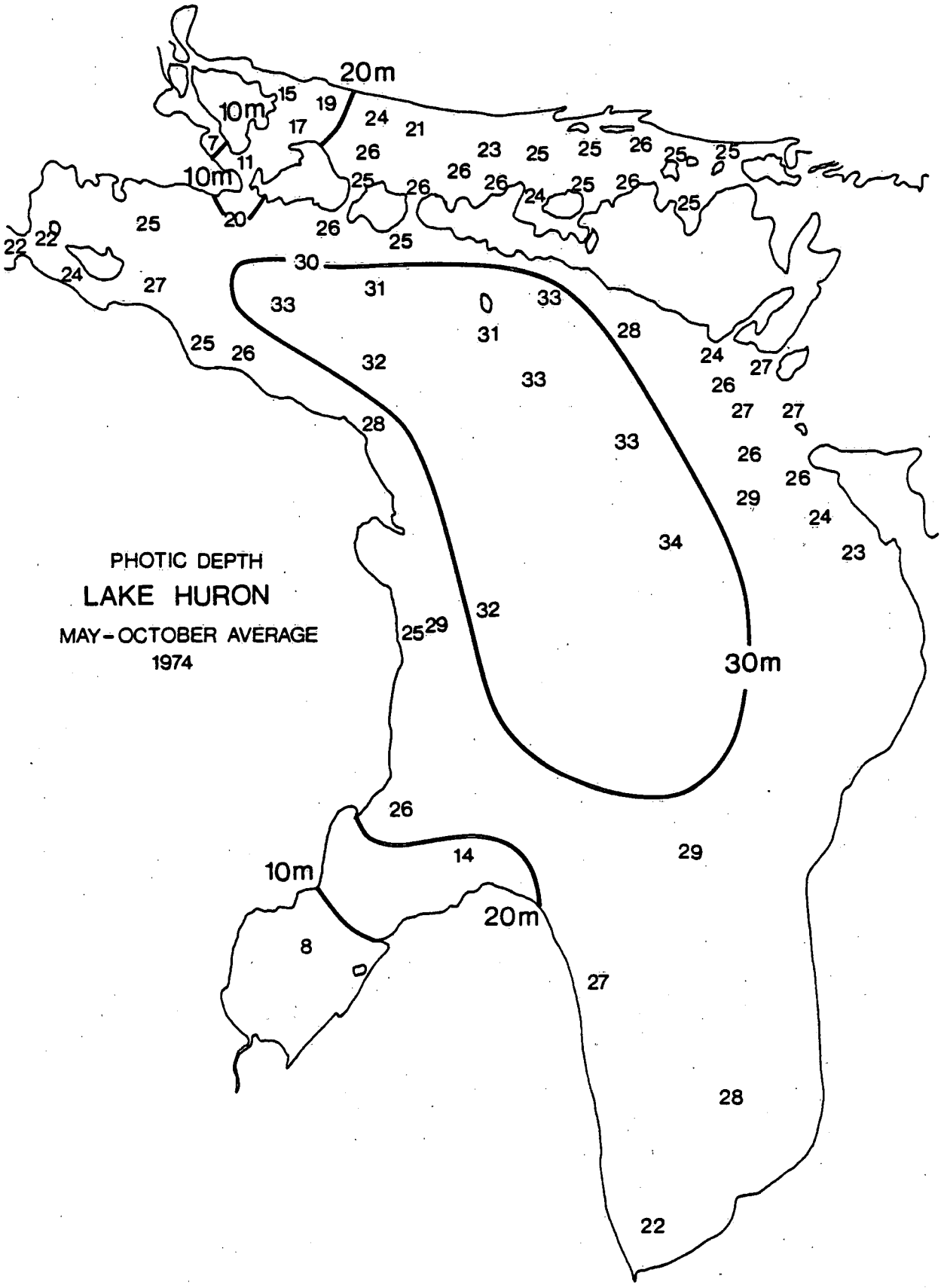
20m
10m
10m
30m
10m
20m
PHOTIC DEPTH
LAKE HURON
MAY-OCTOBER AVERAGE
1974

FIG. 34

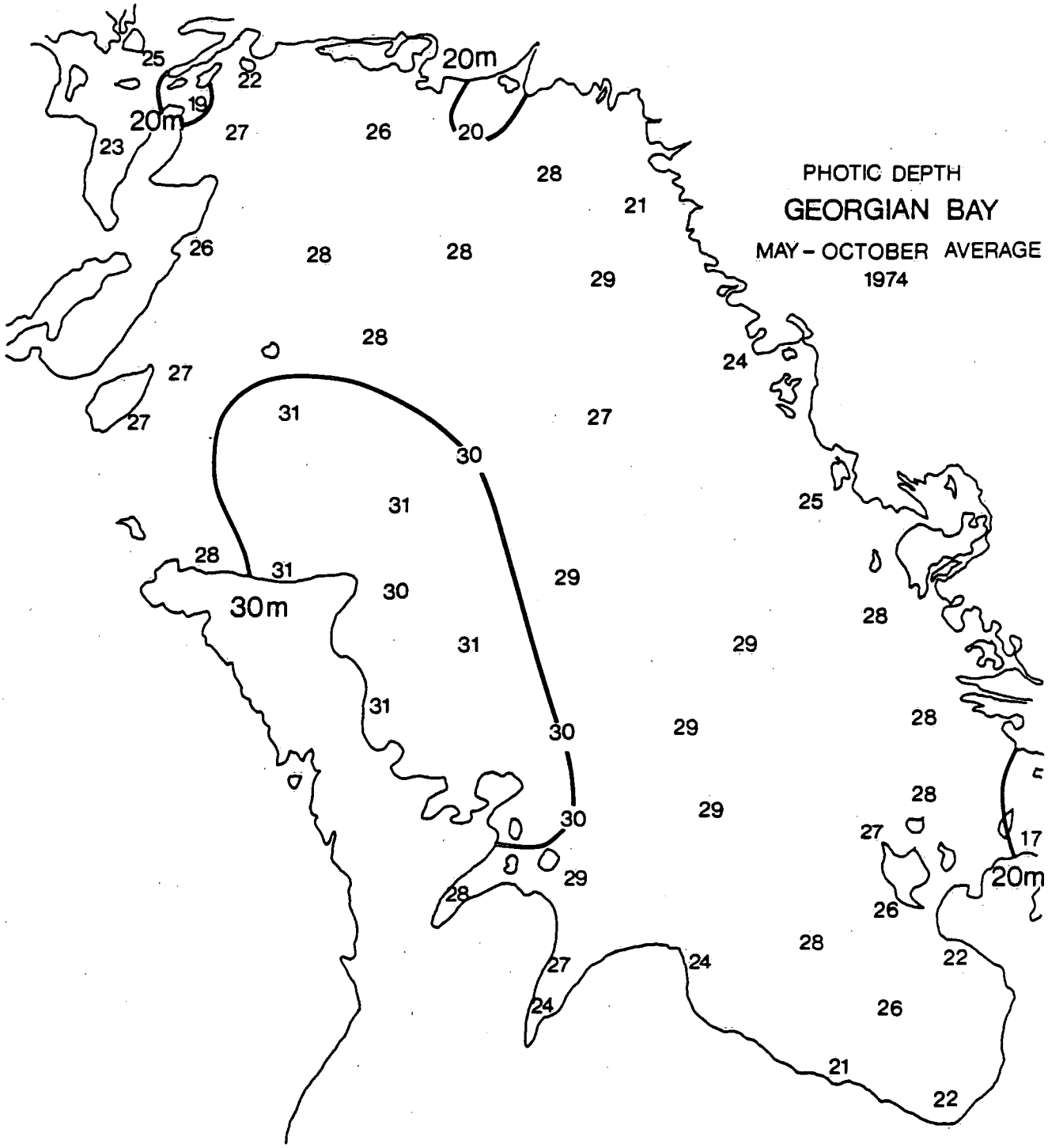
PHOTIC DEPTH
GEORGIAN BAY
MAY - OCTOBER AVERAGE
1974
20m
30m
25
22
19
20m
27
26
20
23
28
21
26
28
28
29
28
24
27
27
31
27
30
31
25
28
31
30m
30
29
31
29
28
31
30
29
28
30
29
28
29
27
17
20m
26
28
27
24
22
24
26
21
22

FIG. 35

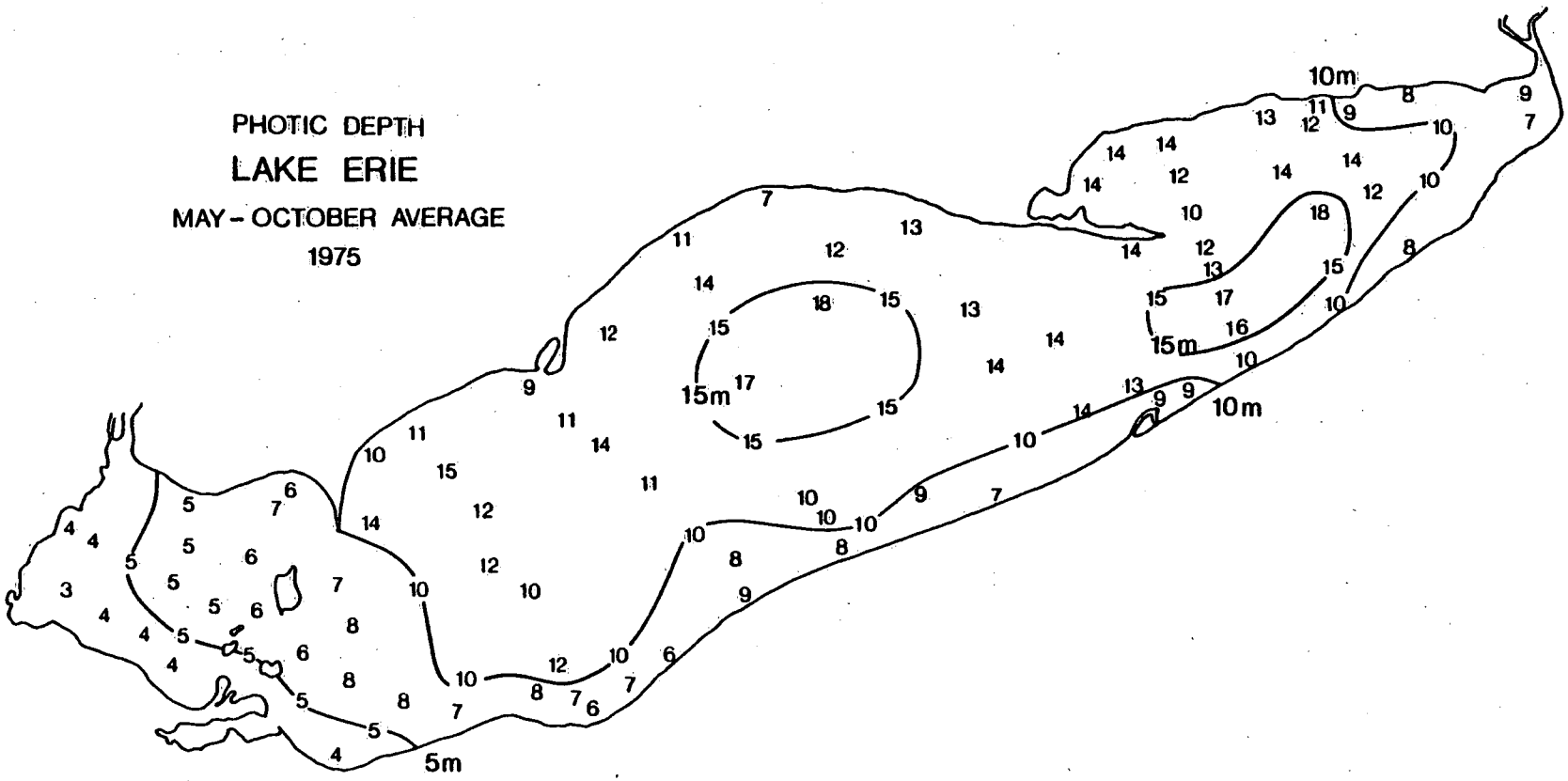
PHOTIC DEPTH
LAKE ERIE
MAY - OCTOBER AVERAGE
1975
10m
15m
15m
10m
5m

FIG. 36

PHOTIC DEPTH

LAKE ONTARIO

SPRING AVERAGE
1974 - 1979

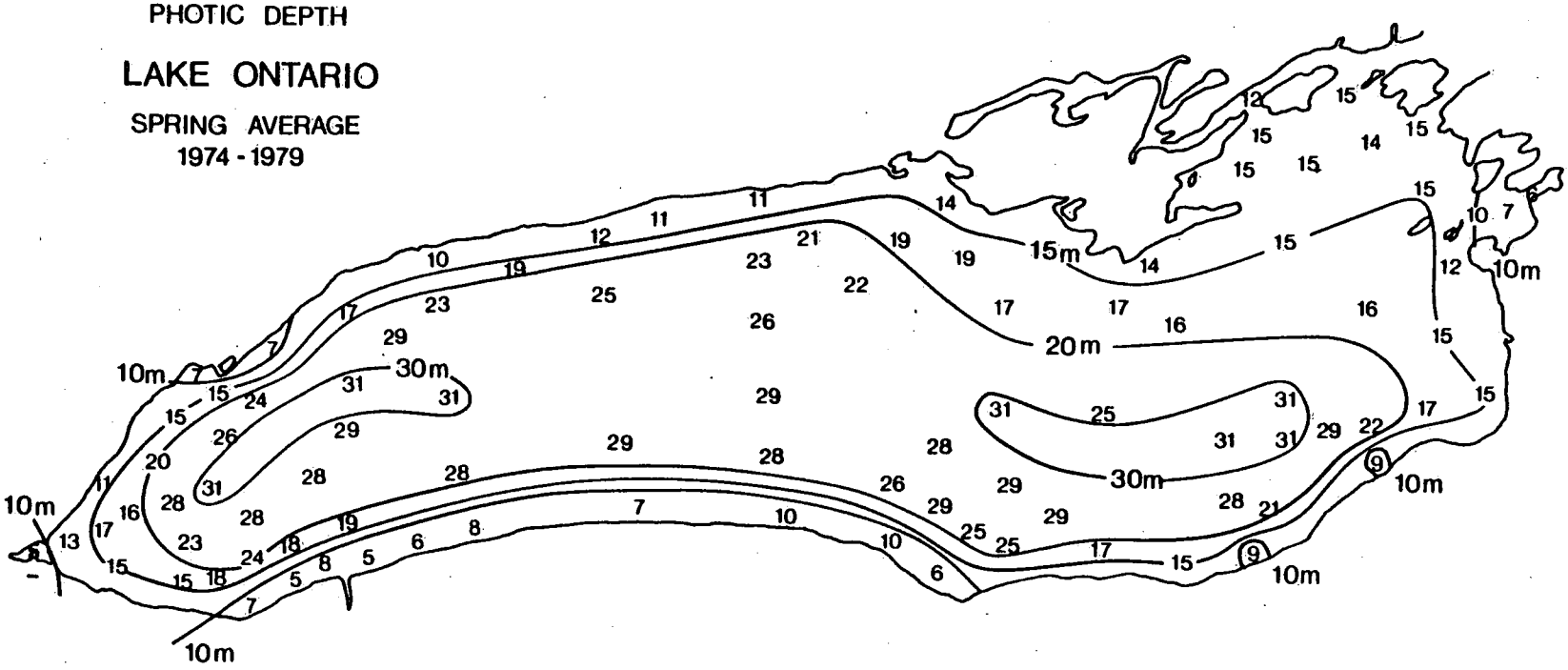

FIG. 37

PHOTIC DEPTH

LAKE ONTARIO

SUMMER AVERAGE

1974 - 1979

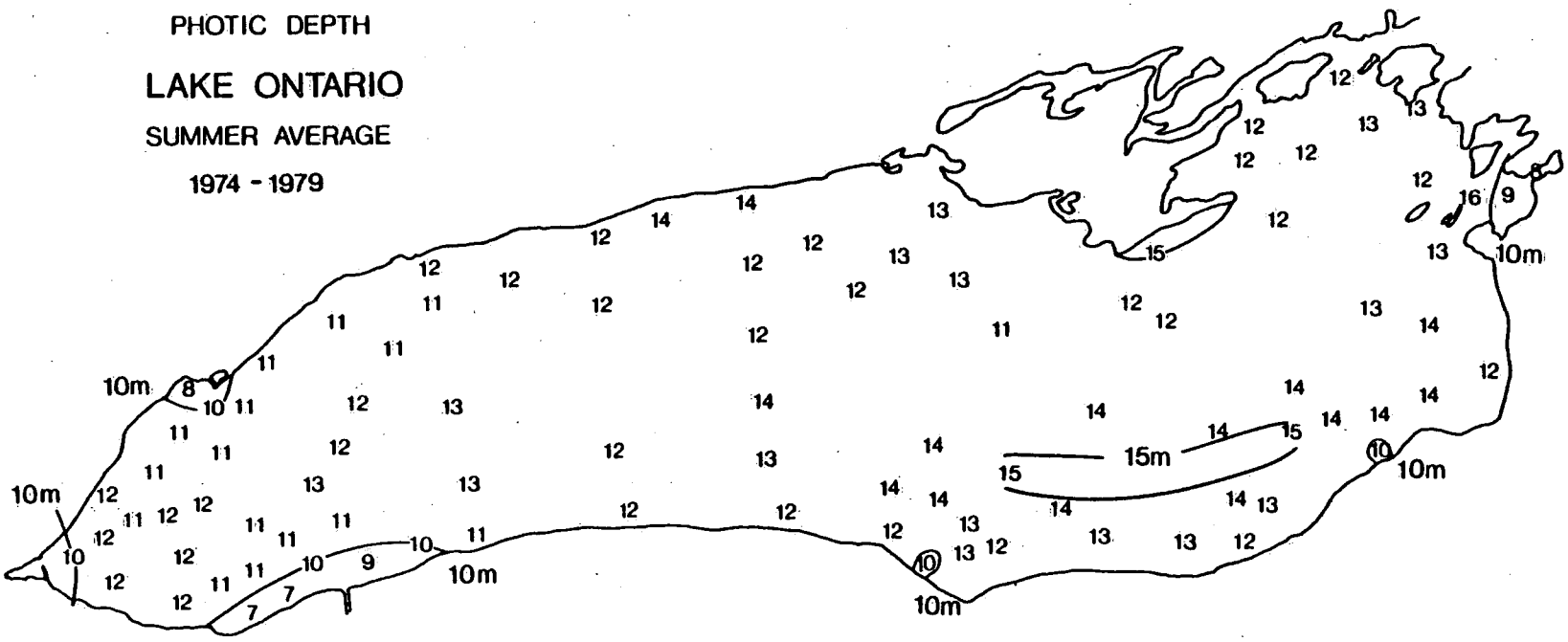

FIG. 38

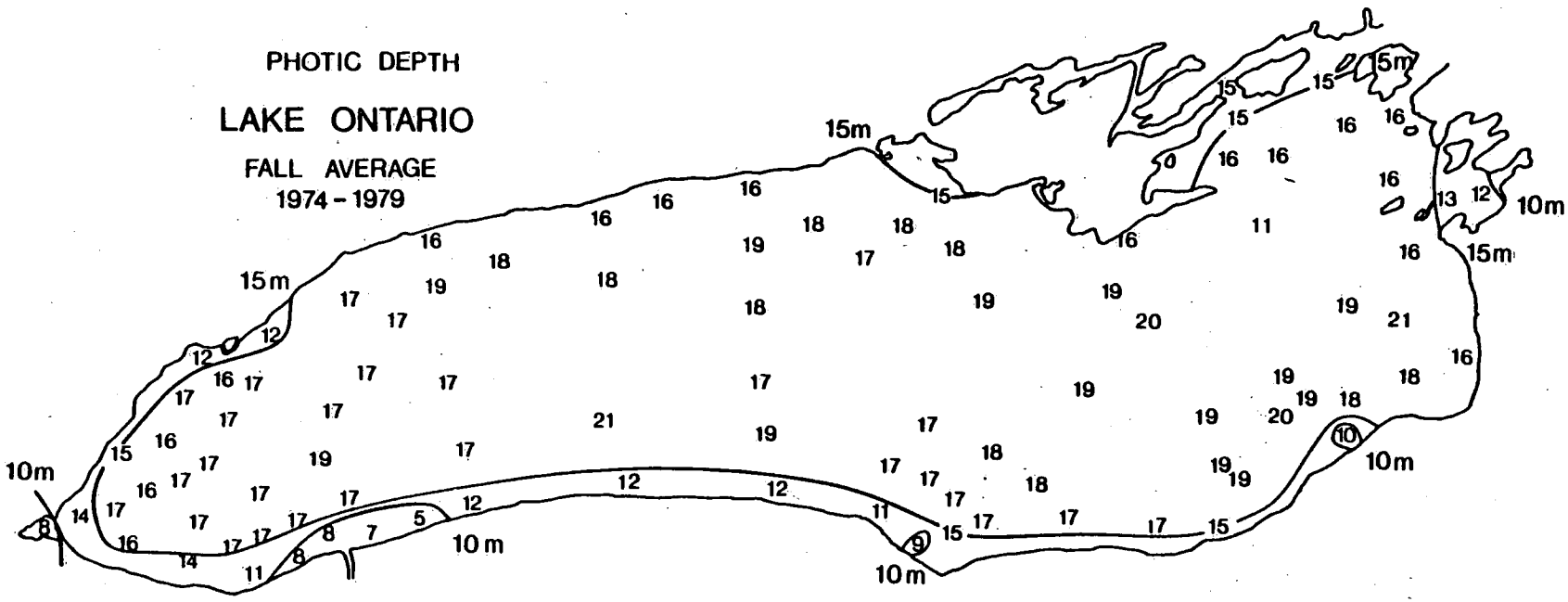
PHOTIC DEPTH
LAKE ONTARIO
FALL AVERAGE
1974 - 1979
15m
10m
10 m

FIG. 39

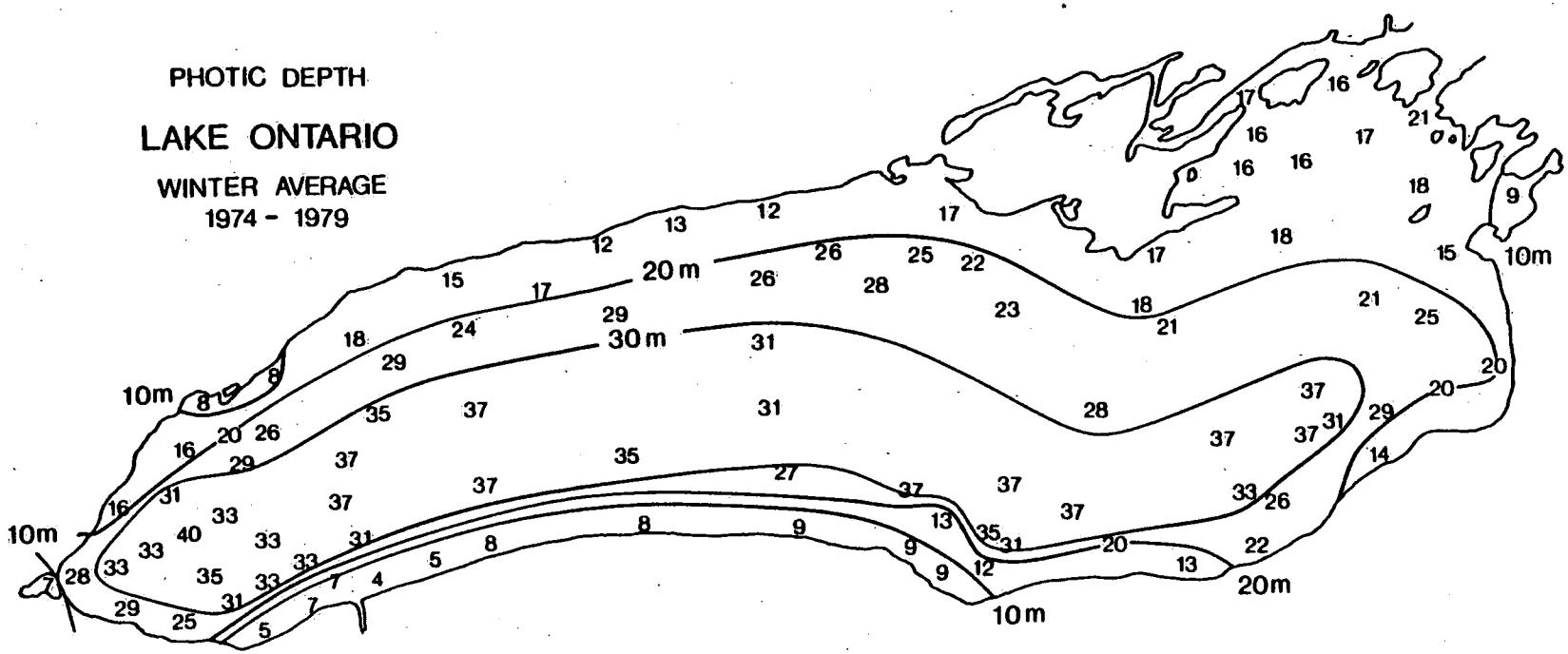
PHOTIC DEPTH
LAKE ONTARIO
WINTER AVERAGE
1974 - 1979
20 m
30 m
10m
10m
10m
20m

FIG. 40

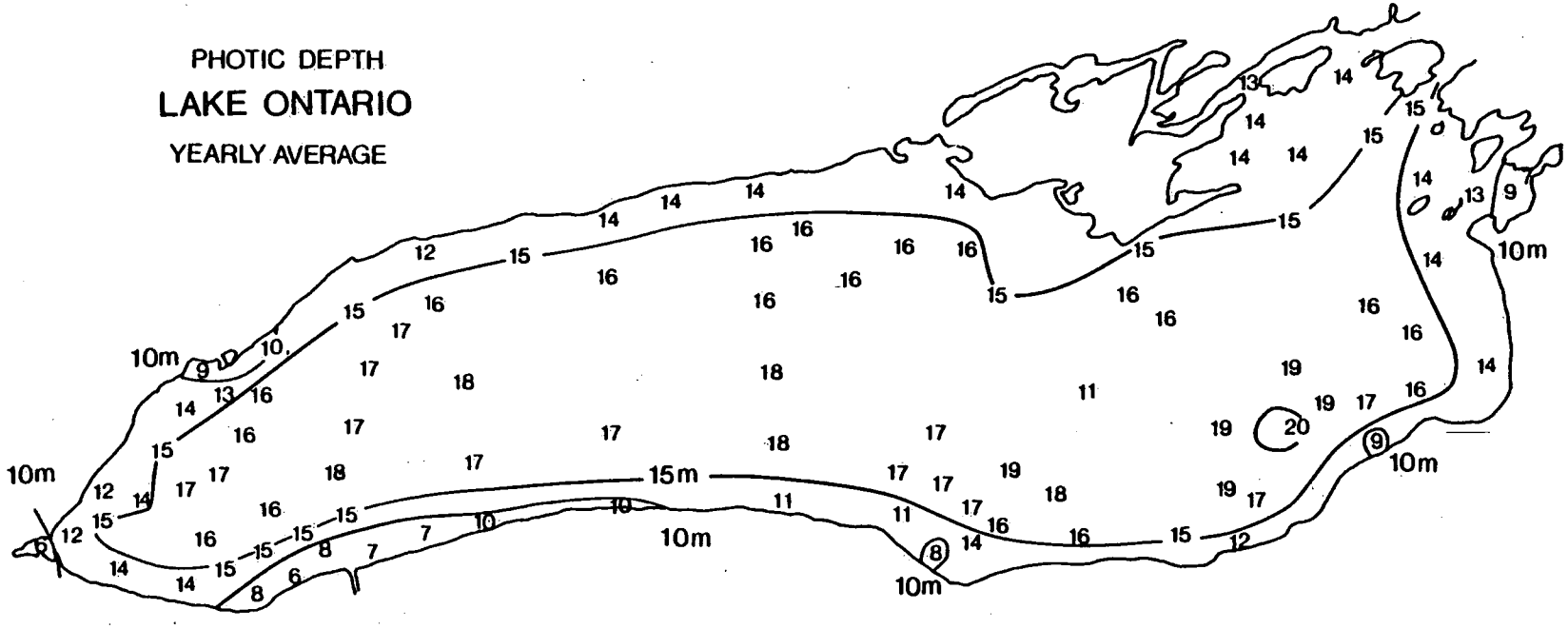
PHOTIC DEPTH
LAKE ONTARIO
YEARLY AVERAGE
10m
15m
10m
10m
10m

FIG. 41

TRANSMISSION TRANSECTS

Figures 42-71 illustrate the geographical locations of the surveillance stations comprising the transects utilized for each Great Lake studied, followed by the transmission transects determined for those station locations. Table 3 lists the particulars for each of these figures. The Lake Superior transmission data are presented as five separate south-to-north transects for the month of September, 1973. The Lakes Huron, Ontario and Erie and Georgian Bay transmission data are presented as one longitudinal transect per month for each lake. While data for only a single year are displayed for each of Lakes Huron and Erie and Georgian Bay, data from three years are included in the transects of Lake Ontario. The transmission data for the Upper Lakes were obtained with a 1 metre path length transmissometer while the transmission data for the Lower Lakes were obtained with a 0.25 metre path length, transmissometer.

Salient features of the transmission transects of Figures 42-71 include:

a) Lakes Huron, Erie and Ontario and Georgian Bay all display the same distinct seasonal cycle. In the spring when the lakes are characterized by isothermal conditions, the transmission transects indicate a similar tendency towards an isotropic condition. No vertical gradient in transmission is in evidence. A slight horizontal gradient in transmission, however, can be

seen. As the season progresses and the lakes become thermally stratified, distinct layering develops among the water masses of equivalent transmission. In general, a significant amount of this layering is associated with the actual location of the thermocline. In Lakes Superior and Huron and Georgian Bay, the thermocline is characterized as the layer of minimum mid-lake transmission. Below and above the thermocline, the waters display a higher degree of clarity. The triple basin nature of Lake Erie, however, produces a considerably more complex transmission transect structure. The shallow western basin of Lake Erie is characterized by both a horizontal and a vertical transmission gradient with extremely low values of transmission being observed at lake-bed. The intermediate-depth central basin is generally characterized by higher transmission values above the thermocline and lower transmission values below the thermocline. The deeper eastern basin tends to display the qualities of the Upper Lakes. In the early summer Lake Ontario displays a transmission structure similar to that of the Upper Lakes (thermocline as the region of minimal transmission). As the summer progresses, however, the eplimnion becomes the most turbid (lowest values of transmission) and the hypolimnion becomes the most clear (highest values of transmission). During the summer, therefore, the deep eastern basin of Lake Erie displays a transmission transect structure similar to those of

the Upper Lakes and Lake Ontario displays an inverse transmission transect structure to that of the central basin of Lake Erie. In the fall, as the lakes return to an isothermal condition, the transmission transect structure also collapses and returns to the spring conditions.

b) Although seasonal data for Lake Superior are not included in this report, existing optical data for this lake indicates its seasonal behaviour is similar to that of Lake Huron and Georgian Bay. Figures 43-47 display a lake-wide regime of minimal transmission in conjunction with the thermocline.

c) An obvious feature of many of the transmission transects of Lakes Erie and Ontario and Georgian Bay is the region of low transmission near the bottom. This region, generally referred to as the nepheloid layer, is most prominent in Lake Ontario during the summer and early fall. This nepheloid layer is most prominent in the western and central basins of Lake Erie during the summer. In fact the entire hypolimnion of central Lake Erie may be considered as comprising the nepheloid layer. The nepheloid layer of Georgian Bay, while most prominent during the summer, is neither as clearly defined nor as physically extensive as its Lower Lake counterparts.

d) An inability to monitor transmission at depths >100 m prohibits any speculations as to the existence and nature of such nepheloid layers in Lakes Superior and Huron.

TABLE 3

Figure	Lake	End Point Stations	Date
42	Superior	Transect Location	-
43	Superior	16, 9	Sept., 1973
44	Superior	17, 28	Sept., 1973
45	Superior	50, 36	Sept., 1973
46	Superior	51, 86	Sept., 1973
47	Superior	165, 177	Sept., 1973
48	Huron	Transect Location	-
49	Huron	33, 1	May, 1974
50	Huron	33, 1	June, 1974
51	Huron	33, 1	July, 1974
52	Huron	33, 1	August, 1974
53	Huron	33, 1	October, 1974
54	Georgian Bay	Transect Location	-
55	Georgian Bay	55, 7	May, 1974
56	Georgian Bay	55, 7	June, 1974
57	Georgian Bay	55, 7	July, 1974
58	Georgian Bay	55, 7	Sept., 1974
59	Georgian Bay	55, 7	October, 1974
60	Erie	Transect Location	-
61	Erie	60, 4	April, 1975
62	Erie	60, 4	May, 1975
63	Erie	60, 4	June, 1975
64	Erie	60, 4	August, 1975
65	Erie	60, 4	October, 1975
66	Ontario	Transect Location	-
67	Ontario	1, 78	May, 1982
68	Ontario	1, 78	July, 1982
69	Ontario	1, 78	August, 1981
70	Ontario	1. 78	October, 1982
71	Ontario	1. 78	October 1983

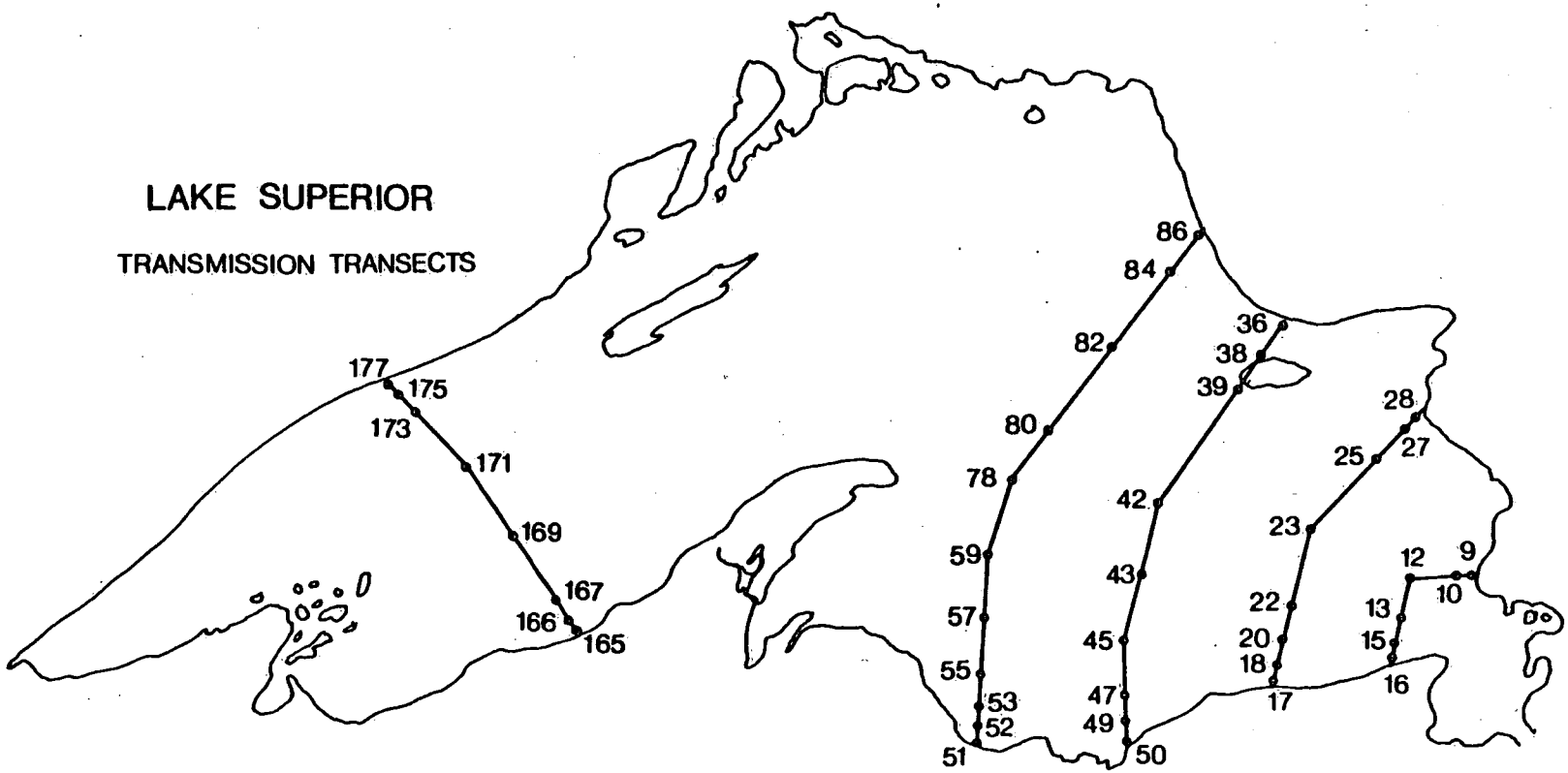
LAKE SUPERIOR
TRANSMISSION TRANSECTS
177
175
173
171
169
167
166
165
86
84
82
80
78
59
57
55
53
52
51
36
38
39
42
43
45
47
49
50
28
27
25
23
22
20
18
17
12
9
10
13
15
16

FIG. 42

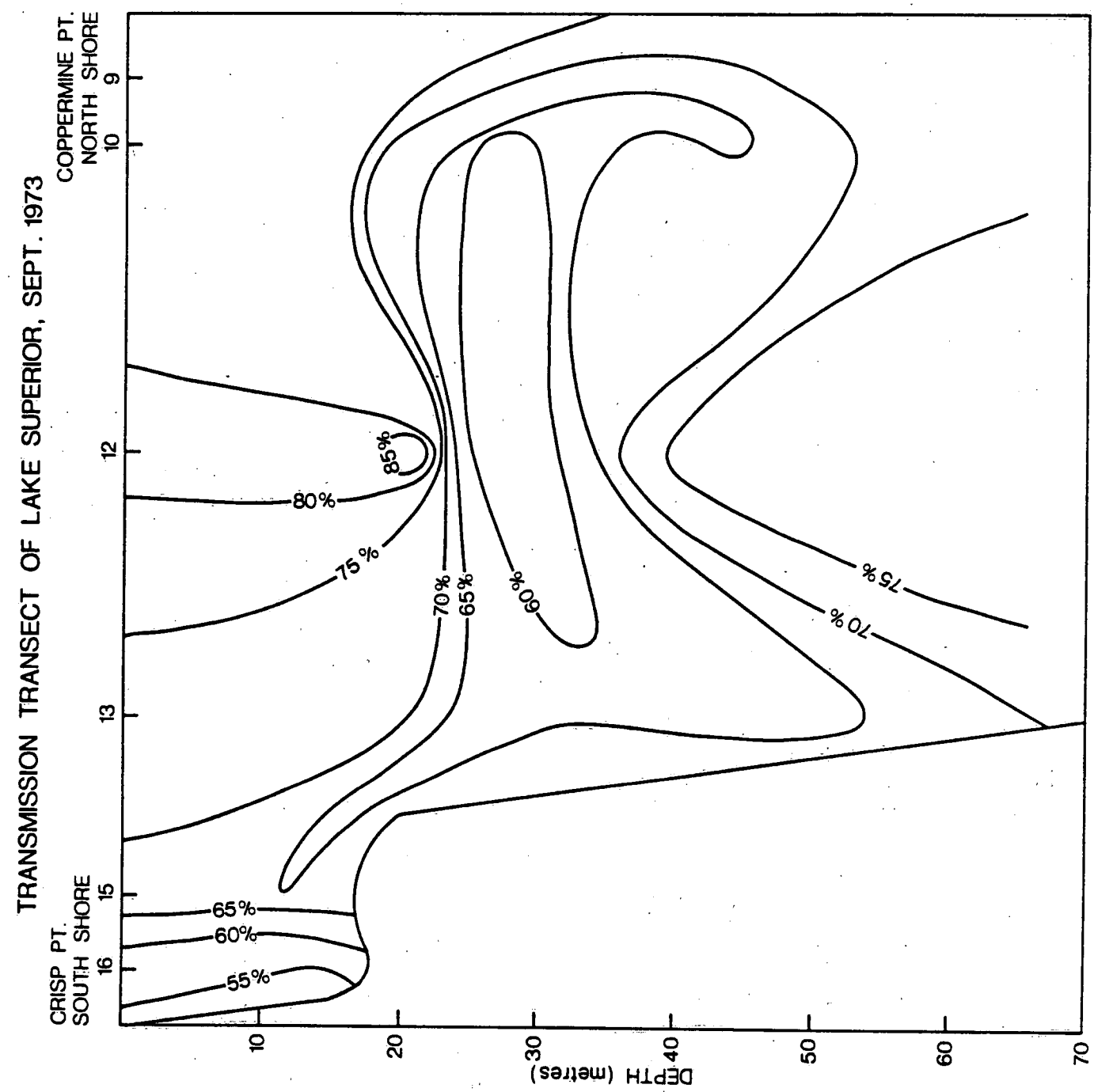
TRANSMISSION TRANSECT OF LAKE SUPERIOR, SEPT. 1973
COPPERMINE PT.
NORTH SHORE
CRISP PT.
SOUTH SHORE
9
10
12
13
15
16
85%
80%
75%
70%
65%
60%
55%
75%
70%
65%
60%
DEPTH (metres)
10
20
30
40
50
60
70

FIG. 43

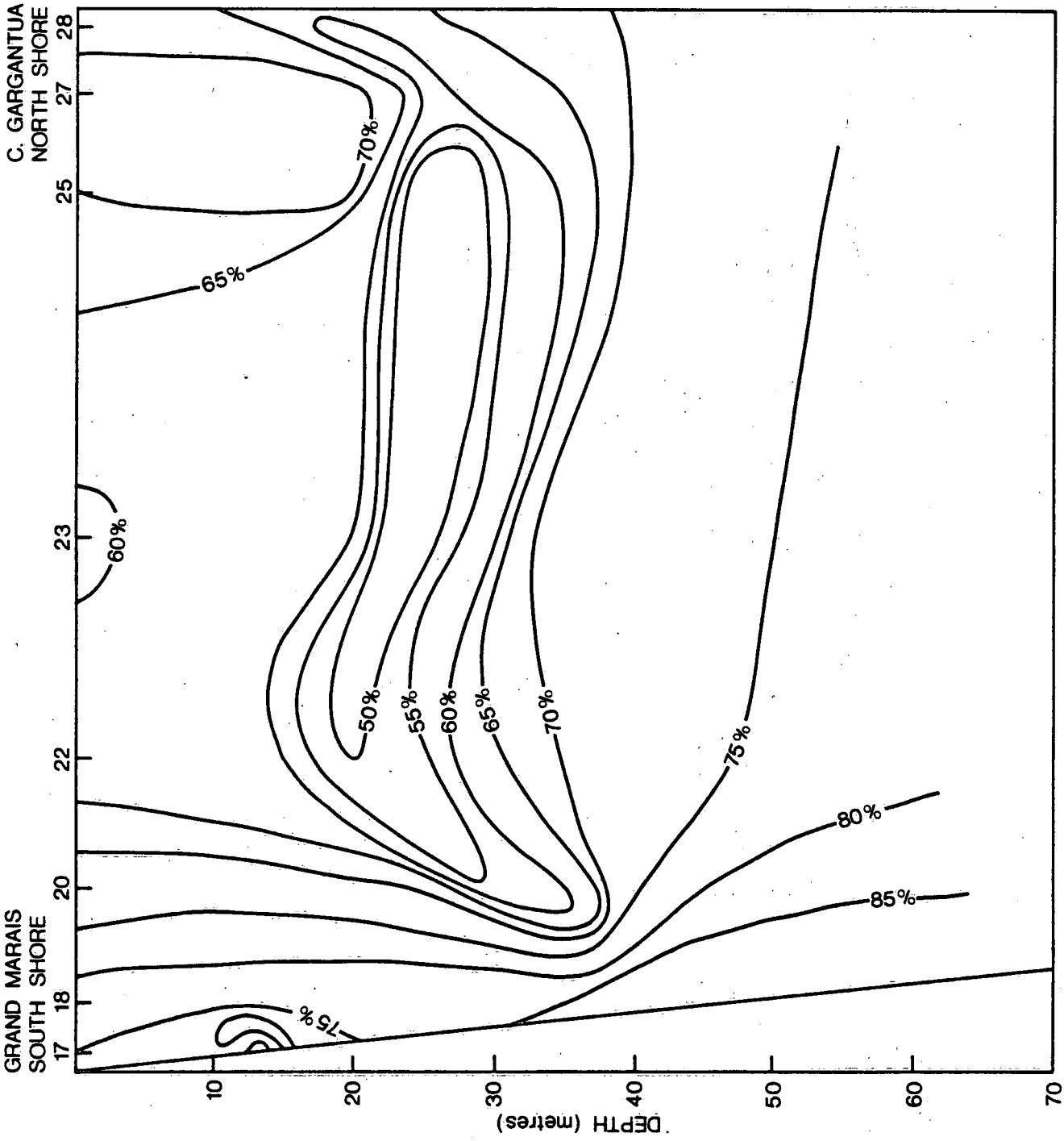
TRANSMISSION TRANSECT OF LAKE SUPERIOR, SEPT. 1973
GRAND MARAIS
SOUTH SHORE
C. GARGANTUA
NORTH SHORE
17
18
20
22
23
25
27
28
50%
55%
60%
65%
70%
75%
80%
85%
DEPTH (meters)
10
20
30
40
50
60
70

FIG. 4

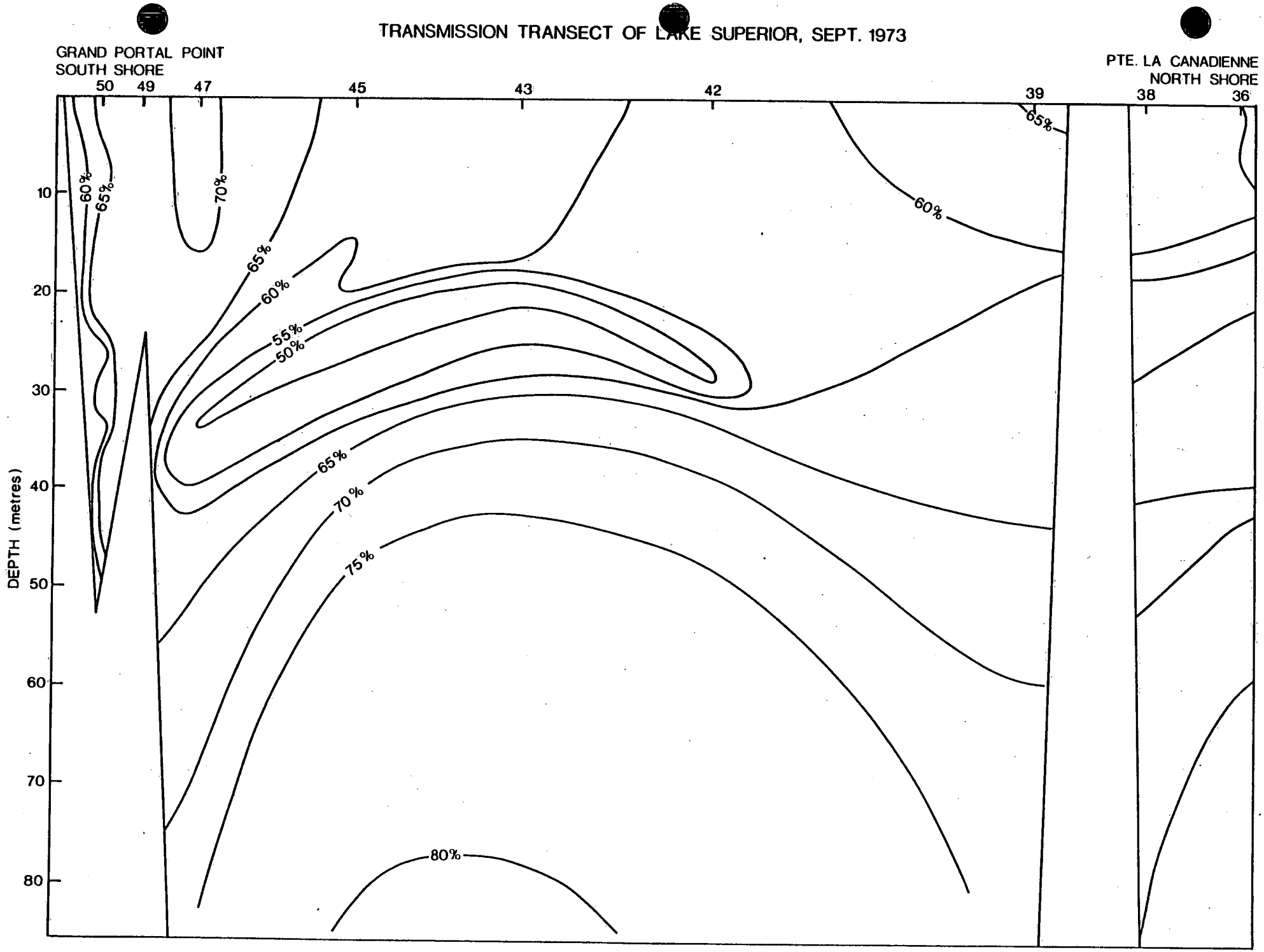
TRANSMISSION TRANSECT OF LAKE SUPERIOR, SEPT. 1973
GRAND PORTAL POINT
SOUTH SHORE
PTE. LA CANADIENNE
NORTH SHORE
50
49
47
45
43
42
39
38
36
DEPTH (metres)
10
20
30
40
50
60
70
80
60%
65%
70%
65%
60%
55%
50%
65%
70%
75%
80%
65%
60%

FIG. 45

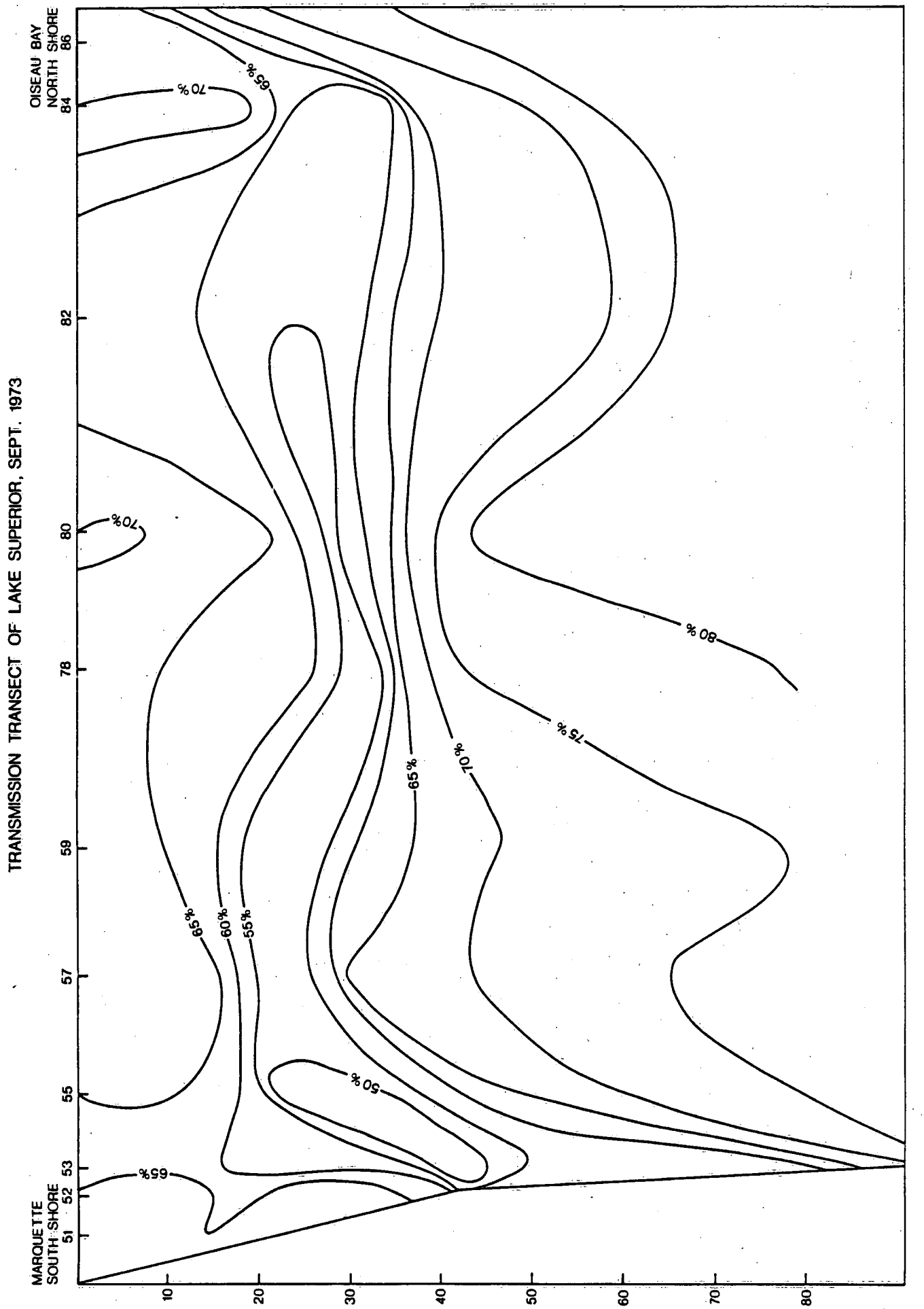
TRANSMISSION TRANSECT OF LAKE SUPERIOR, SEPT. 1973
MARQUETTE SOUTH SHORE
OISEAU BAY NORTH SHORE
51 52 53 55 57 59 78 80 82 84 86
DEPTH (meters)
10 20 30 40 50 60 70 80
65%
70%
70%
65%
60%
55%
65%
50%
70%
75%
80%

FIG. 26

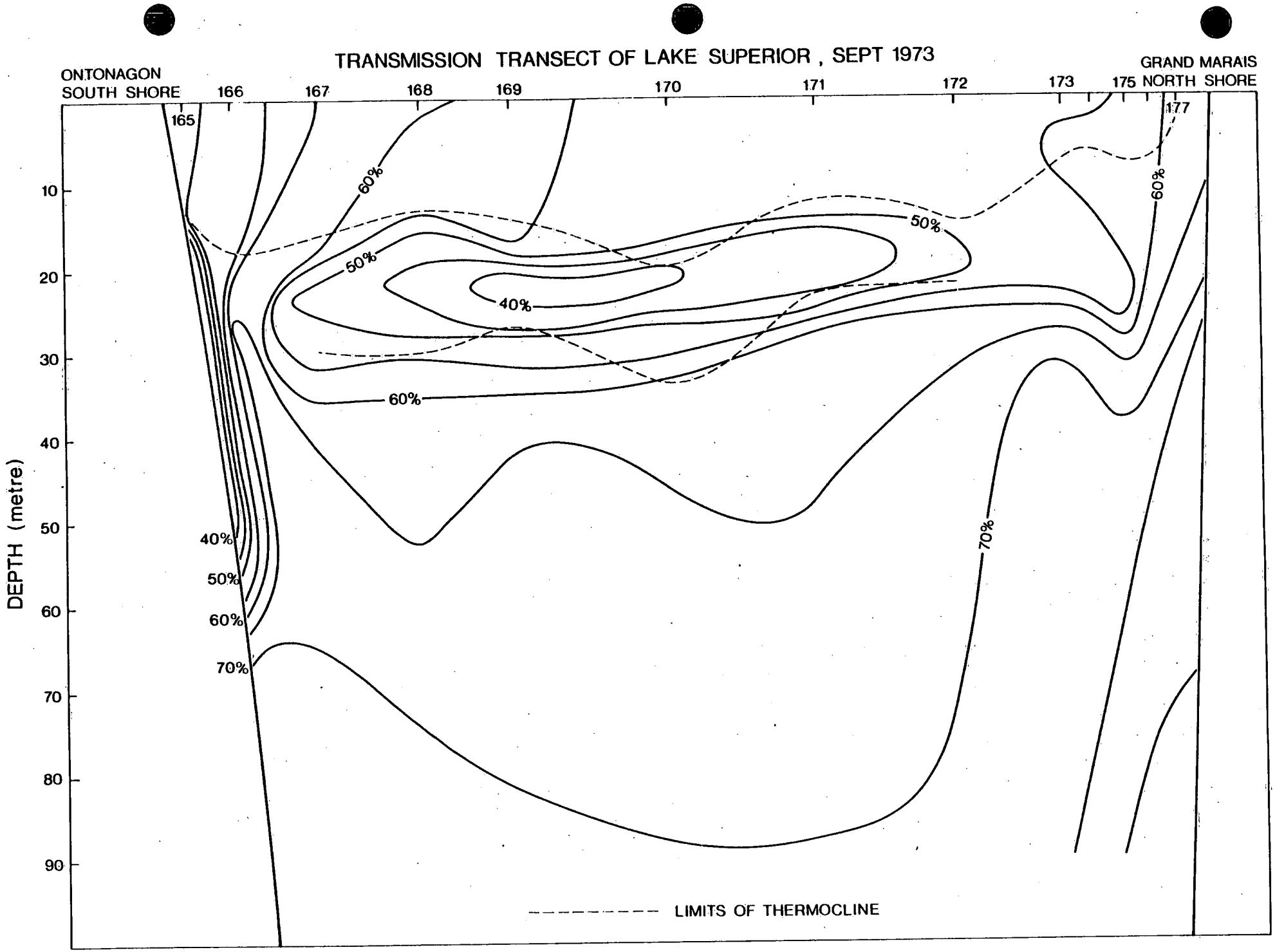
TRANSMISSION TRANSECT OF LAKE SUPERIOR , SEPT 1973
ONTONAGON SOUTH SHORE
GRAND MARAIS NORTH SHORE
165
166
167
168
169
170
171
172
173
175
177
DEPTH (metre)
10
20
30
40
50
60
70
80
90
60%
50%
40%
60%
50%
40%
60%
70%
70%
LIMITS OF THERMOCLINE

FIG. 4.7

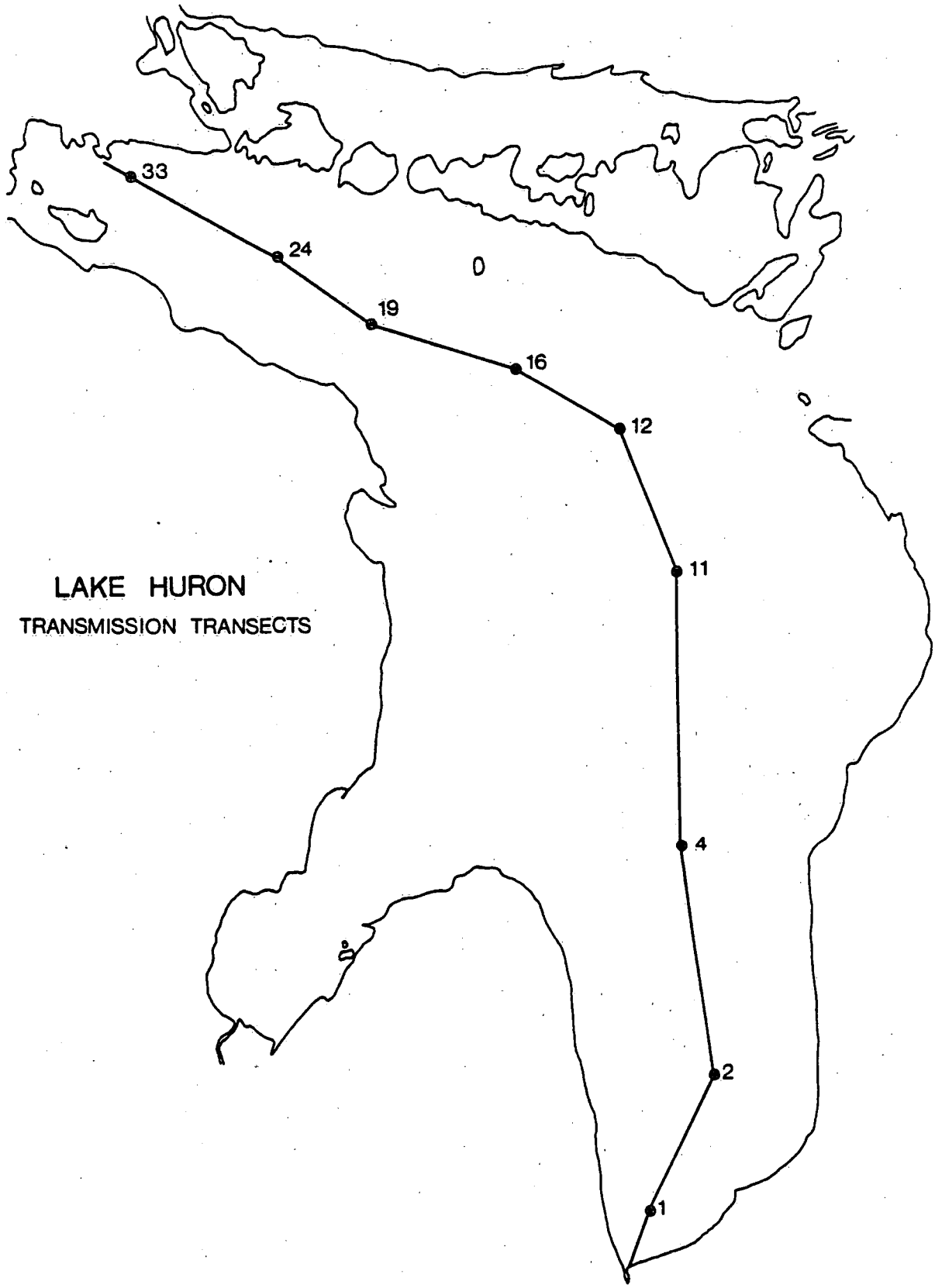

LAKE HURON
TRANSMISSION TRANSECTS

FIG. 48

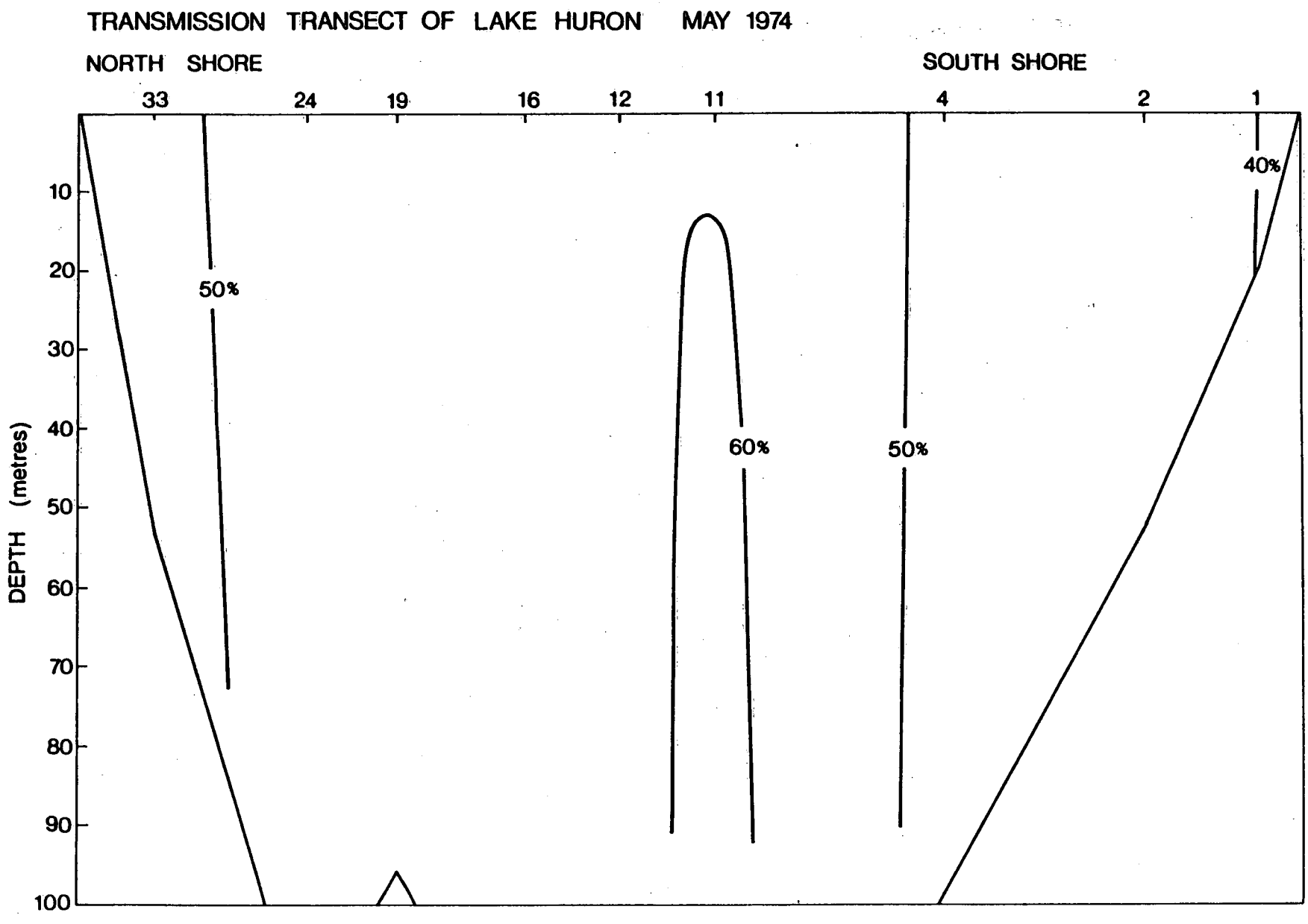
TRANSMISSION TRANSECT OF LAKE HURON MAY 1974
NORTH SHORE
SOUTH SHORE
33
24
19
16
12
11
4
2
1
DEPTH (metres)
10
20
30
40
50
60
70
80
90
100
50%
60%
50%
40%

FIG. 49

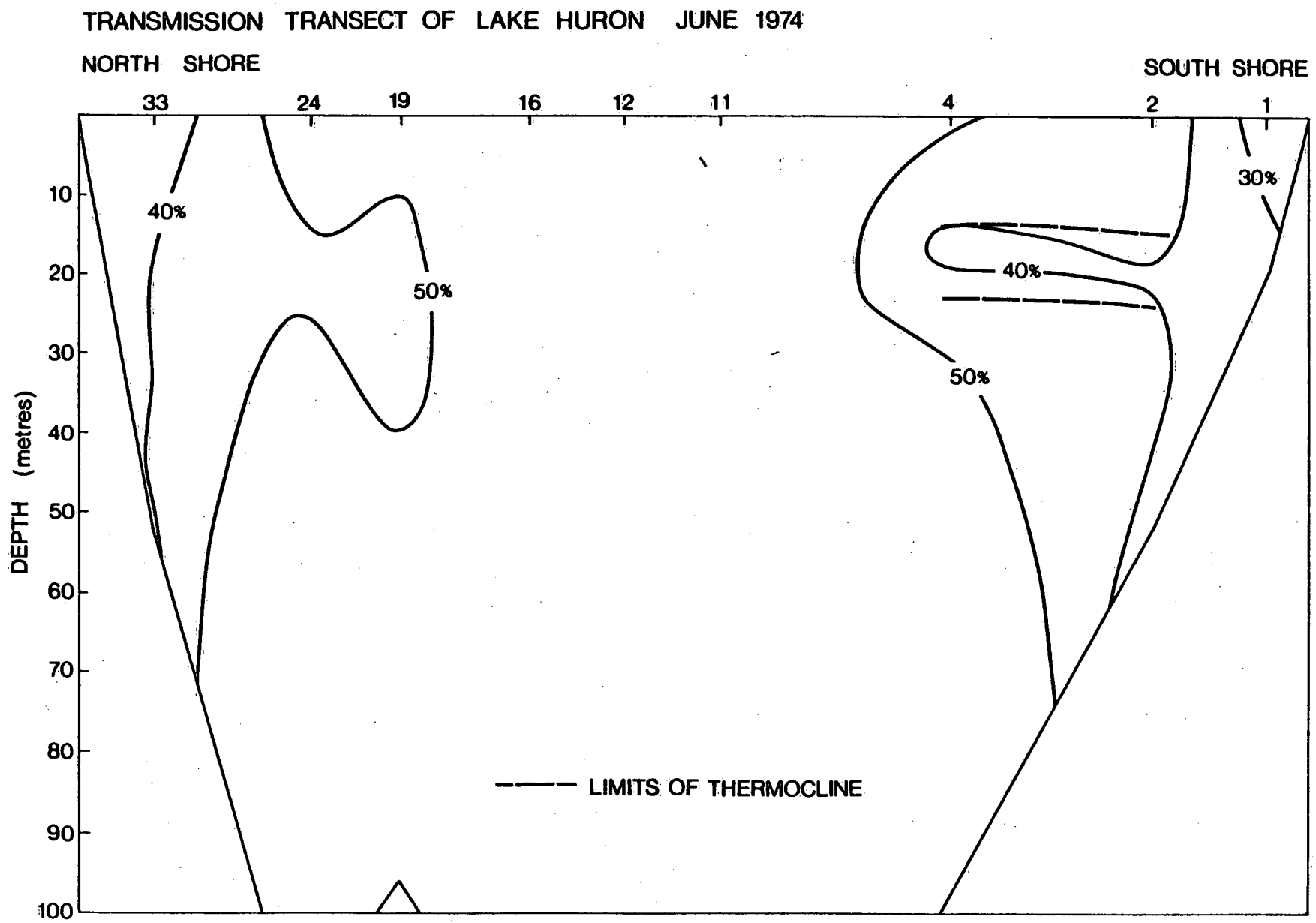
TRANSMISSION TRANSECT OF LAKE HURON JUNE 1974
NORTH SHORE
SOUTH SHORE
33
24
19
16
12
11
4
2
1
DEPTH (metres)
10
20
30
40
50
60
70
80
90
100
40%
50%
40%
50%
30%
LIMITS OF THERMOCLINE

FIG. 5

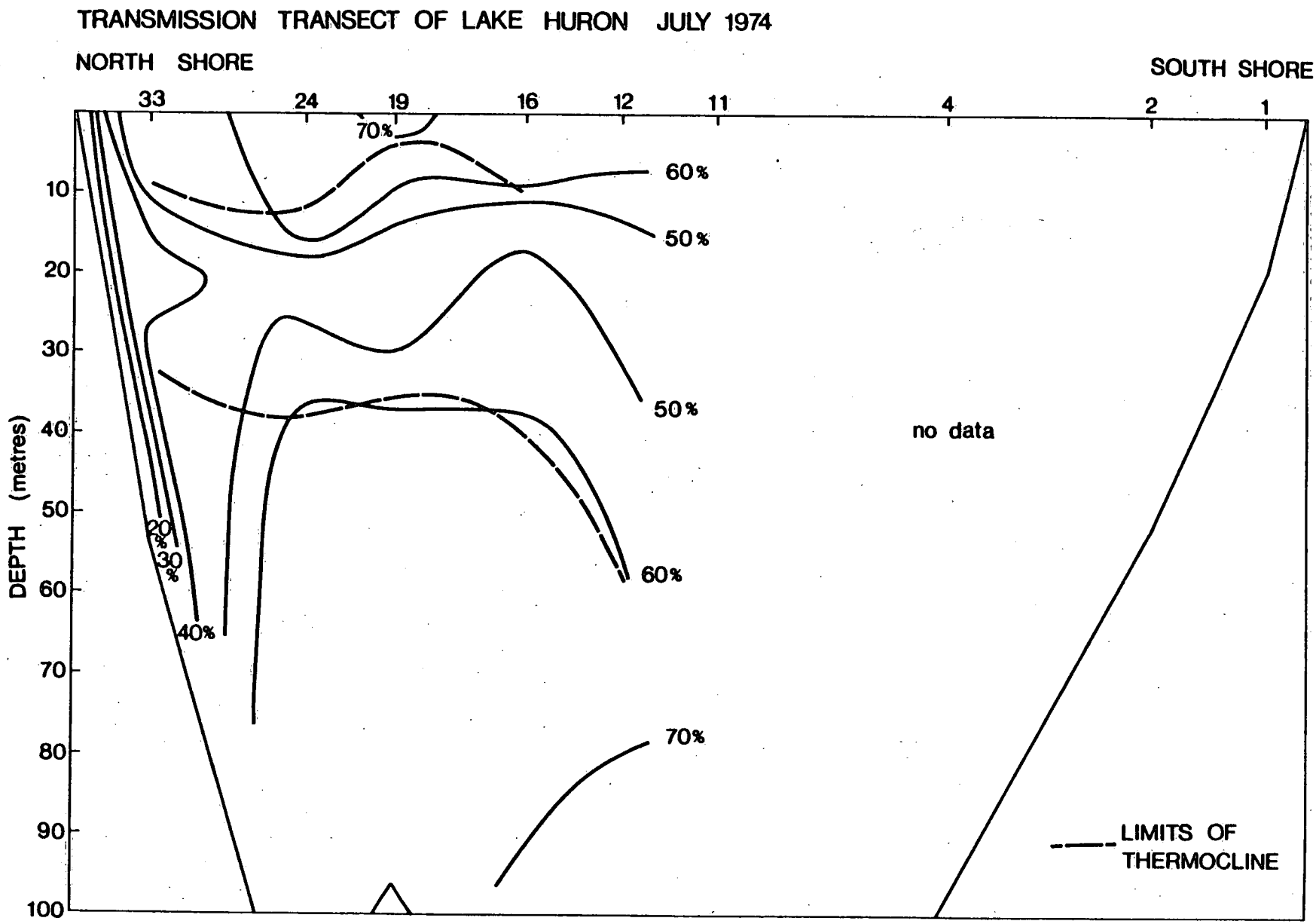
TRANSMISSION TRANSECT OF LAKE HURON JULY 1974
NORTH SHORE
SOUTH SHORE
33
24
19
16
12
11
4
2
1
DEPTH (metres)
10
20
30
40
50
60
70
80
90
100
70%
60%
50%
50%
60%
70%
20%
30%
40%
no data
LIMITS OF THERMOCLINE

FIG. 51

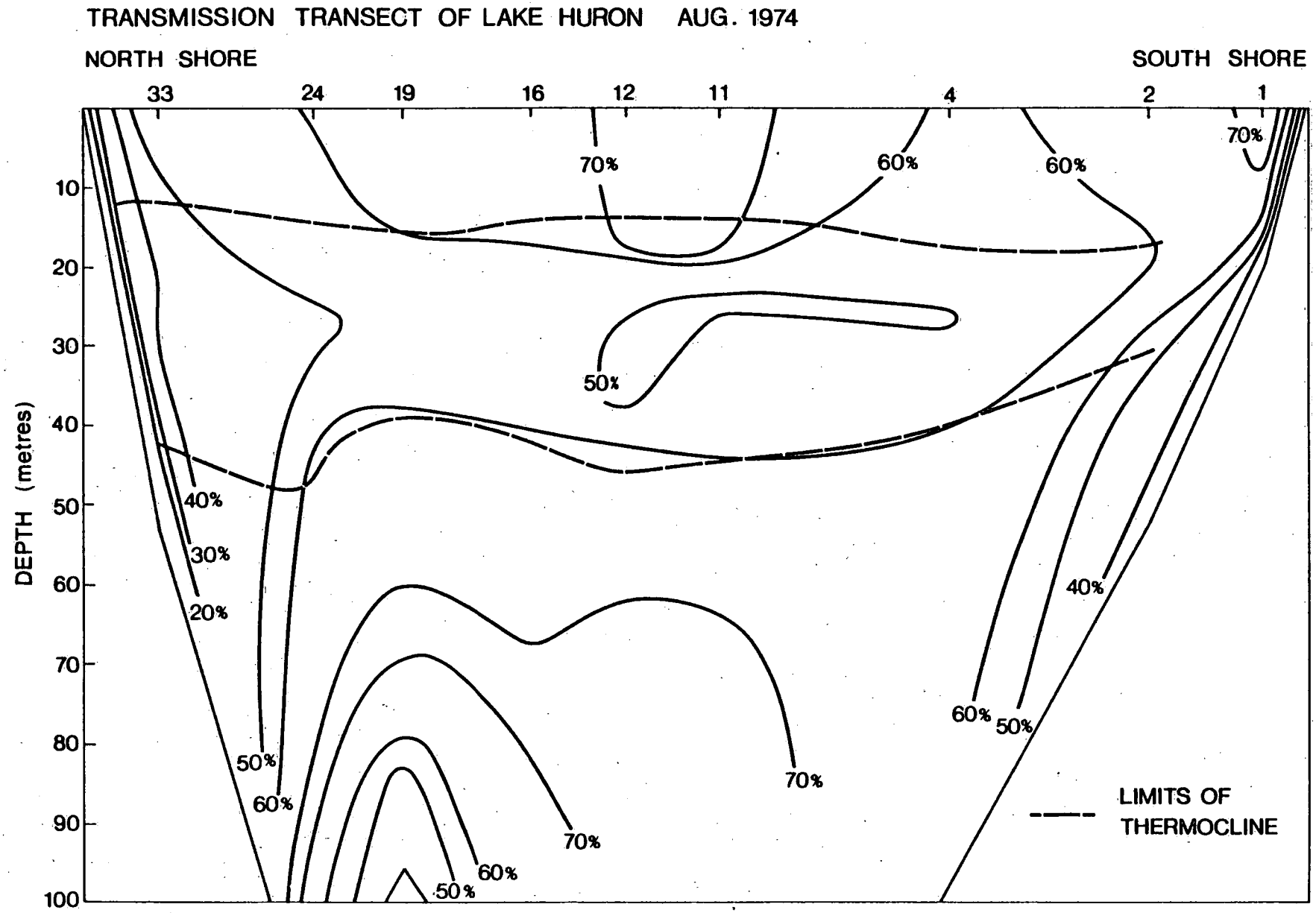
TRANSMISSION TRANSECT OF LAKE HURON AUG. 1974
NORTH SHORE
SOUTH SHORE
33
24
19
16
12
11
4
2
1
DEPTH (metres)
10
20
30
40
50
60
70
80
90
100
70%
60%
60%
70%
50%
40%
30%
20%
50%
60%
70%
60%
50%
40%
60%
50%
70%
LIMITS OF
THERMOCLINE

FIG. 5

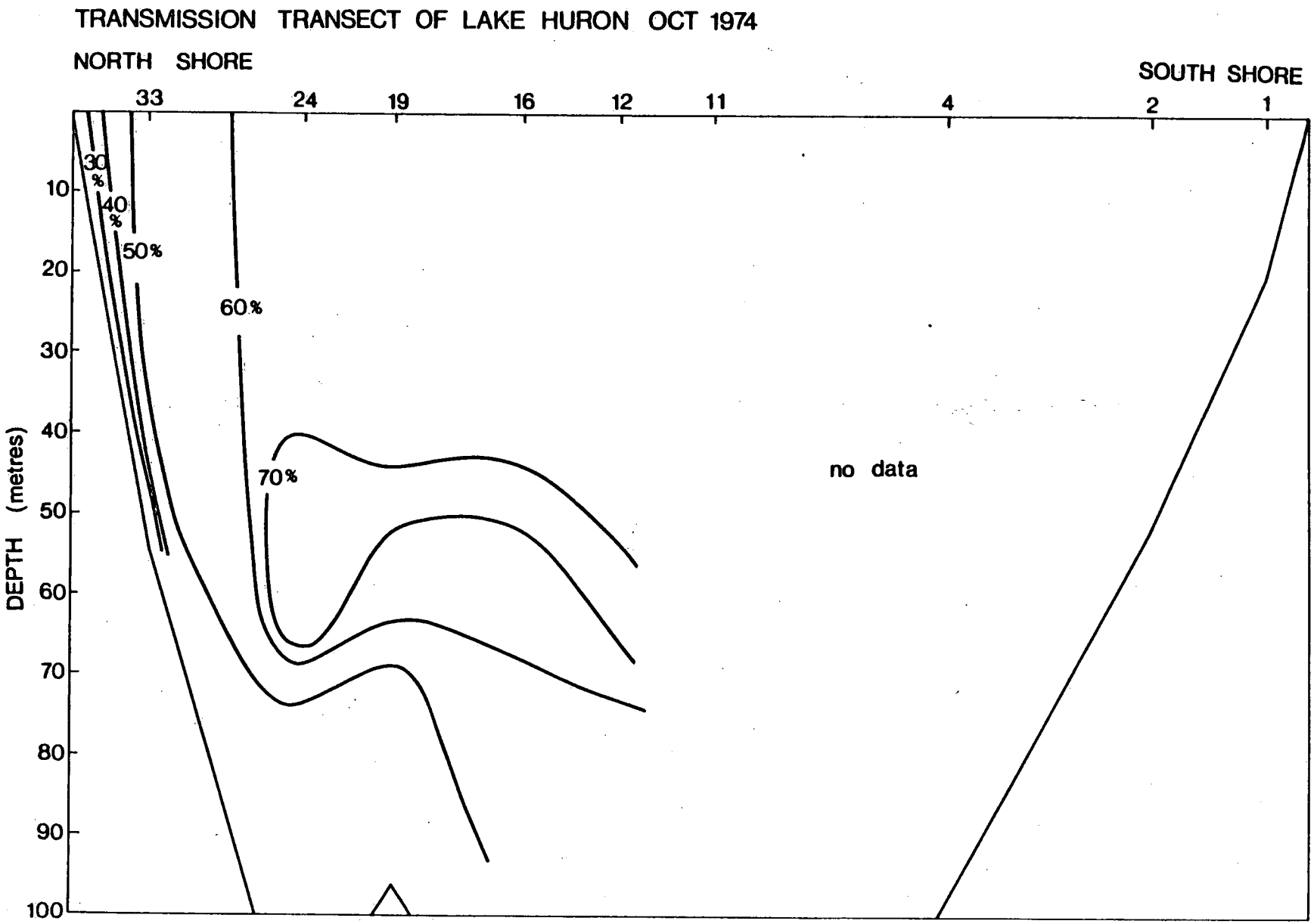
TRANSMISSION TRANSECT OF LAKE HURON OCT 1974
NORTH SHORE
SOUTH SHORE
33
24
19
16
12
11
4
2
1
30%
40%
50%
60%
70%
no data
DEPTH (metres)
10
20
30
40
50
60
70
80
90
100

FIG. 53

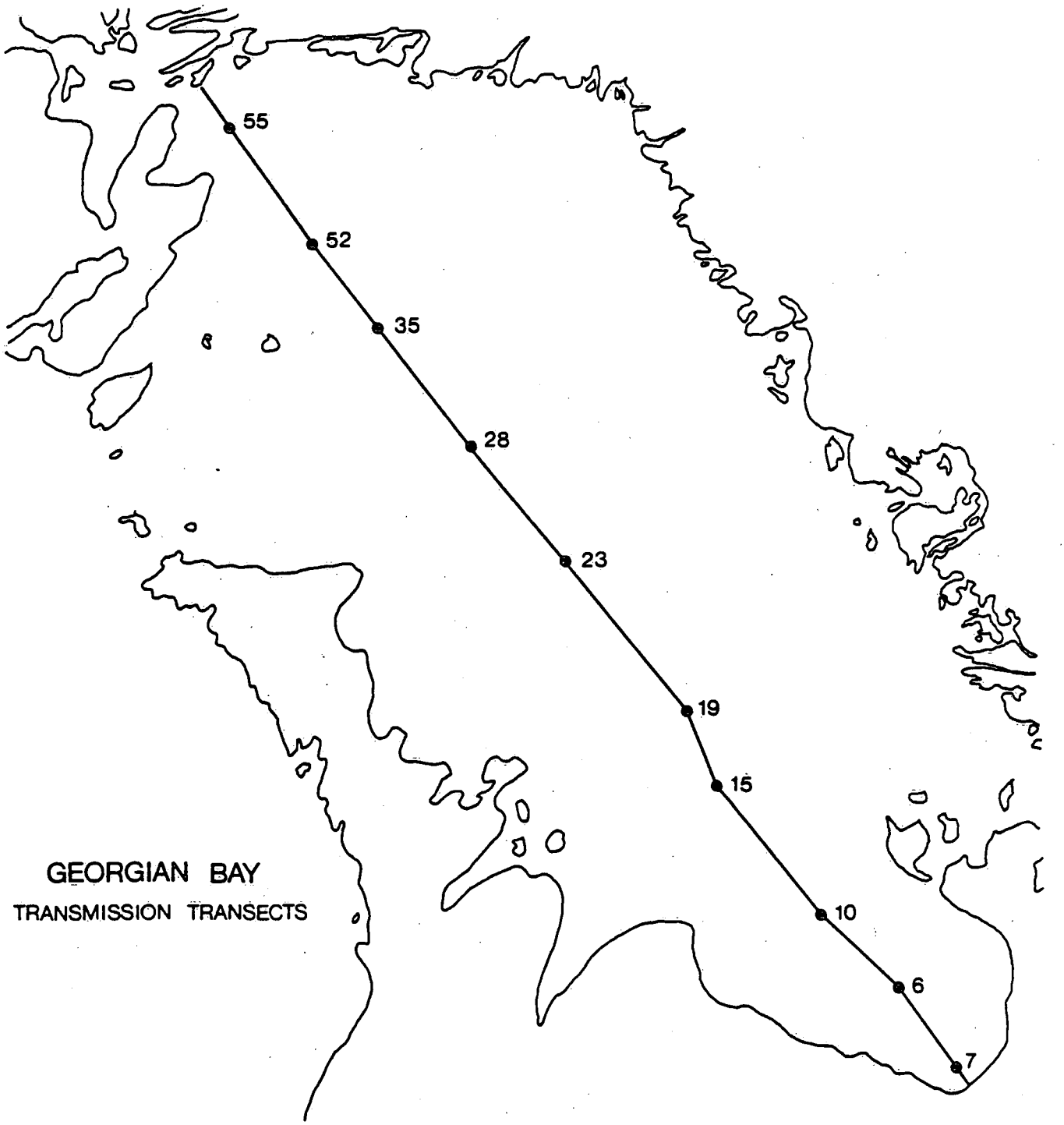
55
52
35
28
23
19
15
10
6
7
GEORGIAN BAY
TRANSMISSION TRANSECTS

FIG. 54

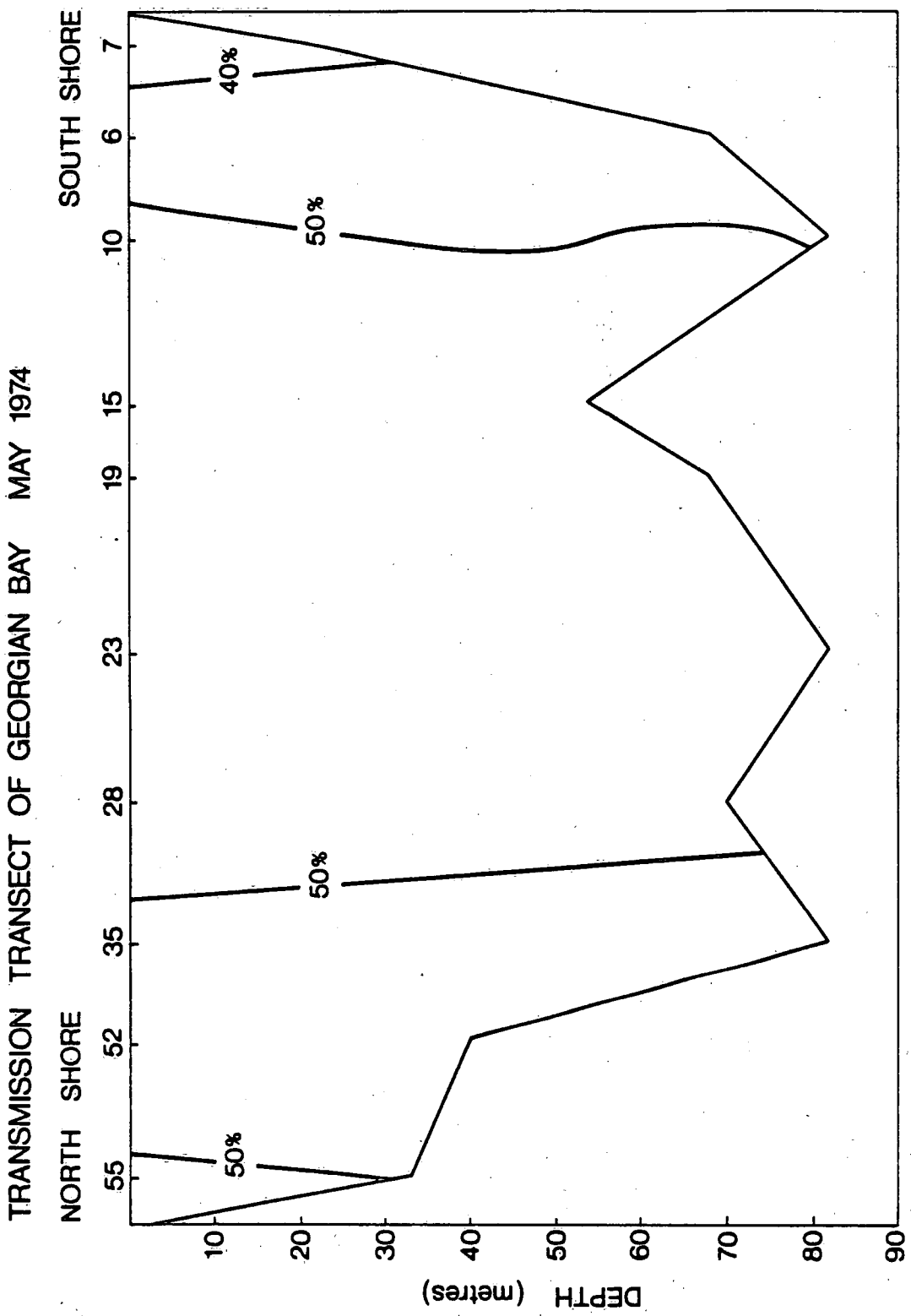
TRANSMISSION TRANSECT OF GEORGIAN BAY MAY 1974
NORTH SHORE
SOUTH SHORE
55
52
35
28
23
19
15
10
6
7
50%
50%
50%
40%
DEPTH (metres)
10
20
30
40
50
60
70
80
90

FIG. 55

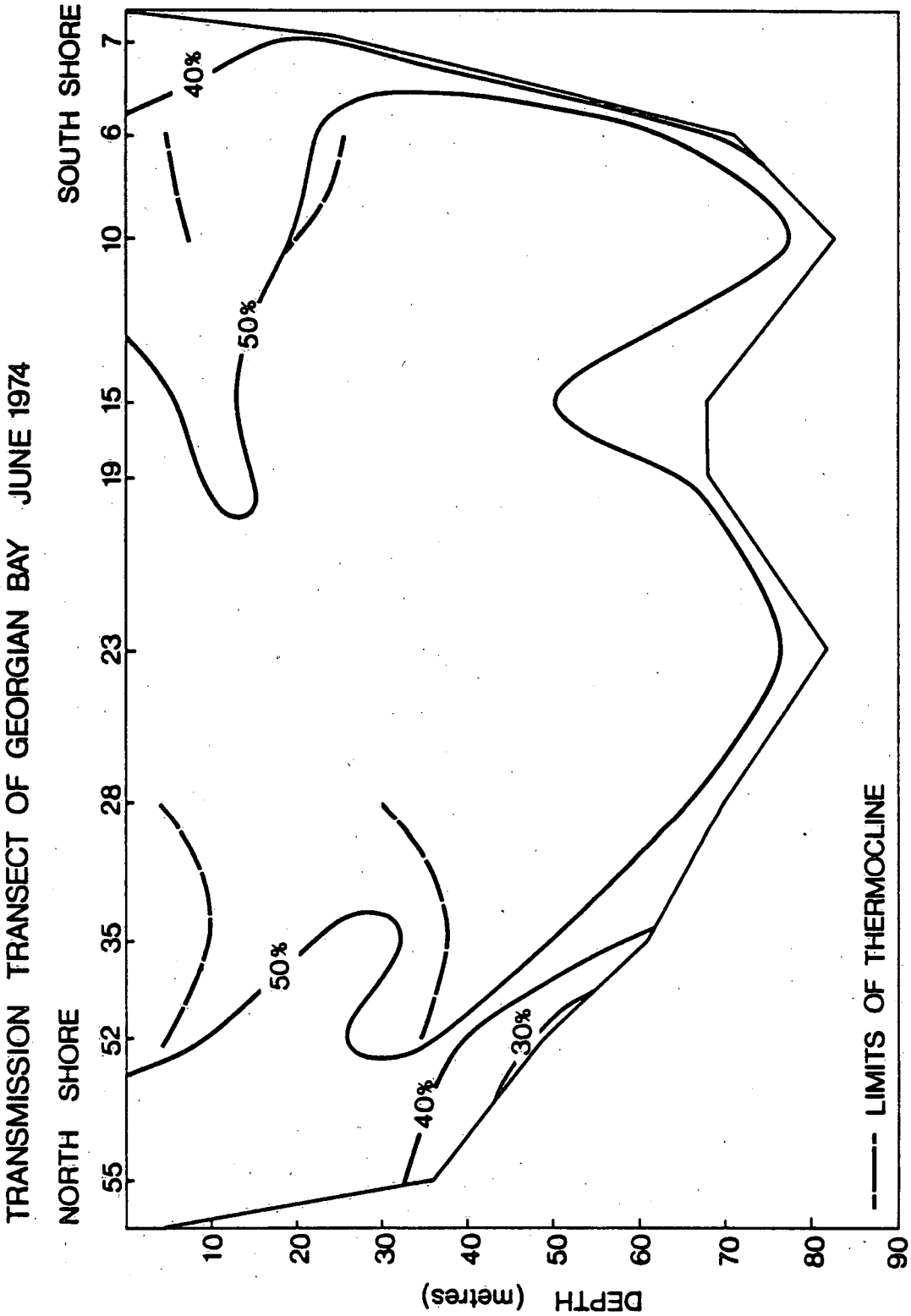
TRANSMISSION TRANSECT OF GEORGIAN BAY JUNE 1974
NORTH SHORE
SOUTH SHORE
55
52
35
28
23
19
15
10
6
7
40%
50%
50%
40%
30%
10
20
30
40
50
60
70
80
90
DEPTH (metres)
LIMITS OF THERMOCLINE

FIG. 56

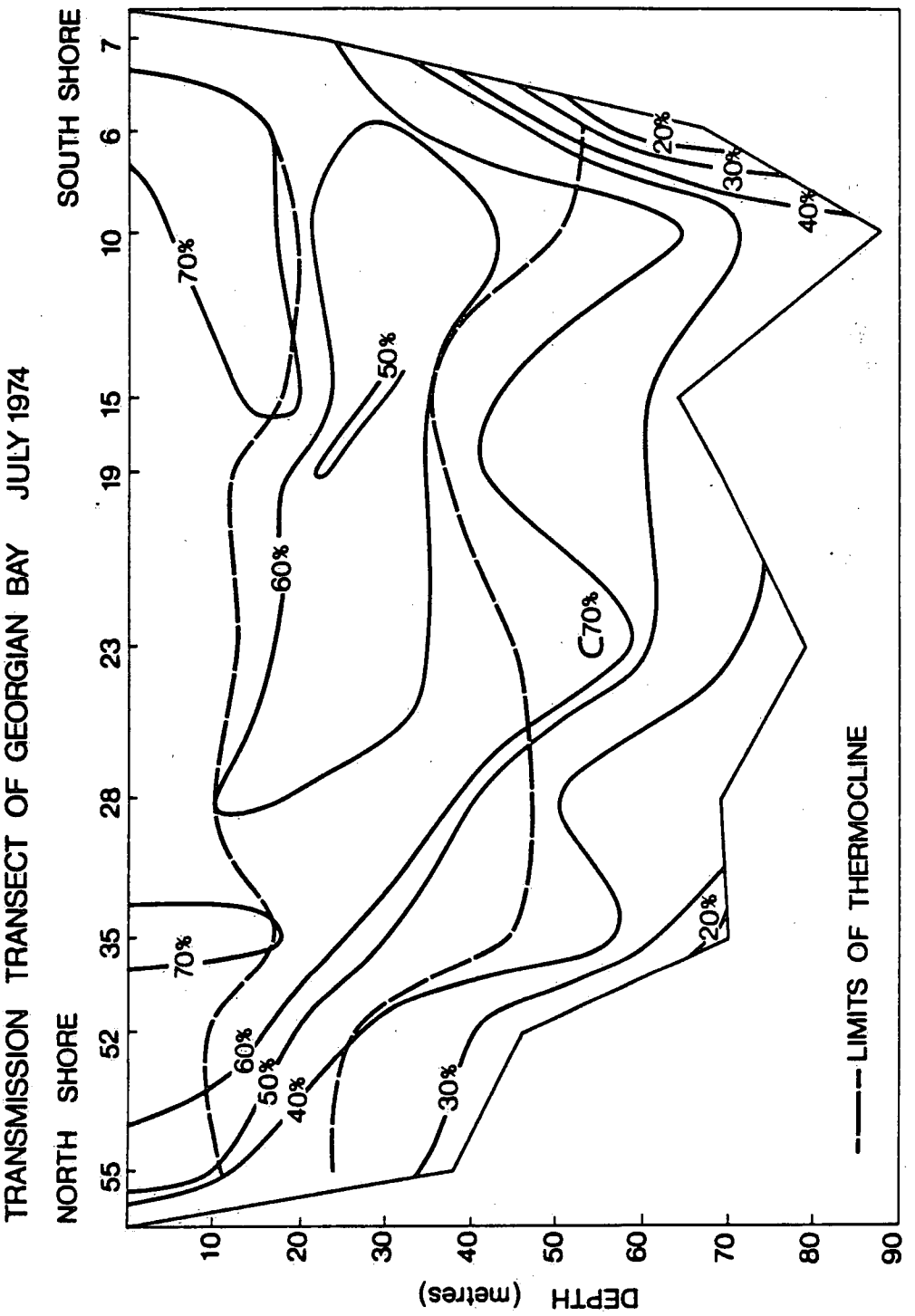
TRANSMISSION TRANSECT OF GEORGIAN BAY JULY 1974
NORTH SHORE
SOUTH SHORE
55 52 35 28 23 19 15 10 6 7
DEPTH (metres)
10 20 30 40 50 60 70 80 90
70%
60%
50%
40%
30%
20%
LIMITS OF THERMOCLINE

FIG. 57

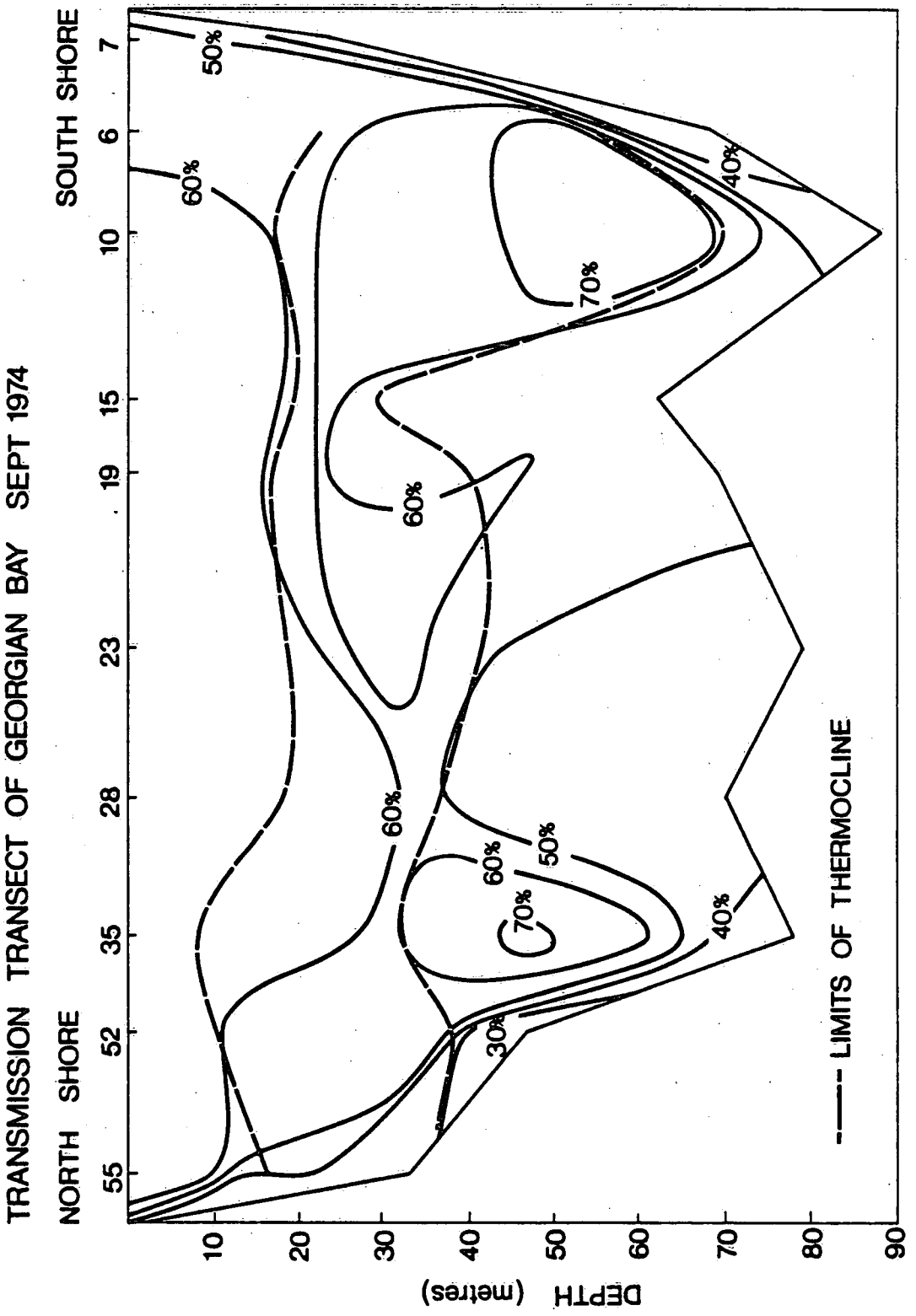
TRANSMISSION TRANSECT OF GEORGIAN BAY SEPT 1974
NORTH SHORE
SOUTH SHORE
55
52
35
28
23
19
15
10
6
7
DEPTH (metres)
10
20
30
40
50
60
70
80
90
50%
60%
70%
40%
30%
LIMITS OF THERMOCLINE

FIG. 58

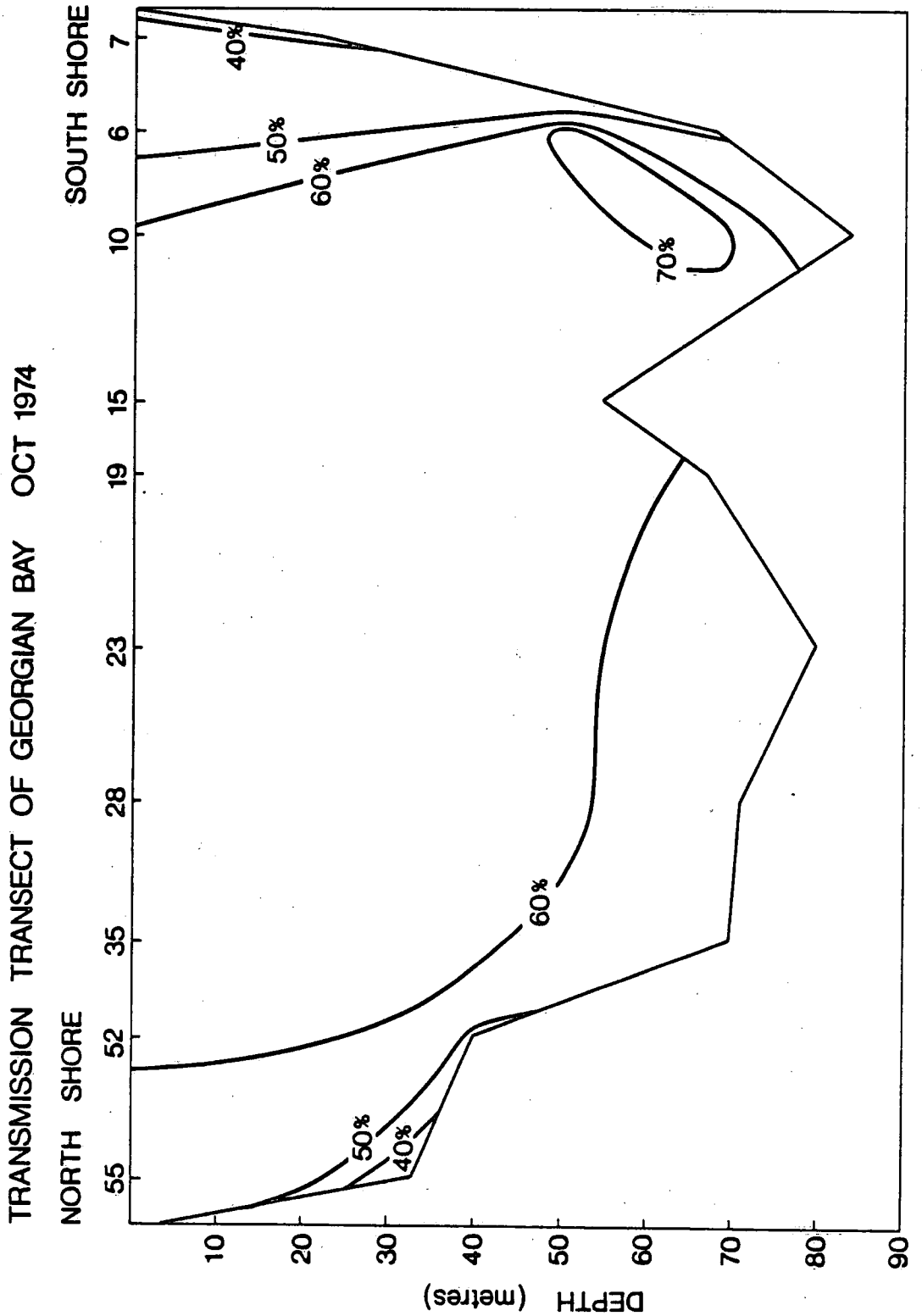
TRANSMISSION TRANSECT OF GEORGIAN BAY OCT 1974
NORTH SHORE
SOUTH SHORE
55
52
35
28
23
19
15
10
6
7
40%
50%
60%
70%
DEPTH (metres)
10
20
30
40
50
60
70
80
90

FIG. 59

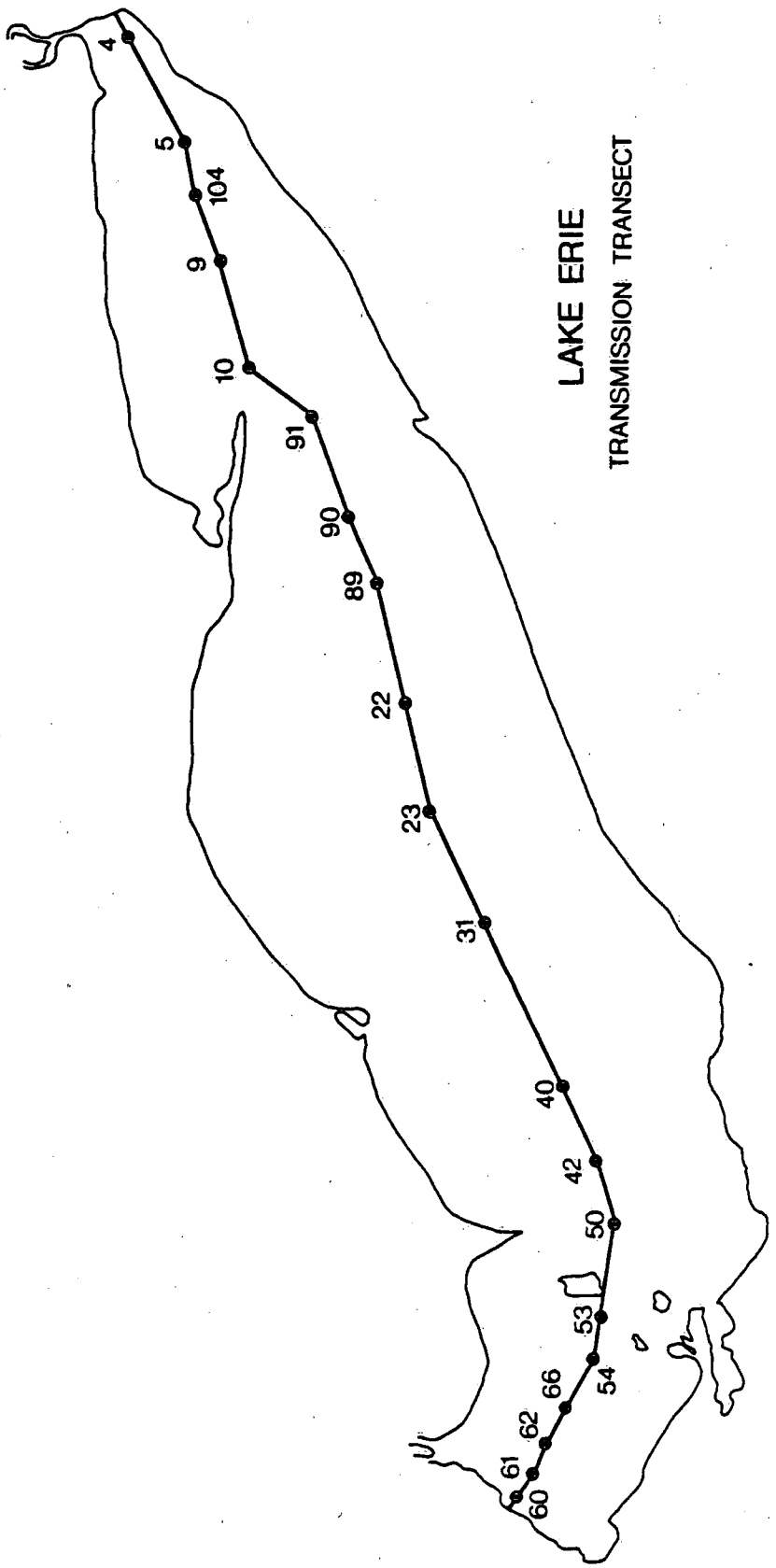
LAKE ERIE
TRANSMISSION TRANSECT
4
5
104
9
10
91
90
89
22
23
31
40
42
50
53
54
66
62
61
60

FIG. 60

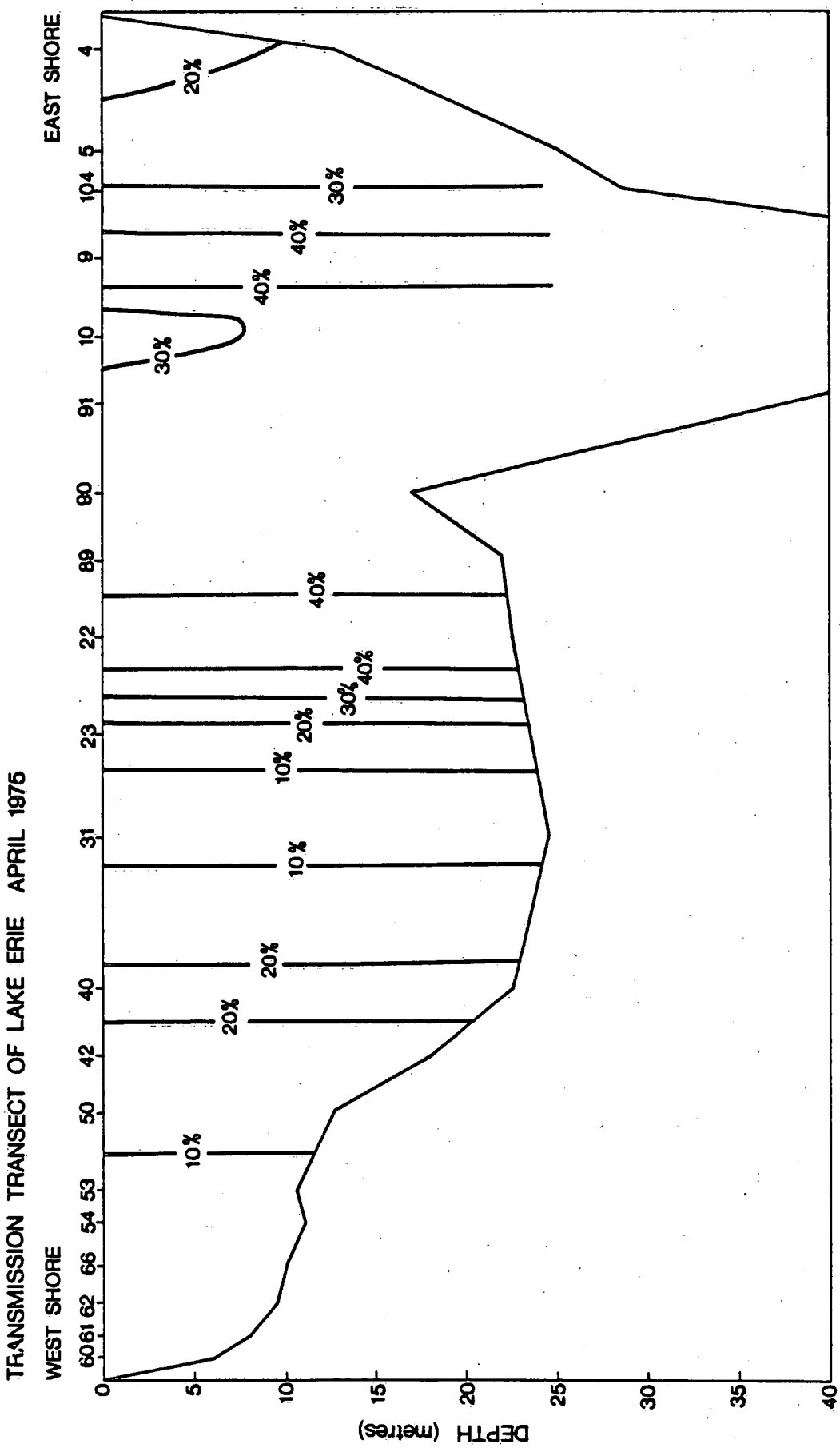
TRANSMISSION TRANSECT OF LAKE ERIE APRIL 1975
WEST SHORE
EAST SHORE
60 61 62 66 54 53 50 42 40 31 23 22 89 90 91 10 9 104 5 4
10%
20%
20%
10%
10%
30%
20%
10%
40%
30%
40%
40%
30%
40%
20%
DEPTH (metres)
0 5 10 15 20 25 30 35 40

FIG. 61

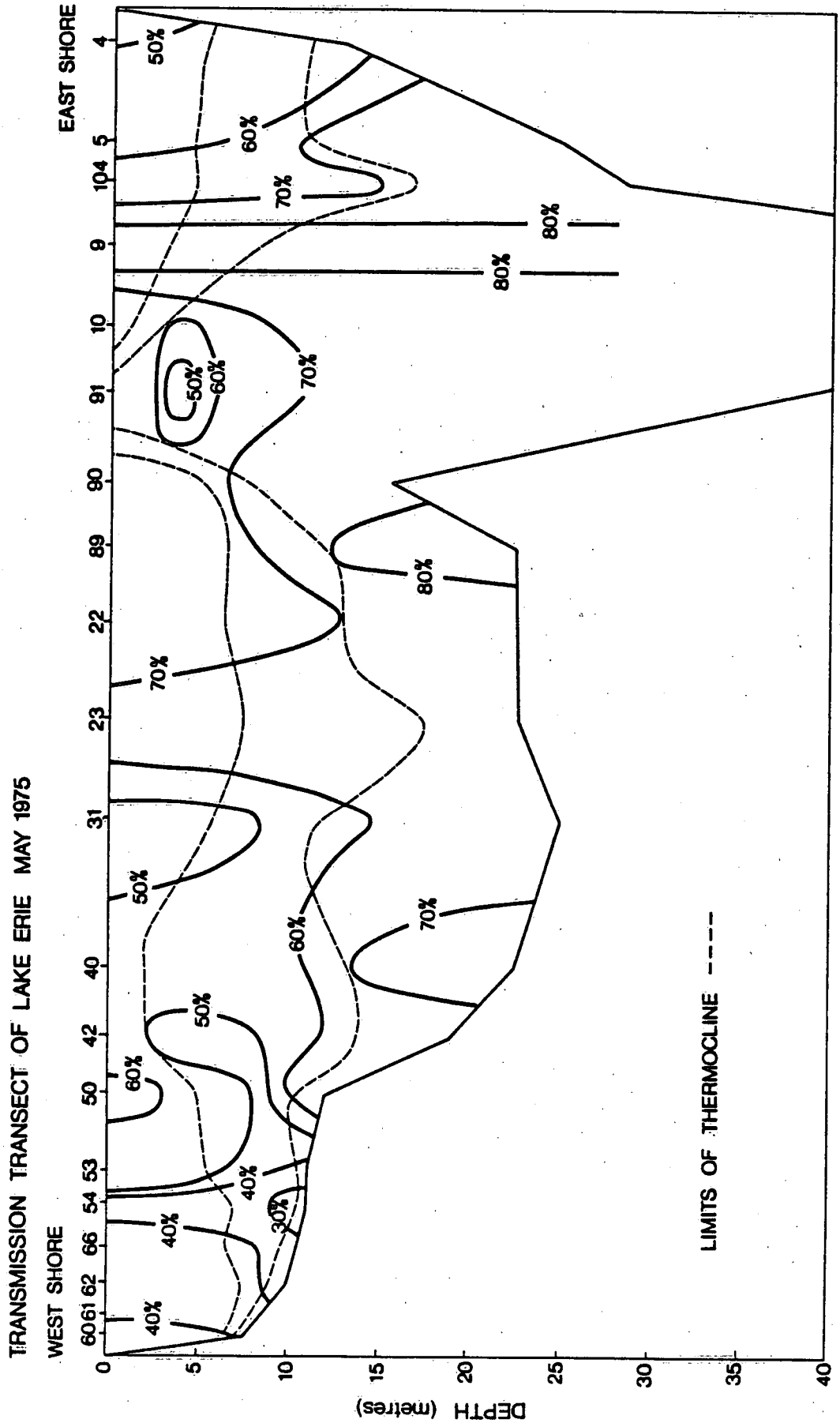
TRANSMISSION TRANSECT OF LAKE ERIE MAY 1975
WEST SHORE
EAST SHORE
60 61 62 66 54 53 50 42 40 31 23 22 89 90 91 10 9 10 4 5 4
50%
60%
70%
80%
40%
30%
LIMITS OF THERMOCLINE ----
DEPTH (meters)
0 5 10 15 20 25 30 35 40

FIG. 62

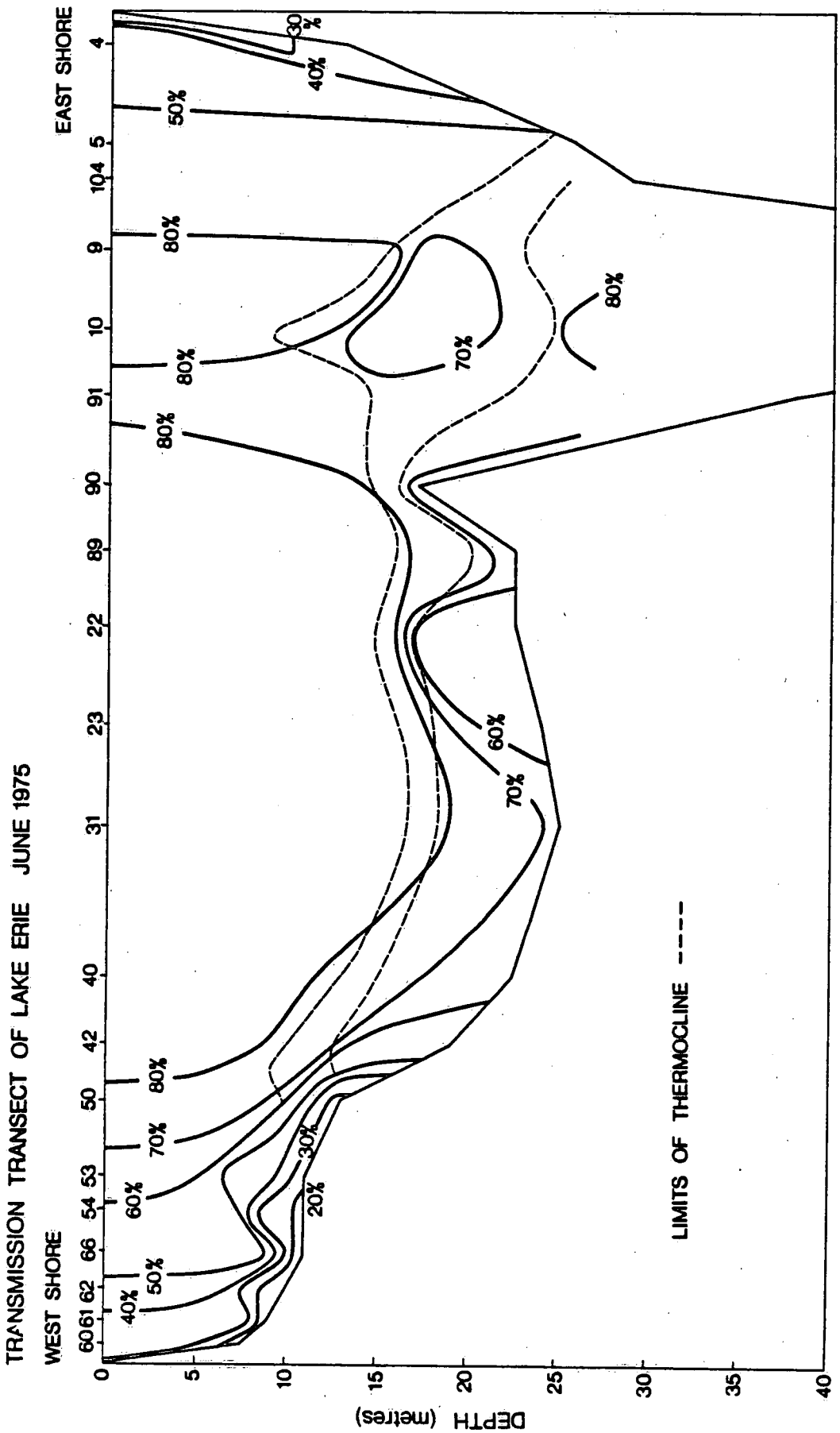
TRANSMISSION TRANSECT OF LAKE ERIE JUNE 1975
WEST SHORE
EAST SHORE
60 61 62 66 54 53 50 42 40 31 23 22 89 90 91 10 9 8 104 5 4
DEPTH (metres)
0 5 10 15 20 25 30 35 40
40%
50%
60%
70%
80%
80%
80%
80%
70%
80%
50%
40%
30%
60%
70%
80%
30%
20%
LIMITS OF THERMOCLINE ----

FIG. 63

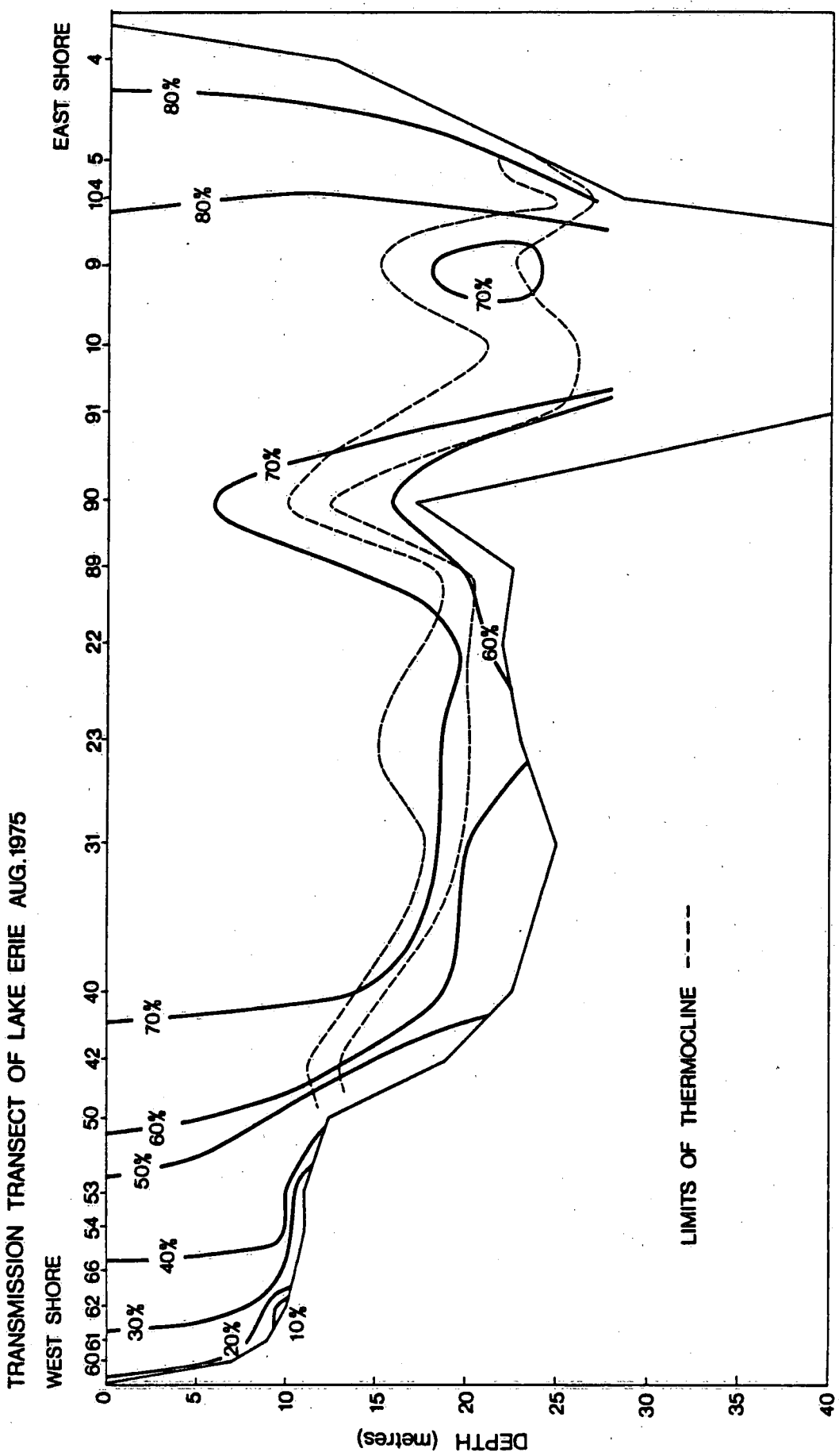
TRANSMISSION TRANSECT OF LAKE ERIE AUG. 1975
WEST SHORE
EAST SHORE
606162 66 54 53 50 42 40 31 23 22 89 90 91 10 9 104 5 4
80%
80%
70%
70%
60%
70%
60%
50%
40%
30%
20%
10%
LIMITS OF THERMOCLINE ----
DEPTH (metres)
0 5 10 15 20 25 30 35 40

FIG. 64

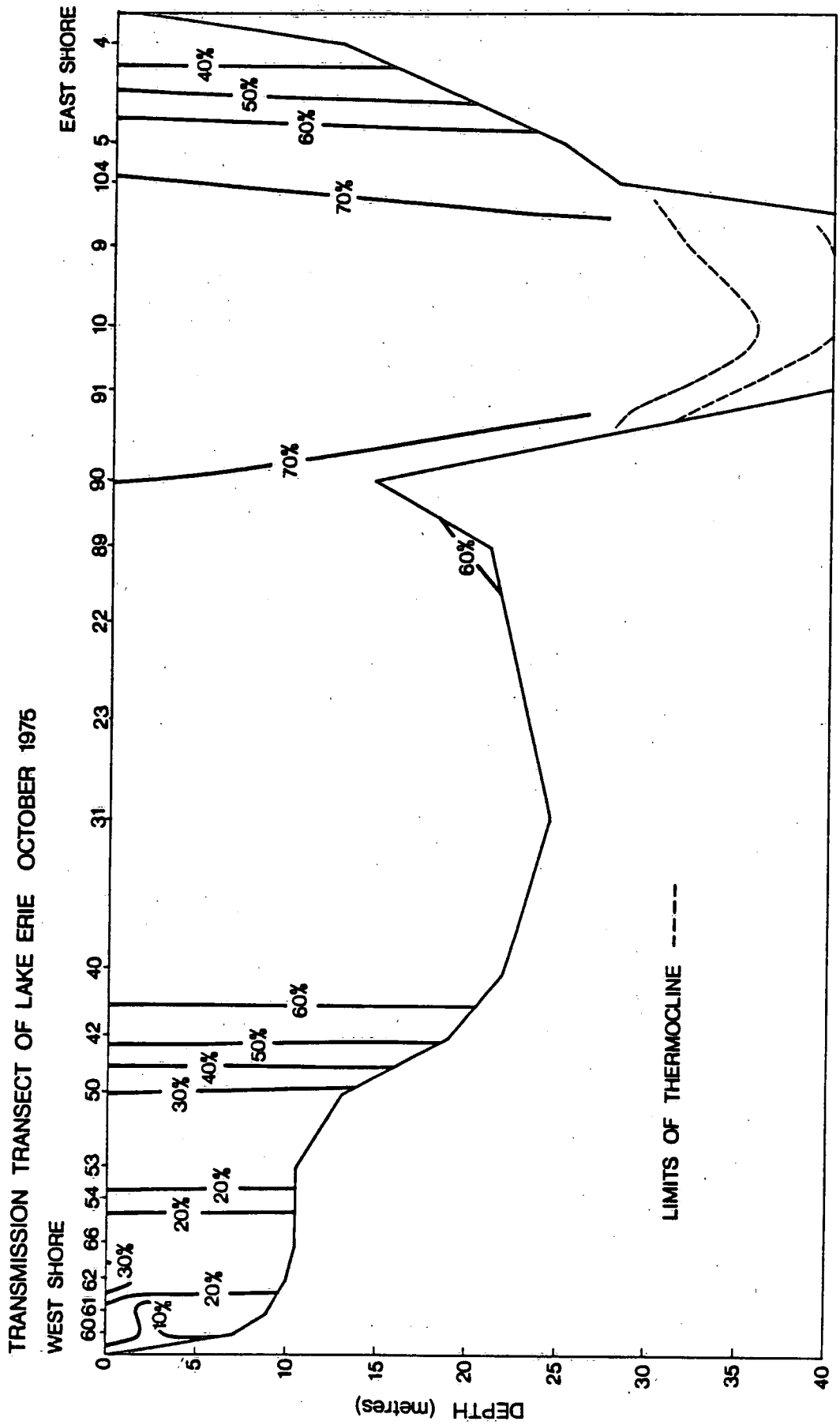
TRANSMISSION TRANSECT OF LAKE ERIE OCTOBER 1975
WEST SHORE
EAST SHORE
DEPTH (metres)
LIMITS OF THERMOCLINE ----
60 61 62 66 54 53 50 42 40 31 23 22 89 90 91 10 9 104 5 4
10%
20%
30%
40%
50%
60%
70%
0 5 10 15 20 25 30 35 40

FIG. 65

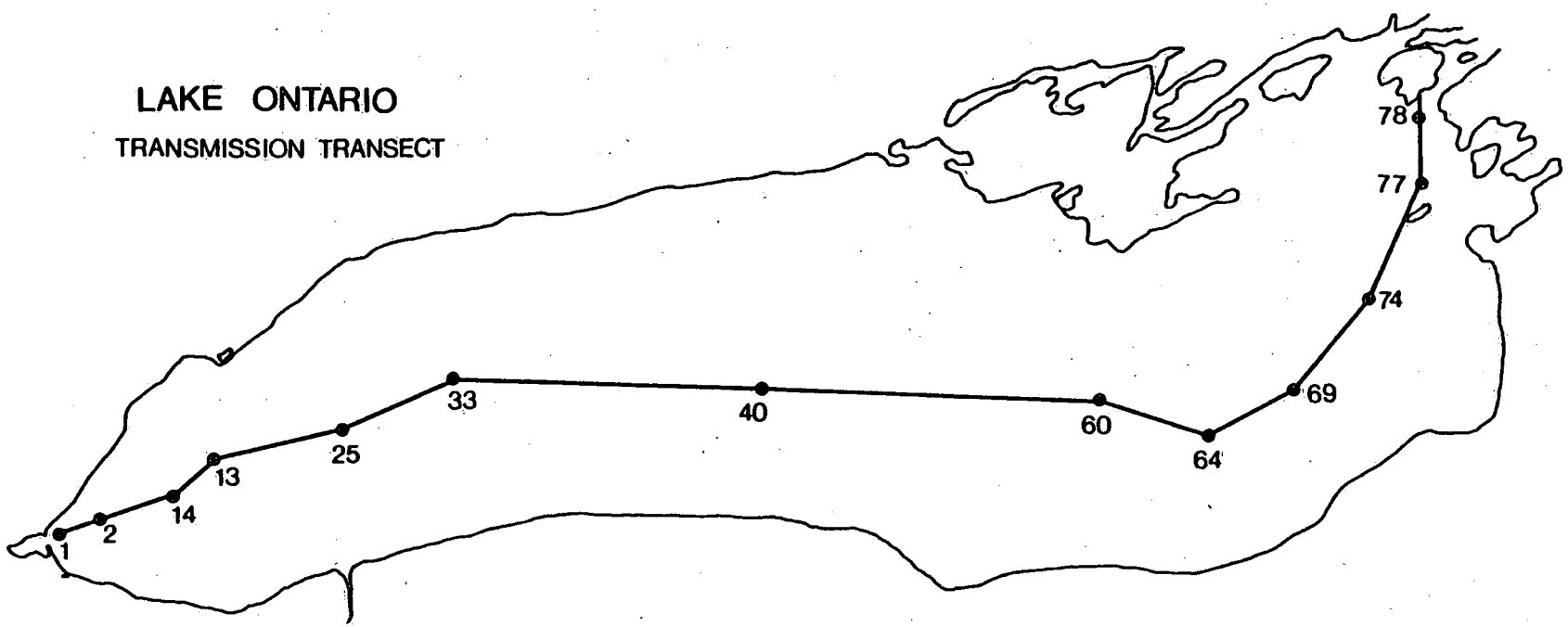
LAKE ONTARIO
TRANSMISSION TRANSECT
1
2
14
13
25
33
40
60
64
69
74
77
78

FIG. 66

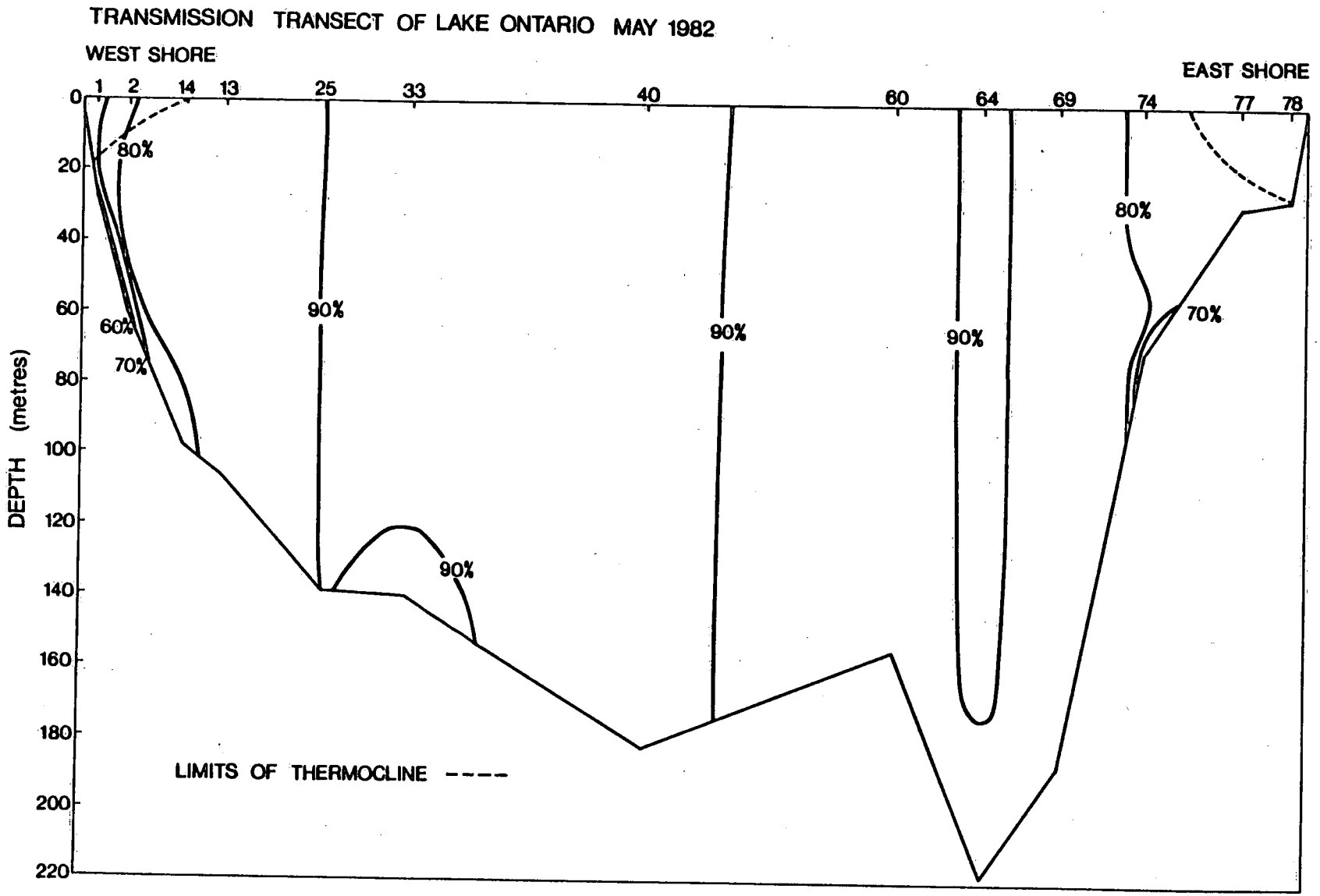
TRANSMISSION TRANSECT OF LAKE ONTARIO MAY 1982
WEST SHORE
EAST SHORE
1
2
14
13
25
33
40
60
64
69
74
77
78
0
20
40
60
80
100
120
140
160
180
200
220
DEPTH (metres)
80%
60%
70%
90%
90%
90%
90%
80%
70%
LIMITS OF THERMOCLINE ----

FIG. 67

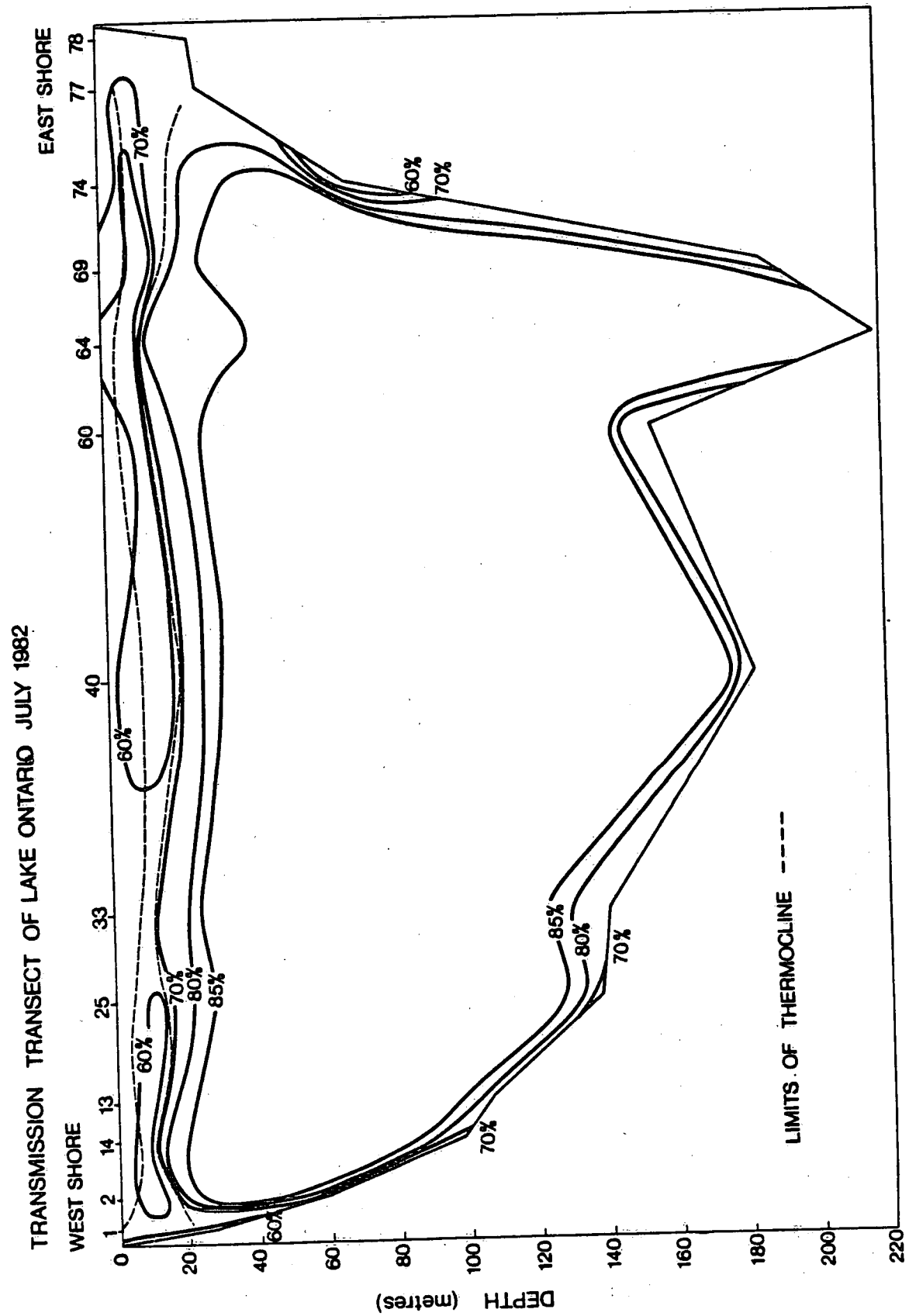
TRANSMISSION TRANSECT OF LAKE ONTARIO JULY 1982
WEST SHORE
EAST SHORE
1
2
14
13
25
33
40
60
64
69
74
77
78
0
20
40
60
80
100
120
140
160
180
200
220
DEPTH (meters)
60%
70%
80%
85%
LIMITS OF THERMOCLINE -----

FIG. 68

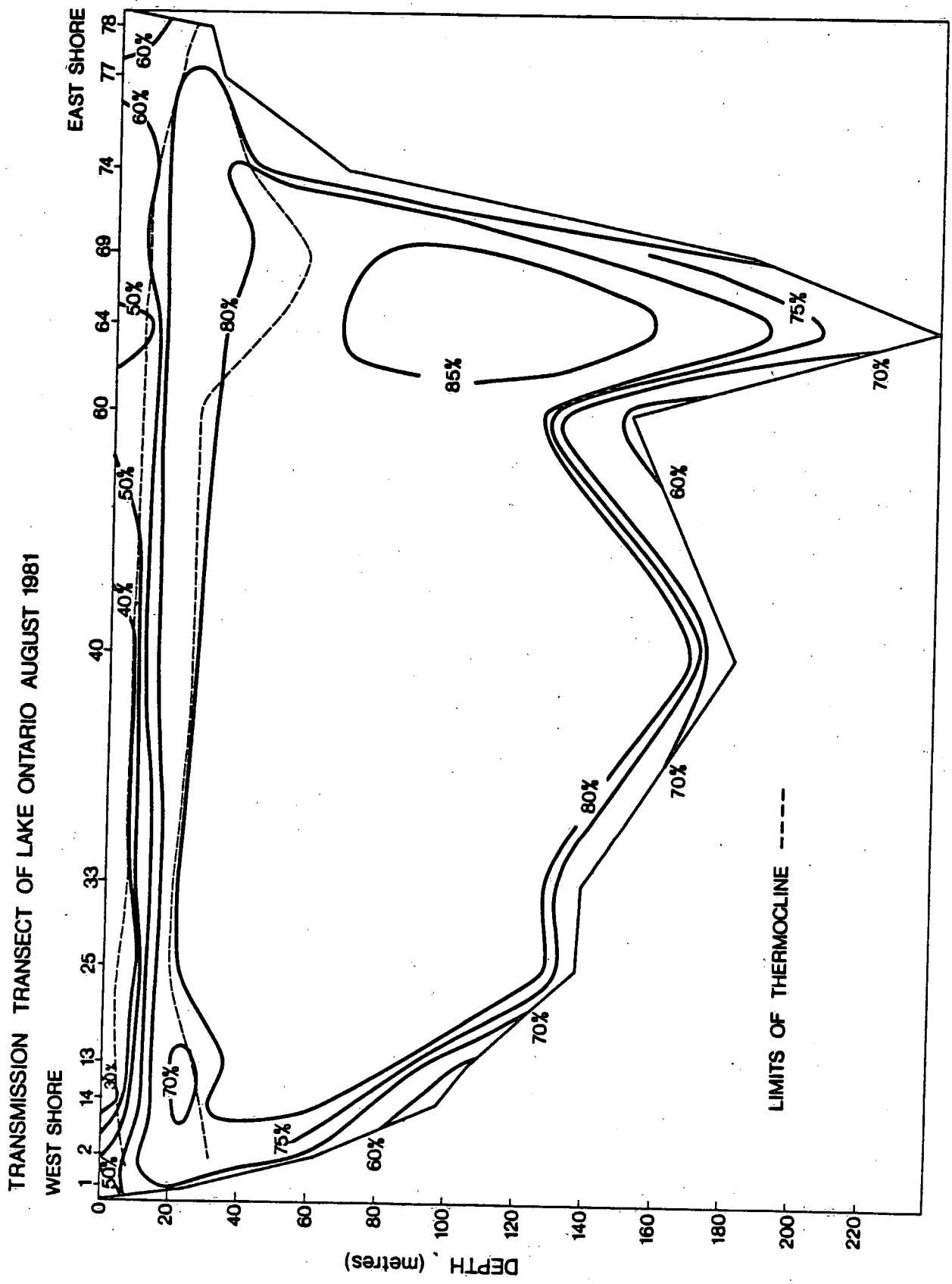
TRANSMISSION TRANSECT OF LAKE ONTARIO AUGUST 1981
WEST SHORE
EAST SHORE
0 1 2 13 14 25 33 40 60 64 69 74 77 78
DEPTH (metres)
0 20 40 60 80 100 120 140 160 180 200 220
50%
30%
70%
75%
60%
80%
85%
40%
LIMITS OF THERMOCLINE -----

FIG. 69

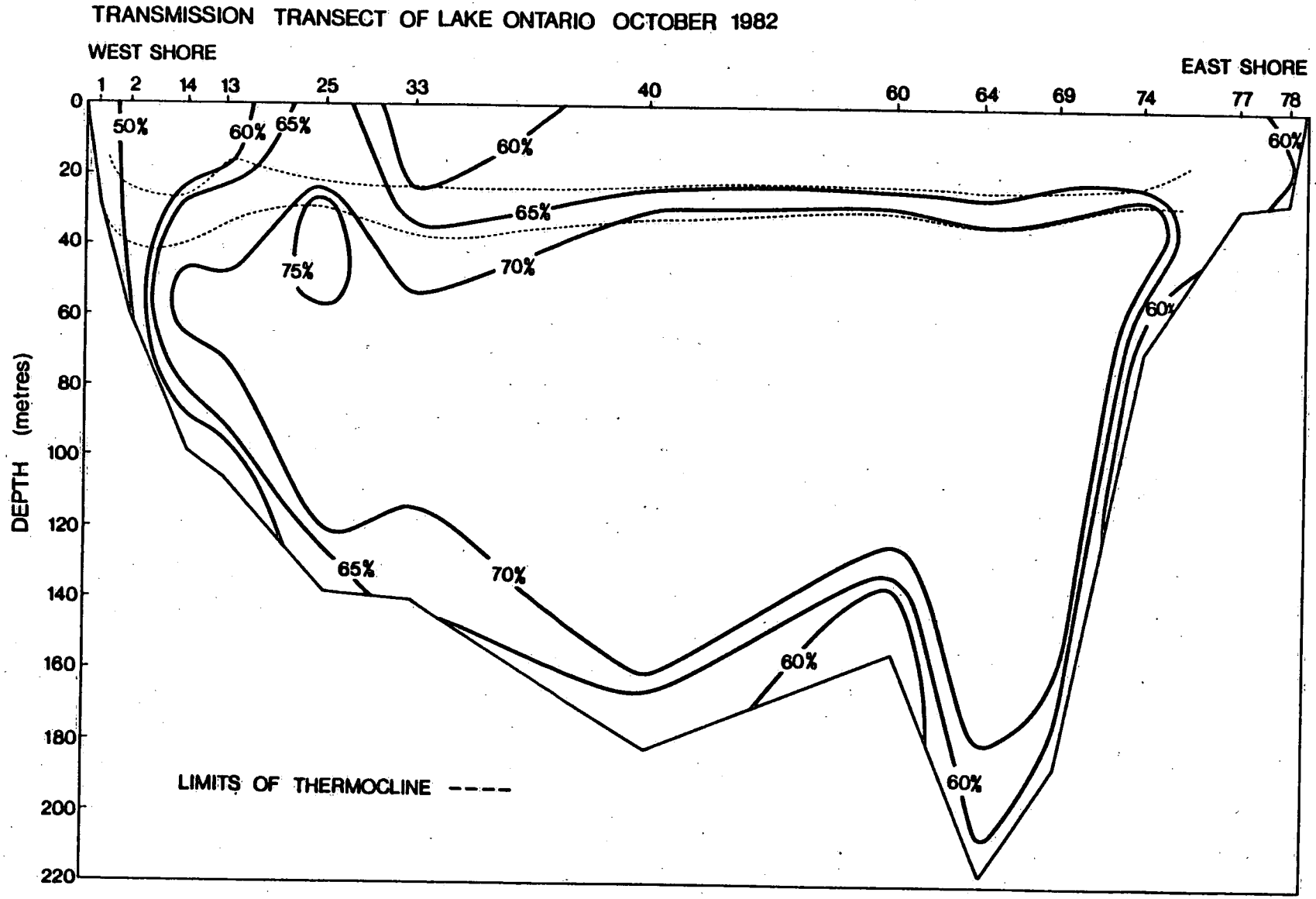
TRANSMISSION TRANSECT OF LAKE ONTARIO OCTOBER 1982
WEST SHORE
EAST SHORE
1 2 14 13 25 33 40 60 64 69 74 77 78
0 20 40 60 80 100 120 140 160 180 200 220
DEPTH (metres)
50%
60%
65%
60%
65%
75%
70%
60%
60%
65%
70%
60%
60%
LIMITS OF THERMOCLINE ----

FIG. 70

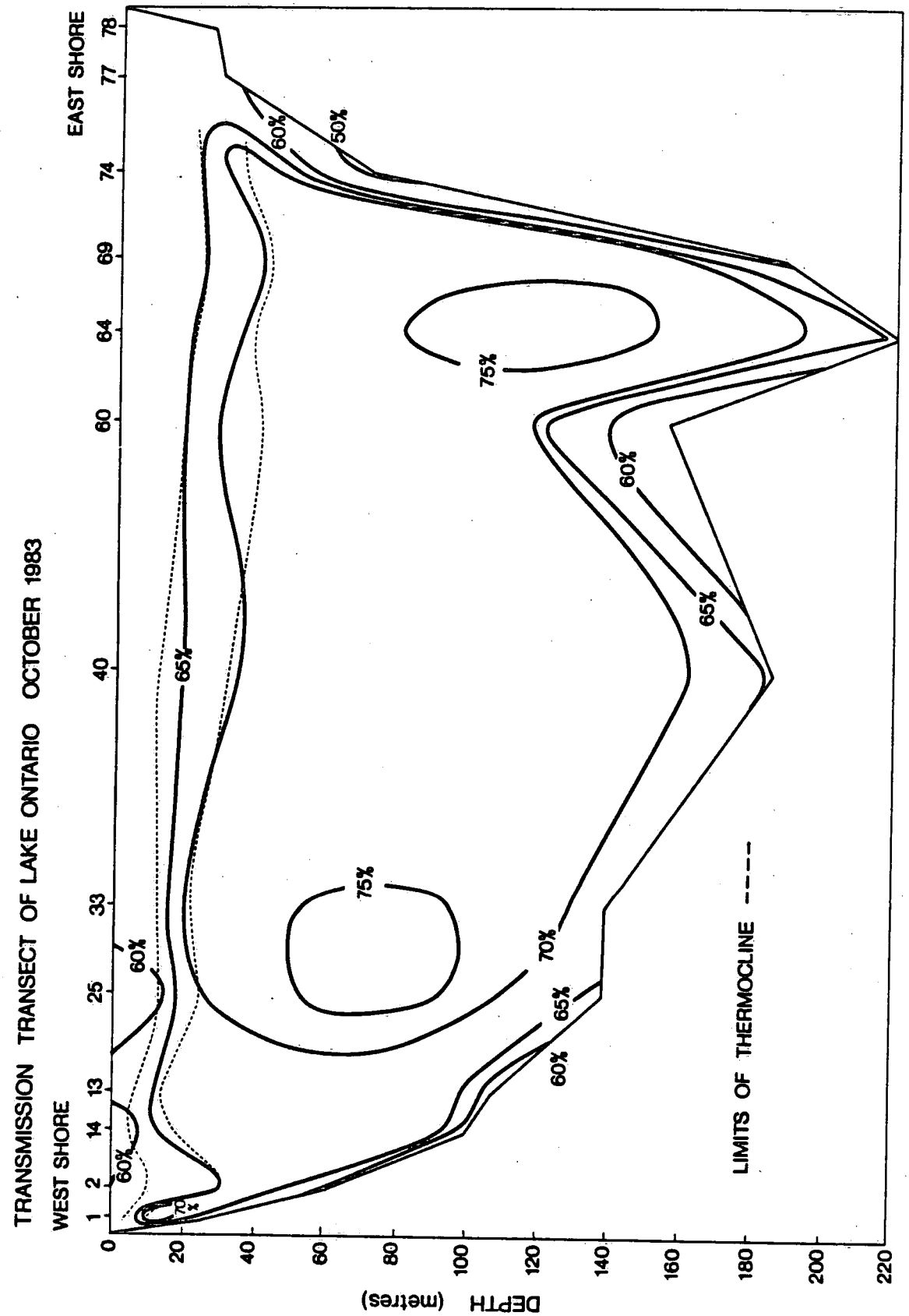
TRANSMISSION TRANSECT OF LAKE ONTARIO OCTOBER 1983
WEST SHORE
EAST SHORE
1 2 14 13 25 33 40 60 84 69 74 77 78
DEPTH (metres)
0 20 40 60 80 100 120 140 160 180 200 220
60%
65%
70%
75%
LIMITS OF THERMOCLINE ----

FIG. 71

BEAM ATTENUATION COEFFICIENT AND SECCHI DISC DEPTH

Figures 72-77 illustrate the intercomparisons between the inverse Secchi depth S^{-1} and the beam attenuation coefficient c. The values of c were calculated in the manner described in Part I of this report utilizing the percent transmission values directly obtained at a depth of 1 metre. Power law regressions between the (c, S^{-1}) data pairs were performed for each lake and the results are illustrated in Table 4. From Table 4 it is seen that the number of data pairs used in the regressions varied from 171 to 1442. The number of points defining the regressions illustrated in Figures 72-77 appear to be considerably less. For display purposes only, the data pairs have been averaged. All data pairs, however, have been included in the regression analyses.

Figure 78 illustrates an intercomparison of the regressions between c and S^{-1} for each of the lakes. It is evident that, in progressing from Lake Superior to Georgian Bay to Lake Ontario to Lake Huron to Lake Erie, a higher ratio of c to S^{-1} is generally encountered.

TABLE 4

Figure	Lake	Date	Path Length	FOV	Range of Secchi Disc Values	Number of Points in Regression	Mathematical Relationship
72	Superior	1973	1 m	2.3°	3 < S < 21 m	291	$C=2.85(S^{-1})^{0.80}$
73	Huron	1974	1 m	2.3°	1.5 < S < 20 m	184	$C=4.55(S^{-1})^{0.95}$
74	Georgian Bay	1974	1 m	2.3°	4 < S < 12 m	171	$C=3.90(S^{-1})^{0.90}$
75	Erie	1975	0.25 m	2.3°	0.5 < S < 10 m	347	$C=5.85(S^{-1})^{1.00}$
76	Ontario	1976-79	0.25 m	2.3°	1 < S < 10 m	1442	$C=4.35(S^{-1})^{0.90}$
77	Ontario	1980-82	0.25 m	0.9°	1 < S < 10 m	796	$C=5.45(S^{-1})^{0.70}$

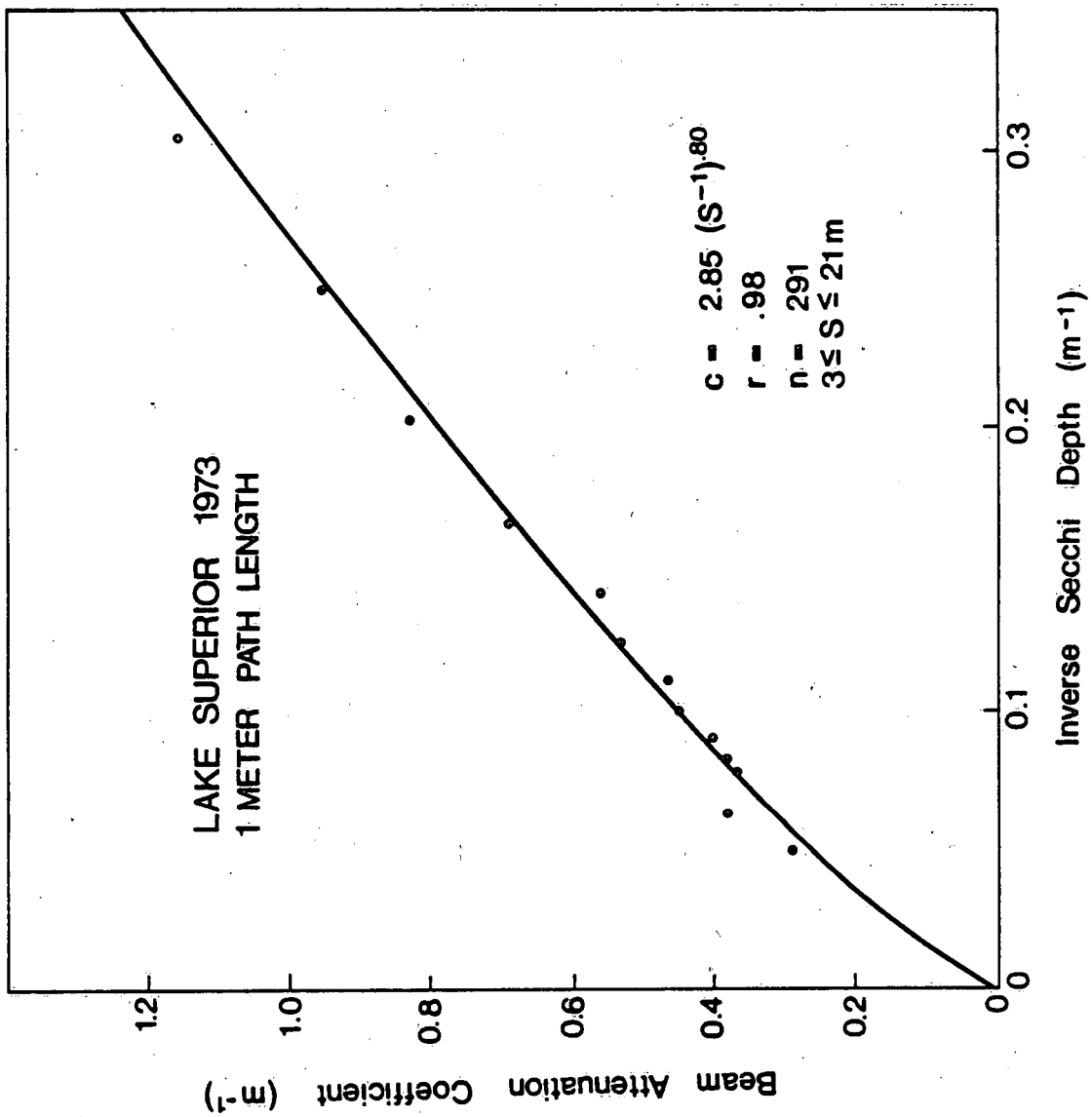
LAKE SUPERIOR 1973
1 METER PATH LENGTH
c = 2.85 (S⁻¹)·⁸⁰
r = .98
n = 291
3 ≤ S ≤ 21 m
Beam Attenuation Coefficient (m⁻¹)
Inverse Secchi Depth (m⁻¹)
0
0.2
0.4
0.6
0.8
1.0
1.2
0.1
0.2
0.3

FIG. 72

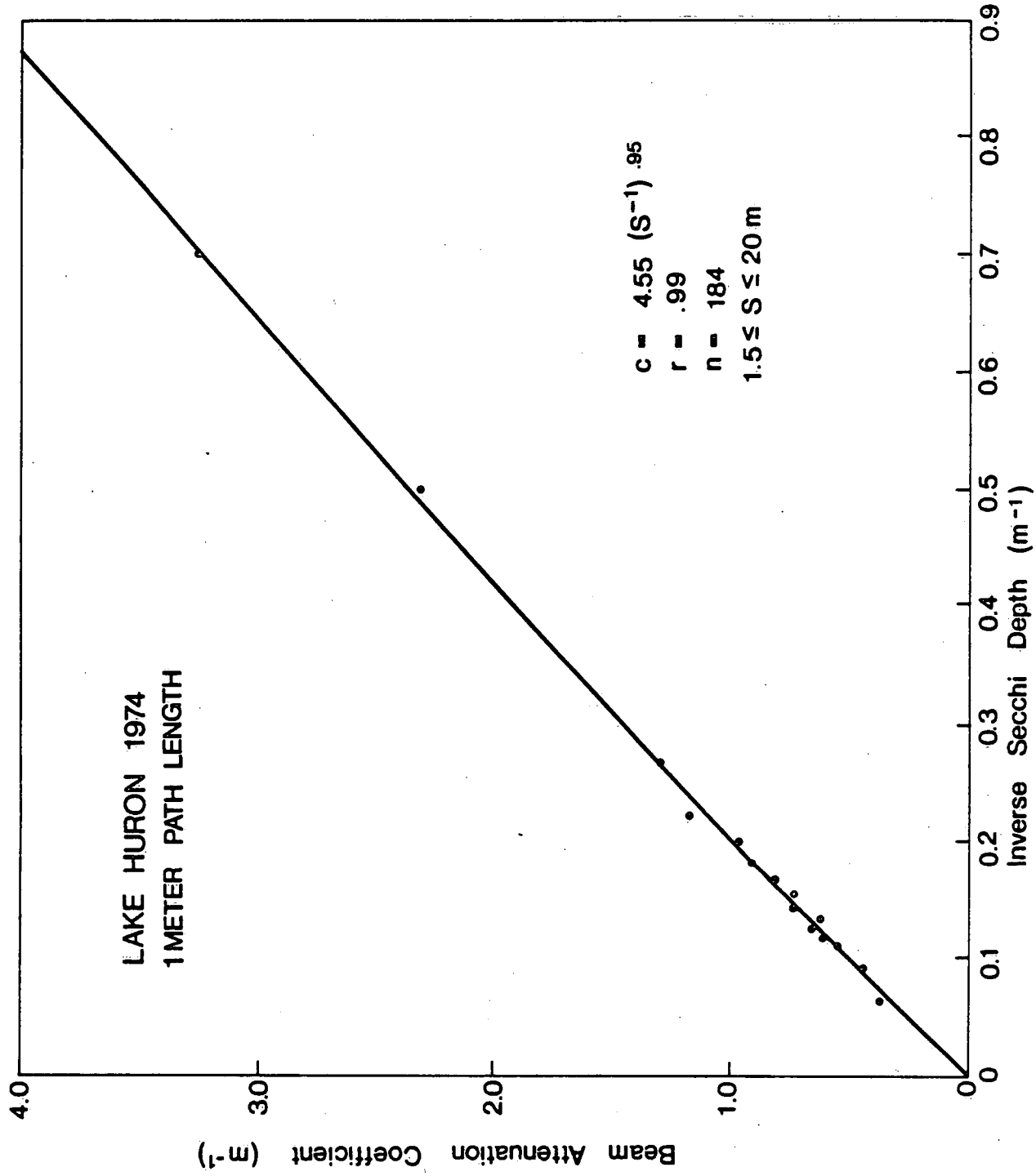
LAKE HURON 1974
1 METER PATH LENGTH
c = 4.55 (S⁻¹) .95
r = .99
n = 184
1.5 ≤ S ≤ 20 m
Beam Attenuation Coefficient (m⁻¹)
Inverse Secchi Depth (m⁻¹)
0
1.0
2.0
3.0
4.0
0.1
0.2
0.3
0.4
0.5
0.6
0.7
0.8
0.9

FIG. 73

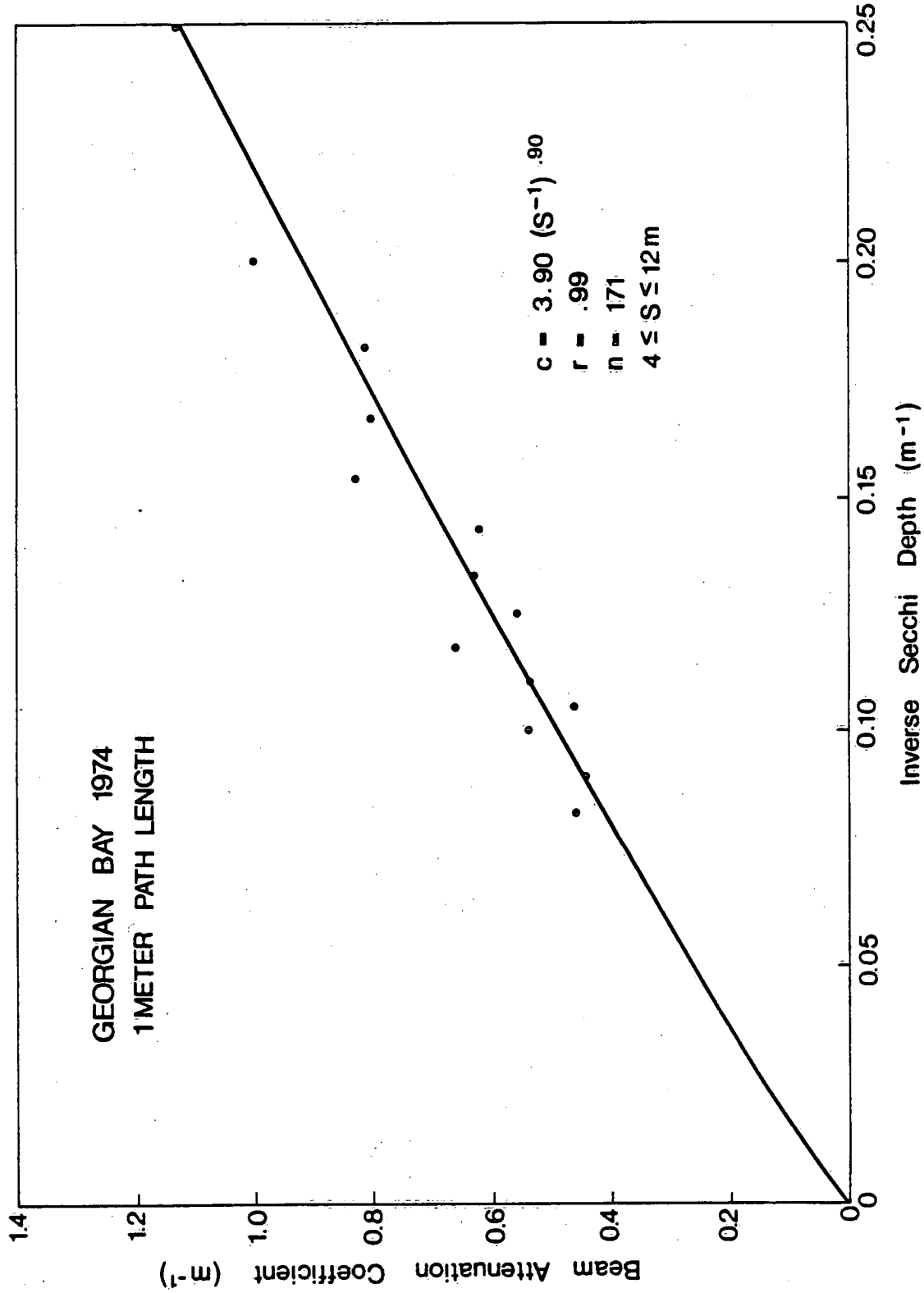
GEORGIAN BAY 1974
1 METER PATH LENGTH
c = 3.90 (S⁻¹) .90
r = .99
n = 171
4 ≤ S ≤ 12 m
Beam Attenuation Coefficient (m⁻¹)
Inverse Secchi Depth (m⁻¹)
0
0.2
0.4
0.6
0.8
1.0
1.2
1.4
0.05
0.10
0.15
0.20
0.25

FIG. 74

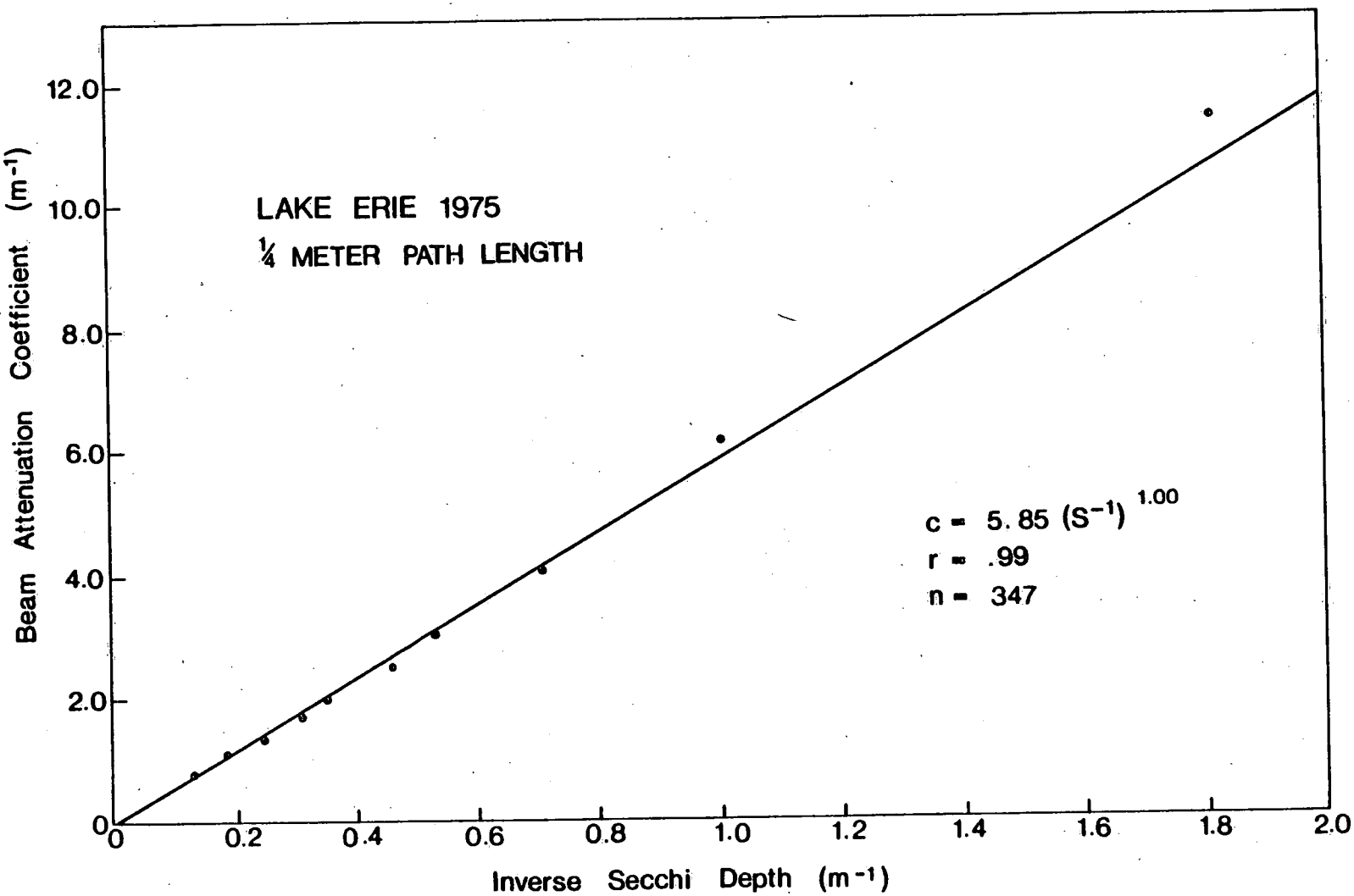
LAKE ERIE 1975
¼ METER PATH LENGTH
c = 5.85 (S⁻¹) 1.00
r = .99
n = 347
Beam Attenuation Coefficient (m⁻¹)
Inverse Secchi Depth (m⁻¹)
0
2.0
4.0
6.0
8.0
10.0
12.0
0.2
0.4
0.6
0.8
1.0
1.2
1.4
1.6
1.8
2.0

FIG. 75

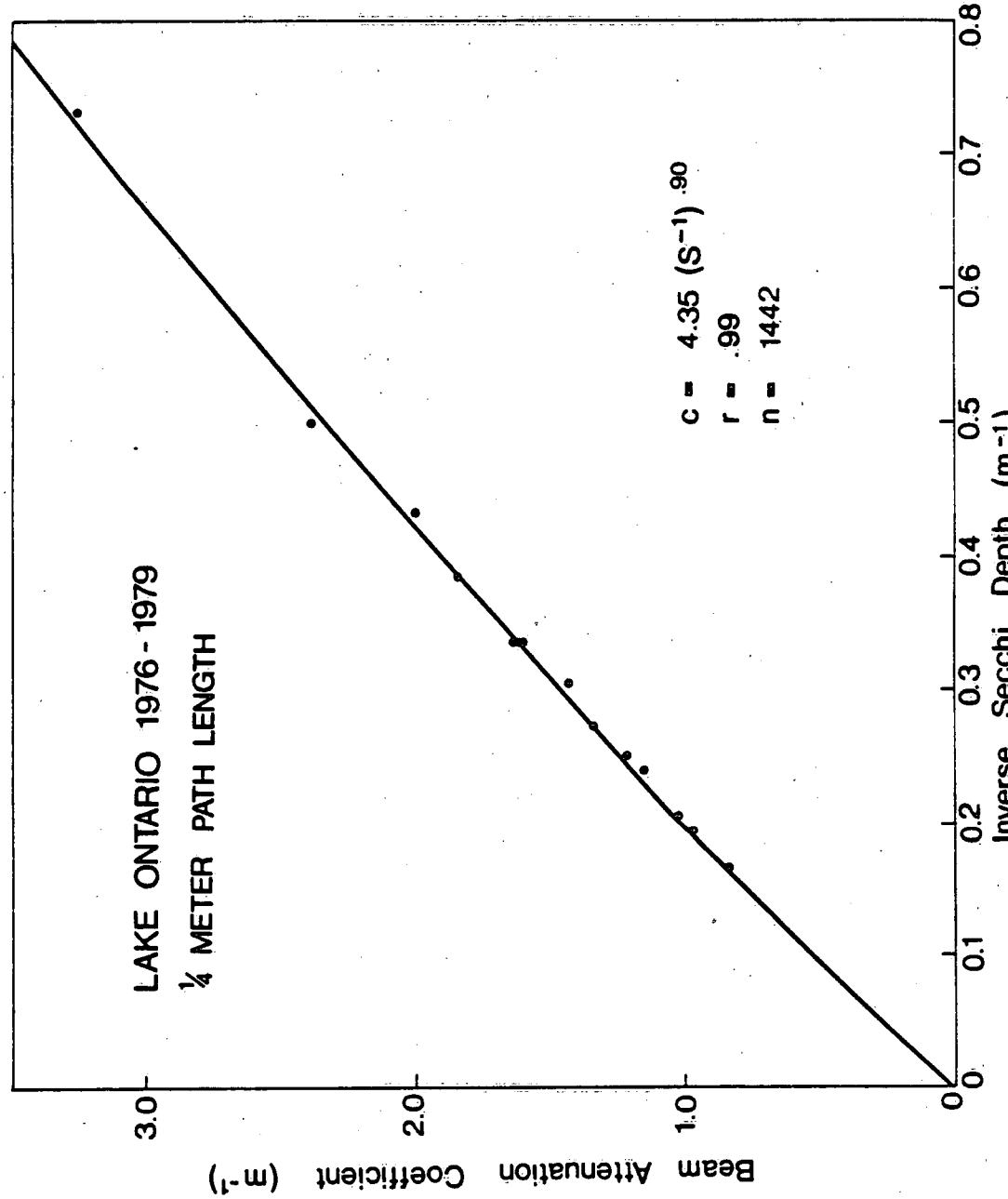
LAKE ONTARIO 1976 - 1979
¼ METER PATH LENGTH
c = 4.35 (S⁻¹) ·90
r = .99
n = 1442
Beam Attenuation Coefficient (m⁻¹)
Inverse Secchi Depth (m⁻¹)
0
1.0
2.0
3.0
0
0.1
0.2
0.3
0.4
0.5
0.6
0.7
0.8

FIG. 76

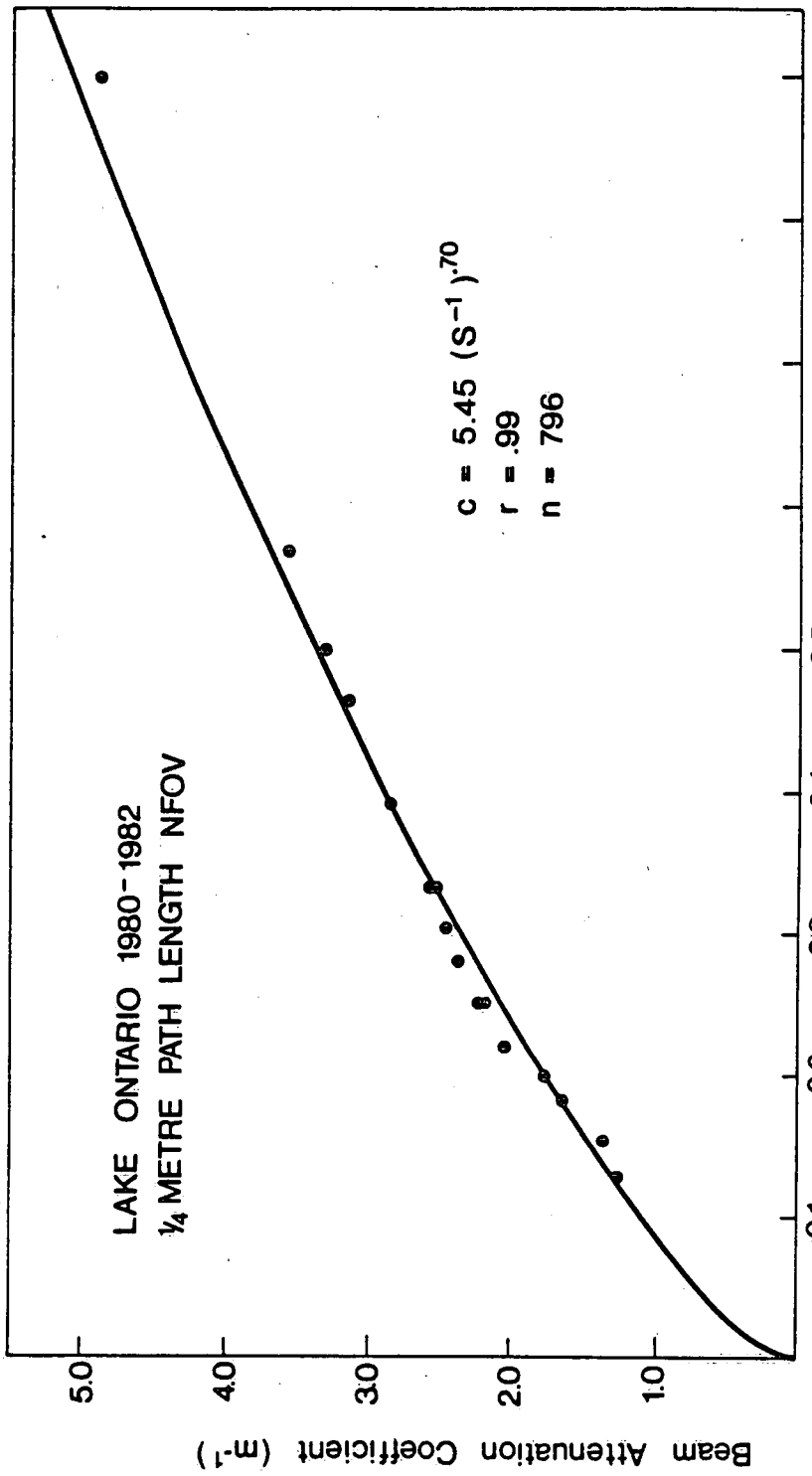
LAKE ONTARIO 1980-1982
¼ METRE PATH LENGTH NFOV
c = 5.45 (S⁻¹).70
r = .99
n = 796
Beam Attenuation Coefficient (m⁻¹)
Inverse Secchi Depth (m⁻¹)
1.0
2.0
3.0
4.0
5.0
0.1
0.2
0.3
0.4
0.5
0.6
0.7
0.8
0.9

FIG. 77

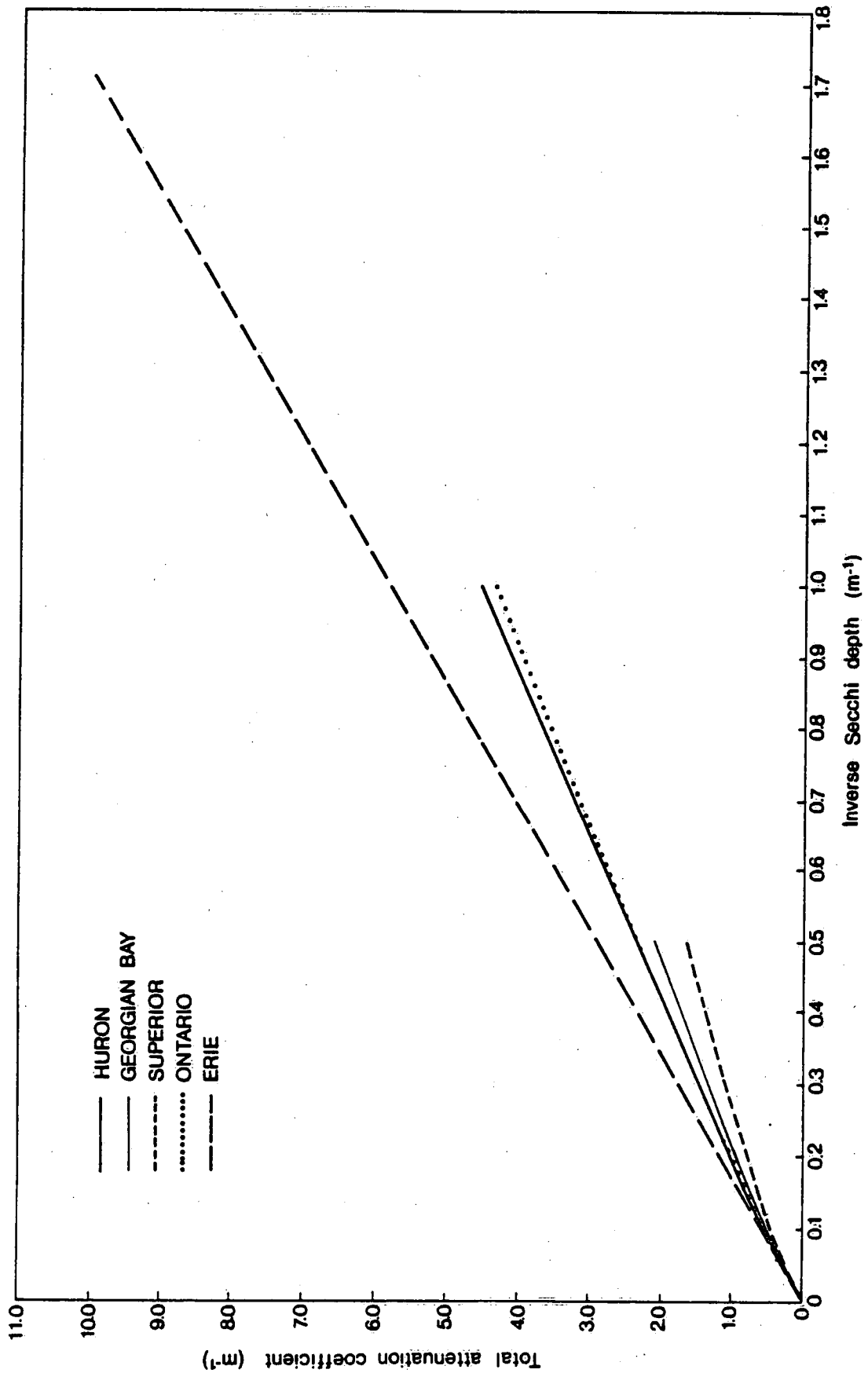
HURON
GEORGIAN BAY
SUPERIOR
ONTARIO
ERIE
Total attenuation coefficient (m⁻¹)
Inverse Secchi depth (m⁻¹)
0
1.0
2.0
3.0
4.0
5.0
6.0
7.0
8.0
9.0
10.0
11.0
0.1
0.2
0.3
0.4
0.5
0.6
0.7
0.8
0.9
1.0
1.1
1.2
1.3
1.4
1.5
1.6
1.7
1.8

FIG. 78

IRRADIANCE ATTENUATION COEFFICIENT AND BEAM ATTENUATION COEFFICIENT

Figures 79-83 illustrate the intercomparisons between the beam attenuation coefficient c and the irradiance attenuation coefficient of the photosynthetic available radiation, k_{PAR}, (See Part I of this report). Linear regressions were performed for the (c,k_{PAR}) data pairs, and the results are summarized in Table 5. The path length and field of view (FOV) appropriate for all the data utilized to calculate c are 1 m and 2.3°, respectively.

Figure 84 illustrates an intercomparison of these regressions between c and k_{PAR} for the general range of values of these parameters observable in each lake.

TABLE 5

Figure	Lake	Date	Number of Points in Regression	Mathematical Relationship
79	Superior	1973	34	k_{PAR}=0.195C+0.08
80	Huron	1974	29	k_{PAR}=0.160C+0.06
81	Georgian Bay	1974	23	k_{PAR}=0.185C+0.06
82	Erie	1975	25	k_{PAR}=0.220C+0.01
83	Ontario	1975	22	k_{PAR}=0.185C+0.02

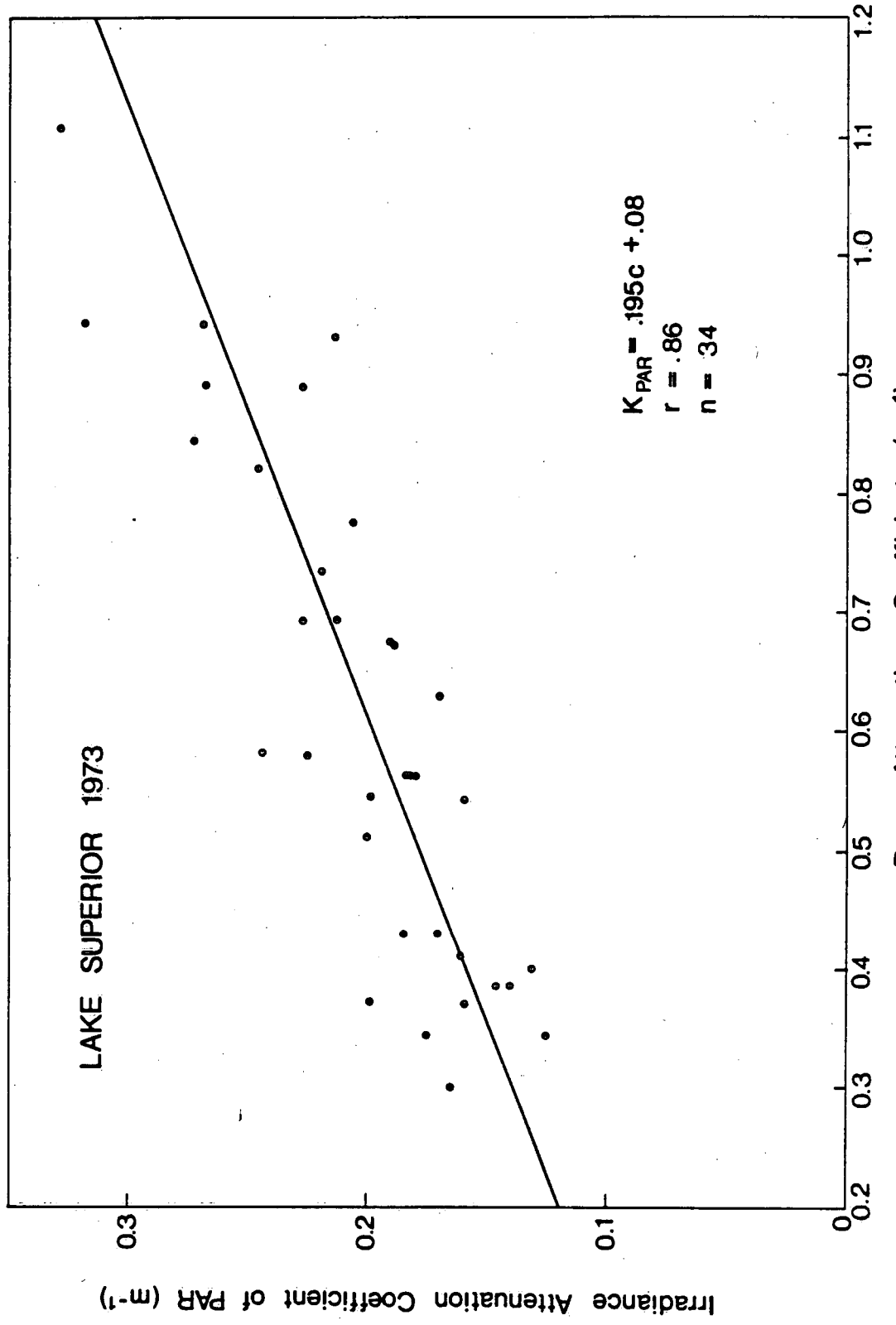
LAKE SUPERIOR 1973
K_{PAR} = .195c + .08
r = .86
n = 34
Irradiance Attenuation Coefficient of PAR (m^{-1})
Beam Attenuation Coefficient (m^{-1})
0.1
0.2
0.3
0
0.2
0.3
0.4
0.5
0.6
0.7
0.8
0.9
1.0
1.1
1.2

FIG. 79

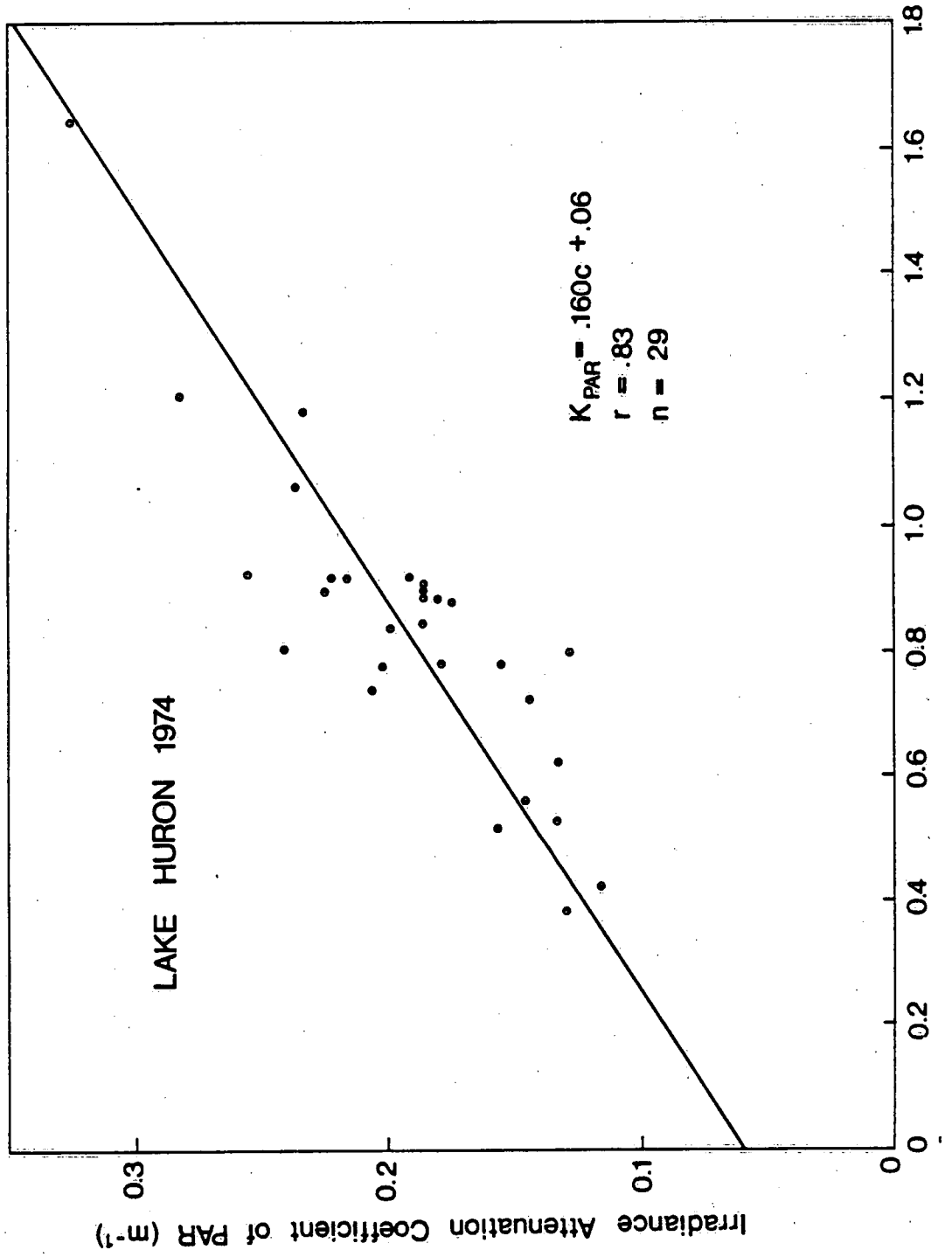
LAKE HURON 1974
K_{PAR} = .160c + .06
r = .83
n = 29
Irradiance Attenuation Coefficient of PAR (m^{-1})
Beam Attenuation Coefficient (m^{-1})
0
0.1
0.2
0.3
0.2
0.4
0.6
0.8
1.0
1.2
1.4
1.6
1.8

FIG. 80

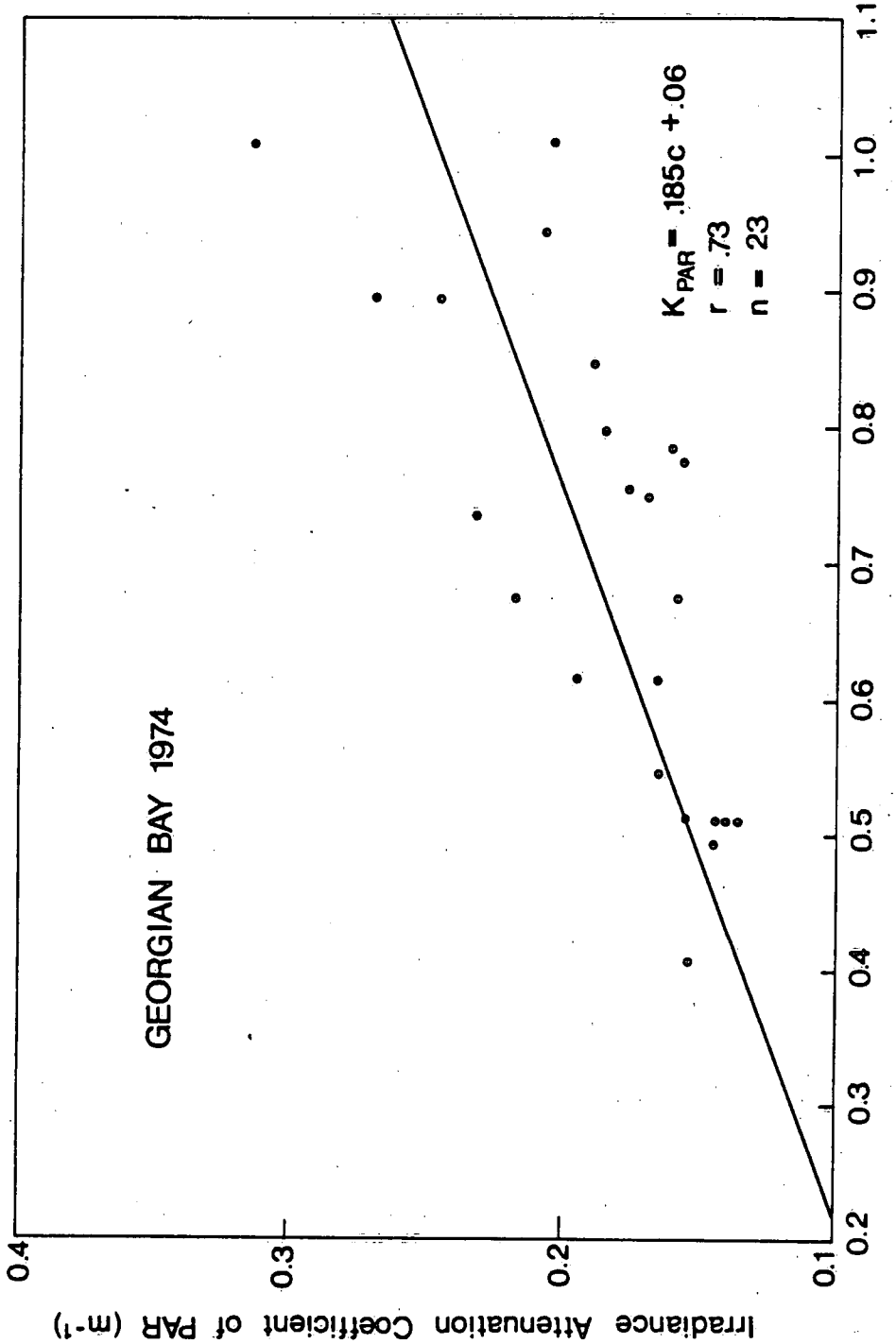
GEORGIAN BAY 1974
K_{PAR} = .185c + .06
r = .73
n = 23
Irradiance Attenuation Coefficient of PAR (m^{-1})
Beam Attenuation Coefficient (m^{-1})
0.1
0.2
0.3
0.4
0.2
0.3
0.4
0.5
0.6
0.7
0.8
0.9
1.0
1.1

FIG. 81

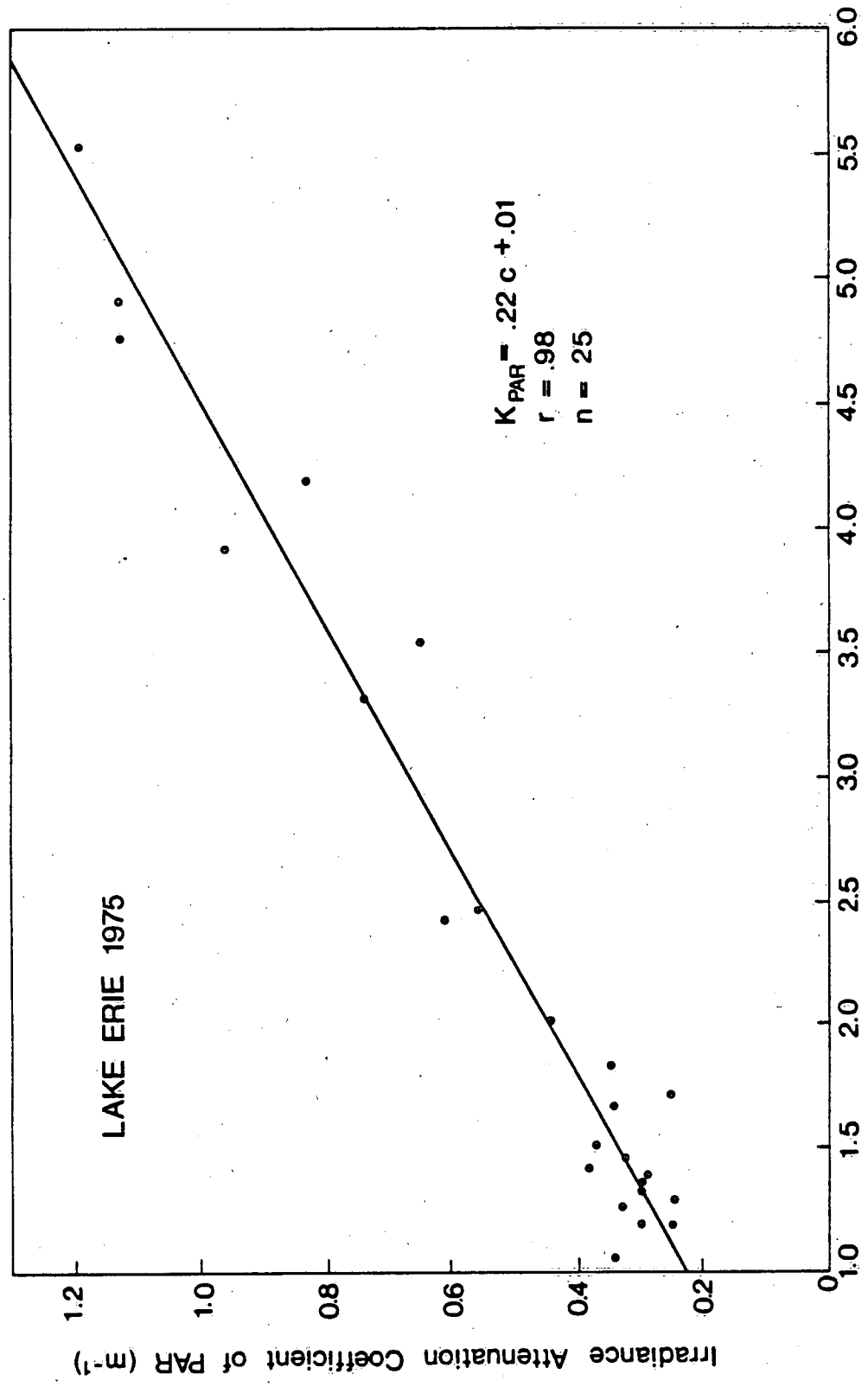
LAKE ERIE 1975
K_{PAR} = .22 c + .01
r = .98
n = 25
Irradiance Attenuation Coefficient of PAR (m^{-1})
Beam Attenuation Coefficient (m^{-1})
0.2
0.4
0.6
0.8
1.0
1.2
1.0
1.5
2.0
2.5
3.0
3.5
4.0
4.5
5.0
5.5
6.0

FIG. 82

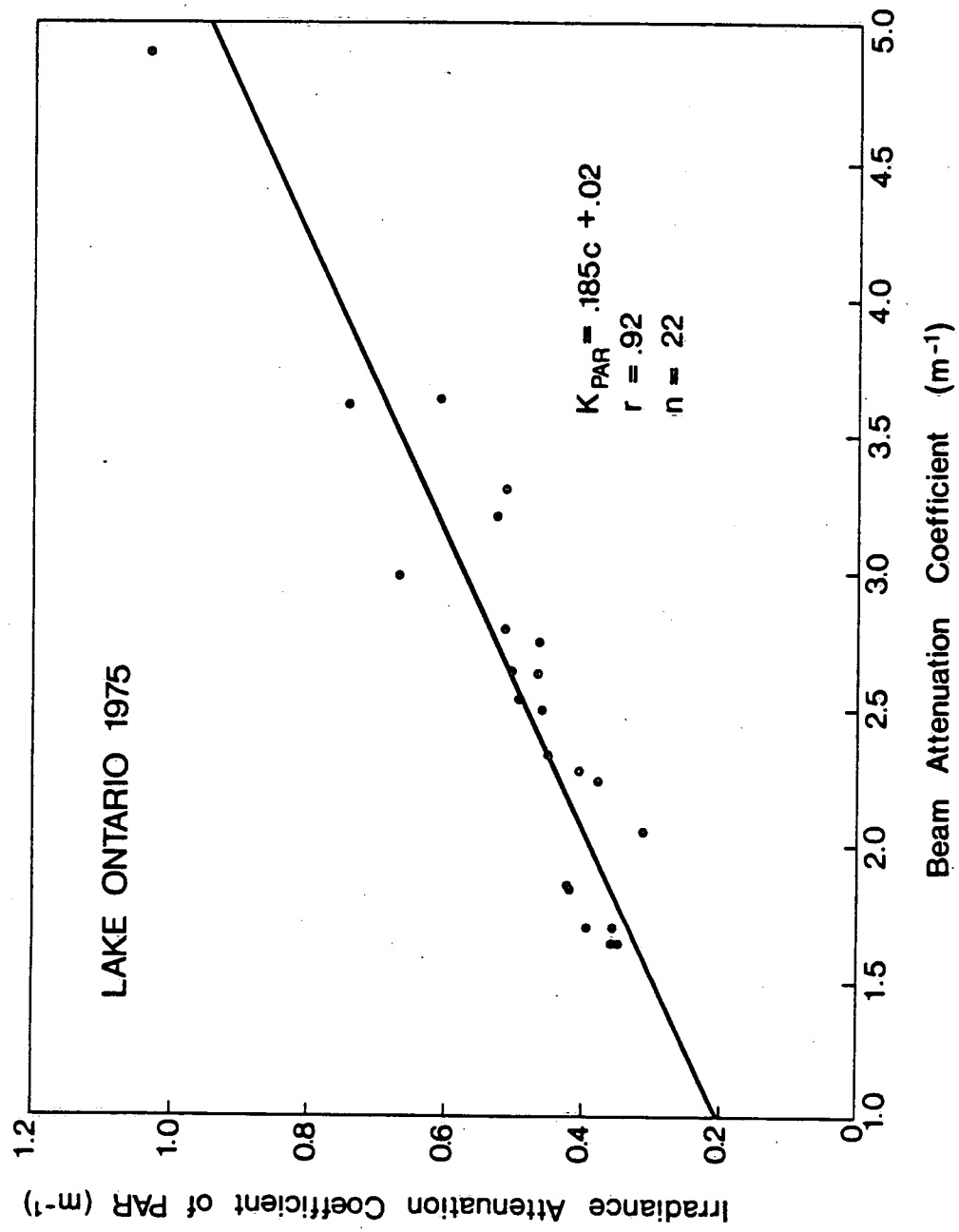
LAKE ONTARIO 1975
K_{PAR} = .185c + .02
r = .92
n = 22
Irradiance Attenuation Coefficient of PAR (m^{-1})
Beam Attenuation Coefficient (m^{-1})
0
0.2
0.4
0.6
0.8
1.0
1.2
1.0
1.5
2.0
2.5
3.0
3.5
4.0
4.5
5.0

FIG. 83

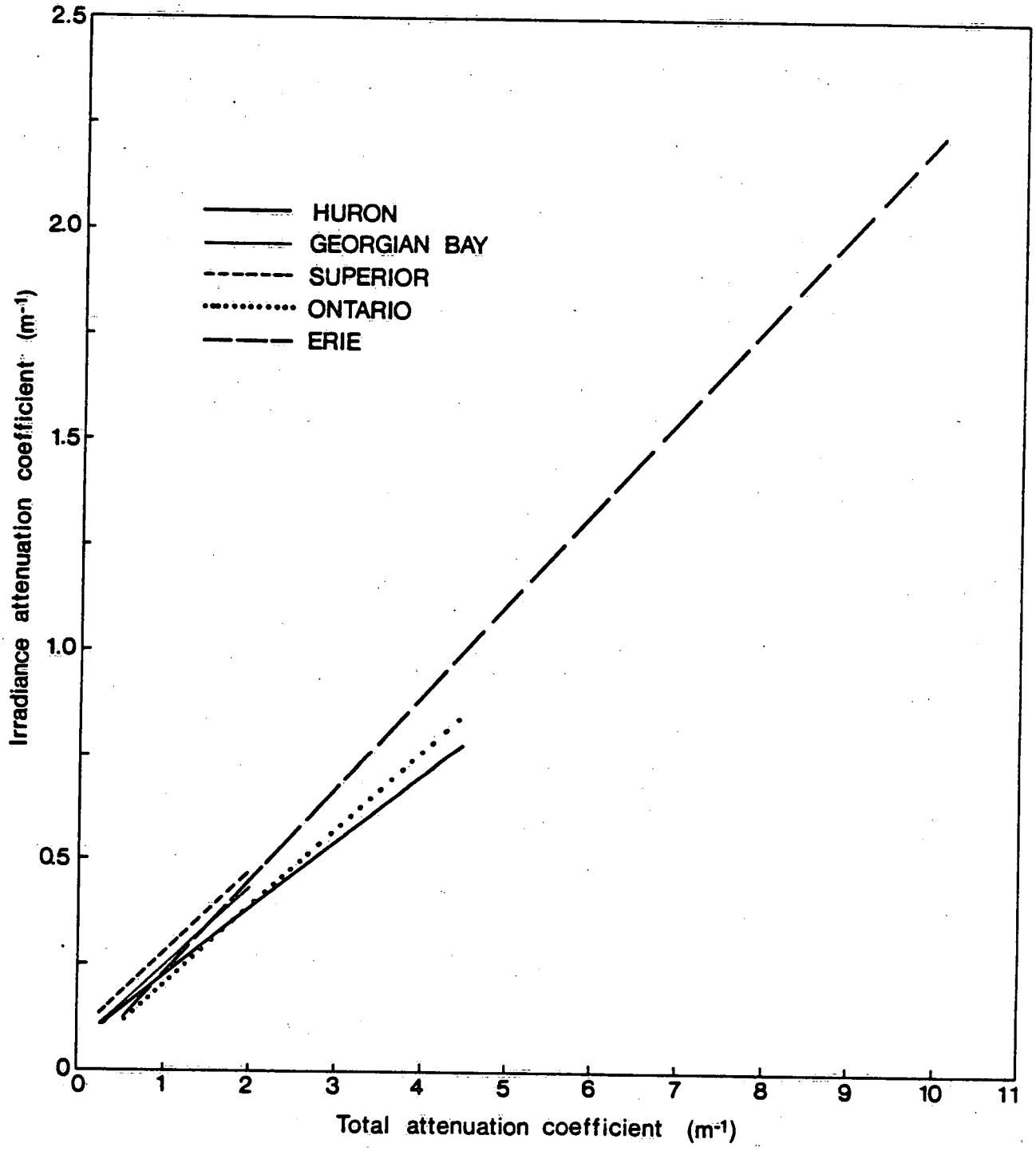
HURON
GEORGIAN BAY
SUPERIOR
ONTARIO
ERIE
Irradiance attenuation coefficient (m-1)
Total attenuation coefficient (m-1)
0
0.5
1.0
1.5
2.0
2.5
0
1
2
3
4
5
6
7
8
9
10
11

FIG. 84

IRRADIANCE ATTENUATION COEFFICIENT AND SECCHI DISC DEPTH

The equations defining the irradiance attenuation coefficient for PAR (k_{PAR}) as a function of the beam attenuation coefficient, c, for each lake monitored are given in Table 5. The equations defining the beam attenuation coefficient, c, as a function of the inverse Secchi disc depth, S^{-1}, are given in Table 4. Clearly, therefore, k_{PAR} may be expressed as a function of S^{-1}. These mathematical relationships between k_{PAR} and S^{-1} would reflect the power law relationship that exists between c and S^{-1}. However, since the power exponents recorded in Table 4 for the 2.3° FOV transmissometer data are very close to unity (the largest departure from unity is the 0.80 exponent appropriate to Lake Superior), the regression curves of Figures 72-77 were fitted to straight lines. Thus the relationships between k_{PAR} and S^{-1} have been simplified to linear representations. These relationships relating k_{PAR} to S^{-1} for each lake are included in Table 6 along with the range of Secchi disc depth values for which the linearity approximation will apply. These ranges of Secchi disc depth values, however, generally encompass the range of values normally observed in those waters.

Figure 85 illustrates the relationships between k_{PAR} and S^{-1} for each lake monitored. It is readily seen that Lakes Huron, Superior and Ontario and Georgian Bay display distinctly similar

similar (k_{PAR}, S^{-1}) regressions, while Lake Erie displays a markedly different regression with a slope which is ~50% higher than the slopes observed for the other water bodies. Figure 86 illustrates the (k_{PAR}, S^{-1}) regressions over the common range of Secchi disc depths $\geq$2 m. Figure 87 illustrates the effect of averaging the regressions of Lakes Superior, Huron and Ontario and Georgian Bay into a single relationship over the range $2m \leq S \leq 10$ m. Consequently, with the exclusion of Lake Erie, the Great Lakes waters monitored by the NWRI surveillance program may be defined by the single relationship

$$k_{PAR} = 0.757\ S^{-1} + 0.07$$

over the range $2\ m \leq S \leq 10$ m.

The average percent difference between the use of this single equation and the actual regression obtained for each lake is as follows:

Lake Huron : 2%

Lake Superior : 5%

Lake Ontario : 7%

Georgian Bay : 5%

TABLE 6

Lake	Range of Secchi Disc Values	Mathematical Relationship
Superior	2 m < S < 20 m	$k_{PAR}=0.67S^{-1}+0.10$
Huron	1 m < S < 20 m	$k_{PAR}=0.74S^{-1}+0.07$
Georgian Bay	2 m < S < 20 m	$k_{PAR}=0.81S^{-1}+0.07$
Erie	0.5 m < S < 10 m	$k_{PAR}=1.28S^{-1}$
Ontario	1 m < S < 3 m	$k_{PAR}=0.76S^{-1}+0.06$
Ontario	3 m < S < 10 m	$k_{PAR}=0.86S^{-1}+0.03$

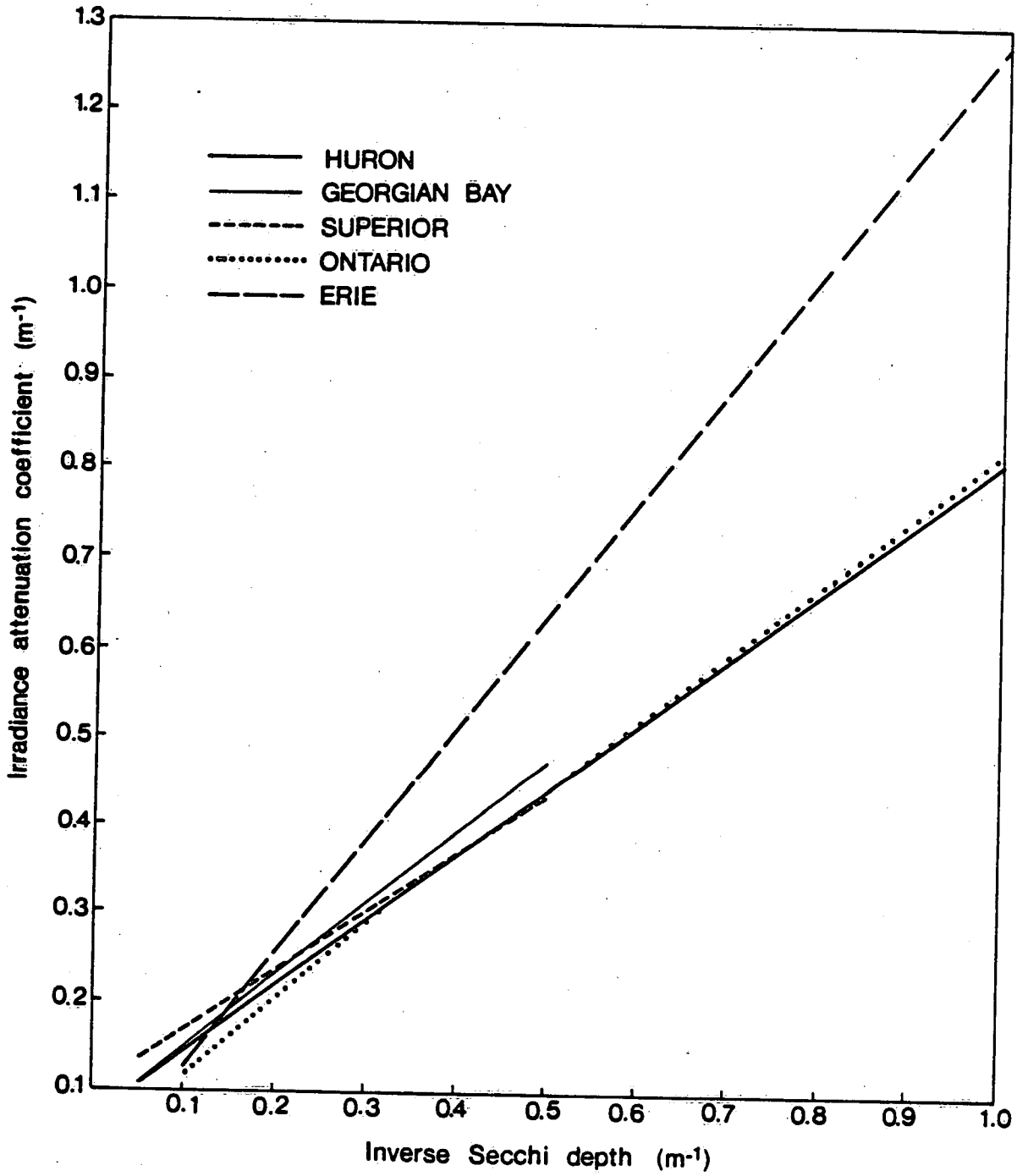
HURON
GEORGIAN BAY
SUPERIOR
ONTARIO
ERIE
Irradiance attenuation coefficient (m-1)
Inverse Secchi depth (m-1)
1.3
1.2
1.1
1.0
0.9
0.8
0.7
0.6
0.5
0.4
0.3
0.2
0.1
0.1
0.2
0.3
0.4
0.5
0.6
0.7
0.8
0.9
1.0

FIG. 85

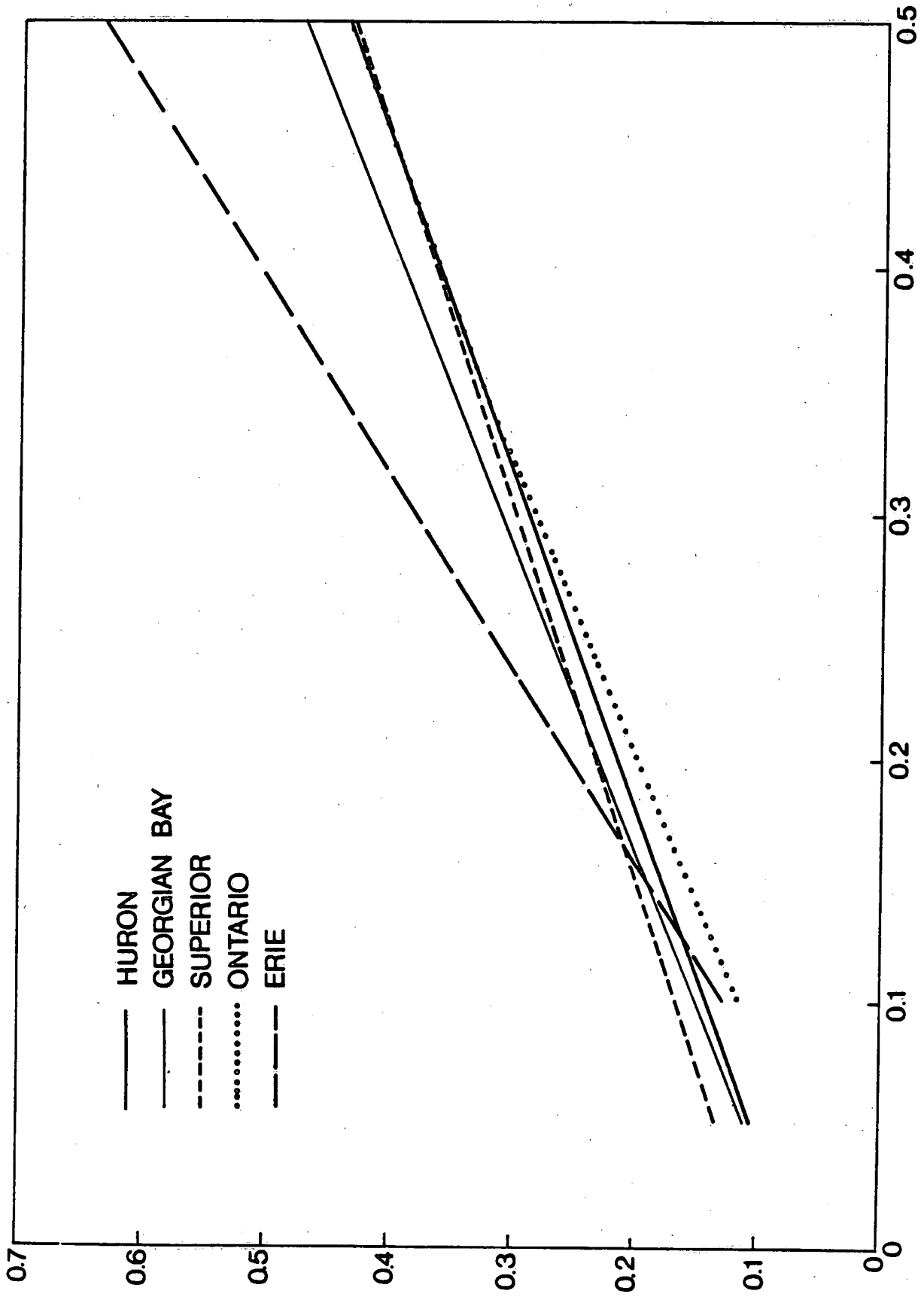
HURON
GEORGIAN BAY
SUPERIOR
ONTARIO
ERIE
Irradiance attenuation coefficient (m-1)
Inverse Secchi depth (m-1)
0
0.1
0.2
0.3
0.4
0.5
0.6
0.7

FIG. 86

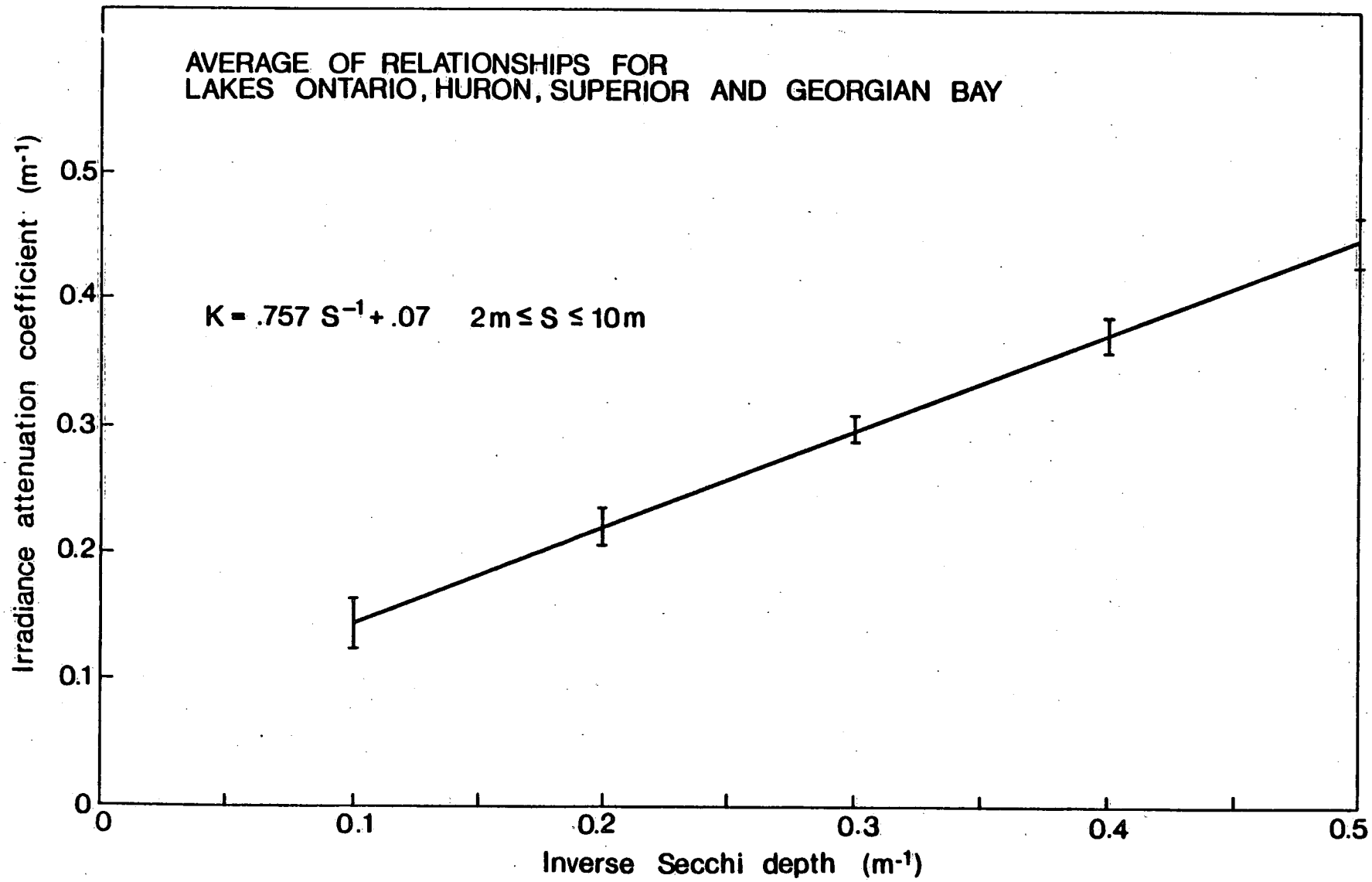
AVERAGE OF RELATIONSHIPS FOR
LAKES ONTARIO, HURON, SUPERIOR AND GEORGIAN BAY
K = .757 S⁻¹ + .07 2m ≤ S ≤ 10m
Irradiance attenuation coefficient (m⁻¹)
0
0.1
0.2
0.3
0.4
0.5
Inverse Secchi depth (m⁻¹)

FIG. 8

SPECTRAL BAND VALUES OF IRRADIANCE ATTENUATION COEFFICIENTS

Figures 88-99 illustrate the results of regressing the irradiance attenuation coefficients appropriate for each of the spectral bands 400nm-500nm (blue); 500nm-600nm (green); 600nm-700nm (red) against the irradiance attenuation coefficient for PAR, k_{PAR}, (400nm-700nm). Specific breakdown of these regressions are given in Table 7 which includes the least squares regression relationships between k_{PAR} ($k_{400-700}$) and each of $k_{400-500}$, $k_{500-600}$ and $k_{600-700}$ and for each lake monitored.

The salient features of Figures 88-99 are as follows:

a) For the Upper Lakes, the statistical scatter between $k_{400-500}$ (blue) and k_{PAR} and between $k_{500-600}$ (green) and k_{PAR} are quite small. The statistical scatter between $k_{600-700}$ (red) and k_{PAR}, however, is quite large.

b) For the Lower Lakes the statistical scatter between k_{PAR} and any of the three spectral band values of the irradiance attenuation coefficients is quite small.

c) The high intercept value of the regressions between $k_{600-700}$ (red) and k_{PAR} apparent in all the lakes is due to the high absorption of pure water in this wavelength band.

d) For each lake the slopes between $k_{500-600}$ (green) and k_{PAR} and between $k_{600-700}$ (red) and k_{PAR} are generally comparable but significantly lower than the slope between $k_{400-500}$ (blue) and k_{PAR}.

e) On a per-lake basis, the relationships between $k_{400-500}$ (blue) and k_{PAR} show the least amount of variance while the relationships between $k_{500-600}$ (green) and k_{PAR} show the greatest amount of variance.

TABLE 7

Figure	Lake	Number of Regression Points	Per-Band Mathematical Relationship
88	Superior	66	$k_{400-500}=1.24k_{PAR}-0.04$
89	Superior	66	$k_{500-600}=0.76k_{PAR}+0.01$
90	Superior	66	$k_{600-700}=0.74k_{PAR}+0.27$
91	Huron & Georgian Bay	102	$k_{400-500}=1.31k_{PAR}-0.05$
92	Huron & Georgian Bay	102	$k_{500-600}=0.76k_{PAR}+0.01$
93	Huron & Georgian Bay	102	$k_{600-700}=0.84k_{PAR}+0.24$
94	Erie	40	$k_{400-500}=1.31k_{PAR}-0.05$
95	Erie	40	$k_{500-600}=0.92k_{PAR}-0.04$
96	Erie	40	$k_{600-700}=0.86k_{PAR}+0.24$
97	Ontario	57	$k_{400-500}=1.23k_{PAR}+0.04$
98	Ontario	57	$k_{500-600}=0.82k_{PAR}$
99	Ontario	57	$k_{600-700}=0.77k_{PAR}+0.28$

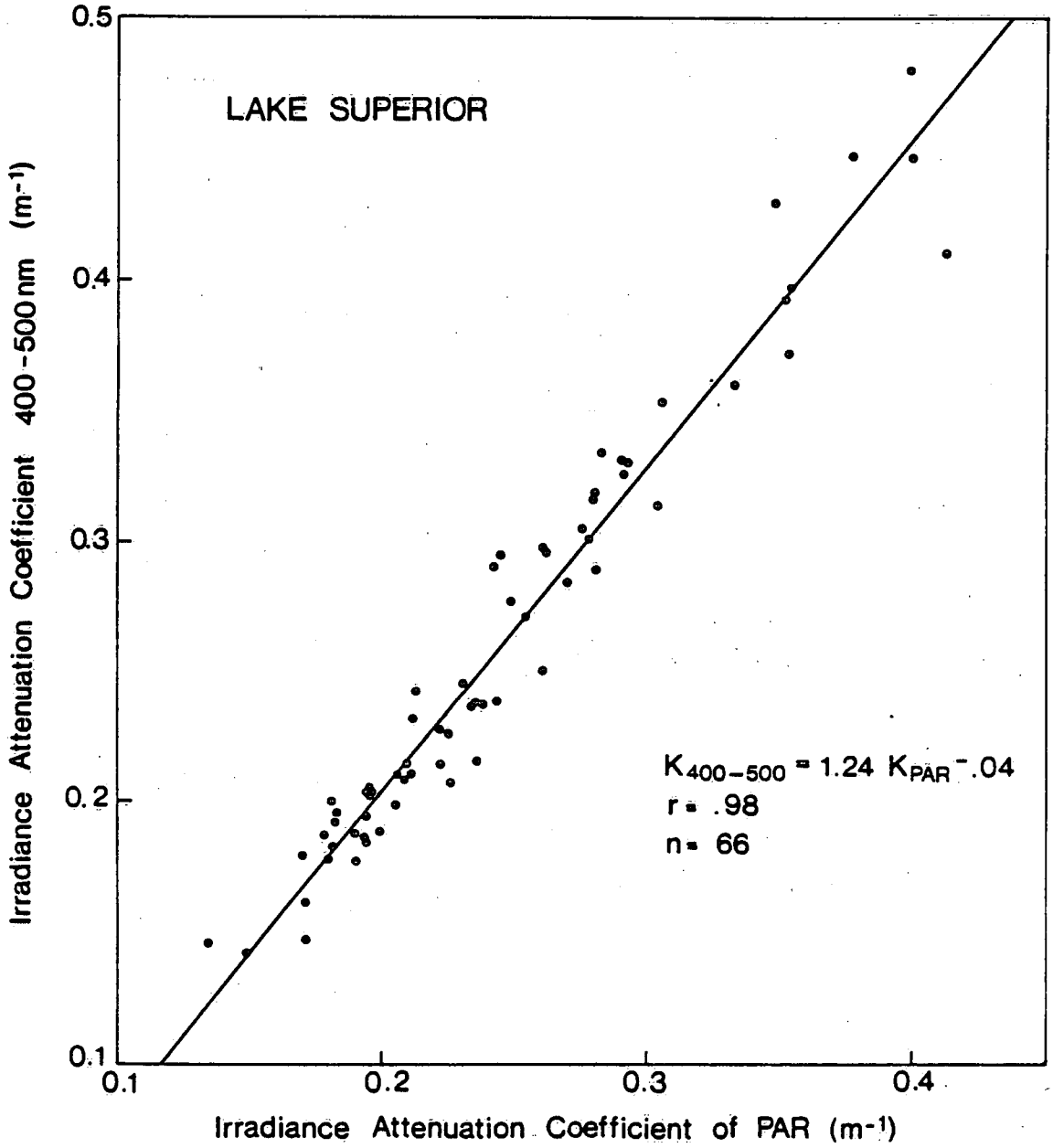
LAKE SUPERIOR
$K_{400-500} = 1.24\ K_{PAR}^{-.04}$
r = .98
n = 66
Irradiance Attenuation Coefficient 400-500nm (m^{-1})
Irradiance Attenuation Coefficient of PAR (m^{-1})
0.1
0.2
0.3
0.4
0.5

FIG. 88

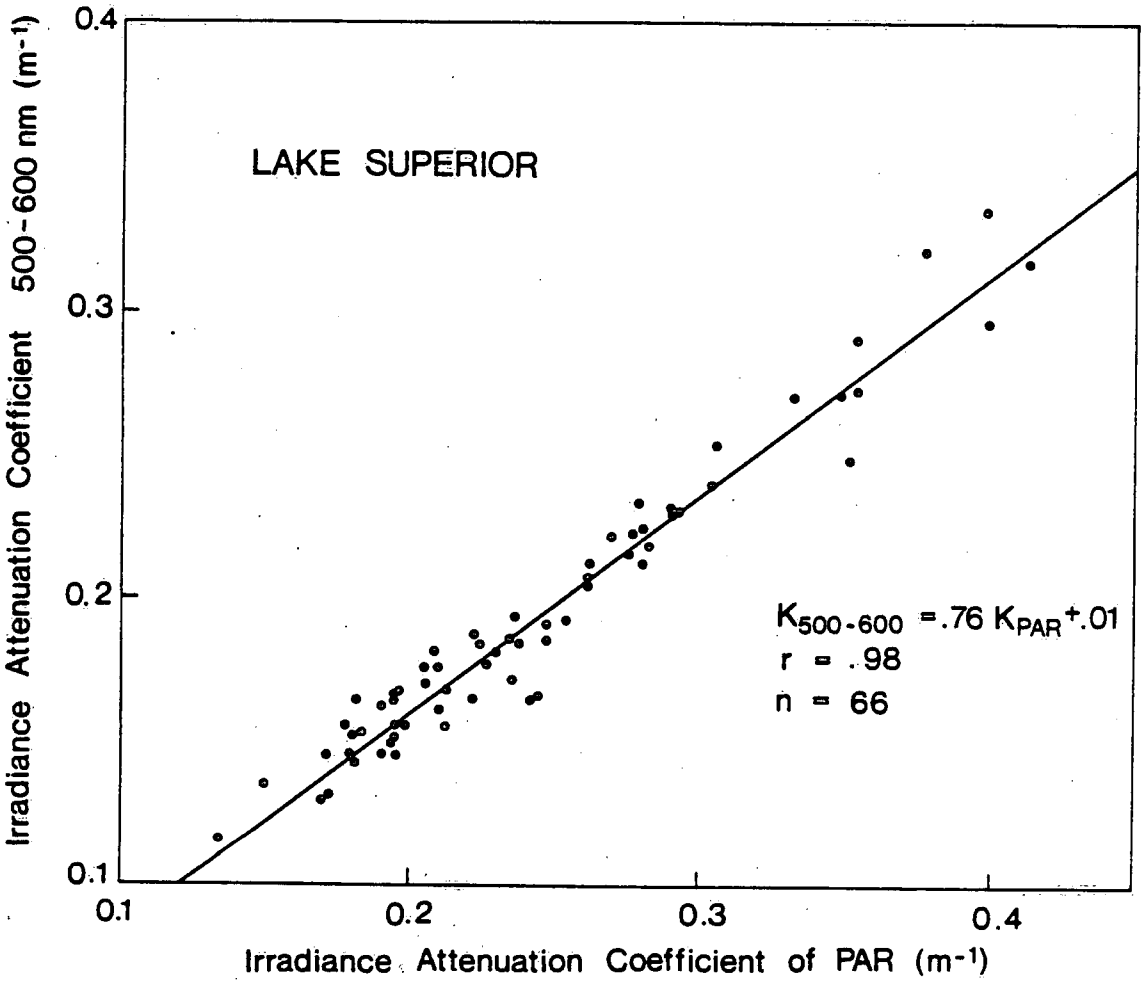
LAKE SUPERIOR
$K_{500-600}$ =.76 K_{PAR}+.01
r = .98
n = 66
Irradiance Attenuation Coefficient 500-600 nm (m^{-1})
Irradiance Attenuation Coefficient of PAR (m^{-1})
0.1
0.2
0.3
0.4

FIG. 89

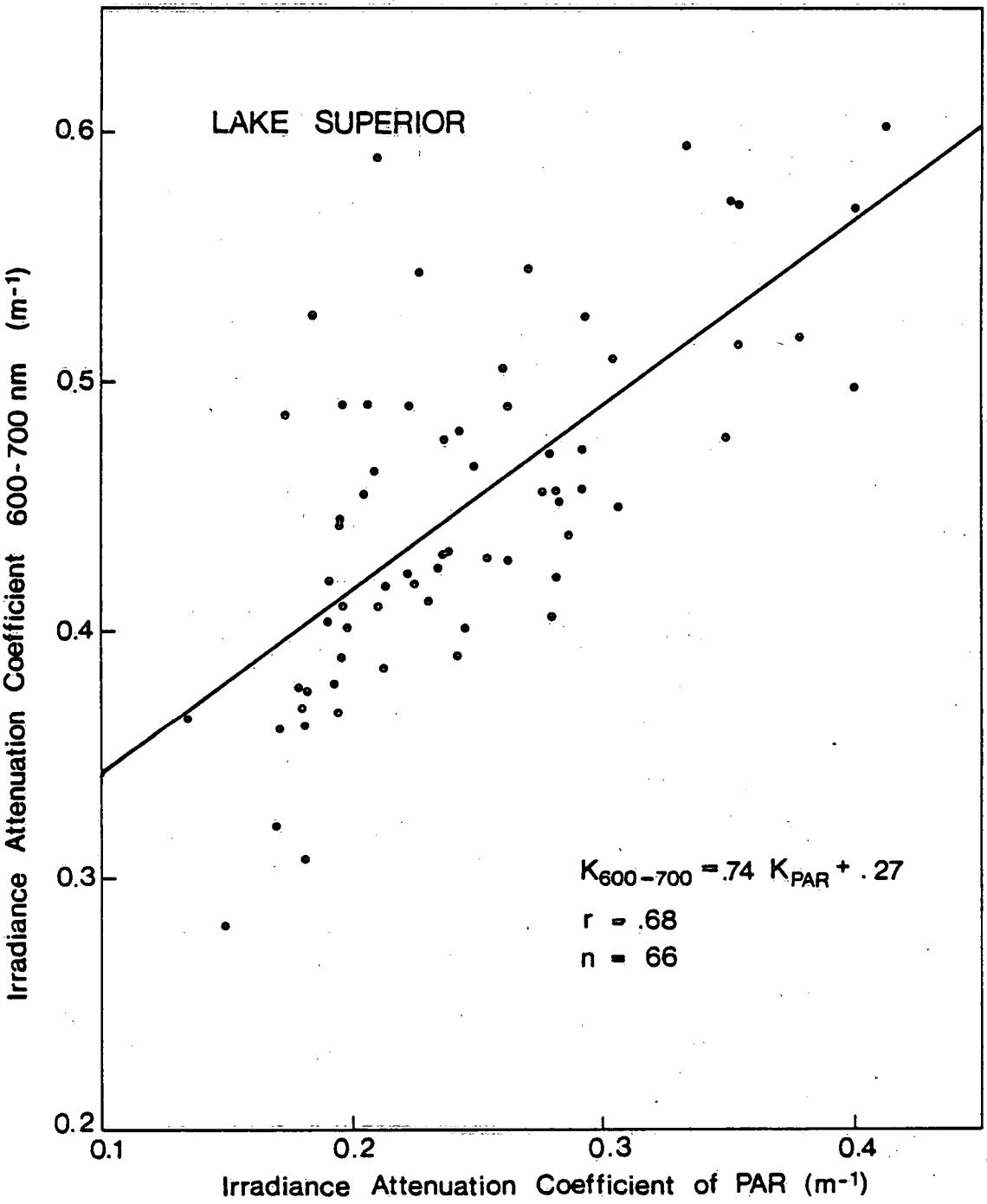
LAKE SUPERIOR
0.6
0.5
0.4
0.3
0.2
0.1
0.2
0.3
0.4
Irradiance Attenuation Coefficient 600-700 nm (m-1)
Irradiance Attenuation Coefficient of PAR (m-1)
K600-700 = .74 KPAR + .27
r = .68
n = 66

FIG. 90

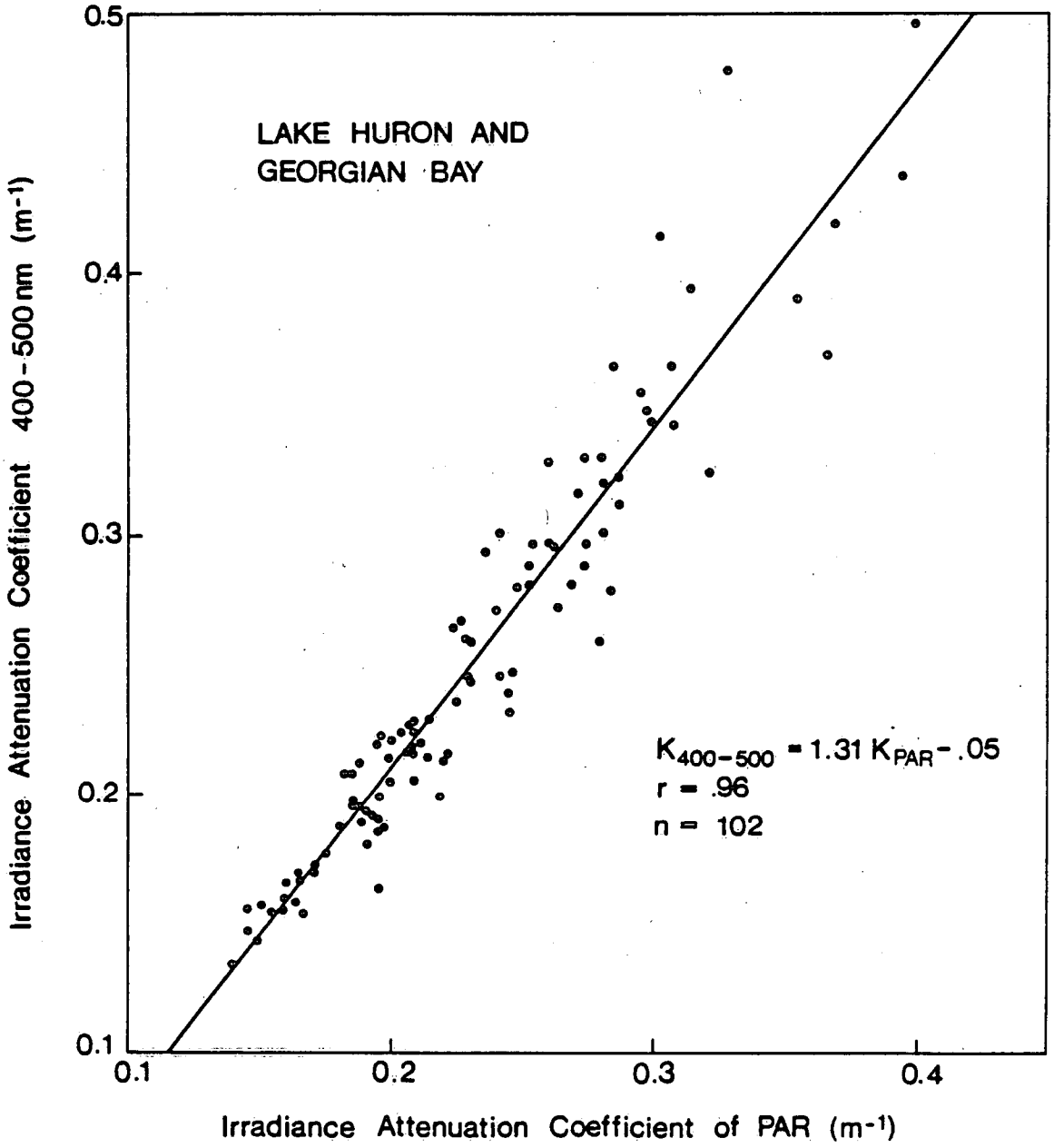
LAKE HURON AND
GEORGIAN BAY
$K_{400-500} = 1.31\ K_{PAR} - .05$
r = .96
n = 102
Irradiance Attenuation Coefficient 400-500 nm (m^{-1})
Irradiance Attenuation Coefficient of PAR (m^{-1})
0.1
0.2
0.3
0.4
0.5

FIG. 91

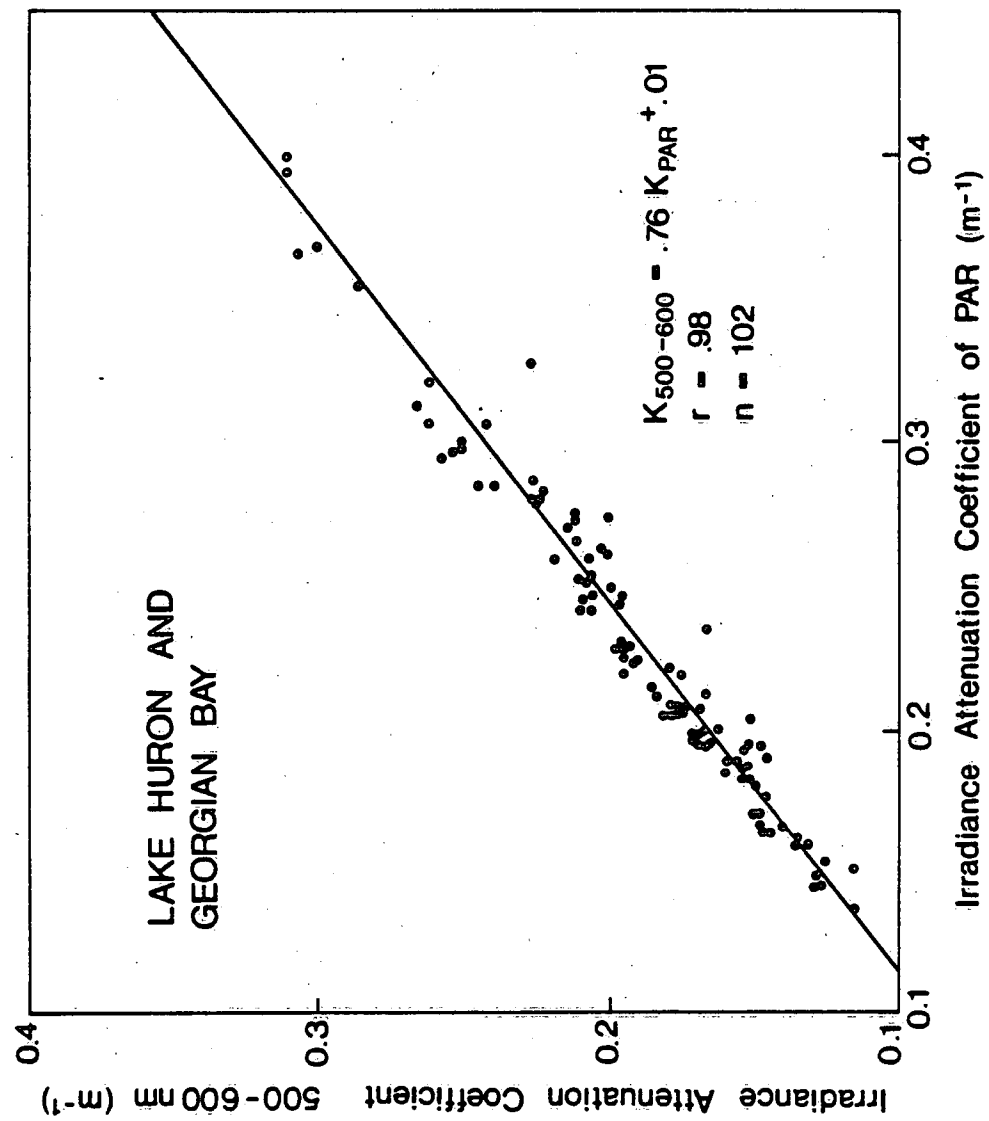
LAKE HURON AND
GEORGIAN BAY
$K_{500-600} = .76\ K_{PAR} + .01$
r = .98
n = 102
Irradiance Attenuation Coefficient 500-600 nm (m^{-1})
Irradiance Attenuation Coefficient of PAR (m^{-1})
0.1
0.2
0.3
0.4

FIG. 92

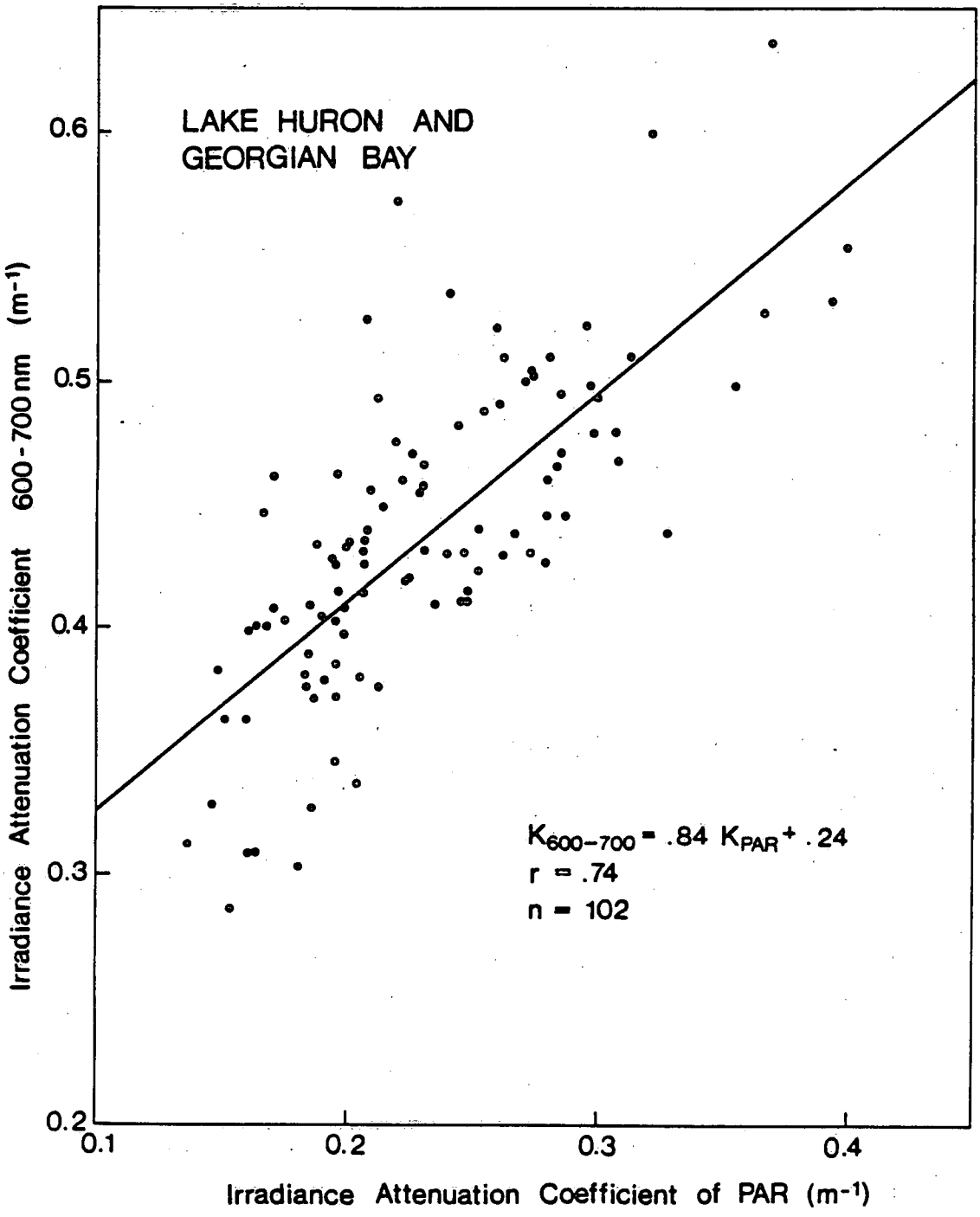
LAKE HURON AND
GEORGIAN BAY
$K_{600-700} = .84\ K_{PAR} + .24$
r = .74
n = 102
Irradiance Attenuation Coefficient 600-700nm (m^{-1})
Irradiance Attenuation Coefficient of PAR (m^{-1})
0.6
0.5
0.4
0.3
0.2
0.1
0.2
0.3
0.4

FIG. 93

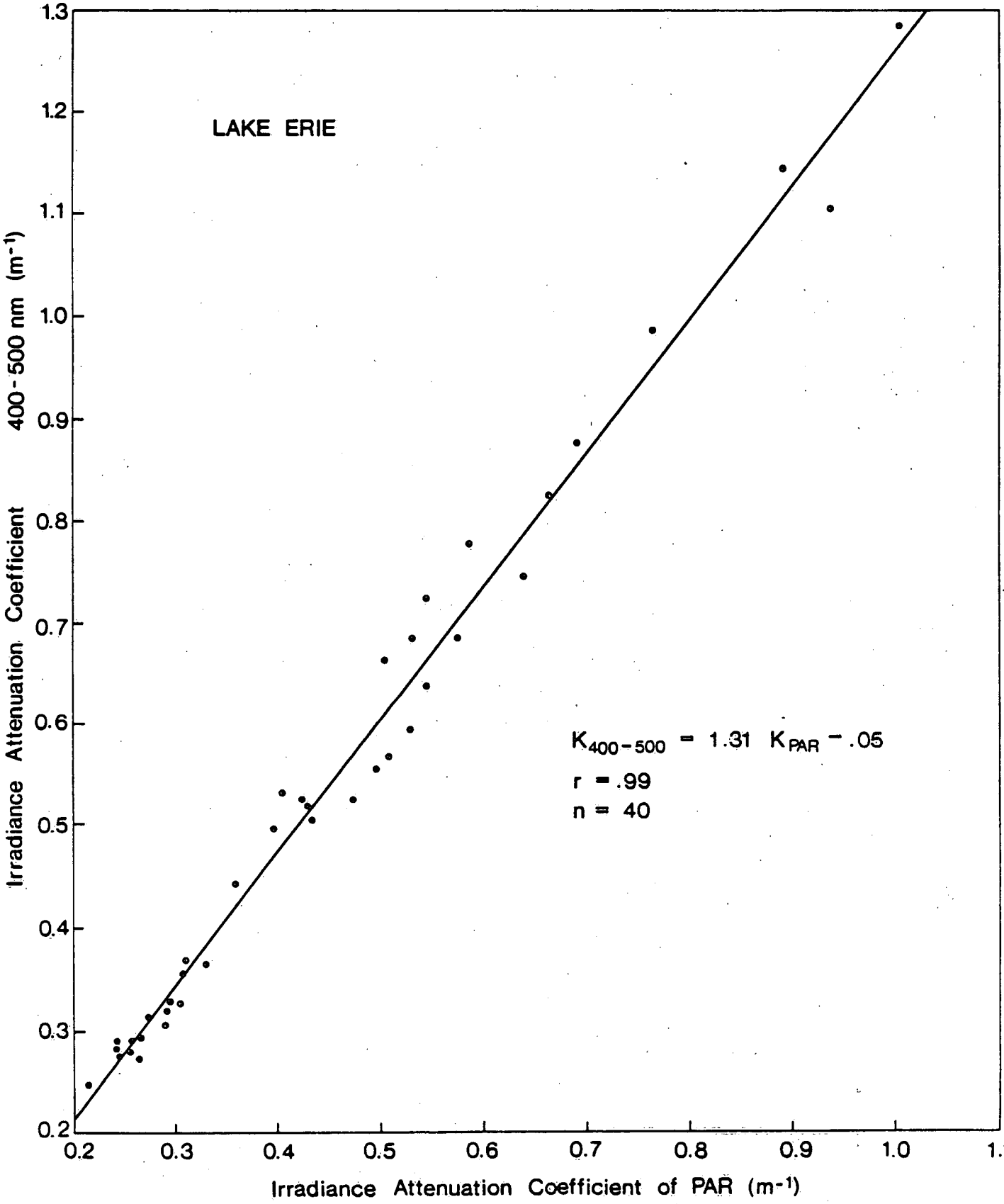
LAKE ERIE
$K_{400-500} = 1.31\ K_{PAR} - .05$
r = .99
n = 40
Irradiance Attenuation Coefficient 400-500 nm (m^{-1})
Irradiance Attenuation Coefficient of PAR (m^{-1})
0.2
0.3
0.4
0.5
0.6
0.7
0.8
0.9
1.0
1.1
1.2
1.3

FIG. 94

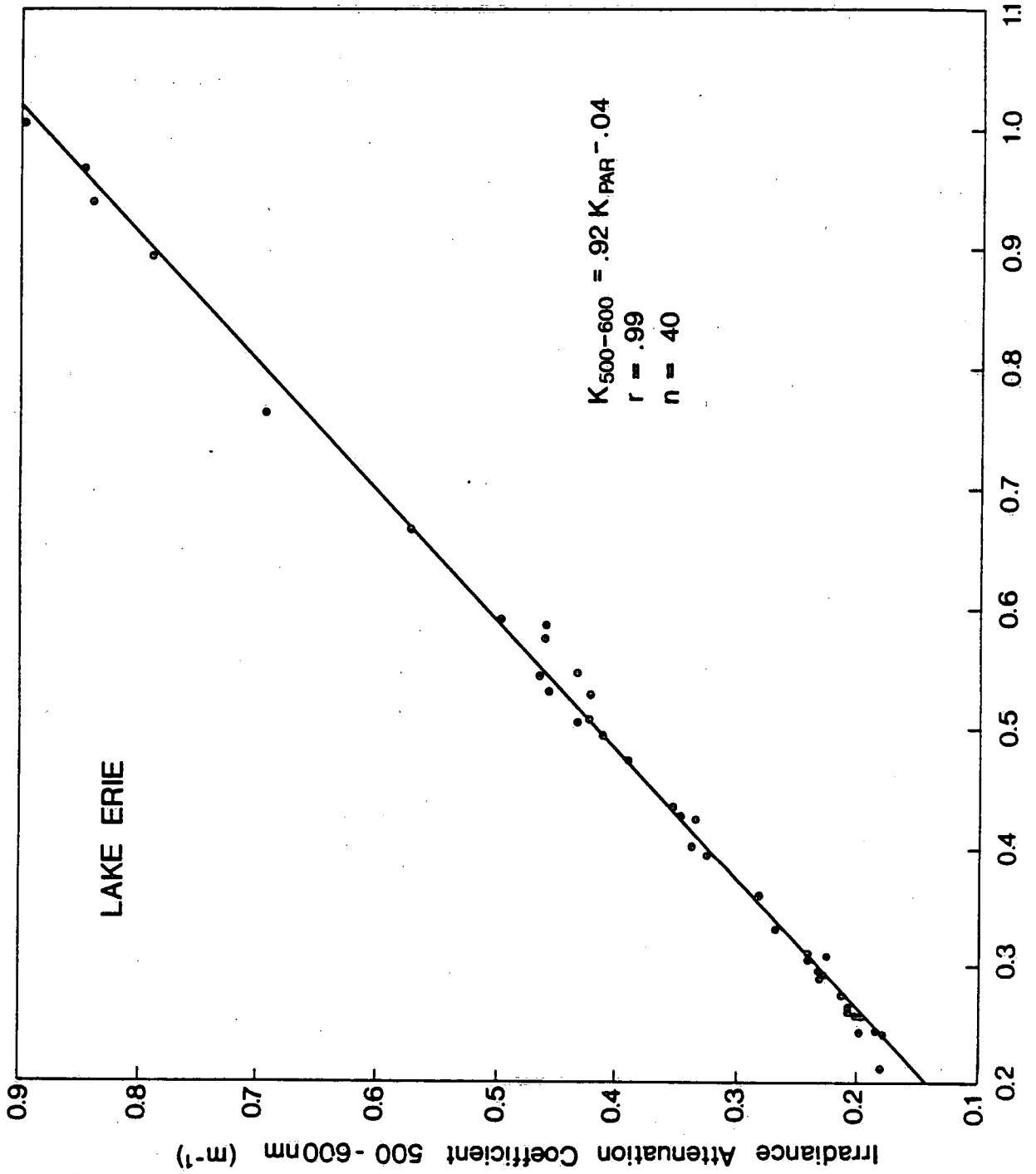
LAKE ERIE
$K_{500-600} = .92\ K_{PAR} - .04$
r = .99
n = 40
Irradiance Attenuation Coefficient 500 -600nm (m^{-1})
Irradiance Attenuation Coefficient of PAR (m^{-1})
0.1
0.2
0.3
0.4
0.5
0.6
0.7
0.8
0.9
1.0
1.1

FIG. 95

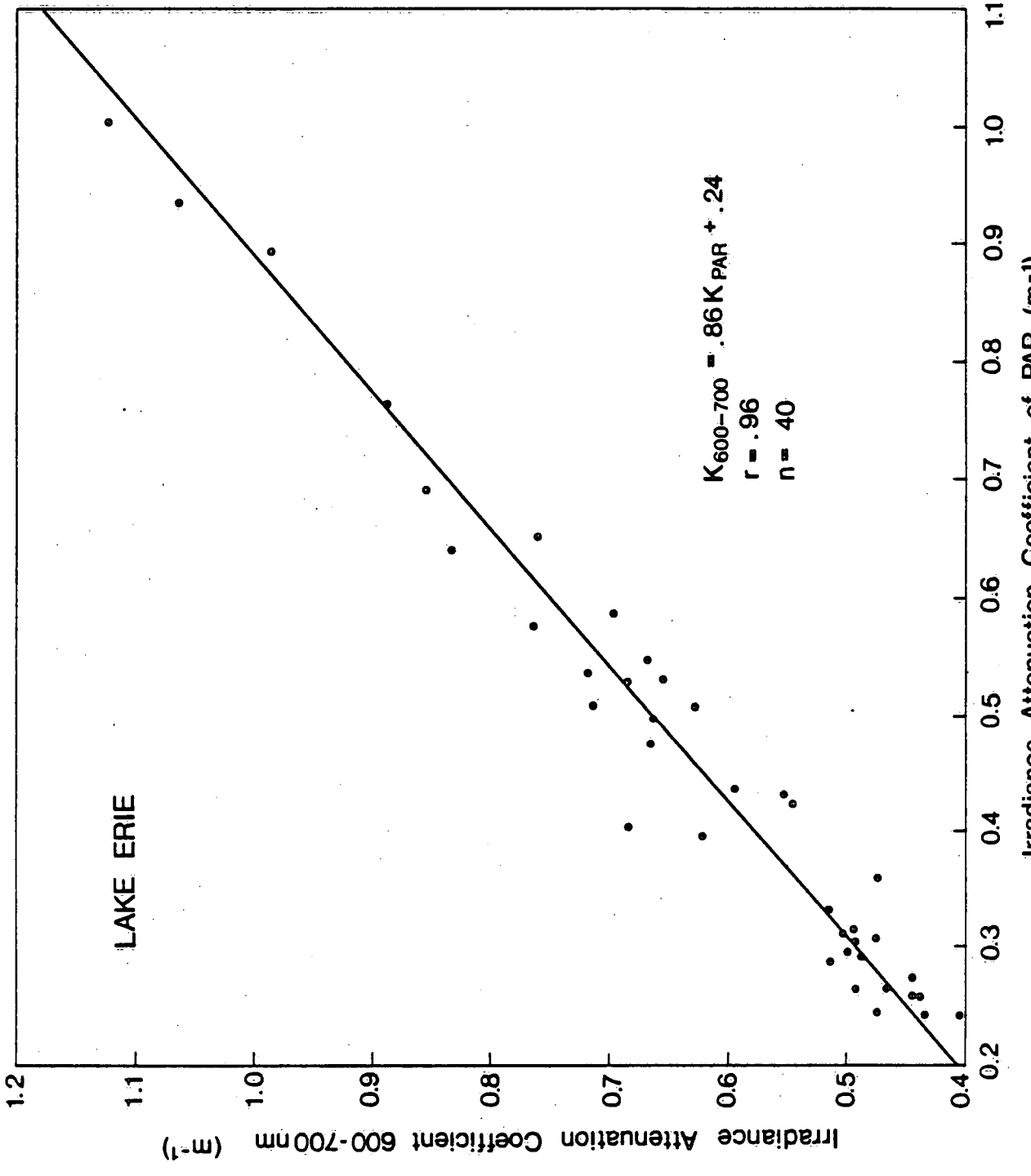
LAKE ERIE
$K_{600-700} = .86 K_{PAR} + .24$
r = .96
n = 40
Irradiance Attenuation Coefficient 600-700 nm (m^{-1})
Irradiance Attenuation Coefficient of PAR (m^{-1})
1.2
1.1
1.0
0.9
0.8
0.7
0.6
0.5
0.4
0.2
0.3
0.4
0.5
0.6
0.7
0.8
0.9
1.0
1.1

FIG. 96

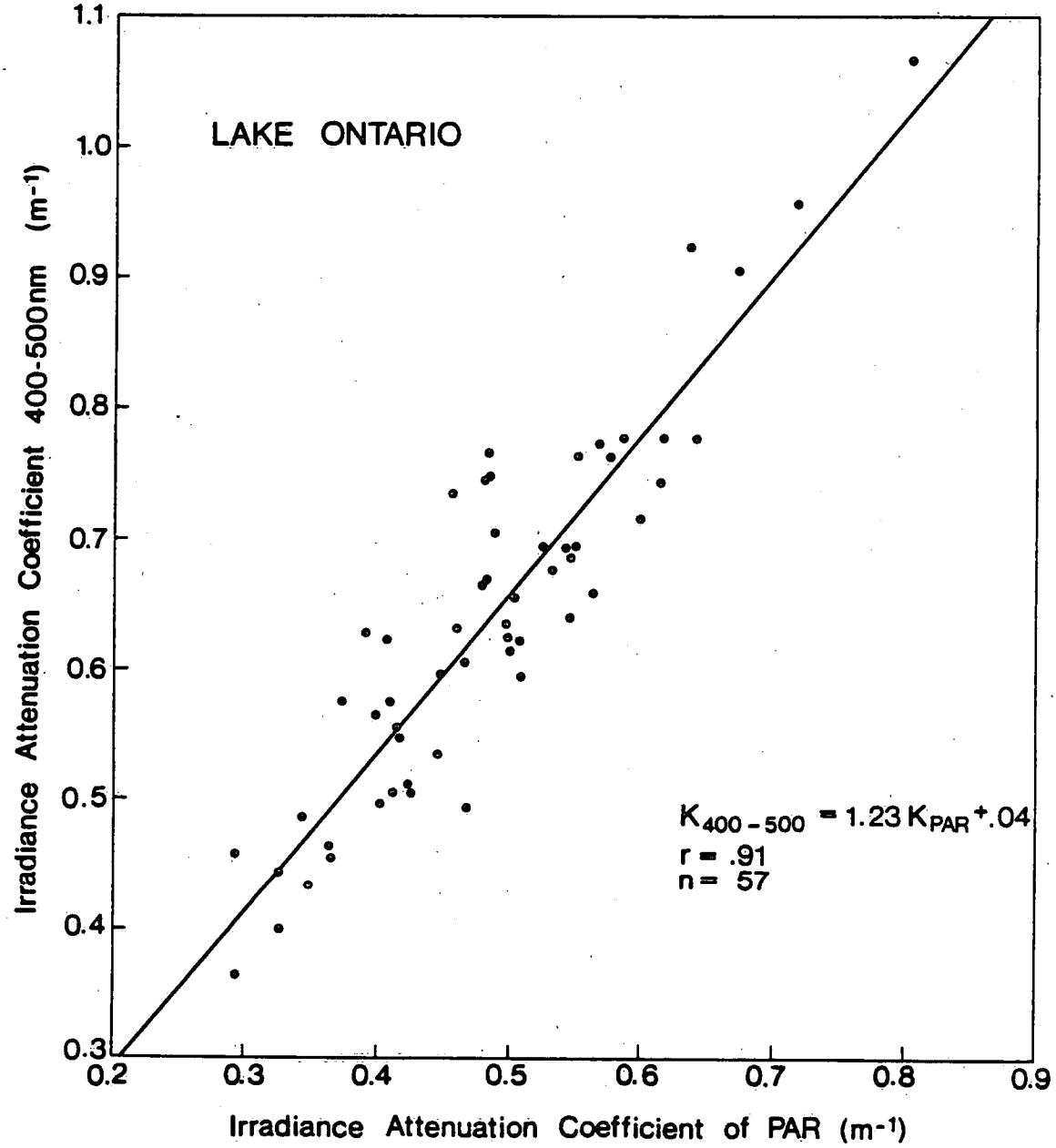
LAKE ONTARIO
$K_{400-500} = 1.23 K_{PAR} + .04$
r = .91
n = 57
Irradiance Attenuation Coefficient 400-500nm (m^{-1})
Irradiance Attenuation Coefficient of PAR (m^{-1})
1.1
1.0
0.9
0.8
0.7
0.6
0.5
0.4
0.3
0.2
0.3
0.4
0.5
0.6
0.7
0.8
0.9

FIG. 97

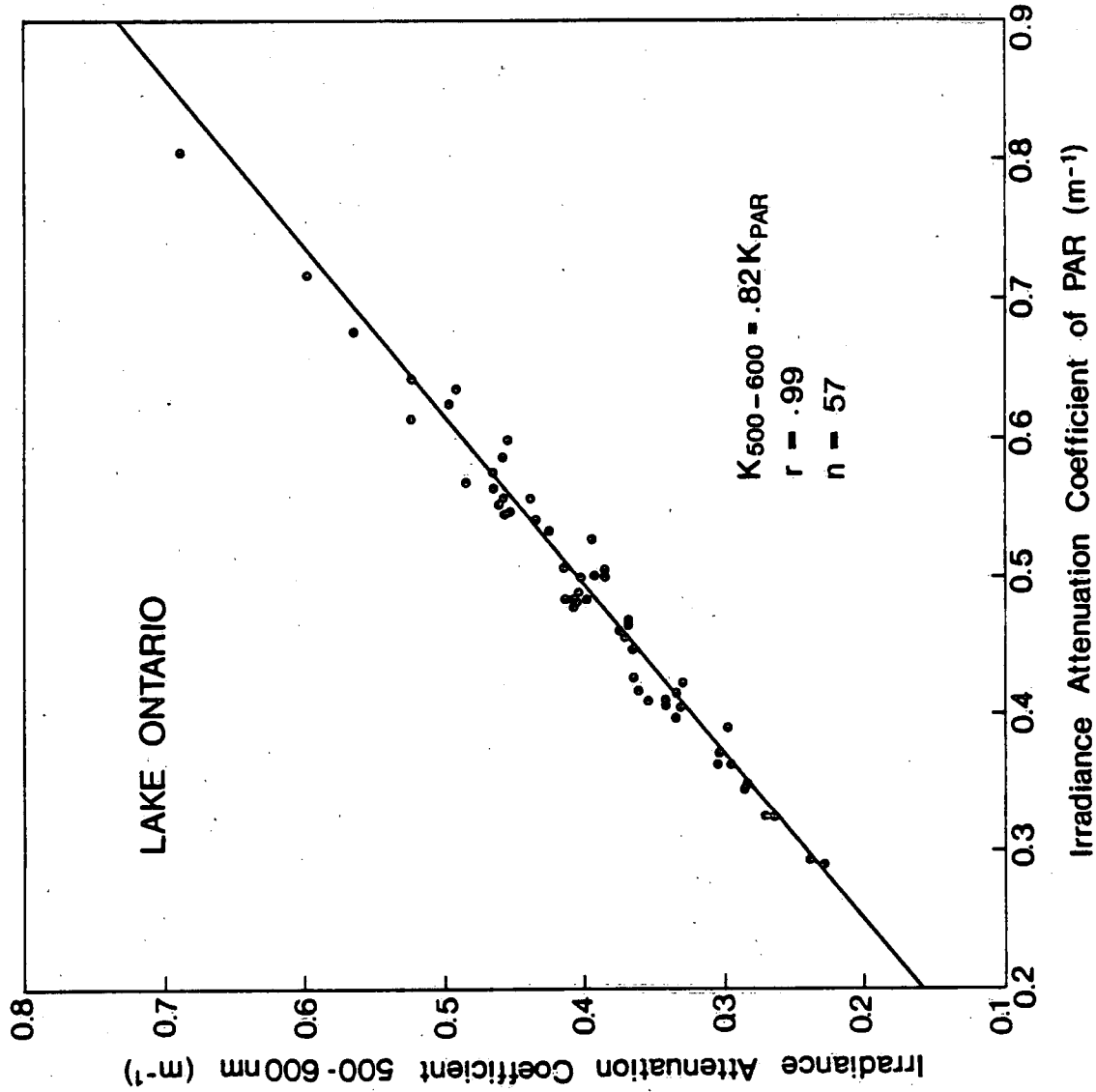
LAKE ONTARIO
$K_{500-600} = .82 K_{PAR}$
r = .99
n = 57
Irradiance Attenuation Coefficient 500-600nm (m^{-1})
Irradiance Attenuation Coefficient of PAR (m^{-1})
0.1
0.2
0.3
0.4
0.5
0.6
0.7
0.8
0.9

FIG. 98

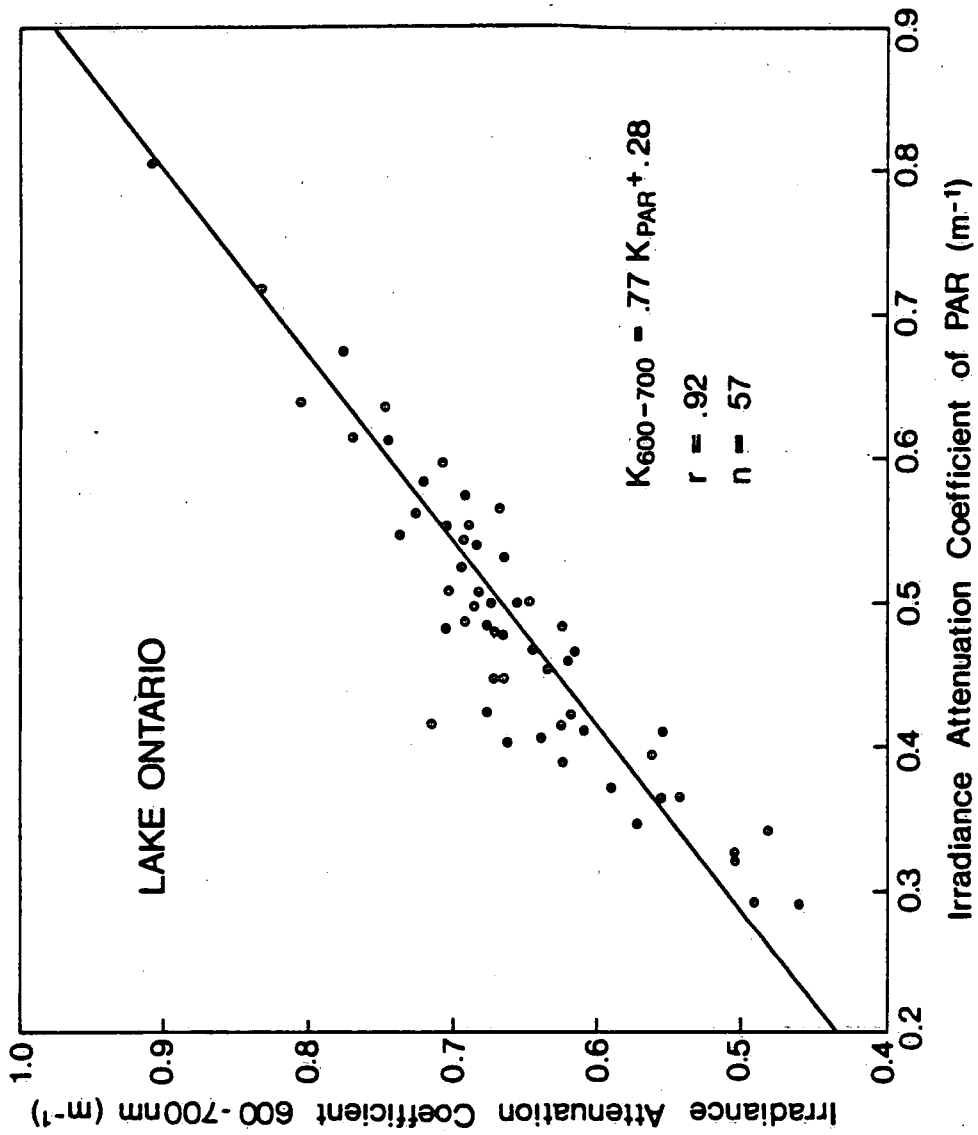
LAKE ONTARIO
$K_{600-700} = .77\ K_{PAR} + .28$
r = .92
n = 57
Irradiance Attenuation Coefficient 600-700nm (m^{-1})
Irradiance Attenuation Coefficient of PAR (m^{-1})
1.0
0.9
0.8
0.7
0.6
0.5
0.4
0.2
0.3
0.4
0.5
0.6
0.7
0.8
0.9

FIG. 99

SPECTRAL DEPENDENCE OF IRRADIANCE ATTENUATION COEFFICIENTS

Figures 100 and 101 illustrate the 15-point spectra obtained from the calculation of the irradiance attenuation coefficient at 20 nanometer increments over the spectral range 410 nm to 690 nm for each lake and for several k_{PAR} values ranging from 0.10 to 0.50 m^{-1} for the Upper Lakes and ranging from 0.20 to 1.20 m^{-1} for the Lower Lakes.

Figures 102 and 103 illustrate the 15-point spectra of the subsurface irradiance at the 100% level (incident) and at the 10% and 1% levels for two values of k_{PAR} for each of Lakes Huron (0.10 m^{-1} and 0.50 m^{-1}) and Erie (0.20 m^{-1} and 1.20 m^{-1}).

The salient features of Figures 100-103 include:

a) For the Upper Lakes, the wavelength with which the minimum attenuation coefficient is associated gradually shifts from ~490 nm to ~570 nm as the k_{PAR} increases. Due to the rapid increase in attenuation for the blue region of the visible spectrum, the wavelength at which minimum attenuation coefficient is observed becomes more sharply defined.

b) For the Lower Lakes, the wavelength with which the minimum attenuation coefficient is associated displays a very slight shift from ~550 nm to ~590 nm as the k_{PAR} increases. Once again the wavelength at which minimum attenuation coefficient is observed becomes more sharply defined as k_{PAR} increases.

c) For low values of k_{PAR} in Lake Huron, the irradiance at the 1% level has virtually lost its red component while retaining a considerable portion of its blue component. Consequently, the subsurface irradiance rapidly becomes "bluer" with increasing depth in Lake Huron waters displaying low k_{PAR}.

d) For high values of k_{PAR} in Lake Huron the subsurface irradiance rapidly becomes peaked in the green with increasing depth.

e) For low values of k_{PAR} in Lake Erie the irradiance at the 1% level has virtually lost its red component but has retained a significant portion of its green component and some of its blue.

f) For high values of k_{PAR} in Lake Erie, the irradiance at the 1% level has lost most of its blue component while retaining significant portions of both its green and red components.

Figure 104 plots the photosynthetic usable radiation (PUR) against the photosynthetic available radiation (PAR) [see Part I of this report], both expressed as a percentage of their incident values for Lakes Huron and Erie utilizing both the upper and lower limits of k_{PAR} for each lake (0.1 m^{-1} and 0.5 m^{-1} for Huron and 0.2 m^{-1} and 1.2 m^{-1} for Erie). As a result of the spectral changes with depth discussed above, the maximum amount of PUR per PAR is displayed for low k_{PAR} in Lake Huron. The minimum amount of PUR per PAR is displayed by high k_{PAR} in both Lakes Huron and Erie. Low values of k_{PAR} in Lake Erie produce almost a 1:1 ratio of PUR to PAR.

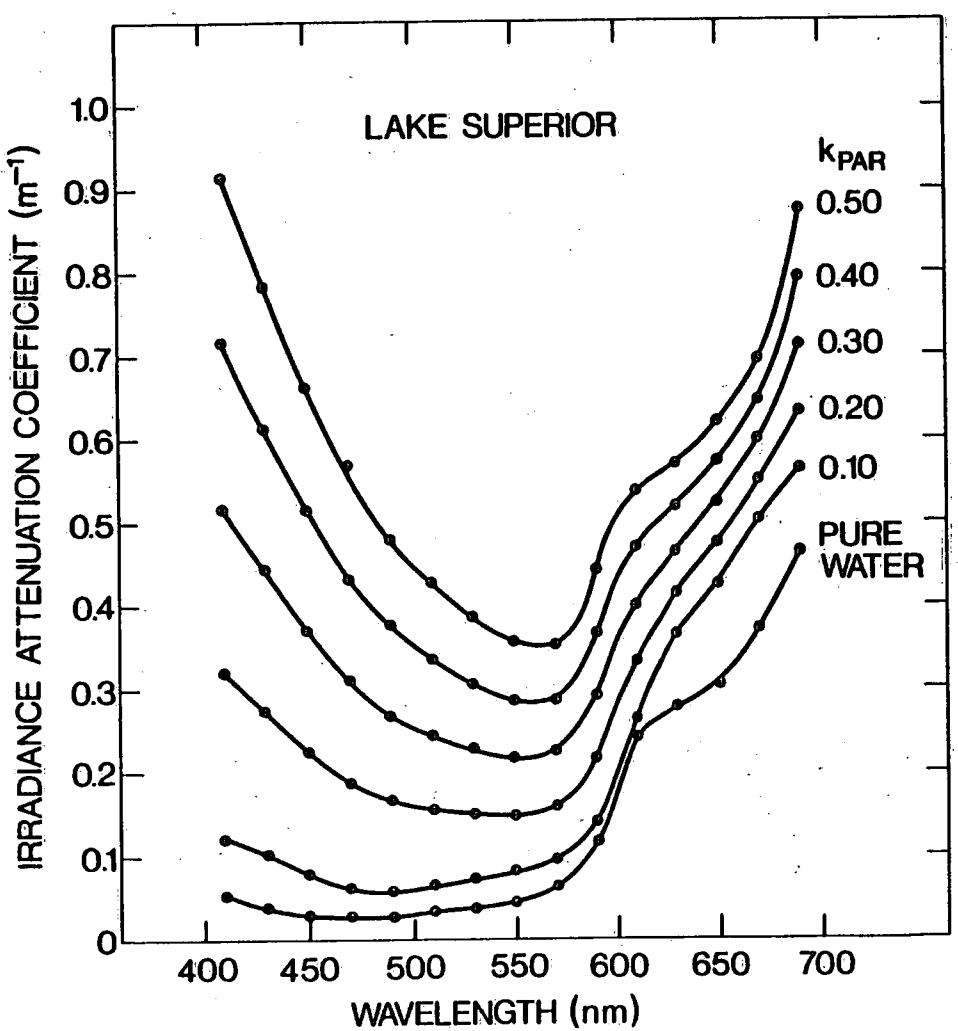
LAKE SUPERIOR
IRRADIANCE ATTENUATION COEFFICIENT (m⁻¹)
WAVELENGTH (nm)
kPAR
0.50
0.40
0.30
0.20
0.10
PURE WATER

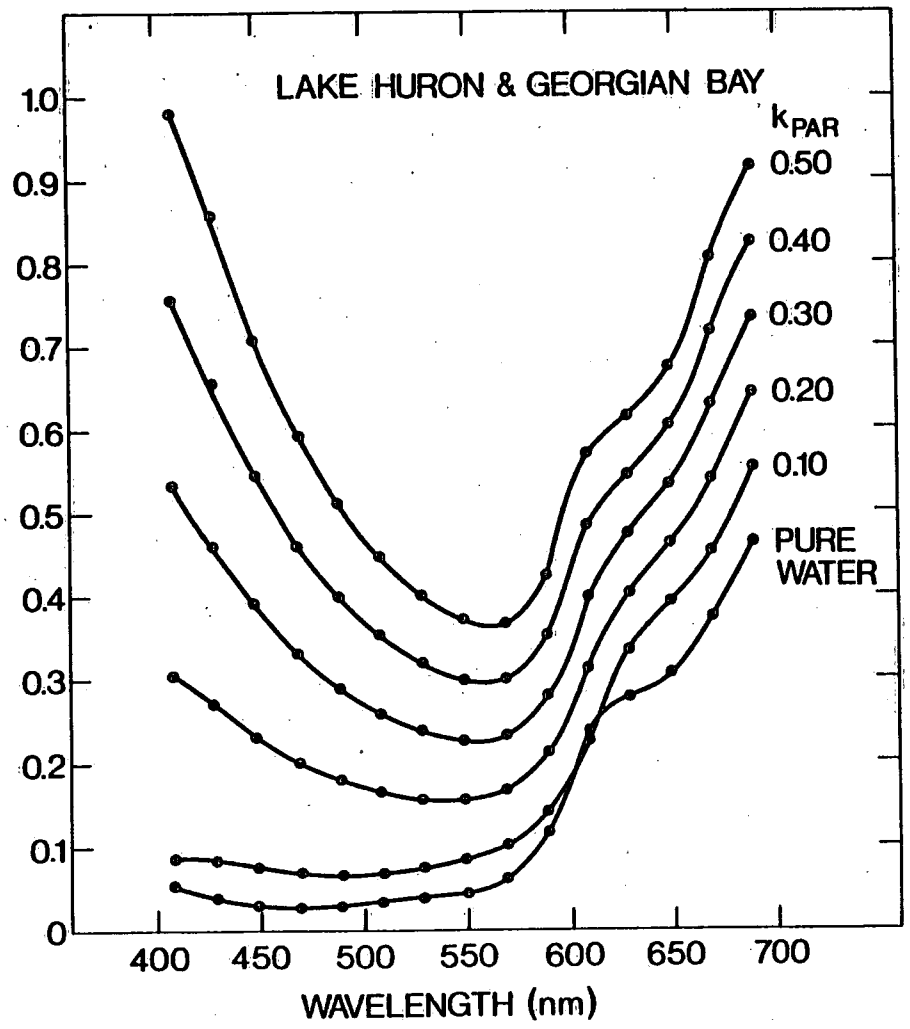
LAKE HURON & GEORGIAN BAY
WAVELENGTH (nm)
kPAR
0.50
0.40
0.30
0.20
0.10
PURE WATER

FIG. 108

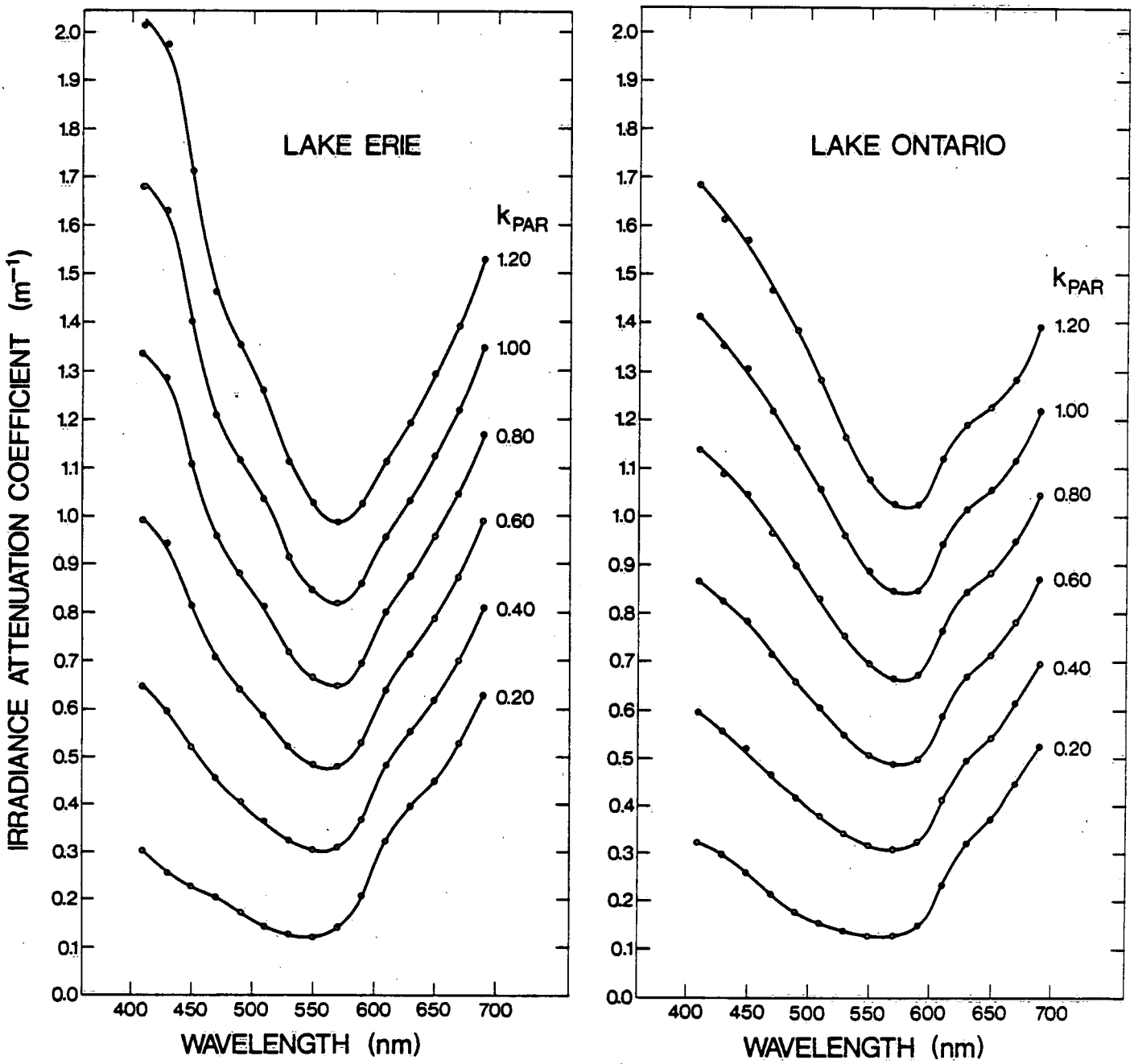
LAKE ERIE
LAKE ONTARIO
IRRADIANCE ATTENUATION COEFFICIENT (m⁻¹)
WAVELENGTH (nm)
kPAR
1.20
1.00
0.80
0.60
0.40
0.20
0.0
0.1
0.2
0.3
0.4
0.5
0.6
0.7
0.8
0.9
1.0
1.1
1.2
1.3
1.4
1.5
1.6
1.7
1.8
1.9
2.0
400
450
500
550
600
650
700

FIG. 101

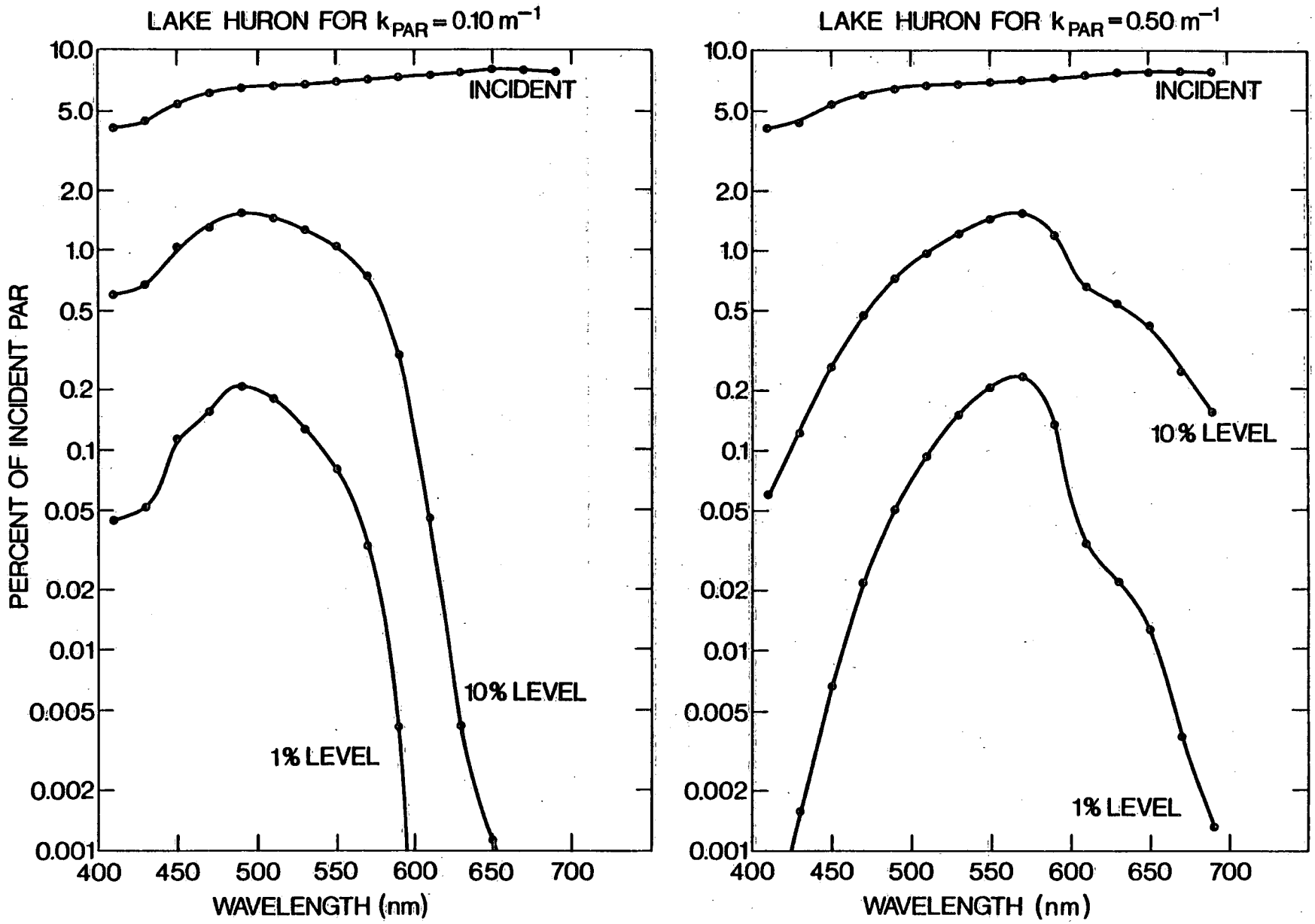
LAKE HURON FOR $k_{PAR} = 0.10\ m^{-1}$
LAKE HURON FOR $k_{PAR} = 0.50\ m^{-1}$
PERCENT OF INCIDENT PAR
10.0
5.0
2.0
1.0
0.5
0.2
0.1
0.05
0.02
0.01
0.005
0.002
0.001
INCIDENT
10% LEVEL
1% LEVEL
400
450
500
550
600
650
700
WAVELENGTH (nm)

FIG. 102

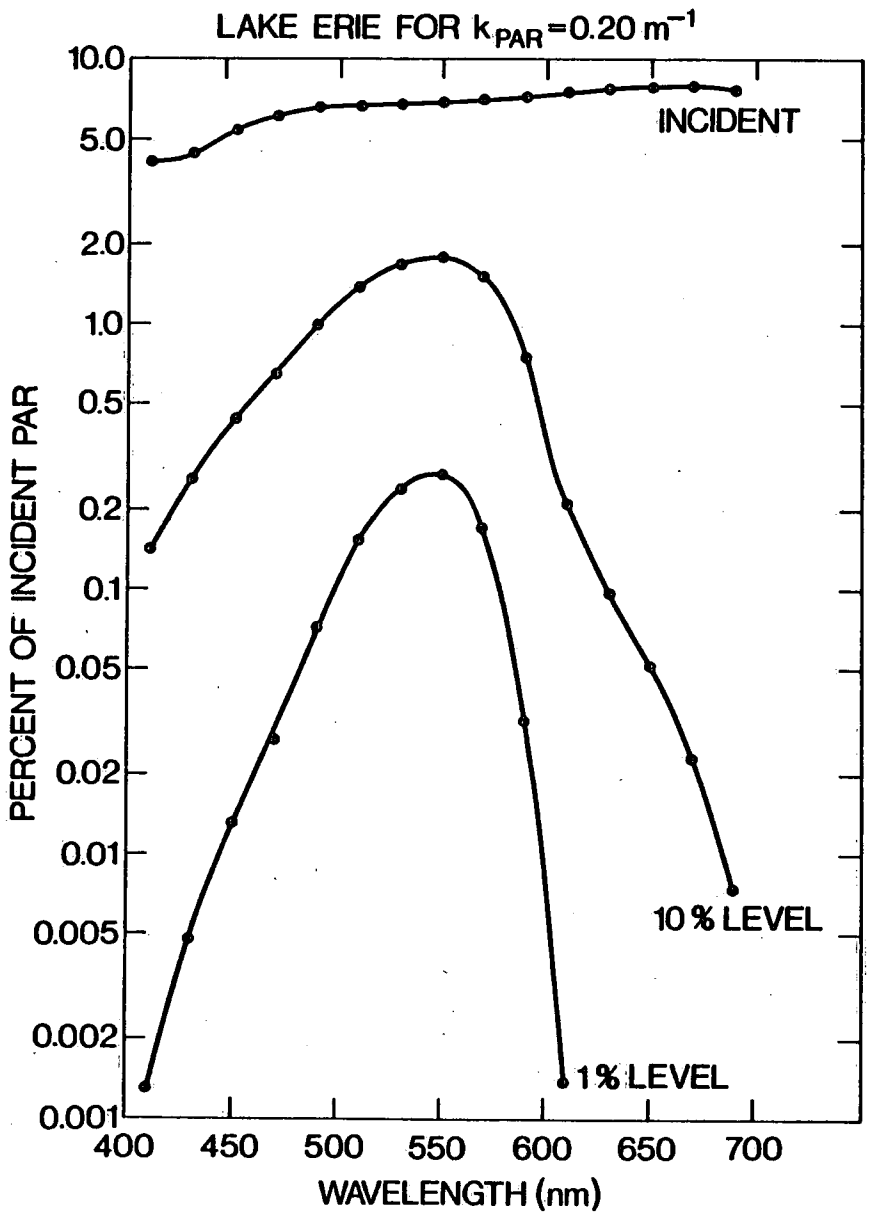
LAKE ERIE FOR k_{PAR}=0.20 m^{-1}
PERCENT OF INCIDENT PAR
10.0
5.0
2.0
1.0
0.5
0.2
0.1
0.05
0.02
0.01
0.005
0.002
0.001
INCIDENT
10% LEVEL
1% LEVEL
400
450
500
550
600
650
700
WAVELENGTH (nm)

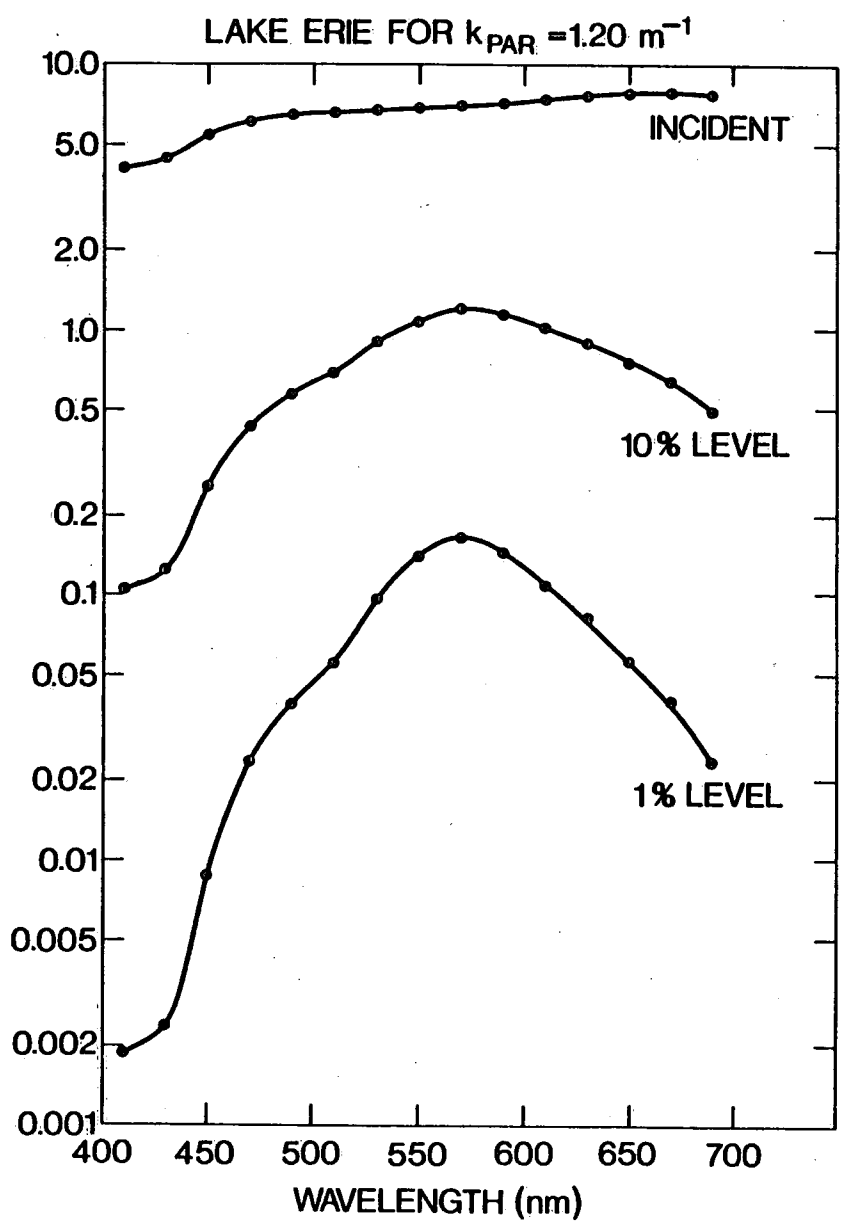
LAKE ERIE FOR k_{PAR} =1.20 m^{-1}
10.0
5.0
2.0
1.0
0.5
0.2
0.1
0.05
0.02
0.01
0.005
0.002
0.001
INCIDENT
10% LEVEL
1% LEVEL
400
450
500
550
600
650
700
WAVELENGTH (nm)

FIG. 103

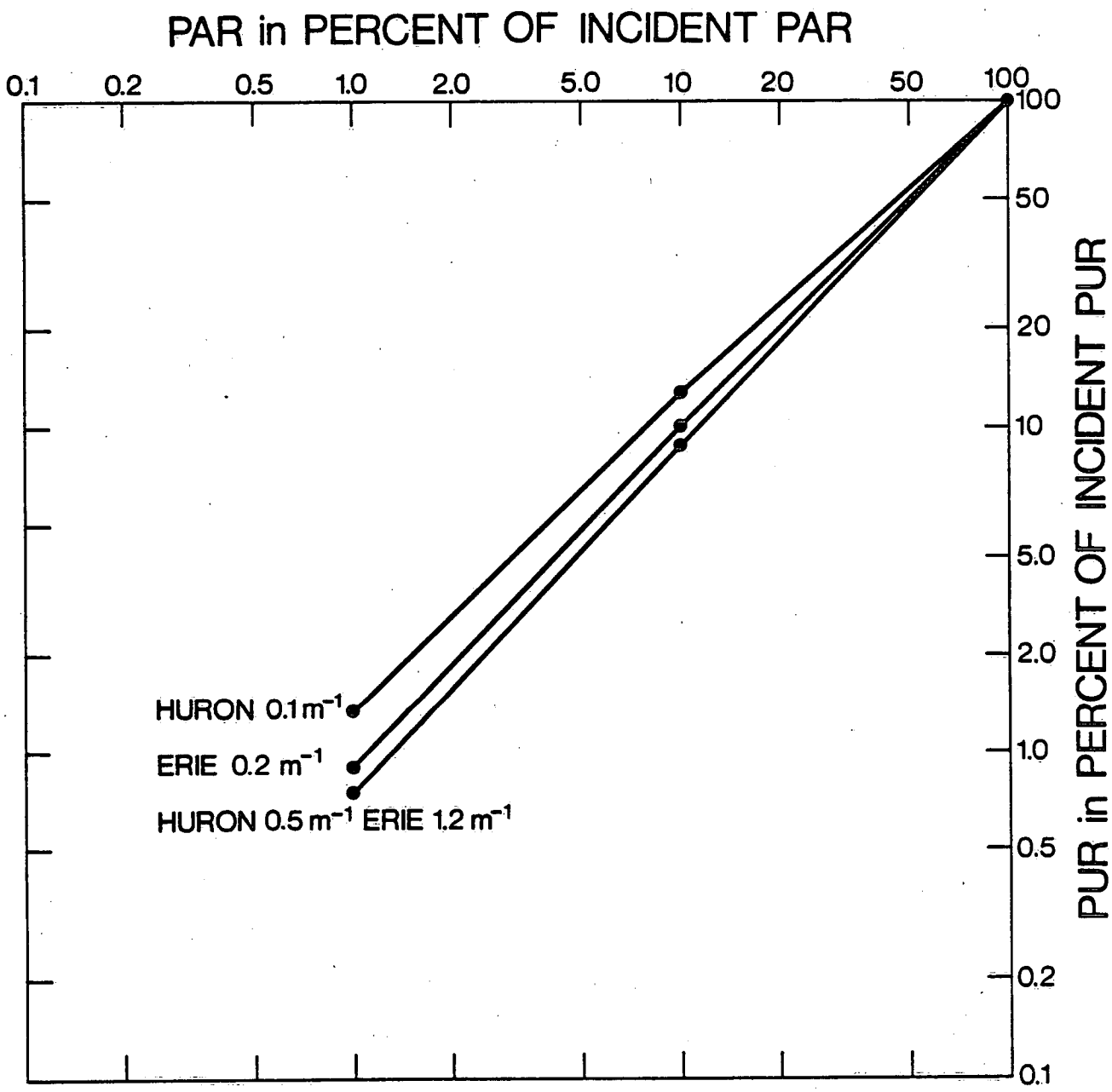
PAR in PERCENT OF INCIDENT PAR
0.1
0.2
0.5
1.0
2.0
5.0
10
20
50
100
PUR in PERCENT OF INCIDENT PUR
HURON 0.1 m⁻¹
ERIE 0.2 m⁻¹
HURON 0.5 m⁻¹ ERIE 1.2 m⁻¹

FIG. 104

SUBSURFACE SIGHTING RANGE

The subsurface sighting range is generally taken to represent the maximum distance at which an object may be detected underwater. Although the term is somewhat subjective, the largest impact on its numerical value is, obviously, the optical properties of the water. Large values of subsurface sighting range are associated with waters of high clarity, while small values of subsurface sighting range are associated with turbid waters. The two most obvious turbidity indicators from an optical standpoint are the beam attenuation coefficient c and the irradiance attenuation coefficient k. The sum of these two optical properties $(k + c)\ m^{-1}$ is frequently employed as an indication of the state of optical clarity.

In addition to the aquatic medium influencing the subsurface sighting range associated with a submerged object, the properties of the submerged object itself strongly influences its ability to be visually detected. In particular, the contrast of the object to its surroundings is of major importance. The reflectivity of the object, R_T and the reflectivity of the background, R_B (this latter parameter is well approximated by either the bottom reflectance if the object is near lake bottom, or the volume reflectance of the water column if the object is not near lake bottom) are the two factors that determine the contrast of the object.

The remaining factors of major influence on the subsurface sighting range associated with a submerged object are the physical

size of the object, the direction of viewing, and the availability of subsurface light (this latter factor being directly related to the incident radiation).

Figure 105 illustrates a nomograph by which the sighting range can be obtained once the optical parameters k, c, R_T, and R_B are known. This particular figure considers physical objects of projected area >100 cm^2 viewed from the surface vertically downward for all lighting conditions between one hour subsequent to sunrise and one hour prior to sunset. To determine the subsurface sighting range, therefore, a direct measurement of the total attenuation coefficient c is first required. For a particular location and time the transmission contours of Figures 1-32 may be used if direct measurements are not readily available. The corresponding value of the irradiance attenuation coefficient k may be calculated from the mathematical relationships of Table 5. The value of R_B, to a first approximation, can be expressed as $0.015(c + 1.0)$. The reflectivity of the object, R_T may be estimated as a number between 0 and 1 depending upon its colour and finish (shiny objects would display higher R_T values, for example, than would objects with a matte finish. Secchi discs are generally described by an R_T of 0.70). Thus the parameters $(c+k)$ and $R_T-R_B/50R_B$ may be readily determined, and a straight line drawn between these values yields the sighting range as its interception point with the curve of Figure 105. For smaller objects, non-vertical viewing directions, and differing conditions of incident

radiation, other nomographs describing these situations would be required. Additional information on the nature and applications of such nomographs may be found in Preisendorfer (1976).

Using the above nomograph technique, the sighting ranges for an object >100 cm^2 projected area and characterized by an R_T of 0.70 were calculated for Lakes Ontario, Erie, Superior, Huron and Georgian Bay. Figure 106 displays these calculated sighting ranges as a function of the transmission values appropriate to the offshore near-surface waters of each of the Great Lakes during the summer months. As is evident from the figure, sighting ranges vary from as high as 20 metres in Lake Superior to as low as 1 or 2 metres in Lakes Erie and Ontario.

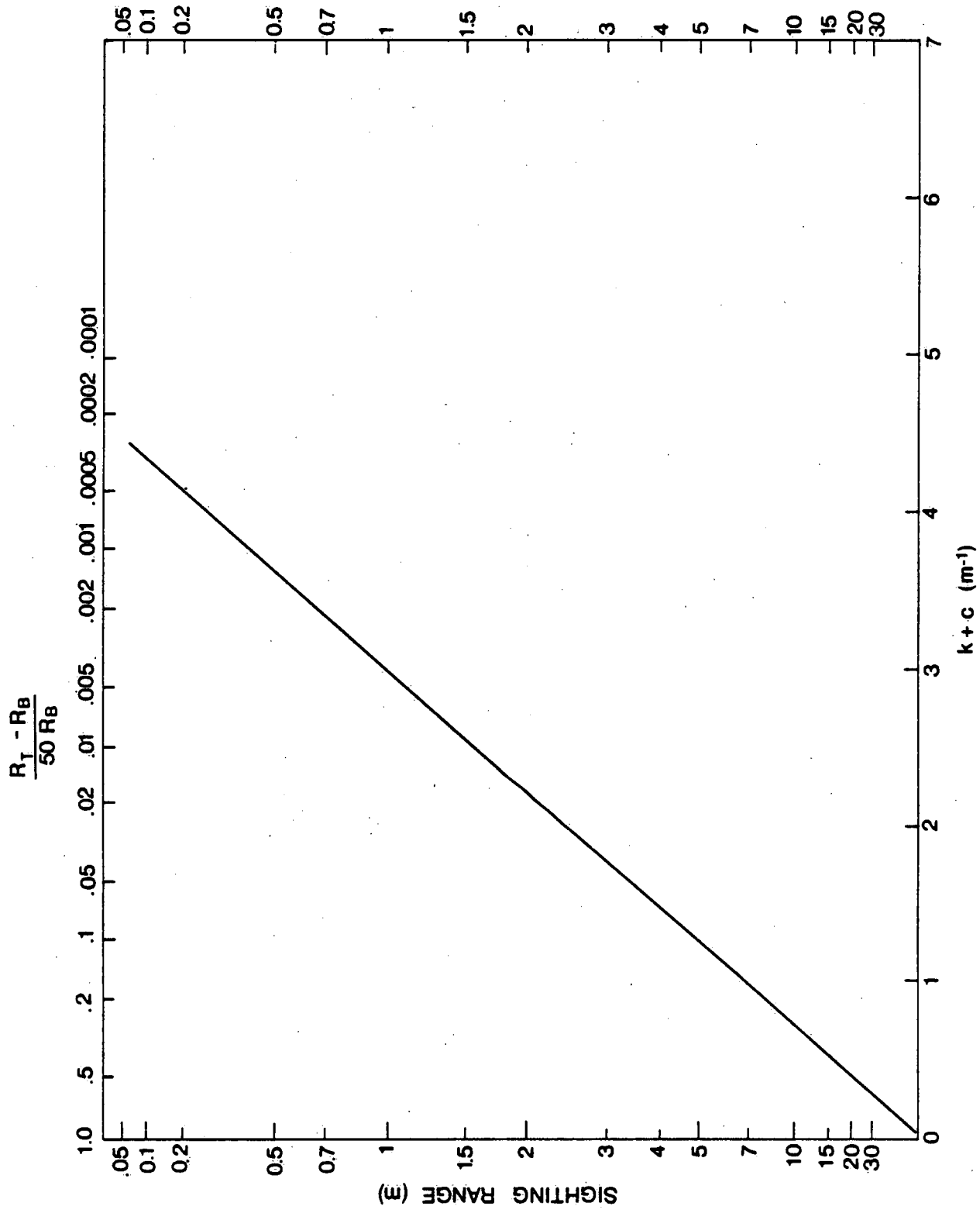
$\frac{R_T - R_B}{50\,R_B}$
1.0
.5
.2
.1
.05
.02
.01
.005
.002
.001
.0005
.0002
.0001
SIGHTING RANGE (m)
.05
0.1
0.2
0.5
0.7
1
1.5
2
3
4
5
7
10
15
20
30
0
1
2
3
4
5
6
7
k + c (m⁻¹)

FIG. 105

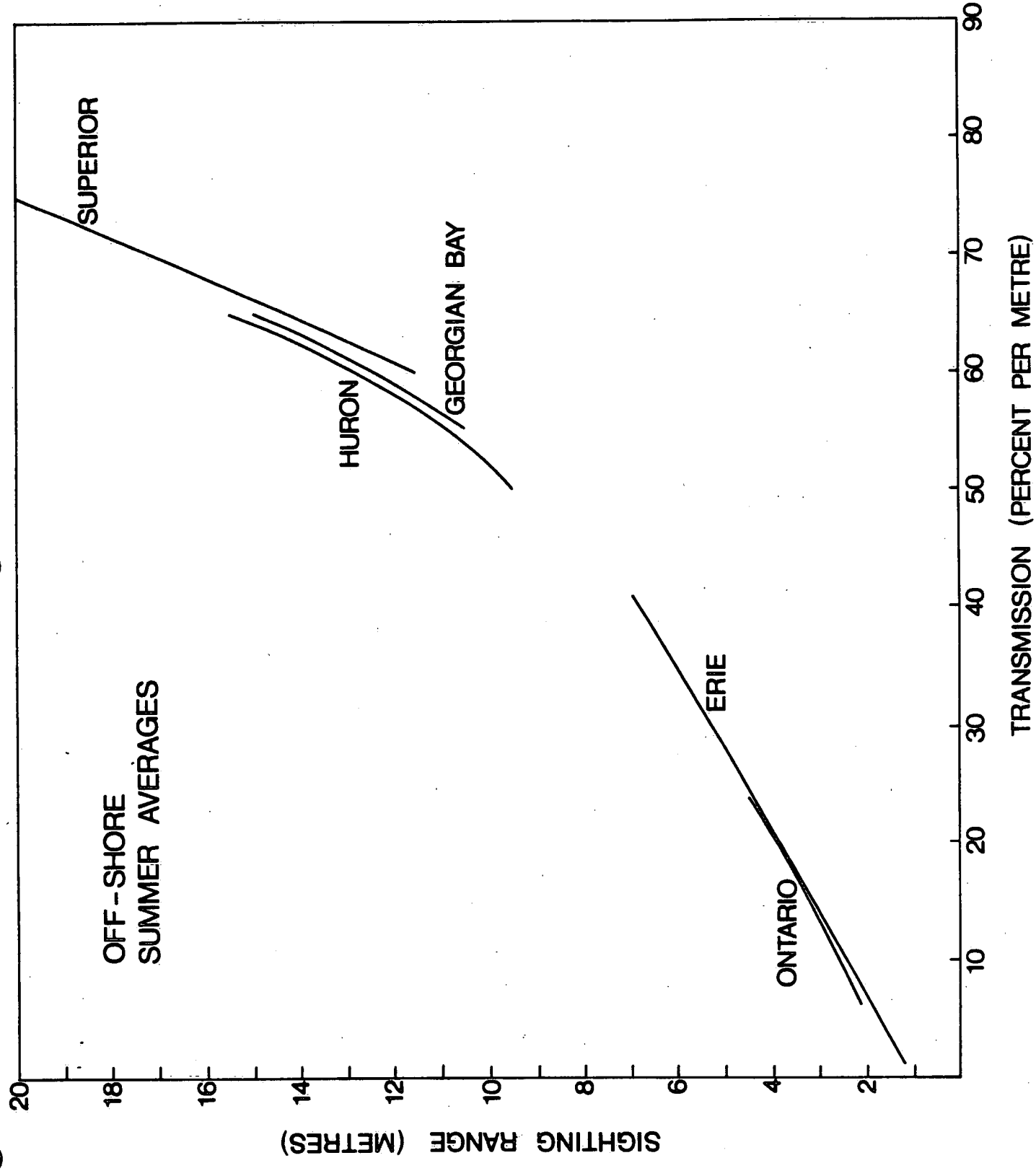
SUPERIOR
HURON
GEORGIAN BAY
ERIE
ONTARIO
OFF-SHORE
SUMMER AVERAGES
SIGHTING RANGE (METRES)
TRANSMISSION (PERCENT PER METRE)
20
18
16
14
12
10
8
6
4
2
10
20
30
40
50
60
70
80
90

FIG. 106

DETERMINATION OF THE PHOTOSYNTHETIC AVAILABLE RADIATION, PAR

The spectral distribution of the incident PAR was measured during both clear and cloudy sky conditions from near sunrise to near sunset. Simultaneous measurements of the total downwelling irradiance E_{TOT}, from 300 to 2800 nm were made with an Eppley pyranometer. Figure 107 displays the regression of PAR on E_{TOT} for 71 incident spectra collected under conditions of constant incident radiation. The regression is defined by

$$\text{PAR } (\mu\text{einsteins/m}^2\text{/sec}) = 1.848\ E_{TOT}\ (\text{W/m}^2)$$

For each of the incident spectra the spectral distribution of quanta in PAR was determined for 20 nm bands, centred at 20 nm intervals from 410 nm to 690 nm. The quanta irradiance in each band was then calculated as a percentage of PAR. The spectral distribution of incident PAR is shown in Figure 108. Also indicated in the figure are the percentages of blue, green and red light comprising PAR.

Figures 107 and 108 can therefore be utilized, along with pyranometer measurements, to determine both PAR and its spectral distribution.

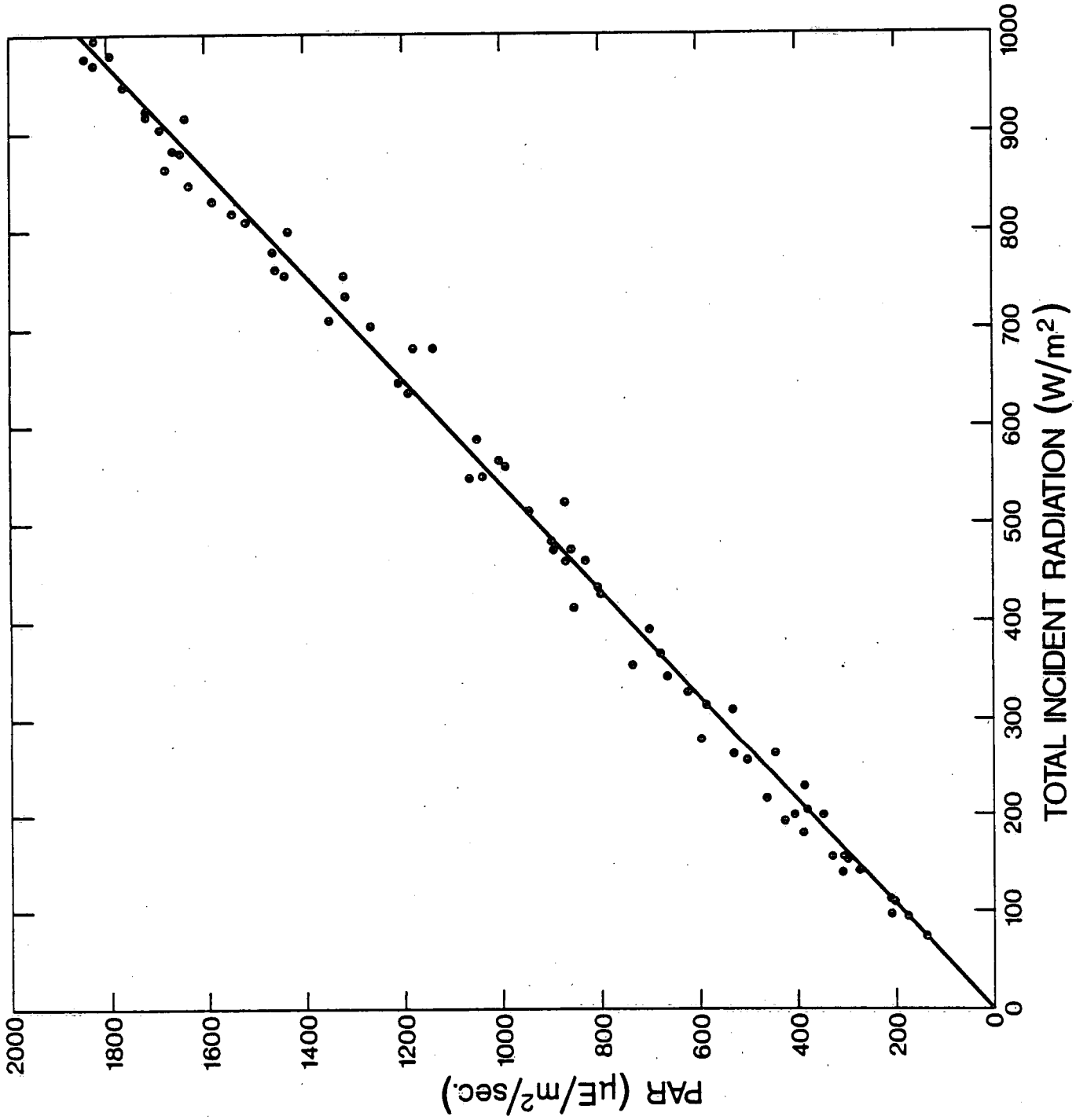
PAR (μE/m²/sec.)
2000
1800
1600
1400
1200
1000
800
600
400
200
0
100
200
300
400
500
600
700
800
900
1000
TOTAL INCIDENT RADIATION (W/m²)

FIG. 107

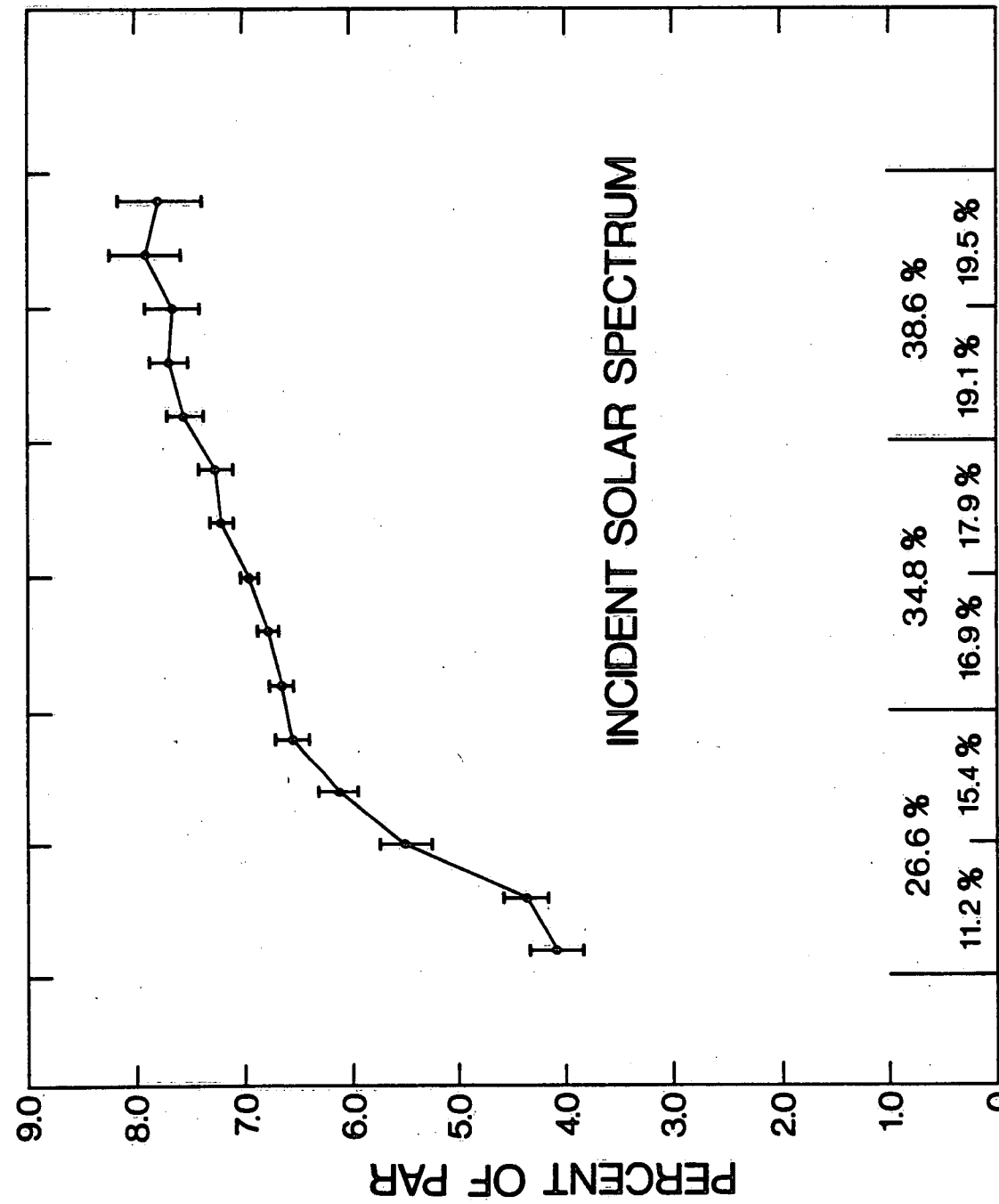
INCIDENT SOLAR SPECTRUM
PERCENT OF PAR
WAVELENGTH (nm)
9.0
8.0
7.0
6.0
5.0
4.0
3.0
2.0
1.0
0
400
450
500
550
600
650
700
11.2 %
15.4 %
26.6 %
16.9 %
17.9 %
34.8 %
19.1 %
19.5 %
38.6 %

FIG. 10B

DETECTION OF OPTICAL LAYERING

Figure 109 illustrates representative vertical transmission and temperature profiles for a mid-lake station in Lake Huron during the summer. The optical layering in the vicinity of the thermocline is a most obvious feature of the transmission profile.

Similarly, Figures 110 and 111 illustrate optical layering in the summer in Lakes Erie and Ontario, respectively. Such structure has been discussed in a previous section.

Figures 112 and 113 illustrate a time series of transmission profiles in Georgian Bay and Lake Erie, respectively. Generation, decay and migration of optical layers are apparent. Of particular note is the development of an epilimnionic layer in Lake Erie (Figure 113) in the late morning on August 19 and again on August 20, 1980.

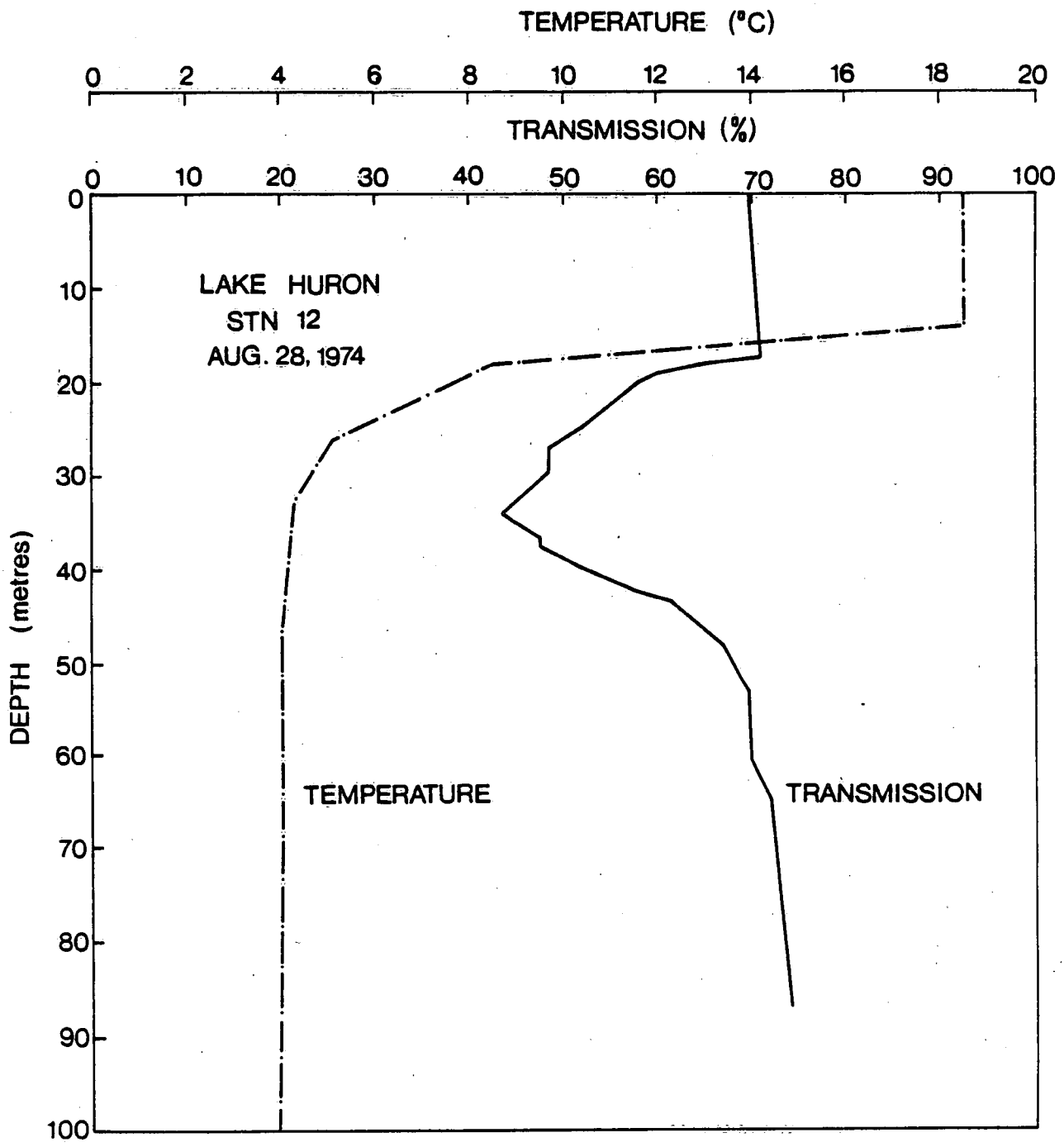
TEMPERATURE (°C)
0 2 4 6 8 10 12 14 16 18 20
TRANSMISSION (%)
0 10 20 30 40 50 60 70 80 90 100
DEPTH (metres)
0 10 20 30 40 50 60 70 80 90 100
LAKE HURON
STN 12
AUG. 28, 1974
TEMPERATURE
TRANSMISSION

FIG. 109

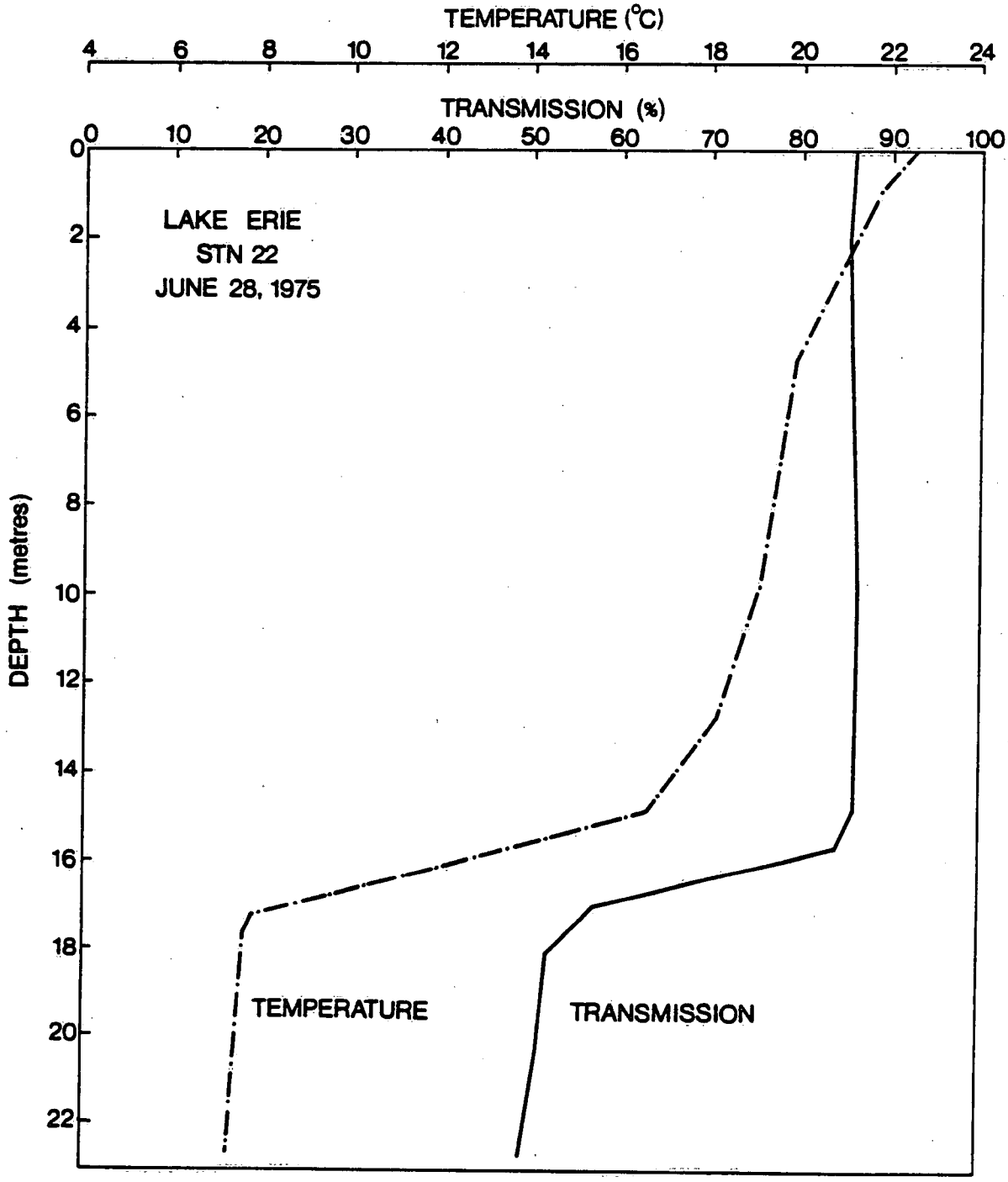
TEMPERATURE (°C)
4 6 8 10 12 14 16 18 20 22 24
TRANSMISSION (%)
0 10 20 30 40 50 60 70 80 90 100
LAKE ERIE
STN 22
JUNE 28, 1975
DEPTH (metres)
0 2 4 6 8 10 12 14 16 18 20 22
TEMPERATURE
TRANSMISSION

FIG. 110

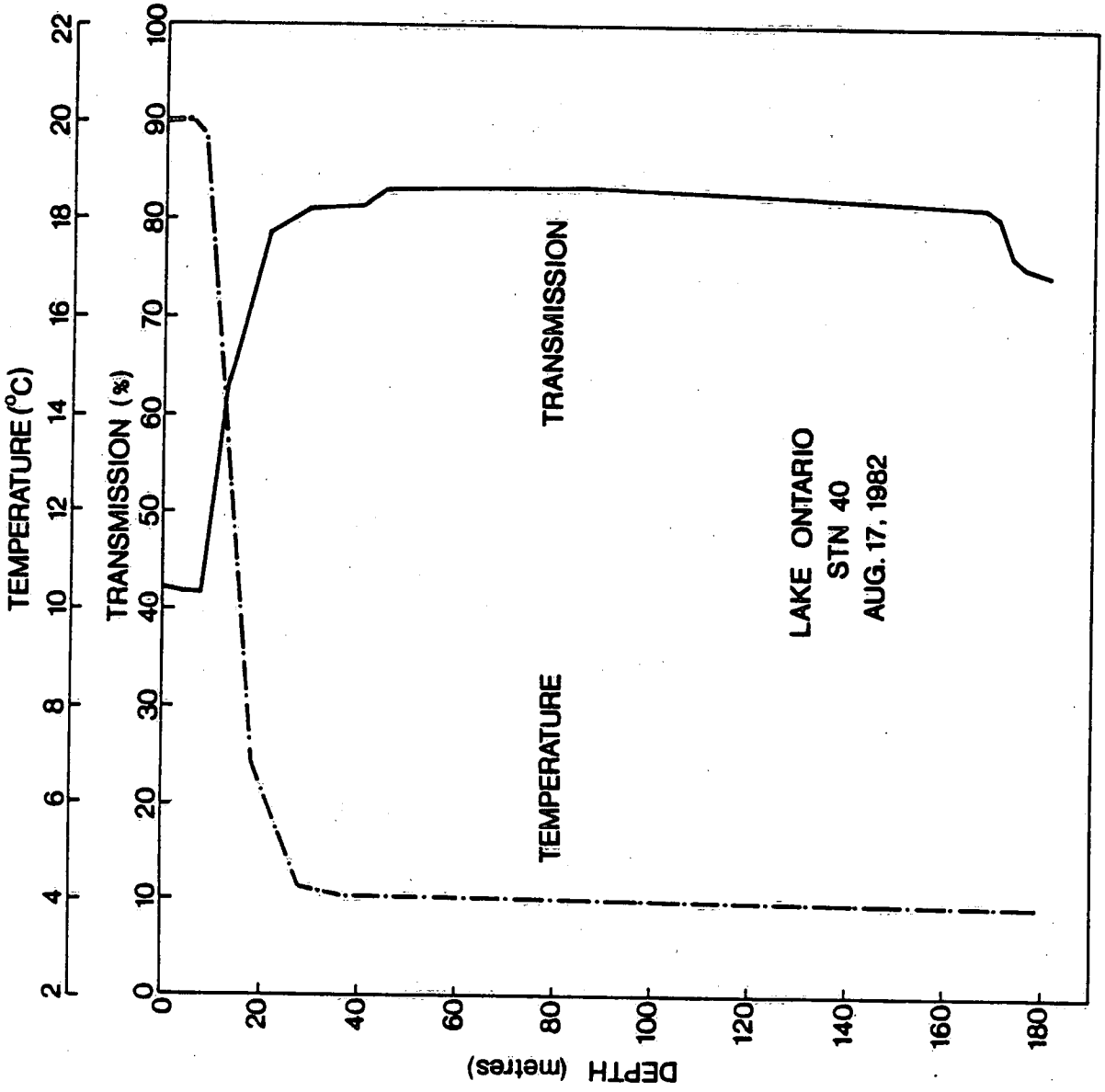
TEMPERATURE (°C)
TRANSMISSION (%)
DEPTH (metres)
TRANSMISSION
TEMPERATURE
LAKE ONTARIO
STN 40
AUG. 17, 1982

FIG. 111

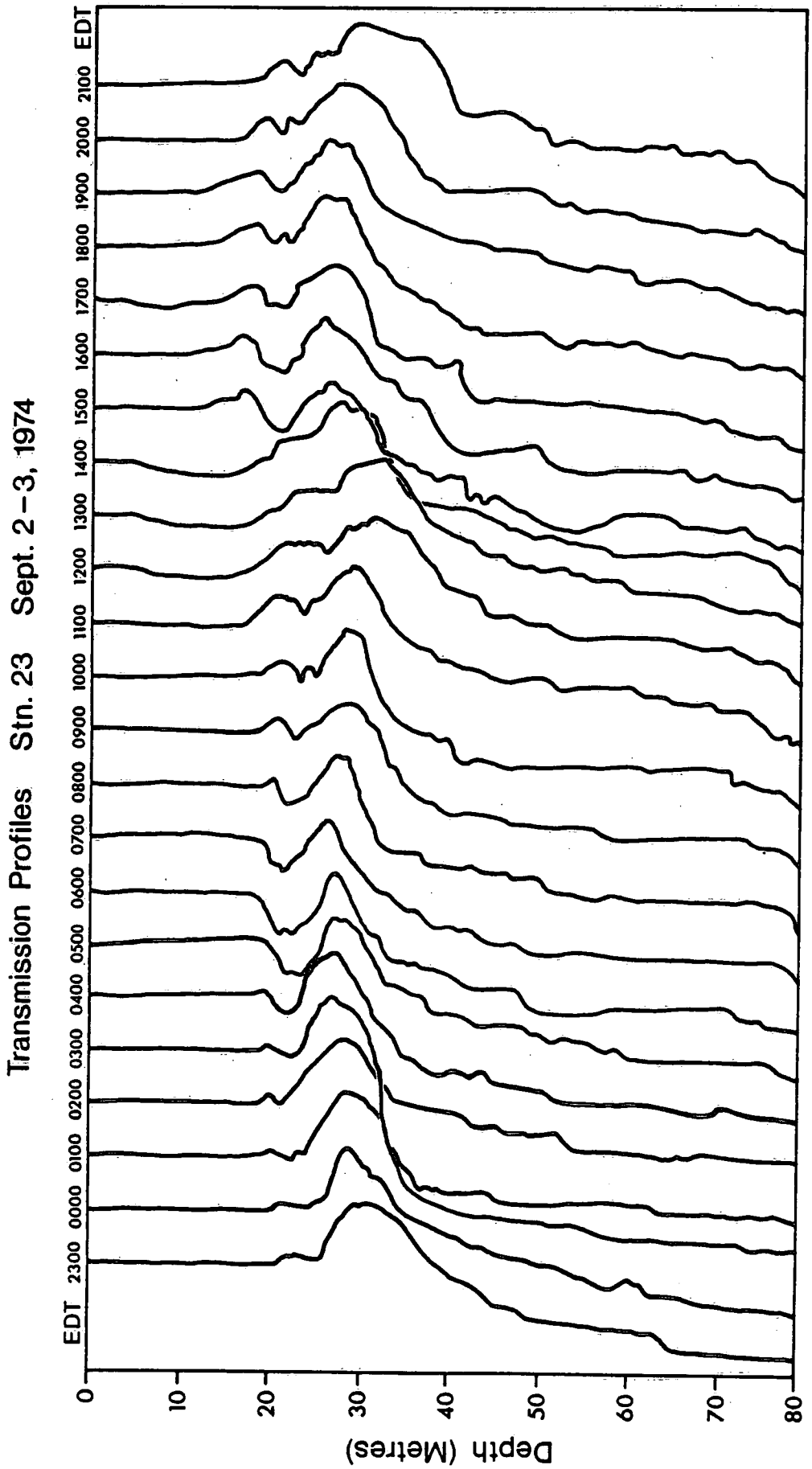
Transmission Profiles Stn. 23 Sept. 2–3, 1974
EDT 2300 0000 0100 0200 0300 0400 0500 0600 0700 0800 0900 1000 1100 1200 1300 1400 1500 1600 1700 1800 1900 2000 2100 EDT
0 10 20 30 40 50 60 70 80
Depth (Metres)

FIG. 112

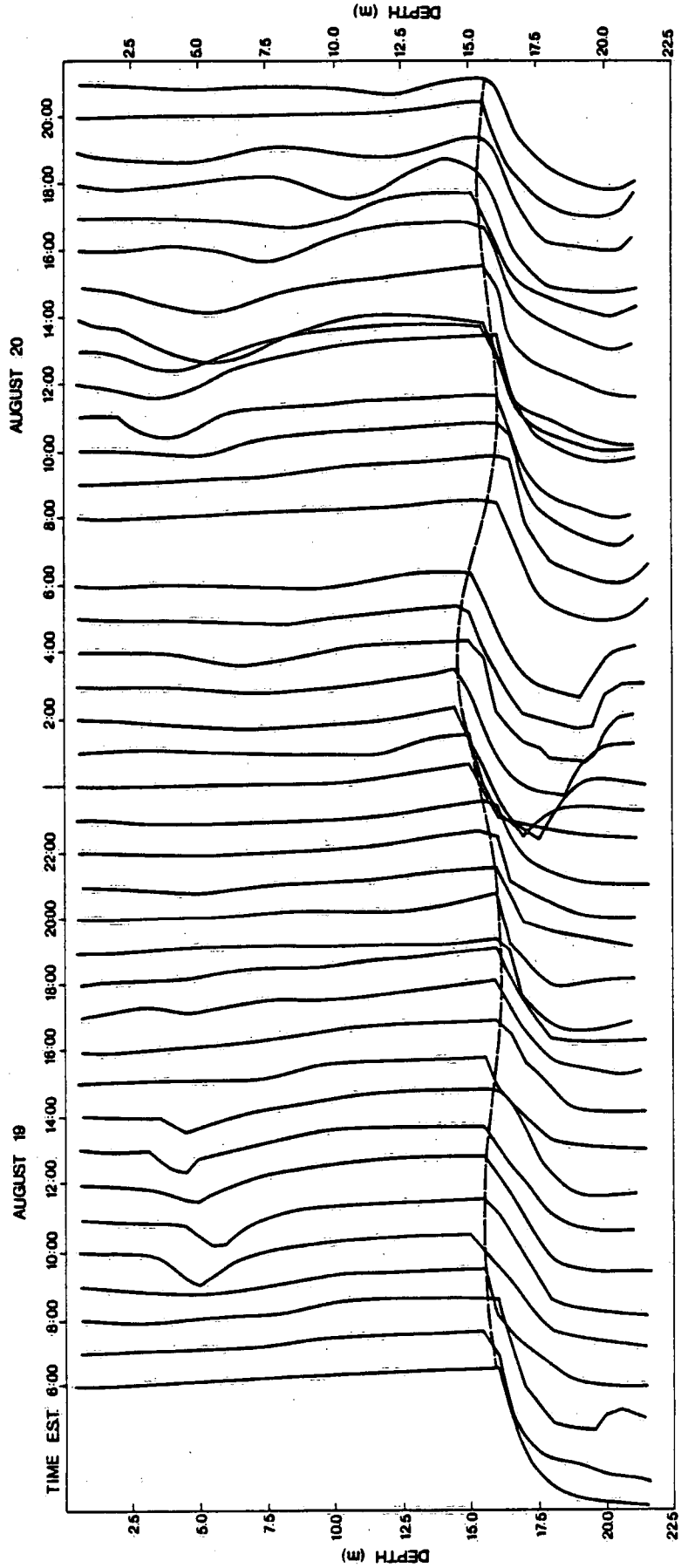
DEPTH (m)
2.5
5.0
7.5
10.0
12.5
15.0
17.5
20.0
22.5
AUGUST 20
AUGUST 19
TIME EST
6:00
8:00
10:00
12:00
14:00
16:00
18:00
20:00
22:00
2:00
4:00
6:00
8:00
10:00
12:00
14:00
16:00
18:00
20:00

FIG. 113

DETERMINATION OF "OPTICAL CROSS SECTIONS"

"Optical cross sections" refer to the attenuating influence on a per unit concentration basis of each component that defines a water mass and can influence its optical properties through the scattering and/or absorption of penetrating radiation. The obvious importance of such "optical cross sections" to the water quality parameters of natural waters has been extensively discussed elsewhere (Bukata et al, 1985; 1983; 1981a; 1981b) and will not be belaboured here. Rather, a brief discussion of three generally used methods of estimating such "cross sections" will be presented.

1) Defining the "optical cross section" of a component of a water mass as the change in the value of the irradiance attenuation coefficient k per unit change in concentration of the component (irrespective of whether the predominant process responsible for the change in k is scattering, absorption, or a combination of both), one technique for estimating such "optical cross sections" consists simply of linearly regressing k against the concentrations of each of the components. Figures 114 and 115 show such linear regressions of k on chlorophyll a concentrations and particulate organic carbon concentrations, respectively. It must be cautioned, however, that this is a highly hazardous approach to the analysis. Such regressions represent, at best, partial derivatives existing between the variables at the time that the regression was performed, and are strongly dependent

upon the influences of the components not being considered. Such partial derivatives can be confidently considered to be equivalent to a total derivative only in either the absence of other influencing components, or in the presence of constant concentrations of such other influencing components. If the component being regressed was the only variable influencing the irradiance attenuation coefficient, then curves such as shown in Figures 114 and 115 could be readily used, with subsequent measurements of k, to reliably infer the concentrations of such water quality indicators as chlorophyll a and particulate organic carbon. However, since such conditions of constancy and/or absence of convoluted components are virtually non-existent in the waters comprising the Laurentian Great Lakes, this first method of estimating "optical cross sections" utilizing linear regressions cannot be generally recommended.

One instance, however, where such a simple linear regression approaches a reasonable degree of reliability is shown in Figure 116. Herein is the regression between the beam attenuation coefficient, c, and the suspended mineral concentration in Lake Erie. It is known that the high concentrations of suspended mineral optically overwhelm the small-to-moderate concentrations of chlorophyll a and other water quality indicators. Consequently, the suspended mineral concentration may be confidently considered to be the predominant factor influencing the beam attenuation coefficient. In this instance, therefore,

direct measurements of c may be utilized to directly infer the suspended mineral concentrations in Lake Erie, provided that the range of c values plotted in Figure 116 is not exceeded. As will be seen later relationships such as considered here do not necessarily retain their linearity over extended ranges of values of independent variables.

2) Again defining the "optical cross section" of a component of a water mass as the change in the value of the attenuation coefficient per unit change in concentration of the responsible aquatic component, a second method suggested by Tyler (1976) has often been used. Figures 117 and 118 illustrate applications of this method. Therein are plotted scatter diagrams of all the data pairs. (The enormous amount of scatter evident in Figures 117 and 118 vividly illustrate the general futility of the single linear regression technique described above). A straight line is generated and taken as defining the lower limit of the envelope containing all the data pairs. The y-intercept of this line is taken as the distilled water value of the optical parameter being regressed (c and k_v for Figures 117 and 118, respectively). The basic premise of this method is that the data points defining this bottom envelope represent water masses which are comprised solely of the water quality component of interest. All other water quality components are absent (not merely constant, but totally absent). If this is indeed the case (i.e. the constructed line applies to water masses comprised of but a

single component), then the slope of the line truly represents a total derivative, and therefore a true "optical cross section". However, if such is not the case (a situation which could easily arise if, for instance, no such uni-component water masses have been encountered in the sampling activities), then this technique would clearly overestimate the numerical values of the "optical cross sections".

3) Defining the "optical cross section" of a component of a water mass more specifically as the amount of either absorption or scattering at wavelength λ for a unit concentration of a particular component [two distinct "cross sections" therefore emerge for the ith component of a water mass: an "absorption cross section", $a_i(\lambda)$, and a "scattering cross section, $b_i(\lambda)$], a third and more rigorous method of estimating cross sections involving the use of multiple linear regressions and/or non-linear optimization techniques has been employed at NWRI. These techniques and the results of such analyses and their applications to water quality estimations have been discussed in great depth in a recent report (Bukata et al, 1985). The discussions will not be repeated here. However, Figures 119 and 120 illustrate the spectral nature of the absorption and scattering "cross sections", respectively, for total suspended mineral, chlorophyll a and dissolved organic carbon. These "cross sections" were determined for Lake Ontario waters.

The use of such absorption and scattering "cross sections" in estimating water quality parameters is illustrated in the next section of this report.

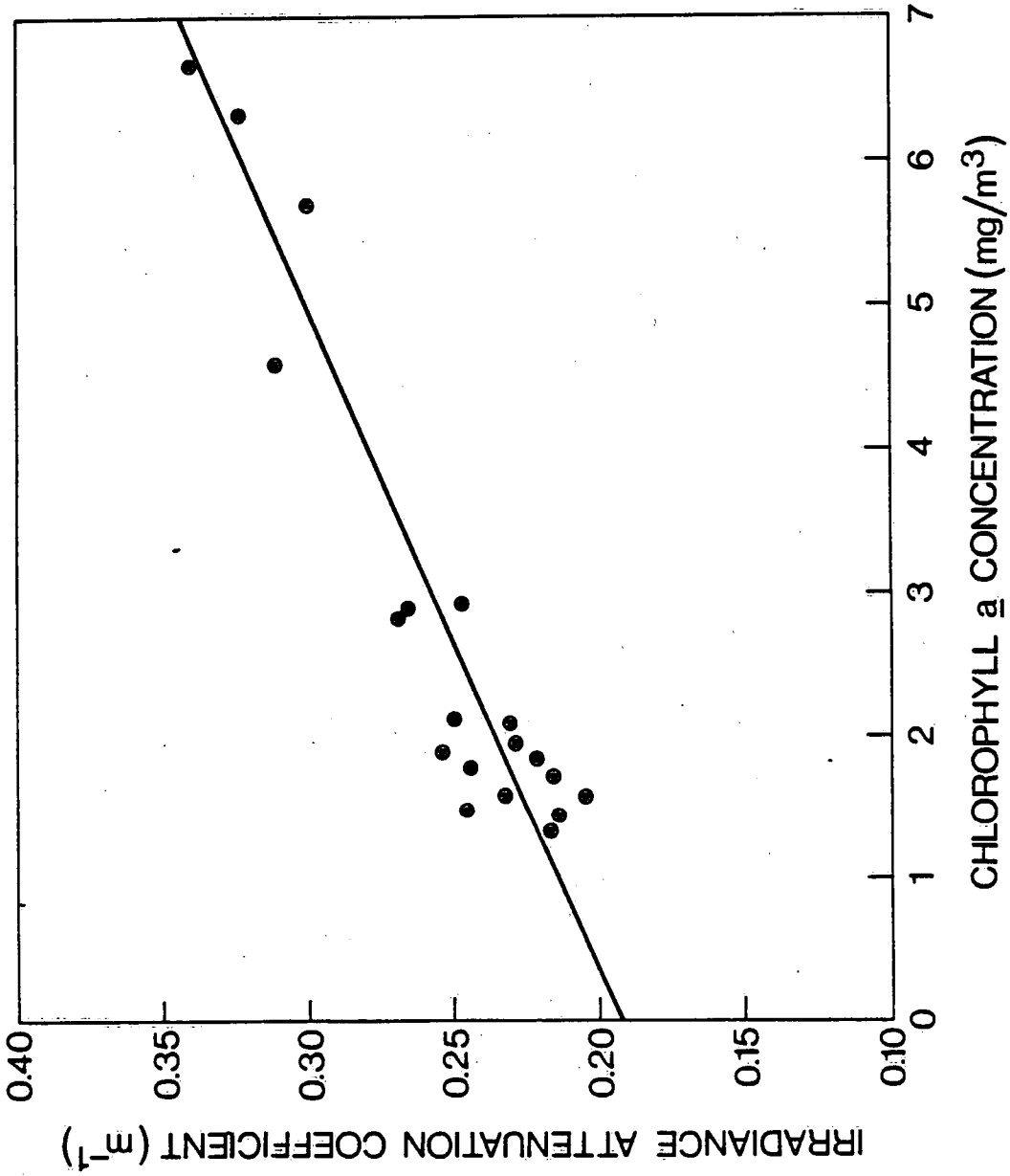
IRRADIANCE ATTENUATION COEFFICIENT (m^{-1})
0.40
0.35
0.30
0.25
0.20
0.15
0.10
0
1
2
3
4
5
6
7
CHLOROPHYLL a CONCENTRATION (mg/m^3)

FIG. 114

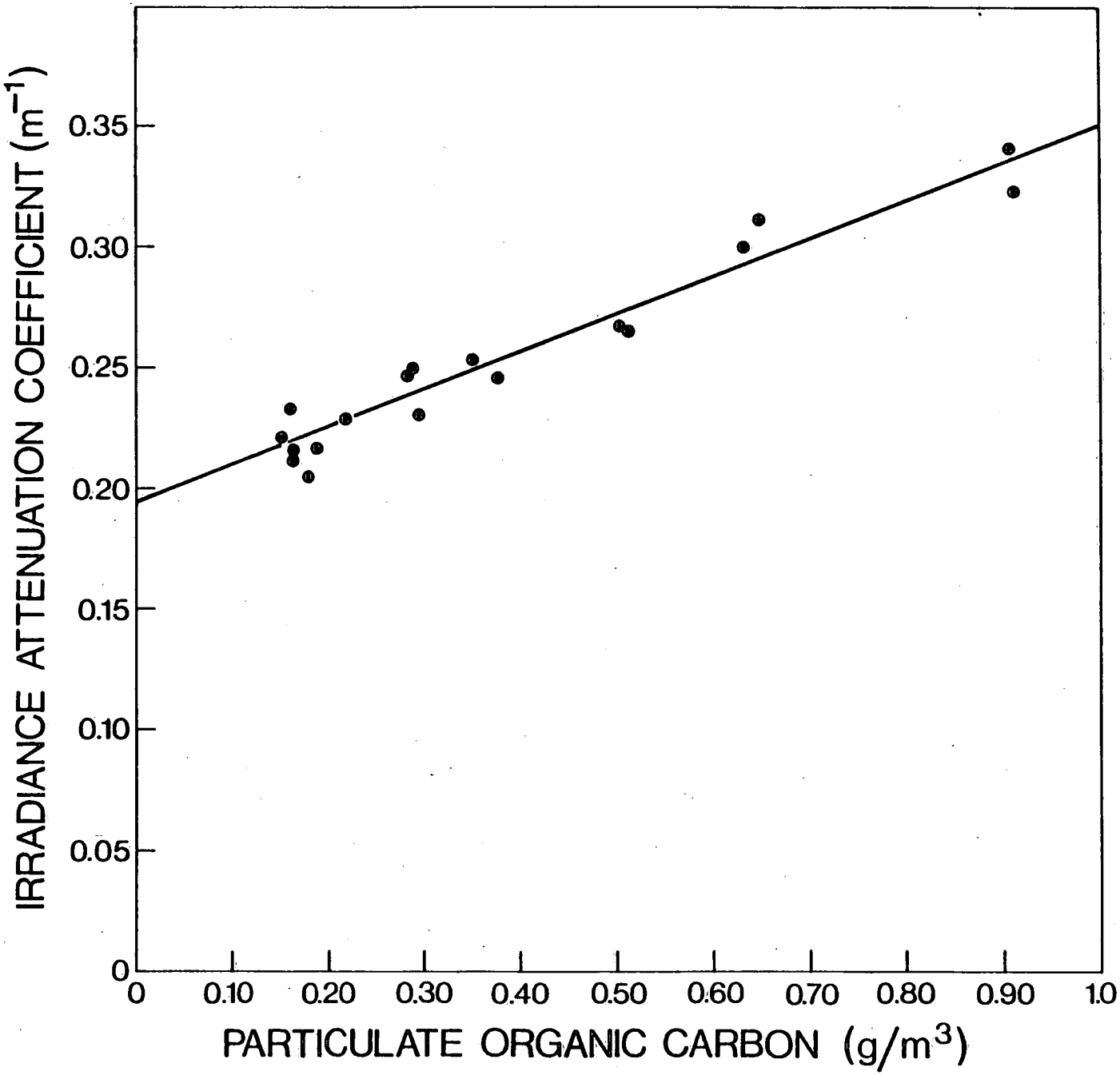
IRRADIANCE ATTENUATION COEFFICIENT (m^{-1})
0.35
0.30
0.25
0.20
0.15
0.10
0.05
0
0
0.10
0.20
0.30
0.40
0.50
0.60
0.70
0.80
0.90
1.0
PARTICULATE ORGANIC CARBON (g/m^3)

FIG. 115

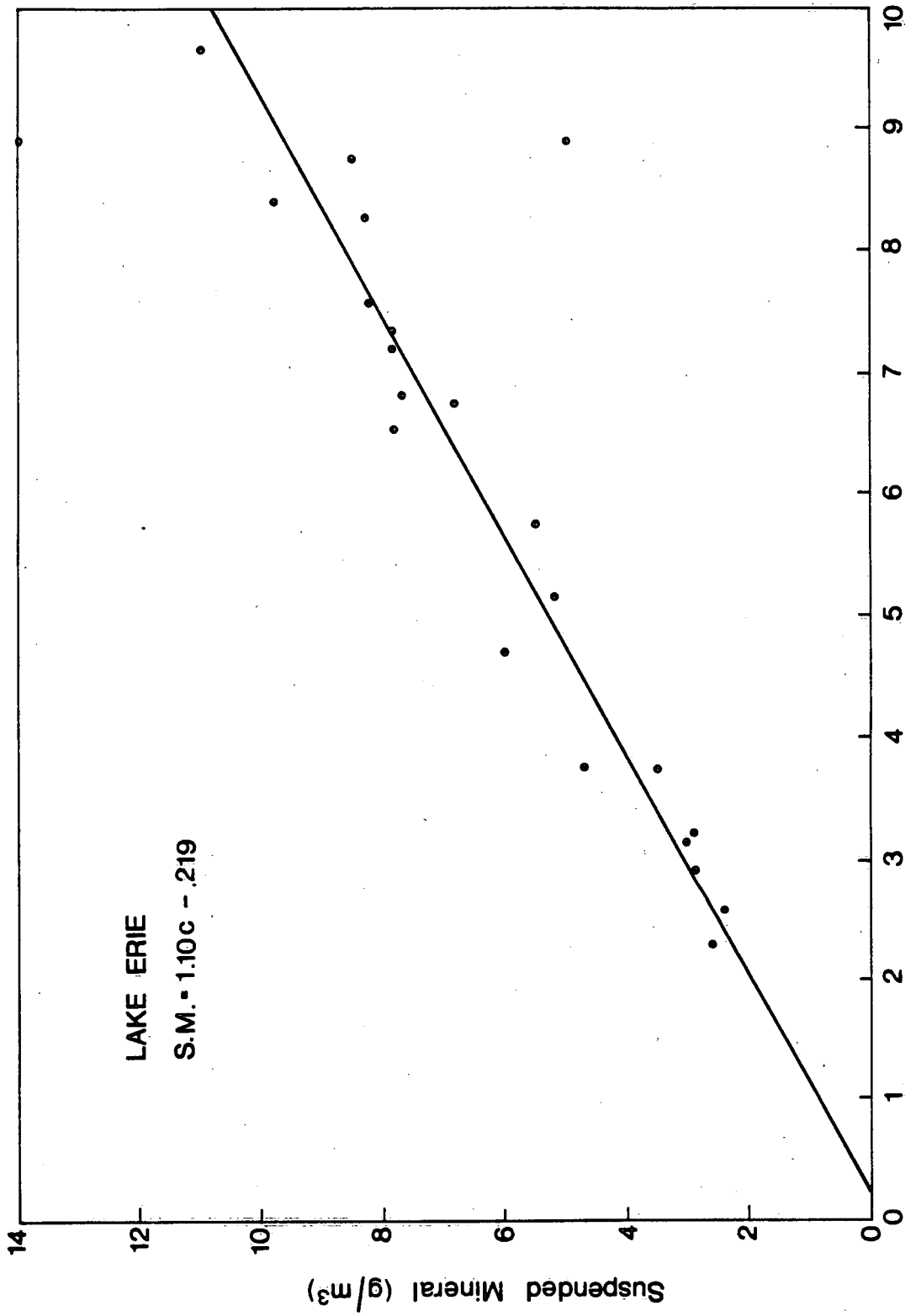
LAKE ERIE
S.M. = 1.10c - .219
Suspended Mineral (g/m³)
Beam Attenuation Coefficient (m⁻¹)
0
2
4
6
8
10
12
14
0
1
2
3
4
5
6
7
8
9
10

FIG. 116

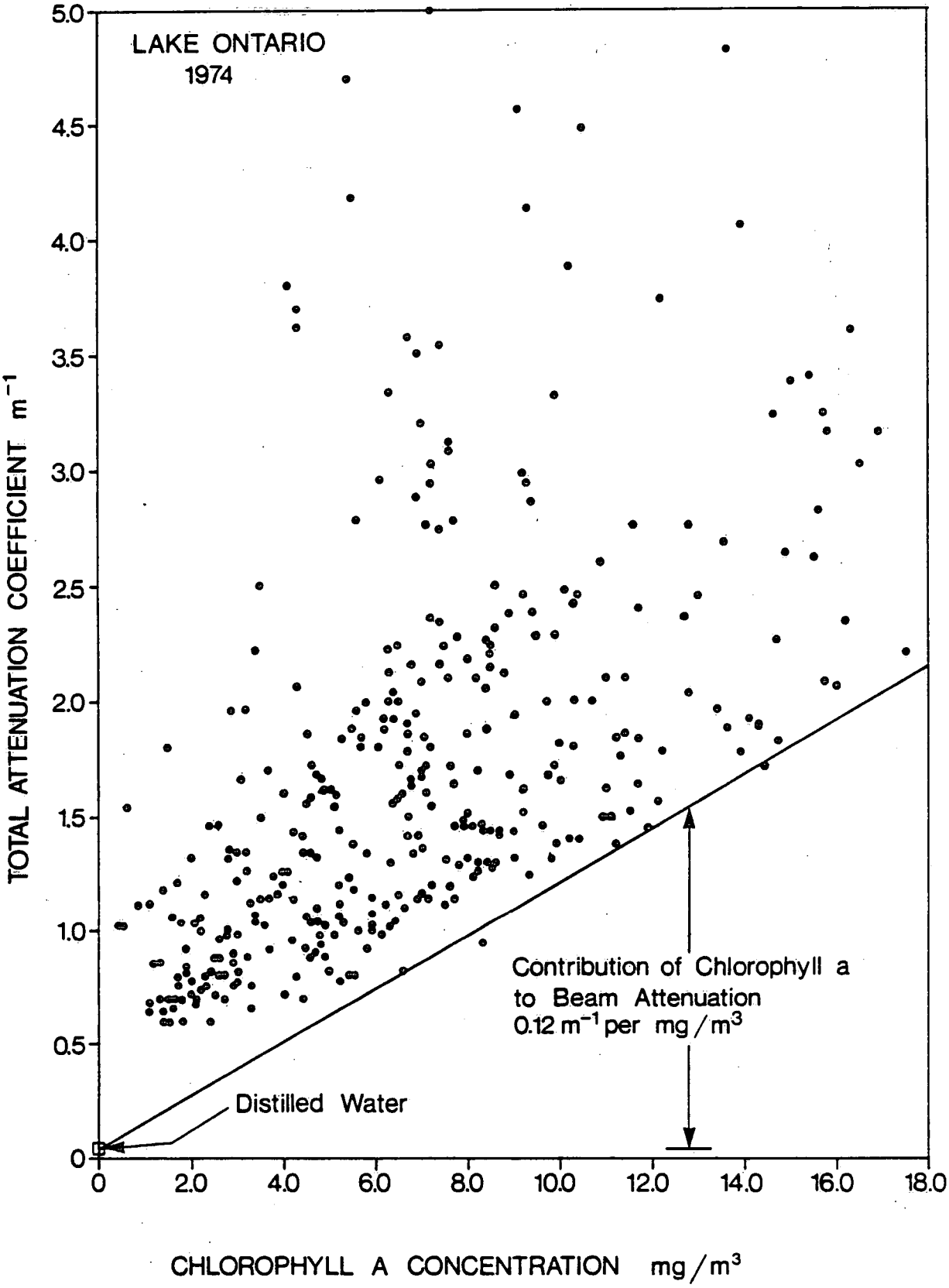
LAKE ONTARIO
1974
TOTAL ATTENUATION COEFFICIENT m⁻¹
CHLOROPHYLL A CONCENTRATION mg/m³
Contribution of Chlorophyll a
to Beam Attenuation
0.12 m⁻¹ per mg/m³
Distilled Water
0
0.5
1.0
1.5
2.0
2.5
3.0
3.5
4.0
4.5
5.0
0
2.0
4.0
6.0
8.0
10.0
12.0
14.0
16.0
18.0

FIG. 117

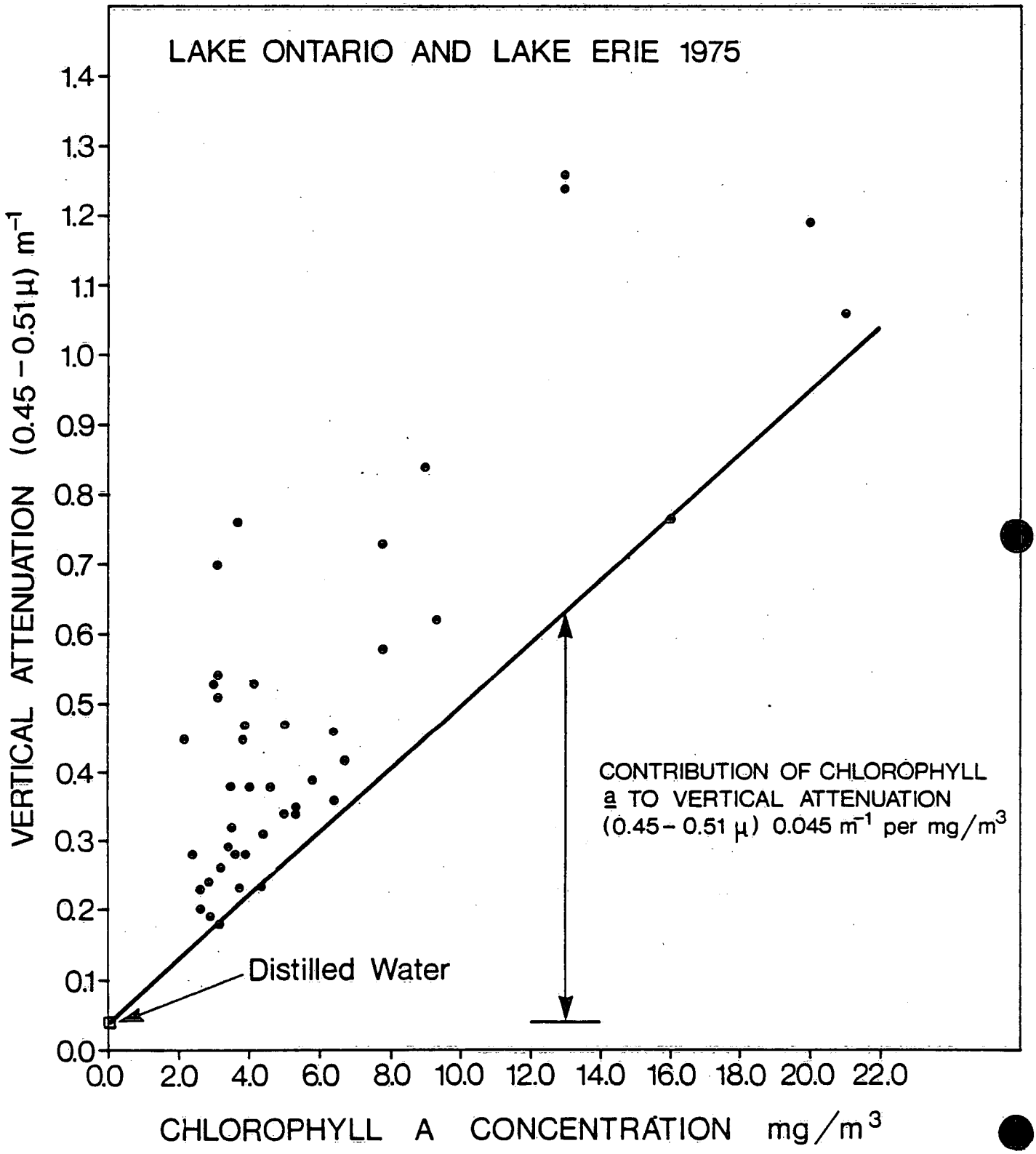
LAKE ONTARIO AND LAKE ERIE 1975
VERTICAL ATTENUATION (0.45 – 0.51 μ) m⁻¹
1.4
1.3
1.2
1.1
1.0
0.9
0.8
0.7
0.6
0.5
0.4
0.3
0.2
0.1
0.0
0.0 2.0 4.0 6.0 8.0 10.0 12.0 14.0 16.0 18.0 20.0 22.0
CHLOROPHYLL A CONCENTRATION mg/m³
CONTRIBUTION OF CHLOROPHYLL a TO VERTICAL ATTENUATION (0.45 – 0.51 μ) 0.045 m⁻¹ per mg/m³
Distilled Water

FIG. 118

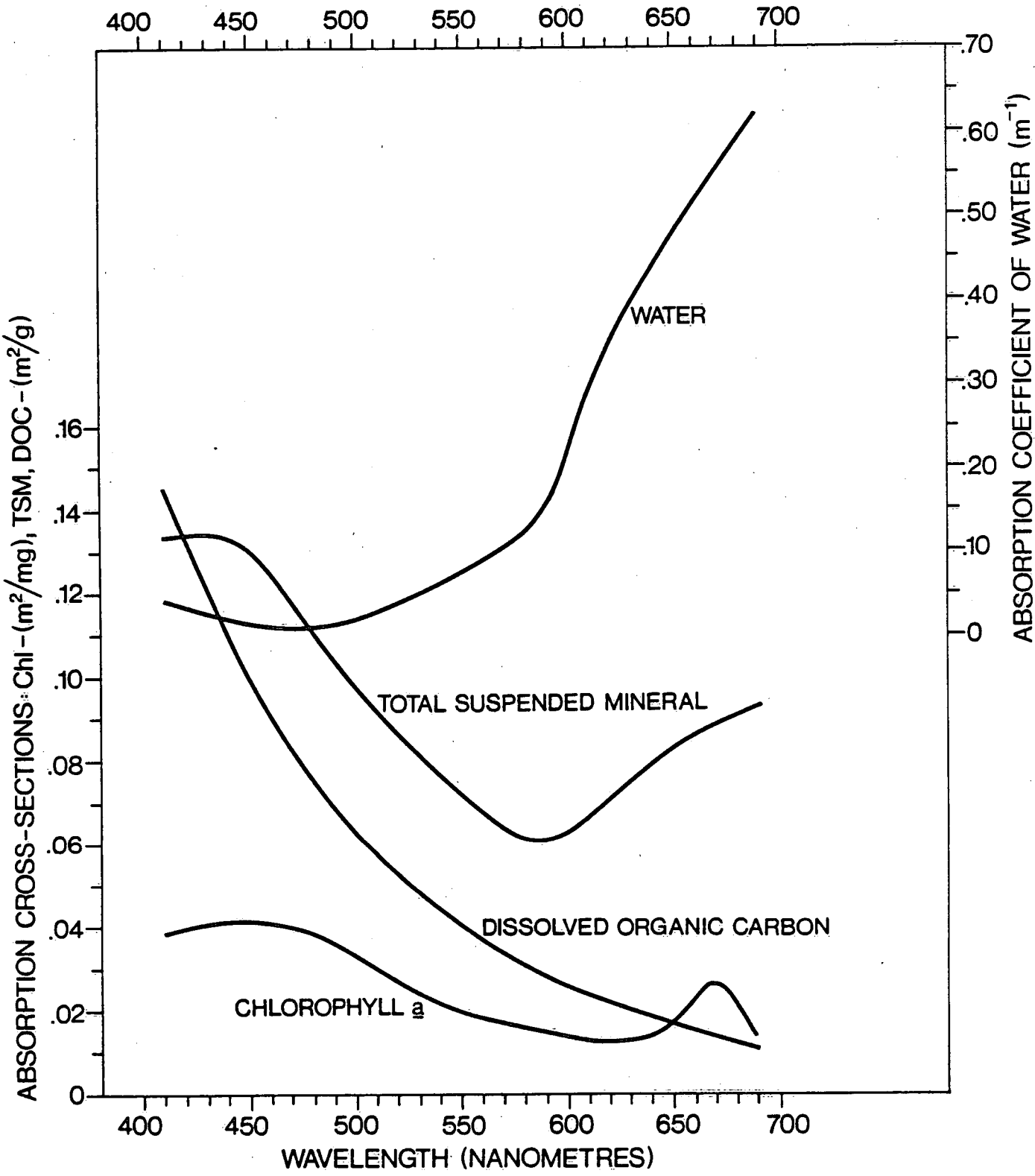
400
450
500
550
600
650
700
.70
.60
.50
.40
.30
.20
.10
0
ABSORPTION COEFFICIENT OF WATER (m^{-1})
WATER
.16
.14
.12
.10
.08
.06
.04
.02
0
ABSORPTION CROSS-SECTIONS-Chl-(m^2/mg), TSM, DOC-(m^2/g)
TOTAL SUSPENDED MINERAL
DISSOLVED ORGANIC CARBON
CHLOROPHYLL a
400
450
500
550
600
650
700
WAVELENGTH (NANOMETRES)

FIG. 119

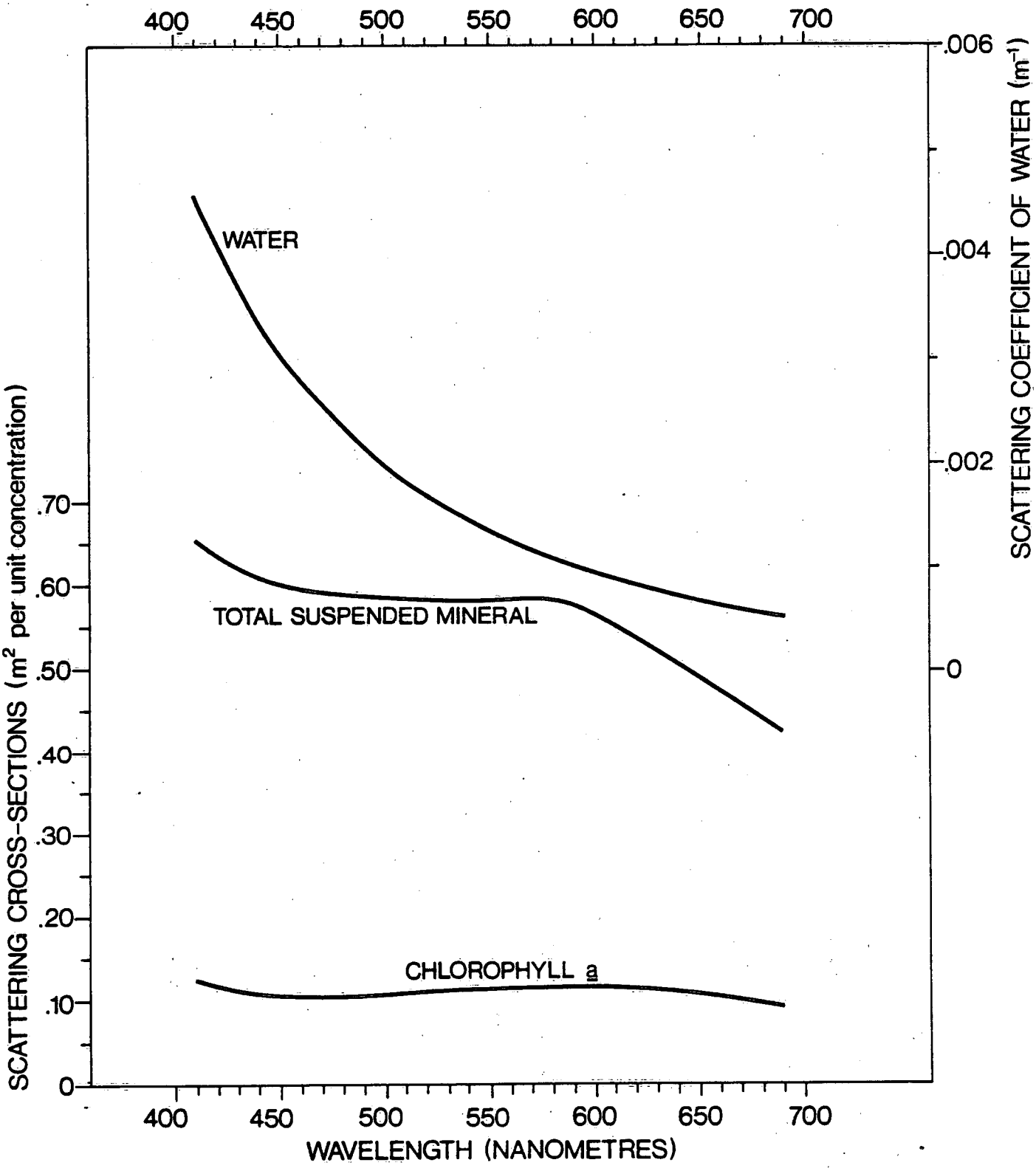
400
450
500
550
600
650
700
.006
.004
.002
0
WATER
TOTAL SUSPENDED MINERAL
CHLOROPHYLL a
.70
.60
.50
.40
.30
.20
.10
0
SCATTERING CROSS-SECTIONS (m² per unit concentration)
SCATTERING COEFFICIENT OF WATER (m⁻¹)
WAVELENGTH (NANOMETRES)

FIG. 120

ESTIMATION OF WATER QUALITY PARAMETERS

As outlined in Bukata et al (1983; 1985), the "optical cross sections" of Figures 119 and 120 may be utilized, along with appropriate radiative transfer theory, to generate the subsurface irradiance reflectance (volume reflectance) spectra that would be observed for water masses comprised of any combination of component concentrations. Figures 121-123 illustrate the mathematically determined volume reflectance spectra for a variety of Lake Ontario water masses displaying variations in their concentrations of suspended minerals, chlorophyll a and dissolved organic carbon.

The estimation of water quality from in situ determinations of subsurface irradiance reflectance spectra would then proceed as follows: The volume reflectance spectrum is directly measured. A non-linear optimization technique (Bukata et al, 1985), along with the spectral values of the "optical cross sections" is used to optimize those values of chlorophyll a, suspended mineral, and dissolved organic carbon that generate a subsurface irradiance reflectance spectrum which most closely resembles the directly measured spectrum.

The above methodology uses the entire visible optical spectrum. Other NWRI attempts to estimate water quality have utilized restrictive regions of the visible spectrum. For example, Figure 124 illustrates a duo-isoplethic curve (the 2 parameters being the concentrations of chlorophyll a as indicated by the first number, and

suspended mineral as indicated by the second number; the DOC concentration is kept constant). Figure 124 utilizes as its axes the subsurface irradiance reflectances at the single wavelength values 550 nm (yellow-green) and 670 nm (red). Clearly, such duo-isopleths may be constructed for any pairs of wavelengths, although not all pairs of wavelengths would be equally appropriate or even usable (Bukata et al, 1981b).

Curves such as shown in Figure 124 may be directly utilized to estimate chlorophyll a and suspended mineral concentrations from in situ measurements of the volume reflectance at two wavelengths. Figure 125 illustrates the scatter between estimated and directly measured chlorophyll a concentrations in Lake Ontario. Similarly Figure 126 illustrates the scatter between estimated and directly measured suspended mineral concentrations.

The use of a single wavelength determination of the subsurface irradiance reflectance in the estimation of water quality in optically complex lake waters can be all but totally eliminated. There exists, however, one very significant exception, namely the use of the volume reflectance at red wavelengths to estimate with a reasonable confidence the suspended mineral concentrations in Great Lake waters. This is illustrated in Figure 127 which displays the anticipated volume reflectance at 650 nm as a function of increasing suspended mineral concentration. The uncertainty bars AB at each plotted point include the range of calculated values of volume

reflectance resulting from varying the chlorophyll *a* and dissolved organic carbon concentrations over the range of values encountered in Lake Ontario. Even with the high degree of optical complexity arising from such large observed fluctuations in component concentrations, a single wavelength measurement of volume reflectance in the red does display an ability to estimate suspended mineral concentration. Figure 128 shows the scatter arising from a direct comparison of directly measured subsurface irradiance reflectance at 670 nm and directly sampled suspended mineral concentrations.

One final technique for estimating suspended mineral concentrations is shown in Figure 129 wherein the relationship between suspended mineral concentration and beam attenuation coefficient c suggests that a determination of c should yield reasonable estimate of the suspended mineral concentration. As stated in the previous section, such a technique may be considered since the impact on c brought about by suspended mineral concentrations is considerably larger than the impacts on c brought about by competitive component concentrations. It should be noted that for $0 \leq c \leq 10\ m^{-1}$ a linear relationship between c and suspended minerals is readily apparent (see previous section). However, for values of $c > 10\ m^{-1}$ the effects of multiple scattering manifest as a distinctly exponential relationship.

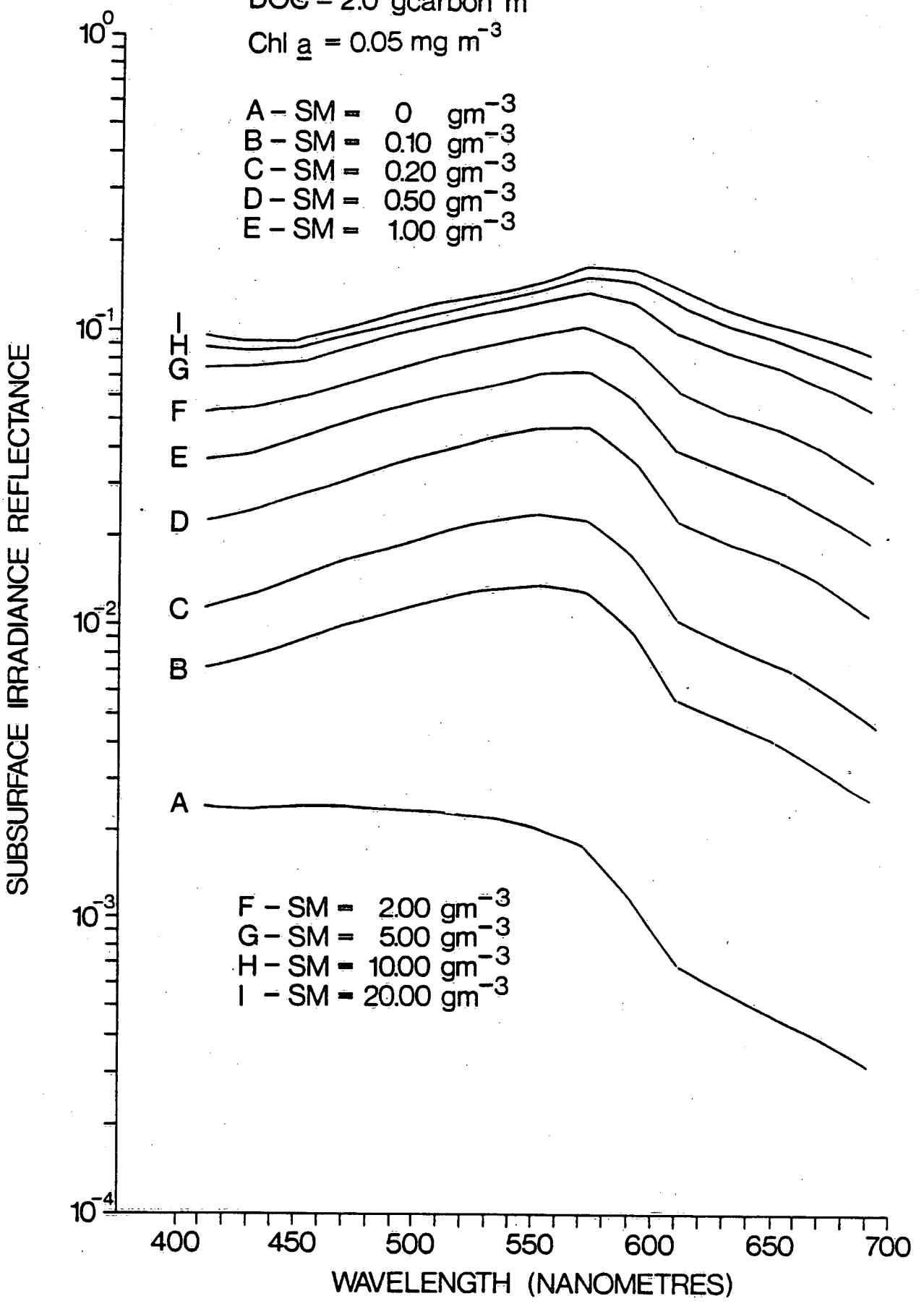
DOC = 2.0 gcarbon m^{-3}
Chl a = 0.05 mg m^{-3}
A – SM = 0 gm^{-3}
B – SM = 0.10 gm^{-3}
C – SM = 0.20 gm^{-3}
D – SM = 0.50 gm^{-3}
E – SM = 1.00 gm^{-3}
F – SM = 2.00 gm^{-3}
G – SM = 5.00 gm^{-3}
H – SM = 10.00 gm^{-3}
I – SM = 20.00 gm^{-3}
SUBSURFACE IRRADIANCE REFLECTANCE
10^{0}
10^{-1}
10^{-2}
10^{-3}
10^{-4}
400
450
500
550
600
650
700
WAVELENGTH (NANOMETRES)

FIG. 121

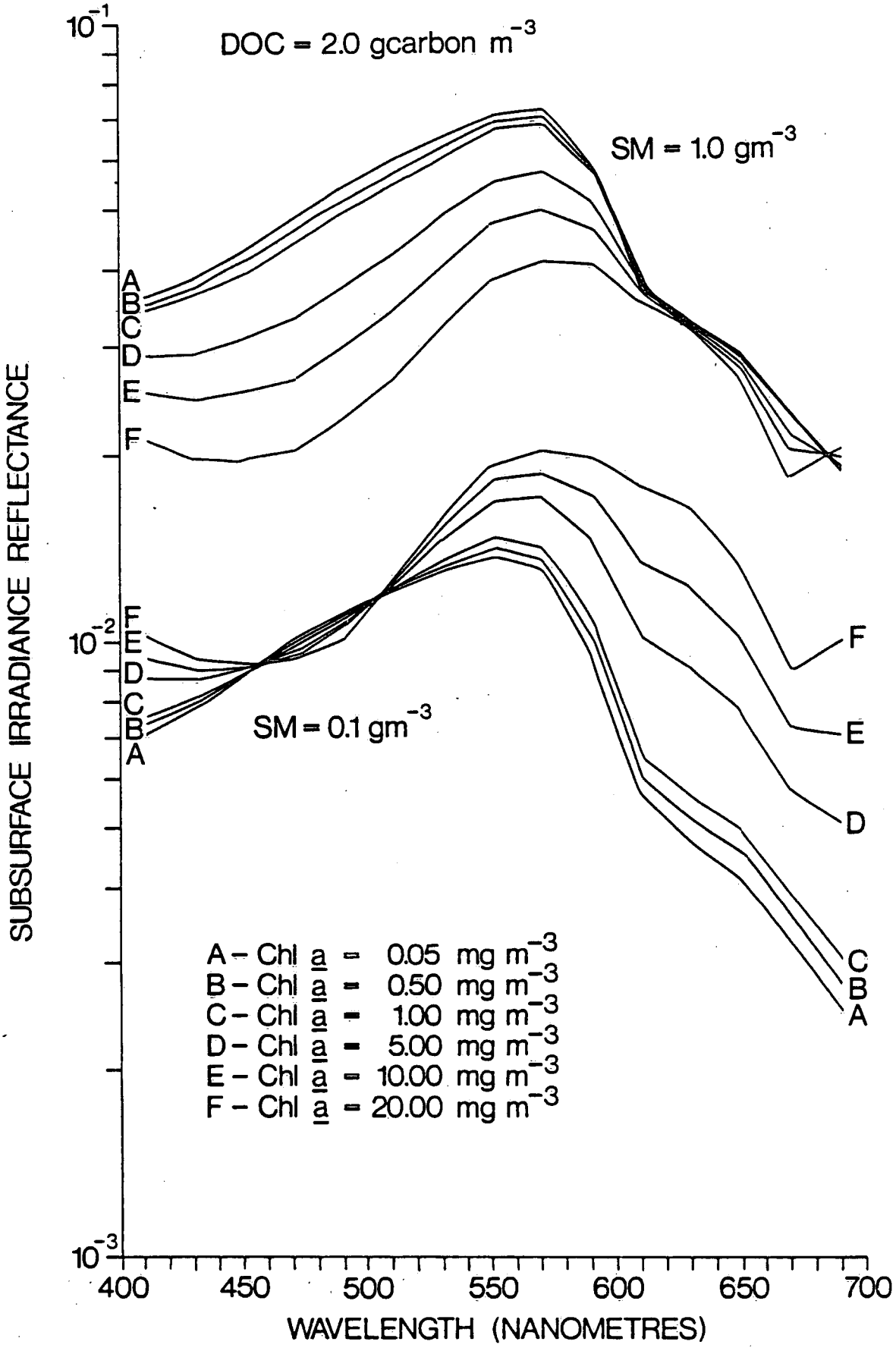
DOC = 2.0 gcarbon m^{-3}
SM = 1.0 gm^{-3}
SM = 0.1 gm^{-3}
SUBSURFACE IRRADIANCE REFLECTANCE
10^{-1}
10^{-2}
10^{-3}
400
450
500
550
600
650
700
WAVELENGTH (NANOMETRES)
A
B
C
D
E
F
A – Chl a = 0.05 mg m^{-3}
B – Chl a = 0.50 mg m^{-3}
C – Chl a = 1.00 mg m^{-3}
D – Chl a = 5.00 mg m^{-3}
E – Chl a = 10.00 mg m^{-3}
F – Chl a = 20.00 mg m^{-3}

FIG. 122

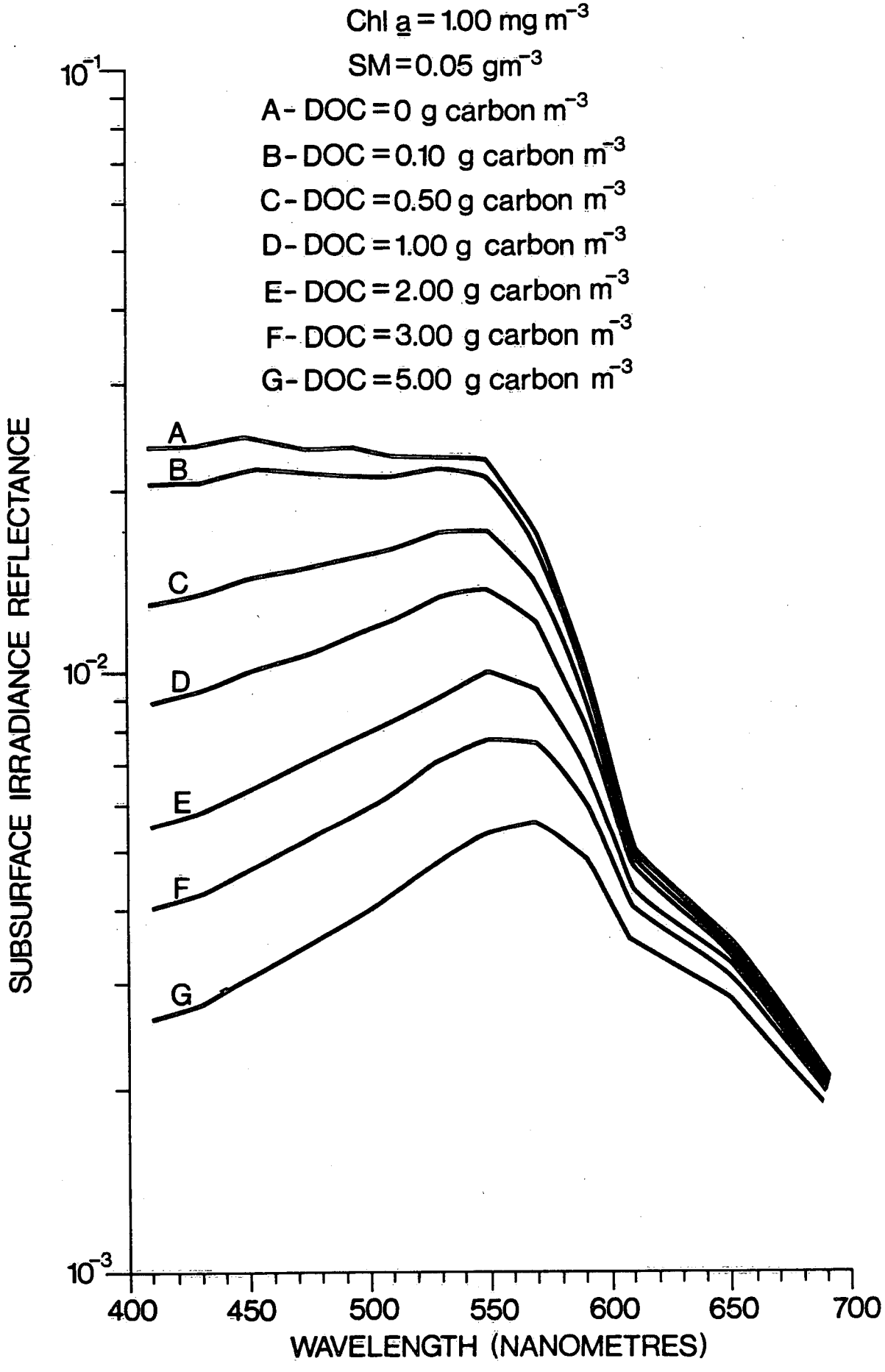
Chl a = 1.00 mg m^{-3}
SM = 0.05 gm^{-3}
A - DOC = 0 g carbon m^{-3}
B - DOC = 0.10 g carbon m^{-3}
C - DOC = 0.50 g carbon m^{-3}
D - DOC = 1.00 g carbon m^{-3}
E - DOC = 2.00 g carbon m^{-3}
F - DOC = 3.00 g carbon m^{-3}
G - DOC = 5.00 g carbon m^{-3}
SUBSURFACE IRRADIANCE REFLECTANCE
10^{-1}
10^{-2}
10^{-3}
A
B
C
D
E
F
G
400
450
500
550
600
650
700
WAVELENGTH (NANOMETRES)

FIG. 123

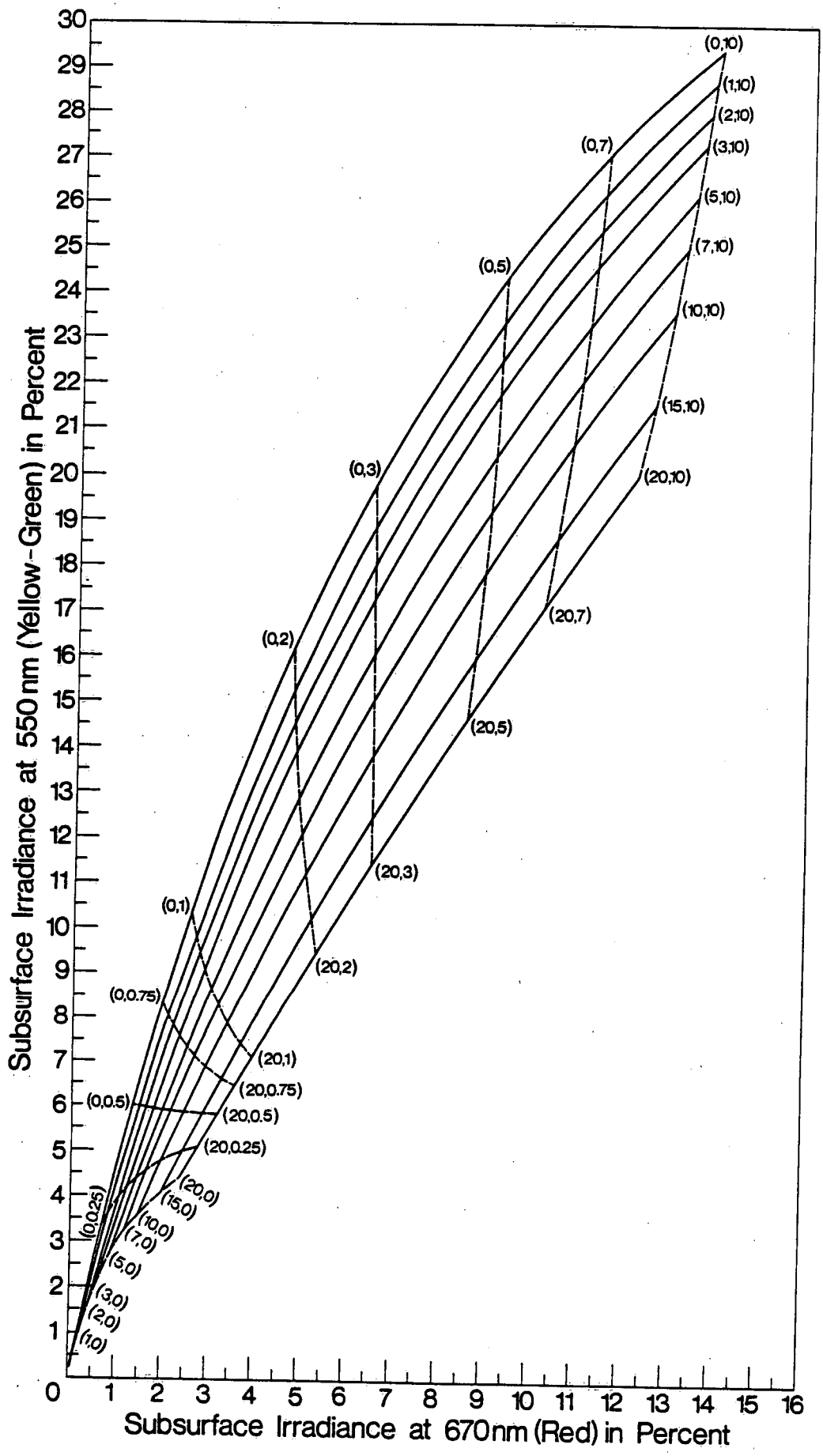
Subsurface Irradiance at 550nm (Yellow-Green) in Percent
Subsurface Irradiance at 670nm (Red) in Percent
0
1
2
3
4
5
6
7
8
9
10
11
12
13
14
15
16
17
18
19
20
21
22
23
24
25
26
27
28
29
30
(0,10)
(1,10)
(2,10)
(3,10)
(5,10)
(7,10)
(10,10)
(15,10)
(20,10)
(0,7)
(20,7)
(0,5)
(20,5)
(0,3)
(20,3)
(0,2)
(20,2)
(0,1)
(20,1)
(0,0.75)
(20,0.75)
(0,0.5)
(20,0.5)
(20,0.25)
(0,0.25)
(20,0)
(15,0)
(10,0)
(7,0)
(5,0)
(3,0)
(2,0)
(1,0)

FIG. 124

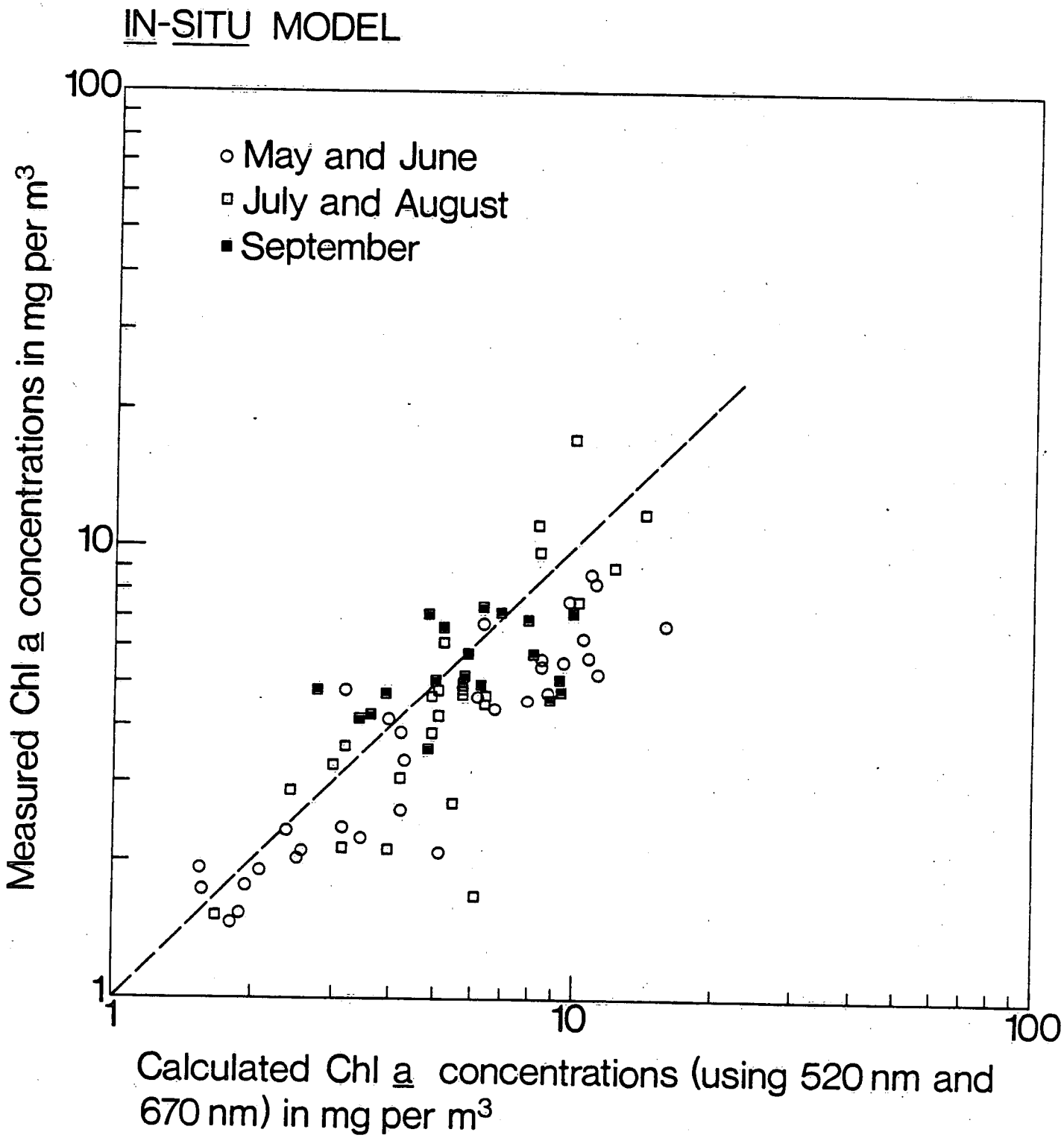
IN-SITU MODEL
100
10
1
1
10
100
May and June
July and August
September
Measured Chl a concentrations in mg per m3
Calculated Chl a concentrations (using 520 nm and 670 nm) in mg per m3

FIG. 125

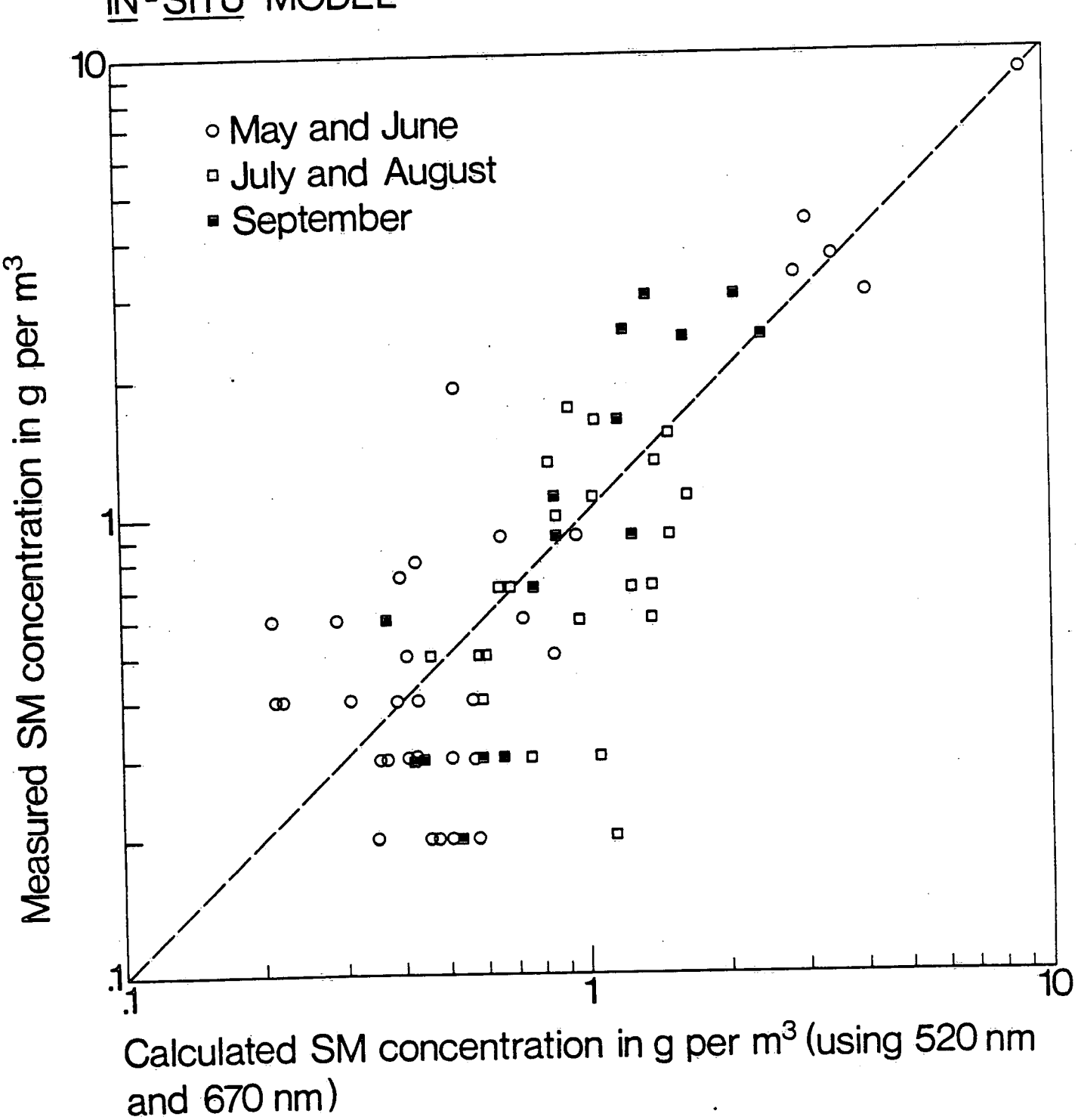
IN-SITU MODEL
10
1
.1
.1
1
10
May and June
July and August
September
Measured SM concentration in g per m3
Calculated SM concentration in g per m3 (using 520 nm and 670 nm)

FIG. 126

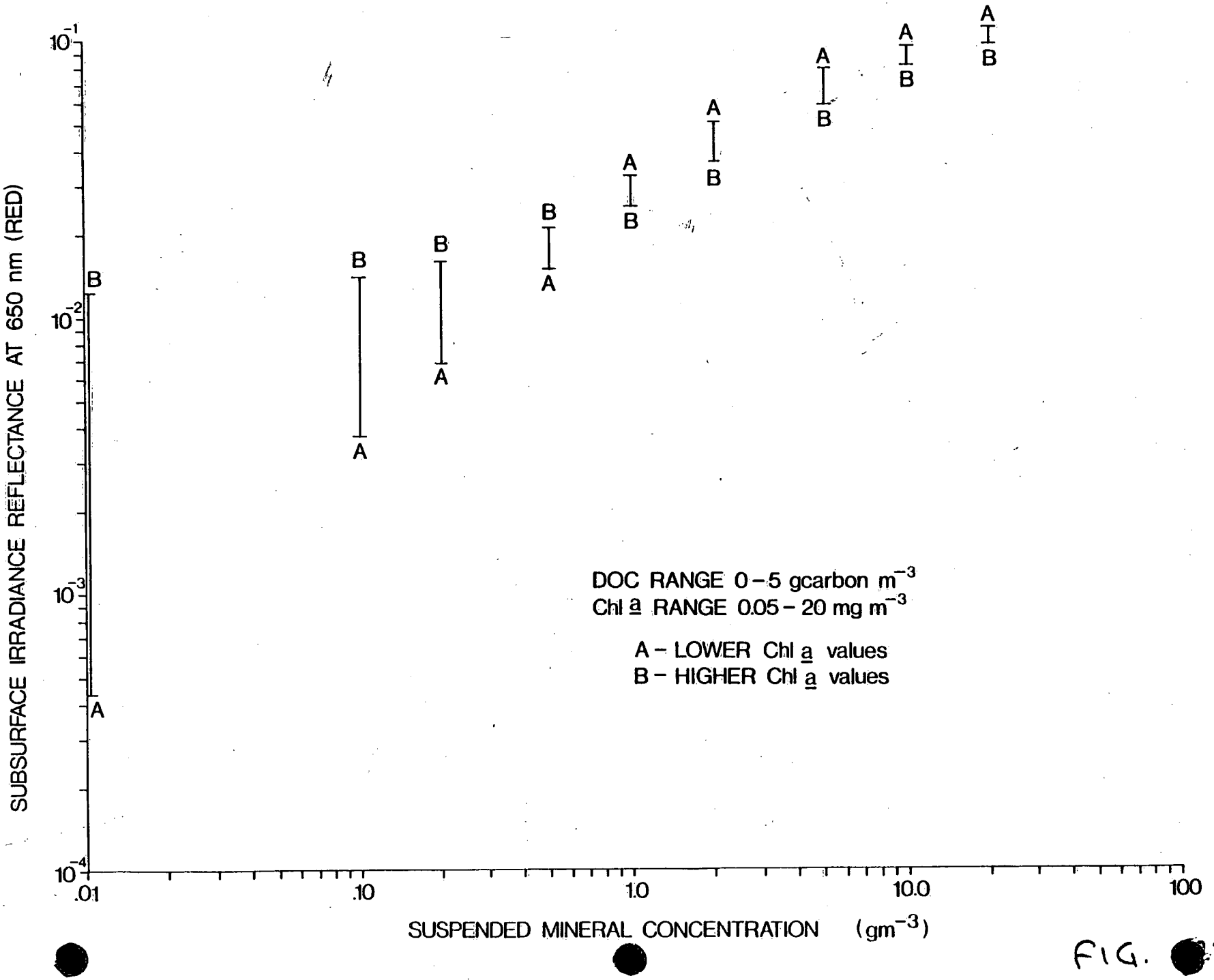
SUBSURFACE IRRADIANCE REFLECTANCE AT 650 nm (RED)
10^{-1}
10^{-2}
10^{-3}
10^{-4}
.01
.10
1.0
10.0
100
SUSPENDED MINERAL CONCENTRATION (gm^{-3})
DOC RANGE 0 – 5 gcarbon m^{-3}
Chl a RANGE 0.05 – 20 mg m^{-3}
A – LOWER Chl a values
B – HIGHER Chl a values

FIG. 7

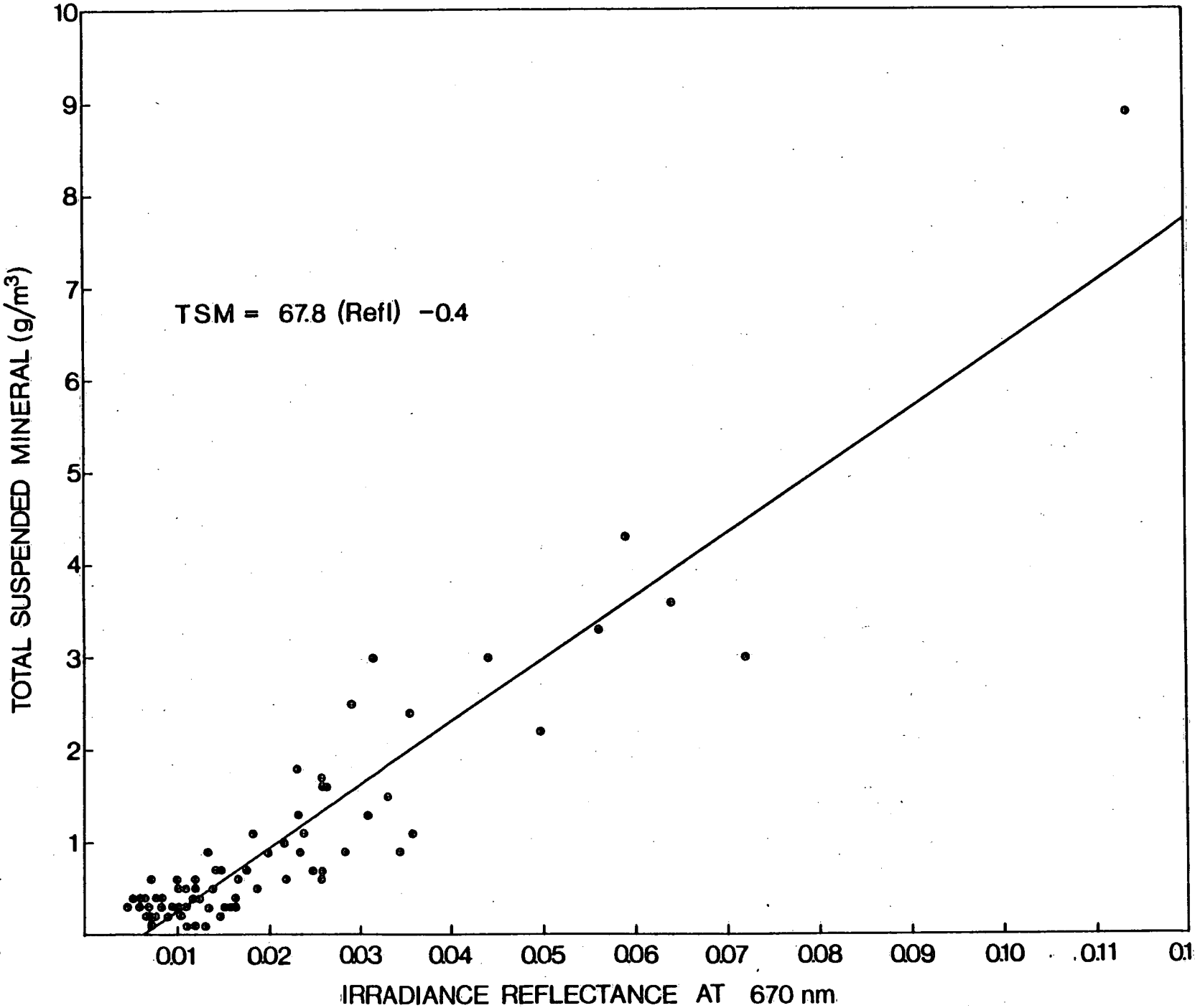
TOTAL SUSPENDED MINERAL (g/m³)
TSM = 67.8 (Refl) −0.4
10
9
8
7
6
5
4
3
2
1
0.01
0.02
0.03
0.04
0.05
0.06
0.07
0.08
0.09
0.10
0.11
0.12
IRRADIANCE REFLECTANCE AT 670 nm

FIG. 128

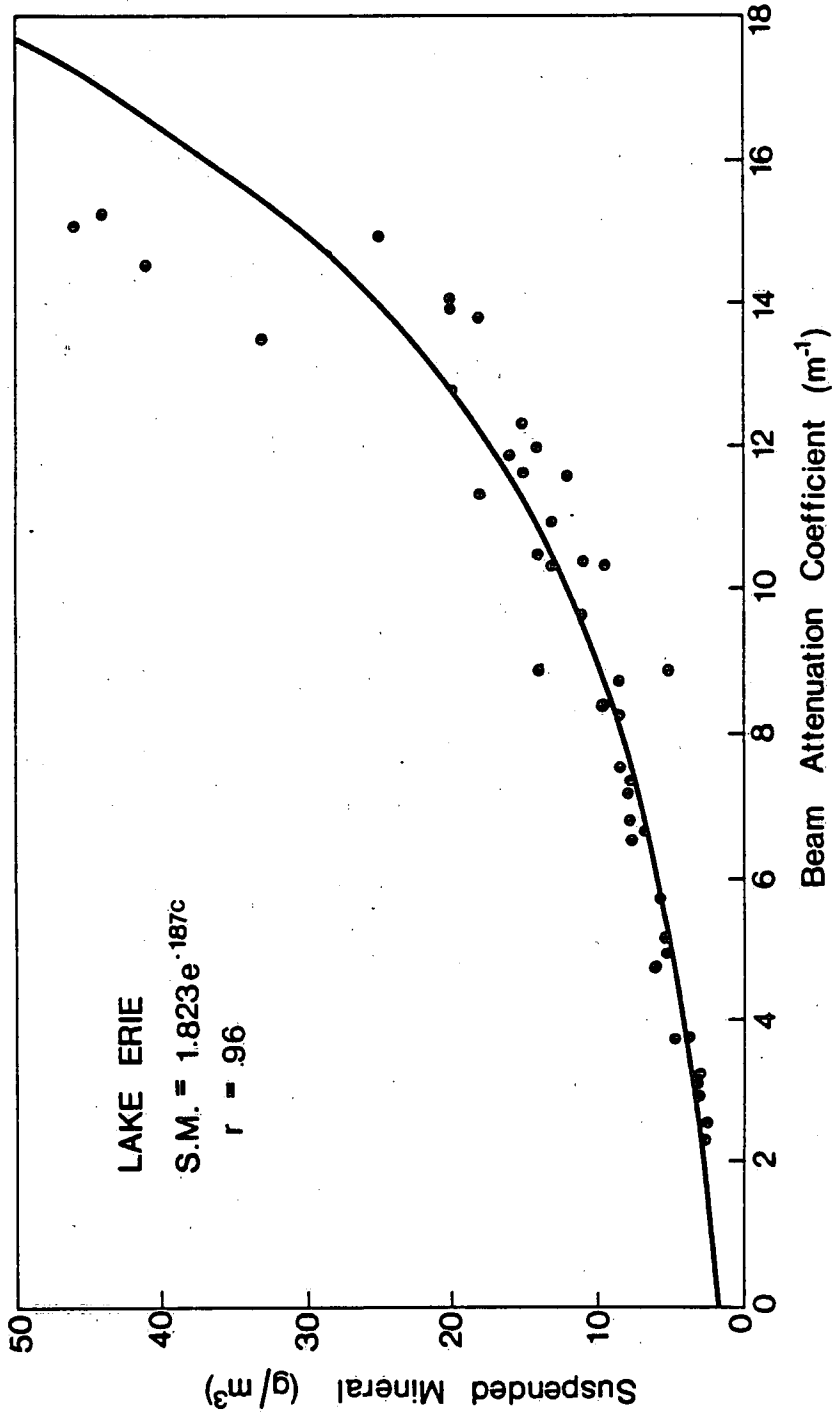
LAKE ERIE
S.M. = 1.823e^.187c
r = .96
Suspended Mineral (g/m³)
Beam Attenuation Coefficient (m⁻¹)
0
10
20
30
40
50
0
2
4
6
8
10
12
14
16
18

FIG. 129

REFERENCES

Bukata, R.P., J.H. Jerome, J.E. Bruton, and S.C. Jain. Determination of Inherent Optical Properties of Lake Ontario Coastal Waters. Appl. Opt., 18, 3926-3932, 1979.

Bukata, R.P., J.H. Jerome, and J.E. Bruton. An Optical Water Quality Model of Lake Ontario. Part I. Determination of the Optical Cross-Sections of Organic and Inorganic Particulates in Lake Ontario. Appl. Opt., 20, 1696-1703, 1981a.

Bukata, R.P., J.E. Bruton, and J.H. Jerome. An Optical Water Quality Model of Lake Ontario. Part II. Determination of Chlorophyll a and Suspended Mineral Concentrations of Natural Waters from Submersible and Low Altitude Optical Sensors. Appl. Opt., 20, 1704-1714, 1981b.

Bukata, R.P., J.E. Bruton, and J.H. Jerome. On the Use of Chromaticity in the Remote Measurements of Water Quality. Remote Sensing of Environment, 13, 161-177, 1983.

Bukata, R.P., J.E. Bruton, and J.H. Jerome. Application of Direct Measurements of Optical Parameters to the Estimation of Lake Water Quality Indicators. IWD Scientific Series No. 140. 1985.

Jerome, J.H., R.P. Bukata, and J.E. Bruton. Spectral Attenuation and Irradiance in the Laurentian Great Lakes. J. Great Lakes Res., 9, 60-68, 1983.

Jerome, J.H., J.E. Bruton, and R.P. Bukata. A Short Discussion on the Intercomparison of Transmissometers Used at CCIW. NWRI Report No. 84-36, 1984.

Preisendorfer, R.W. Hydrologic Optics. Vol. I. Introduction. U.S. Dept. of Commerce, 1976.

Tyler, J.E. Ocean Analysis by Means of Beer's Law. Appl. Opt., 15, 2565-2567, 1976.